Novel aptamer development for cell isolation and targeted drug delivery

Emmeline Ling Yi Cheng

A dissertation
submitted in partial fulfillment of the
requirements for the degree of

Doctor of Philosophy

University of Washington
2021

Reading Committee:
Suzie H. Pun, Chair
Kim A. Woodrow
Julie Shi

Program Authorized to Offer Degree:
Bioengineering

University of Washington

Abstract

Novel aptamer development for cell isolation and targeted drug delivery

Emmeline Ling Yi Cheng

Chair of the Supervisory Committee:

Suzie H. Pun

Department of Bioengineering

Aptamers are oligonucleotides that can bind to their targets with high affinity. These “chemical antibodies” provides numerous advantages over their biological counter parts. It is discussed in **chapter 1** that aptamers are attractive alternatives to antibodies when used in cell sorting technologies and drug delivery systems due to their reversable binding mechanisms, stability, chemical modification flexibility, low cost, and other properties. In our group, we discovered a couple of novel DNA aptamers using cell-SELEX (Systemic Evolution of Ligands by EXponential enrichment) technique. We presented a transferrin receptor 1 (TfR1, CD71) binding aptamer discovery process and application in **chapter 2**. This aptamer was used in a cell sorting system to separate cancerous B cells from healthy white blood cells designated for downstream adoptive cell therapy production. In **chapter 3**, we modified this CD71 aptamer for reversable cell targeting. The new version of CD71 aptamer was paired with a CD8 binding aptamer in a

multiplexed traceless cell isolation method. In **chapter 4**, we sought to identify a CD4 binding aptamer in order to tracelessly isolate both $CD4^+$ and $CD8^+$ T cells from PBMCs (peripheral blood mononuclear cells) for CAR (chimeric antigen receptor) T cell manufacturing. In **chapter 5**, we present one of the aptamers developed in this discovery process that has high binding to cancerous T cells. We modified this newly discovered aptamer for into different targeted drug delivery systems to treat acute lymphoblastic leukemia T cells. Lastly, the major discoveries on characterizing the CD71 aptamer and optimizing the dual selection method were summarized in **chapter 6**, along with recommended future work.

Table of Contents

List of Figures

List of Tables

Acknowledgements

Working towards the aims in this thesis has been challenging. This thesis work would not be possible without the frequent discussions with my mentors, co-workers, and committee members. I am incredibly thankful for everyone who has helped me and encouraged me during my graduate years at the University of Washington.

First and foremost, I want to thank my thesis advisor, **Suzie Pun**, who has provided the resource and advice I needed to make progress. On top of the scientific suggestions, Suzie has also given me detailed feedback on my manuscript writing, made time to meet with me for discussions when I requested, been empathetic and optimistic when my results were negative, and supported me throughout my career-building process. You are truly a role model and all that I wish for as a mentor.

Next, I want to thank my reading committee members, **Suzie Pun**, **Kim Woodrow**, and **Julie Shi**, as well as my supervisory committee members **Suzie Pun**, **Kim Woodrow**, **Julie Shi**, **Mike Jensen**, and **Georg Seelig** for all the guidance and feedback on my thesis work. I am honored to complete this milestone with you.

I would also like to thank our collaborators, **Chris Ramsborg**, **Allison Bianchi**, **Julie Shi**, and **Calvin Chan** who have given us valuable feedback and brainstormed potential applications using our biomaterials.

Stephen Salipante and **Kelsi Penewit** have been helping us with sequencing our DNA library samples and processing the output data for all our aptamer discovery projects. Thank you for your effort in loading the samples, converting the data files, and troubleshooting my sample preparation to improve the sequencing quality.

I would like to thank **Nataly Kacherovsky** for being my direct mentor and introducing me to the aptamer field when I first joined the Pun lab. You continuously inspire me to think outside the box and to come up with methods we have not tried before. I also enjoy cross-country skiing and foraging chanterelle in the mountains with you.

Drew Sellers is one of the most helpful scientists in the group who has helped me improve my HLPC, pull-down, conjugation, and other assays. Our coffee breaks in between experiments are one of my favorite times during the workdays. Even though I do not get your references most of the time, I appreciate you telling jokes to cheer me up when work is not going well.

Thank you, **Abby O'Connor**, for being a fantastic mentee who experimented with lots of new approaches for developing novel aptamers. Your enthusiasm is refreshing. I am proud of all that you have accomplished in the Pun lab. I feel very fortunate to be your direct mentor.

To the fellow Punions in my class, **Meilyn Sylvestre**, **Ian Cardle**, **Alex Prossnitz**, and **Dan Lee**. I am lucky to join the lab along with a group of hard-working and passionate scientists like you. Graduate school looked daunting at first, so I am glad that I was with good company.

I want to thank some of the Punions above my class, **Gary Liu**, **Brynn Olden**, **Bob Lamm**, **David Peeler**, and **Albert Yen** for your mentorship on my presentation and writing skills. I have made the most advancements in the past years by getting feedback from you. I also appreciate you for setting great examples of being resilient and reminding me not taking my experiment results personally.

To the current Punions, **Audrey Olshefsky**, **Clinton Heinze**, **Trey Pichon**, **Lucy Yang**, **Kefan Song**, **Ben Nguyen**, **Melissa Ling**, and **Jai Raman**, it has been a pleasure working with you. You

are one of the reasons I am excited to go to the lab every day. Like Suzie once said, I consider all of you my academic family.

To my friends in the city, **Alfredo Quijano Rubio**, **Camilla Bortolami**, **Yue Zhang**, **Ida Su**, **Sara Keller**, **Jamie Hernandez**, and **Carina Pereira**, I enjoyed all the fun times exploring restaurants and breweries, as well as having viewing parties and board game nights with you. I came to the states to do science. But you have made it become so much more. Thank you for making Seattle more like home to me.

I want to thank my families on the west coast, **J.S. Chen**, **Cindy Young**, **Grace Chen**, **Alex Chen**, and **Jimmy Chen**, who welcomed me with open arms when I first arrived in the United States. I appreciate you for all the advice and for inviting me to your vacation trips.

To **Ian Cardle**, my partner, thank you for your love and support. I am so glad to have you joining me on this journey. You always find a way to make me laugh, even during the tough days. Thank you for reminding me to enjoy the moment and to embrace this learning process. I am excited to see where life takes us next.

I want to thank my brother, **Alvin Cheng**, who continuously inspires me to be courageous by going down a career path that no one in the family has gone before. Thank you to **mom** and **dad** for teaching me to be kind and diligent, and to not give up easily when facing obstacles.

Dedication

To my family:

Fuhui Huang, Chin Hsiang Cheng, and Alvin Cheng

Chapter 1. Background and significance

1.1 Oligonucleotide binding ligands – aptamers

Aptamers are single-stranded oligonucleotides. They can be made of DNA, RNA, or artificial bases. Once aptamers are folded into the three-dimensional structures depend on base-pairing, these molecules can recognize targets ranging from small molecule to proteins, while having high affinity similar to antibodies. Aptamers have been an attractive alternative for antibodies because of their thermostability, low production cost, rapid chemical production process, and insusceptibility to lyophilization.[1] These characteristics lower the cost and facility requirements for long-term storage and temperature controlled transportation of these materials (**Table 1.1**). Therefore, aptamers are favorable for industrial applications.

Table 1.1. Antibody and aptamer comparison.

	Aptamer	**Antibody**	Ref.
Production process	Chemical	Biological	
Cost	~1.50 USD/nmole (IDT, 88bp, biotinylated)	~320 USD/nmole (Thermo Fisher, biotinylated)	
Storage	Room temperature, lyophilization safe	4^{o}C	[2]
Production time	Days-weeks	Months	[1]
Size	Smaller (~25 Å)	Larger (~140 Å)	[3,4]
Affinity	K_D pM-nM	K_D pM-nM	[5]
Binding activity	Reversible	Irreversible	[1]
Immunogenicity	Non-immunogenic	Often immunogenic	[1]

1.2 Reversable binding of aptamers

The binding ability of aptamers rely on their folded structure which is dictated by base-pairing. A thermally stable aptamer has three-dimensional structure consist of different secondary structures such as stems, hairpins, loops, and quadruplex.[1,6] These structures lead to interaction between aptamers and non-nucleic acid targets, such as proteins. The interactions contribute to targeted aptamer binding include electrostatic interactions, van der Waals forces, hydrogen bonding, hydrophobic effect (at the base-pairing core), pi-pi stacking, and steric complementarity.[7]

Different from antibodies, the binding structures of aptamers are reversable. We can achieve this by using chelator (e.g. EDTA), protein (e.g. DNA binding protein, competitors), or complementary strands to disrupt the base-pairing of aptamer.[8–10] Some groups have applied aptamer complementary strands as a safety measure for their therapeutic aptamers and to remove undesired labeling materials from the target proteins. For example, an anticoagulant aptamer targets Factor Xa was applied to patients went through cardiopulmonary bypass surgery to prevent blood clots. Once formed binding to Factor Xa, the aptamer activity can be reversed by its complementary strands. This measure precisely controlled the time of terminating anticoagulant aptamer activity.[11] Another therapeutic aptamer was used in cancer drug delivery system. Gray et al. developed a reversable pancreatic cancer drug delivery system with an aptamer-drug conjugate. A corresponding complementary strand that targets the hairpin structure of the aptamer was tested to successfully neutralizing the cytotoxicity of drug both *in vitro* and *in vivo*.[12] The complementary strand and aptamer pairs were also found useful for traceless isolation of cells. The targeting aptamers can first be applied to a mixed cell population and followed by secondary labeling with solid states (e.g., magnetic beads or resins). The cells can then be purified using the combination of these materials. More importantly, these undesired isolation materials can be removed by reversing aptamer binding with complementary strands for cell product productions and for studies on cellular pathways without their markers being shielded.[13,14]

1.3 Developing novel aptamers with SELEX

The most common way to develop novel aptamers is using a panning method called SELEX (Systemic Evolution of Ligands by Exponential enrichment), first reported by Tuerk and Gold in the 1990's. The group developed a T4 polymerase binding RNA aptamer with this *in vitro* evolution process.[15] Aptamer sequences developed in control environments have since been used in biosensors, diagnostics, drug delivery systems, cell isolations, biomarker discoveries, and other therapeutics,[13,16] including the first aptamer approved by FDA in 2004, Pegaptanib, which inhibits age-related macular degeneration through blocking the actions of vascular endothelial growth factor.[17]

In this thesis, we extensively use cells as selection targets in the SELEX process to discover novel DNA aptamers that bind to cell surface biomarkers.[18] In general, this process, called cell-

SELEX, starts by using a library of DNA that provides ~10^{16} unique sequences. Each sequence is composed of two constant regions flanking one variable region. The constant regions are used for PCR amplification, while the variable region provides sequence diversity. Each selection round has positive selections that enrich desired binders on target cells and negative selections that depletes background binders with control cells. The enriched pool from each selection rounds were amplified with PCR before entering the next round. At the end, the sequences in the pools were identified using NGS.[18] Detailed variations of cell-SELEX we used are presented in chapter 2, 4, and 5. Theoretically, one can develop aptamers that bind to any biomarker of interest by using the proper conditions.

1.4 CAR T cell therapy, a high-cost cancer therapy relies on biological ligands during production

Chimeric Antigen Receptor (CAR) T cell therapy is a type of highly effective cancer immunotherapy that harnesses and amplifies the patient's own immunity to defeat the cancerous cells in their body. Unlike traditional chemotherapy, CAR T cell therapies usually use the autologous T cells collected from the patient. CARs are genetically engineered receptor proteins composed of an extracellular single chain variable region derived from antibodies for cancer cell markers recognition, a transmembrane domain, and an intracellular domain with CD3ζ signaling chain and costimulatory receptors, such as CD28 or 4-1BB.[19,20] This type of therapy is especially effective on blood cancers. The currently approved CD19 CAR T cell therapies, Kymriah (Novartis), Yescarta (Gilead), Tecartus (Gilead), and Breyanzi (Bristol Myers Squibb) are approved to treat patients with relapse or refractory B cell acute lymphoblastic leukemia, diffuse large B cell lymphoma, and mantle cell lymphoma.[21–25] Whereas Abecma (Bristol Myers Squibb), a B cell maturation antigen-targeting CAR T cell, is approved to treat multiple myeloma.[26,27] In brief, the CAR T cell therapy manufacturing process includes (1) isolating or enriching T cells from patient's apheresis product, (2) activating, (3) transducing these T cells to express CAR, (4) expanding these cells in culture, and (5) reinfuse the cells back to the patients (**Figure 1.1**).[28]

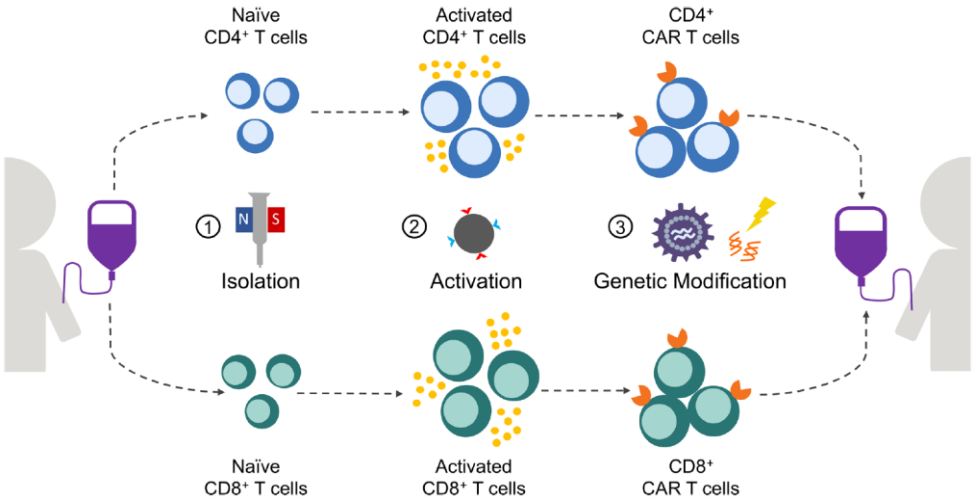

Figure 1.1. Schematic of producing CAR T cells with defined CD4 and CD8 ratio. Reproduced from ref. [29]. Copyright 2020 American Chemical Society.

It takes a median throughput time of 23 days to manufacture Kymriah and the involvement of both clinics and manufacturing sites.[30] The process is time consuming, labor-intensive, and highly relies on biological reagents, such as antibodies. These factors ultimately result in the high price tags of the approved CAR T cell products (Kymriah at $475,000; Yescarta and Tecartus at $373,000 per dose). Therefore, improvements are needed to reduce the manufacturing cost of CAR T cell products. Some progress has been made by using closed automatic systems, upscaling production, and finding less expensive alternative methods and materials.[31,32] Strikingly, the recurrent materials used in the production process, including antibodies, costs 10,000 to 20,000 dollars in producing a single dose of autologous CAR T cells, which contributes to ~18% of the total manufacturing cost.[31,33] Throughout chapter 2 to 4, we ultimately aim at using aptamers to provide better and cheaper cell isolation methods for CAR T cell therapies.

1.5 Challenges and opportunities in antibody-drug conjugate as cancer treatment

Antibody-drug conjugates are targeted drug delivery platforms that directly conjugate bioactive toxin onto cancer cell-specific antibodies to avoid toxicity on healthy cells. However, the use of antibodies has raised a few challenges and concerns. One of them is the immunogenicity of antibodies.[34] Advancement has been made to reduce immunogenicity including making

humanized antibodies by modifying mouse antibodies sequence to increase similarity with human antibodies and chimeric antibodies by replacing mouse Fc region with human Fc using gene editing. One can also generate human antibodies by using human hybridoma cells for production.[35,36] However, we can bypass these engineering processes entirely by using aptamers.

Tumor penetration is another limiting factor for the success of cancer treatment, which can be highly effected by the size of the drug delivery vehicle.[36] As aptamers are about 10 times smaller than antibodies in size[4], Xiang et al. compared the penetration of EpCAM binding aptamer and antibody on colorectal cancer solid tumor models, both *in vitro* and *in vivo*. The authors found fold increase of accumulation, retention, and deeper tumor targeting by using EpCAM aptamer compared to using EpCAM antibody.[3]

Last, modification of antibodies is challenging as the protein structures are easily affected by adding residues with reactive functional groups.[37] These chemical alterations, however, are crucial for forming stable covalent bonds between the antibodies and toxins. Aptamers are easy to modify, both in the middle sequances[38,39], or on the 5'- and 3'-ends[40,41]. Modified aptamers has been used for various applications including fluorescent detection, nanoparticle functionalization, nuclease resistant, and active molecules delivery.[38–43] In addition to precise chemical modification, DNA aptamers also have available intercalating sites between the base pairs the double stranded structure for cytotoxic drugs such as anthracyclines.[44] This is an alternative drug delivery method that takes shorter time to formulate compared to direct conjugation. In chapter 5, we applied a novel aptamer with high binding affinity on toxin delivery to T-ALL cancer cells.

1.6 References

1. Zhou, J. & Rossi, J. Aptamers as targeted therapeutics: Current potential and challenges. *Nature Reviews Drug Discovery* (2017) doi:10.1038/nrd.2016.199.

2. Keefe, A. D., Pai, S. & Ellington, A. Aptamers as therapeutics. *Nature Reviews Drug Discovery* (2010) doi:10.1038/nrd3141.

3. Xiang, D., Zheng, C., Zhou, S.-F., Qiao, S., Tran, P. H.-L., Pu, C., Li, Y., Kong, L., Kouzani, A. Z., Lin, J., Liu, K., Li, L., Shigdar, S. & Duan, W. Superior Performance of Aptamer in Tumor Penetration over Antibody: Implication of Aptamer-Based Theranostics in Solid Tumors. *Theranostics* **5**, 1083–1097 (2015).

4. Lee, J. O., So, H. M., Jeon, E. K., Chang, H., Won, K. & Kim, Y. H. Aptamers as molecular recognition elements for electrical nanobiosensors. *Anal. Bioanal. Chem.* (2008) doi:10.1007/s00216-007-1643-y.

5. Dong, Y., Xu, Y., Yong, W., Chu, X. & Wang, D. Aptamer and Its Potential Applications for Food Safety. *Critical Reviews in Food Science and Nutrition* (2014) doi:10.1080/10408398.2011.642905.

6. Sullivan, R., Adams, M. C., Naik, R. R. & Milam, V. T. Analyzing secondary structure patterns in DNA aptamers identified via compels. *Molecules* (2019) doi:10.3390/molecules24081572.

7. Cai, S., Yan, J., Xiong, H., Liu, Y., Peng, D. & Liu, Z. Investigations on the interface of nucleic acid aptamers and binding targets. *Analyst* (2018) doi:10.1039/c8an01467a.

8. Ellington, A. D. & Szostak, J. W. In vitro selection of RNA molecules that bind specific ligands. *Nature* (1990) doi:10.1038/346818a0.

9. Bunka, D. H. J., Platonova, O. & Stockley, P. G. Development of aptamer therapeutics. *Current Opinion in Pharmacology* (2010) doi:10.1016/j.coph.2010.06.009.

10. Li, L., Chen, X., Cui, C., Pan, X., Li, X., Yazd, H. S., Wu, Q., Qiu, L., Li, J. & Tan, W. Aptamer Displacement Reaction from Live-Cell Surfaces and Its Applications. *J. Am. Chem. Soc.* (2019) doi:10.1021/jacs.9b07191.

11. Gunaratne, R., Kumar, S., Frederiksen, J. W., Stayrook, S., Lohrmann, J. L., Perry, K., Bompiani, K. M., Chabata, C. V., Thalji, N. K., Ho, M. D., Arepally, G., Camire, R. M., Krishnaswamy, S. & Sullenger, B. A. Combination of aptamer and drug for reversible anticoagulation in cardiopulmonary bypass. *Nat. Biotechnol.* (2018) doi:10.1038/nbt.4153.

12. Powell Gray, B., Kelly, L., Ahrens, D. P., Barry, A. P., Kratschmer, C., Levy, M. & Sullenger, B. A. Tunable cytotoxic aptamer–drug conjugates for the treatment of prostate cancer. *Proc. Natl. Acad. Sci.* **115**, 4761 LP – 4766 (2018).

13. Kacherovsky, N., Cardle, I. I., Cheng, E. L., Yu, J. L., Baldwin, M. L., Salipante, S. J., Jensen, M. C. & Pun, S. H. Traceless aptamer-mediated isolation of CD8+ T cells for chimeric antigen receptor T-cell therapy. *Nat. Biomed. Eng.* (2019) doi:10.1038/s41551-019-0411-6.

14. Gray, B. P., Requena, M. D., Nichols, M. D. & Sullenger, B. A. Aptamers as Reversible Sorting Ligands for Preparation of Cells in Their Native State. *Cell Chem. Biol.* (2020) doi:10.1016/j.chembiol.2019.12.004.

15. Tuerk, C. & Gold, L. Systematic evolution of ligands by exponential enrichment: RNA ligands to bacteriophage T4 DNA polymerase. *Science (80-.).* (1990) doi:10.1126/science.2200121.

16. Dunn, M. R., Jimenez, R. M. & Chaput, J. C. Analysis of aptamer discovery and technology. *Nat. Rev. Chem.* (2017) doi:10.1038/s41570-017-0076.

17. Ng, E. W. M., Shima, D. T., Calias, P., Cunningham, E. T., Guyer, D. R. & Adamis, A. P. Pegaptanib, a targeted anti-VEGF aptamer for ocular vascular disease. *Nature Reviews Drug Discovery* vol. 5 123–132 (2006).

18. Sefah, K., Shangguan, D., Xiong, X., O'Donoghue, M. B. & Tan, W. Development of DNA aptamers using cell-selex. *Nat. Protoc.* (2010) doi:10.1038/nprot.2010.66.

19. Z, E., T, W., G, G. & D, S. Specific activation and targeting of cytotoxic lymphocytes through chimeric single chains consisting of antibody-binding domains and the gamma or zeta subunits of the immunoglobulin and T-cell receptors. *Proc. Natl. Acad. Sci. U. S. A.* (1993).

20. Sadelain, M., Brentjens, R. & Rivière, I. The basic principles of chimeric antigen receptor design. *Cancer Discovery* (2013) doi:10.1158/2159-8290.CD-12-0548.

21. Novartis Pharmaceuticals Corporation. KYMRIAH (tisagenlecleucel) - Package insert. *U.S. Food and Drug Administration website* https://www.fda.gov/media/107296/download (2017).

22. Kite Pharma, I. YESCARTA (axicabtagene ciloleucel) - Package insert. *U.S. Food and Drug Administration website* https://www.fda.gov/media/108377/download (2017).

23. Kite Pharma, I. TECARTUS (brexucabtagene autoleucel) - Package insert. *U.S. Food and Drug Administration website* https://www.fda.gov/media/140409/download (2020).

24. Abramson, J. S., Palomba, M. L., Gordon, L. I., Lunning, M. A., Wang, M., Arnason, J., Mehta, A., Purev, E., Maloney, D. G., Andreadis, C., Sehgal, A., Solomon, S. R., Ghosh, N., Albertson, T. M., Garcia, J., Kostic, A., Mallaney, M., Ogasawara, K., Newhall, K., Kim, Y., Li, D. & Siddiqi, T. Lisocabtagene maraleucel for patients with relapsed or refractory large B-cell lymphomas (TRANSCEND NHL 001): a multicentre seamless design study. *Lancet (London, England)* **396**, 839–852 (2020).

25. Abramson, J. S., Palomba, M. L., Gordon, L. I., Lunning, M. A., Wang, M. L., Arnason, J. E., Mehta, A., Purev, E., Maloney, D. G., Andreadis, C., Sehgal, A. R., Solomon, S. R., Ghosh, N., Albertson, T., Garcia, J., Kostic, A., Li, D., Kim, Y. & Siddiqi, T. Pivotal Safety and Efficacy Results from Transcend NHL 001, a Multicenter Phase 1 Study of Lisocabtagene Maraleucel (liso-cel) in Relapsed/Refractory (R/R) Large B Cell Lymphomas. *Blood* **134**, 241 (2019).

26. Munshi, N. C., Anderson, L. D., Shah, N., Madduri, D., Berdeja, J., Lonial, S., Raje, N., Lin, Y., Siegel, D., Oriol, A., Moreau, P., Yakoub-Agha, I., Delforge, M., Cavo, M.,

Einsele, H., Goldschmidt, H., Weisel, K., Rambaldi, A., Reece, D., Petrocca, F., Massaro, M., Connarn, J. N., Kaiser, S., Patel, P., Huang, L., Campbell, T. B., Hege, K. & San-Miguel, J. Idecabtagene Vicleucel in Relapsed and Refractory Multiple Myeloma. *N. Engl. J. Med.* (2021) doi:10.1056/nejmoa2024850.

27. Jagannath, S., Lin, Y., Goldschmidt, H., Reece, D., Nooka, A., Senin, A., Rodriguez-Otero, P., Powles, R., Matsue, K., Shah, N., Anderson, L. D., Streetly, M., Wilson, K., Le, H. Van, Swern, A. S., Agarwal, A. & Siegel, D. S. KarMMa-RW: comparison of idecabtagene vicleucel with real-world outcomes in relapsed and refractory multiple myeloma. *Blood Cancer J.* (2021) doi:10.1038/s41408-021-00507-2.

28. Levine, B. L., Miskin, J., Wonnacott, K. & Keir, C. Global Manufacturing of CAR T Cell Therapy. *Molecular Therapy - Methods and Clinical Development* (2017) doi:10.1016/j.omtm.2016.12.006.

29. Cardle, I. I., Cheng, E. L., Jensen, M. C. & Pun, S. H. Biomaterials in chimeric antigen receptor T-cell process development. *Acc. Chem. Res.* (2020) doi:10.1021/acs.accounts.0c00335.

30. Tyagarajan, S., Spencer, T. & Smith, J. Optimizing CAR-T Cell Manufacturing Processes during Pivotal Clinical Trials. *Mol. Ther. - Methods Clin. Dev.* **16**, 136–144 (2020).

31. Zhu, F., Shah, N., Xu, H., Schneider, D., Orentas, R., Dropulic, B., Hari, P. & Keever-Taylor, C. A. Closed-system manufacturing of CD19 and dual-targeted CD20/19 chimeric antigen receptor T cells using the CliniMACS Prodigy device at an academic medical center. *Cytotherapy* (2018) doi:10.1016/j.jcyt.2017.09.005.

32. Ran, T., Eichmüller, S. B., Schmidt, P. & Schlander, M. Cost of decentralized CAR T-cell production in an academic nonprofit setting. *Int. J. Cancer* (2020) doi:10.1002/ijc.33156.

33. Spink, K. & Steinsapir, A. The long road to affordability: a cost of goods analysis for an autologous CAR-T process. *Cell Gene Ther. Insights* (2018) doi:10.18609/cgti.2018.108.

34. Hamilton, G. S. Antibody-drug conjugates for cancer therapy: The technological and regulatory challenges of developing drug-biologic hybrids. *Biologicals* (2015) doi:10.1016/j.biologicals.2015.05.006.

35. C., J., Jennifer, Y., G., T., Parikh, R., Lou, Y. & Far, D. Monoclonal Antibody Development and Physicochemical Characterization by High Performance Ion Exchange Chromatography. in *Innovations in Biotechnology* (2012). doi:10.5772/30056.

36. Beck, A., Goetsch, L., Dumontet, C. & Corvaïa, N. Strategies and challenges for the next generation of antibody-drug conjugates. *Nature Reviews Drug Discovery* (2017) doi:10.1038/nrd.2016.268.

37. Junutula, J. R., Bhakta, S., Raab, H., Ervin, K. E., Eigenbrot, C., Vandlen, R., Scheller, R. H. & Lowman, H. B. Rapid identification of reactive cysteine residues for site-specific labeling of antibody-Fabs. *J. Immunol. Methods* (2008) doi:10.1016/j.jim.2007.12.011.

38. Van Riesen, A. J., Fadock, K. L., Deore, P. S., Desoky, A., Manderville, R. A., Sowlati-Hashjin, S. & Wetmore, S. D. Manipulation of a DNA aptamer-protein binding site through arylation of internal guanine residues. *Org. Biomol. Chem.* (2018)

doi:10.1039/c8ob00704g.

39. Virgilio, A., Petraccone, L., Vellecco, V., Bucci, M., Varra, M., Irace, C., Santamaria, R., Pepe, A., Mayol, L., Esposito, V. & Galeone, A. Site-specific replacement of the thymine methyl group by fluorine in thrombin binding aptamer significantly improves structural stability and anticoagulant activity. *Nucleic Acids Res.* (2015) doi:10.1093/nar/gkv1224.

40. Zhang, L., Wang, S., Yang, Z., Hoshika, S., Xie, S., Li, J., Chen, X., Wan, S., Li, L., Benner, S. A. & Tan, W. An Aptamer-Nanotrain Assembled from Six-Letter DNA Delivers Doxorubicin Selectively to Liver Cancer Cells. *Angew. Chemie* (2020) doi:10.1002/ange.201909691.

41. Huang, Y. F., Shangguan, D., Liu, H., Phillips, J. A., Zhang, X., Chen, Y. & Tan, W. Molecular assembly of an aptamer-drug conjugate for targeted drug delivery to tumor cells. *ChemBioChem* (2009) doi:10.1002/cbic.200800805.

42. Yang, L., Zhang, X., Ye, M., Jiang, J., Yang, R., Fu, T., Chen, Y., Wang, K., Liu, C. & Tan, W. Aptamer-conjugated nanomaterials and their applications. *Advanced Drug Delivery Reviews* (2011) doi:10.1016/j.addr.2011.10.002.

43. Musumeci, D., Platella, C., Riccardi, C., Moccia, F. & Montesarchio, D. Fluorescence sensing using DNA Aptamers in cancer research and clinical diagnostics. *Cancers* (2017) doi:10.3390/cancers9120174.

44. Macdonald, J., Denoyer, D., Henri, J., Jamieson, A., Burvenich, I. J. G., Pouliot, N. & Shigdar, S. Bifunctional Aptamer-Doxorubicin Conjugate Crosses the Blood-Brain Barrier and Selectively Delivers Its Payload to EpCAM-Positive Tumor Cells. *Nucleic Acid Ther.* (2020) doi:10.1089/nat.2019.0807.

Chapter 2. Discovery of a transferrin receptor 1-binding aptamer for removing cancer cells from adoptive T-cell therapy manufacturing

Emmeline L. Cheng, Ian I. Cardle, Nataly Kacherovsky, Yunshi Zhou, Vamsiraman Raman, Albert Yen, Stephen J. Salipante, Michael C. Jensen, Suzie H. Pun*

Abstract

The clinical manufacturing of chimeric antigen receptor (CAR) T cells includes cell selection, activation, gene transduction, and expansion. The method of T-cell selection varies across companies; some groups collect elutriation-enriched peripheral blood mononuclear cells (PBMCs) to obtain increased percentages of T cells, while other groups use costly antibodies to isolate $CD3^+$, $CD4^+$, and/or $CD8^+$ T cells. However, neither of these methods actively eliminate the cancer cells in the patient's apheresis product from the healthy immune cells. Alarmingly, it has been found that transduction of a single leukemic B cell with the CAR gene can confer resistance to CAR T-cell therapy and lead to treatment failure. In this study, we report the identification of a novel high-affinity aptamer, termed tJBA8.1, that targets transferrin receptor 1 (TfR1), a receptor broadly upregulated by cancer cells. Using competition assays, we reveal that tJBA8.1 shares a binding site on TfR1 with both holo-transferrin and a previously published aptamer, XQ-2d. We then use tJBA8.1 to effectively deplete B lymphoma cells spiked into PBMCs with minimal impact on the healthy immune cell composition. Lastly, we characterize TfR1-independent binding of tJBA8.1 and present opportunities for specificity and affinity improvement. As TfR1 expression is broadly upregulated on many cancers, including difficult-to-treat T-cell leukemias and lymphomas, our work provides a facile, universal, and inexpensive approach for comprehensively removing cancerous cells from patient apheresis products for safe manufacturing of adoptive T-cell therapies.

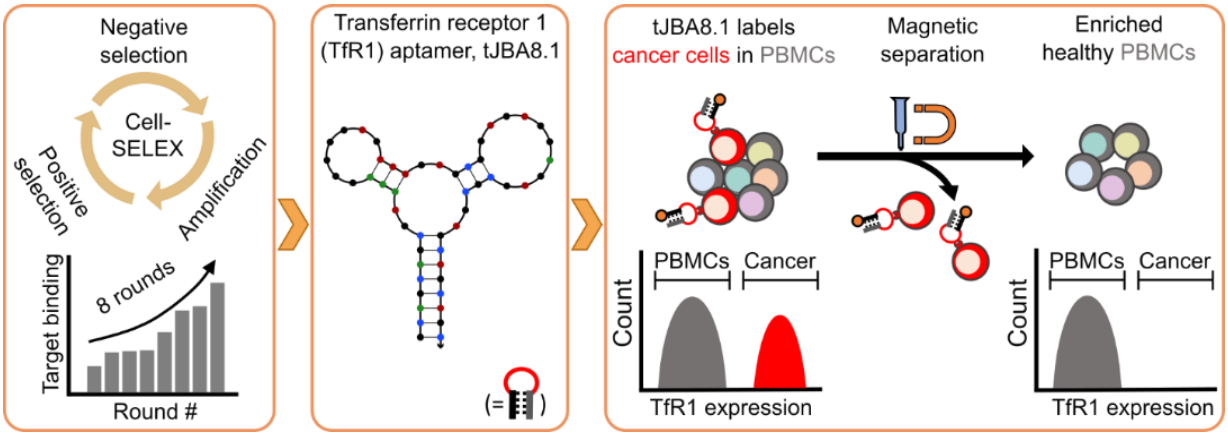

Scheme 2.1. Development and application of a transferrin receptor 1-binding aptamer.

2.1 Introduction

Chimeric antigen receptor (CAR) T-cell therapy has gained significant traction in the oncology field, with five FDA-approved therapies to-date: four for treating relapsed or refractory (r/r) $CD19^+$ B-cell malignancies (Novartis's Kymriah, Gilead-Kite's Yescarta and Tecartus, and Bristol Myers Squibb-Juno Therapeutic's Breyanzi) and another for treating r/r $BCMA^+$ multiple myeloma (Bristol Myers Squibb-bluebird bio's Abecma).[1–7] In these treatments, a patient's T cells journey through an elaborate manufacturing process that consists of 1) enrichment from a leukapheresis product, 2) activation *ex vivo*, 3) lentiviral or retroviral expression of a CAR that directs T-cell function against a tumor-associated antigen, 4) expansion to therapeutically relevant numbers, and 5) re-infusion into the patient's body for cancer elimination.[8] Given the intricate nature of this operation, there is a continual need for further innovation at each production step to reduce the costs and increase the efficacy and safety of these adoptive T-cell therapies.[9]

T-cell enrichment or selection is one of the most pivotal steps in CAR T-cell manufacturing, as the cell composition and purity used in subsequent activation and transduction steps can influence the outcome of the therapy. For Kymriah, Yescarta, and Abecma, T cells are indirectly enriched by collecting peripheral blood mononuclear cells (PBMCs) from leukapheresis product using counterflow centrifugal elutriation, which removes most monocytes, granulocytes, platelets, and residual red blood cells based on differences in cell size and density relative to lymphocytes.[10–14] However, this selection approach is unable to discriminate healthy T cells from circulating

cancerous lymphocytes, meaning that tumor cells can be present in downstream manufacturing steps and thereby drive uncontrollable activation and exhaustion of the CAR T-cell product.[15] Additionally, in 2018, it was found that transduction of a single leukemic B cell with the CAR gene during CAR T-cell manufacturing caused a patient to relapse after treatment and ultimately succumb to their disease.[16] The patient's cancer expressed the CD19 CAR on the cell surface, masking the CD19 antigen in *cis* and thereby protecting the cancer cells from treatment. These issues highlight the need for complete removal of cancerous lymphocytes during the selection step prior to further CAR T-cell manufacturing.

To address this problem, especially for patients with high circulating blast and leukemia cell counts, Tecartus and Breyanzi rely on direct isolation of T cells. Whereas Tecartus isolates bulk $CD3^+$ T cells and does not further consider the composition of T-cell subsets,[5] Breyanzi separately isolates helper $CD4^+$ T cells and cytotoxic $CD8^+$ T cells for CAR T-cell production and later infuses the patient with a defined 1:1 composition of the subsets.[6] In doing so, Breyanzi has proven to be a safer therapy than its counterparts; it has lower rates of cytokine release syndrome and neurotoxicity than Kymriah and Yescarta while remaining equally effective.[2,3,6] However, the direct isolation of T cells is expensive, typically relying on costly antibody- or multimerized Fab-coated magnetic beads that target either the $CD3^+$, $CD4^+$, and/or $CD8^+$ T-cell markers for positive enrichment or unwanted immune cell markers for negative enrichment.[17,18] Furthermore, these approaches do not actively remove the cancer cells from a patient's leukapheresis product. In contrast to B-cell malignancies,[19] malignant T cells can be difficult to separate from healthy T cells used for manufacturing CAR T cell therapies.[20,21] Accordingly, as autologous CAR T-cell therapies are broadened to treat diverse hematological malignancies, an inexpensive and universal method for removing cancerous cells from healthy PBMCs will be imperative for safe manufacturing of these treatments.

DNA aptamers, single-stranded oligonucleotides that fold into sequence-specific secondary structures, are molecular recognition agents that can address the deficiencies of cancer cell removal approaches currently employed in adoptive T-cell manufacturing. Unlike biologically produced antibodies and Fabs, aptamers are inexpensive, owing to their fast chemical synthesis with low lot-to-lot variation.[22] Aptamers can also be controllably modified at any position (5' end, 3' end, or internally) and display binding affinities comparable to antibodies, making them highly amenable

to immobilization onto solid supports for affinity-based separations.[23,24] Demonstrating this, our group previously identified CD8-binding DNA aptamers and used them to isolate $CD8^+$ T cells via magnetic-activated cell sorting (MACS) with comparable purity, yield, and downstream CAR functionality as those isolated from commercial antibody-based methods.[25]

Aptamers can be selected to bind certain cell types without prior knowledge of receptor identity (i.e. receptor-agnostic panning). The subtractive evolutionary process in which aptamers go through rounds of positive and negative selection against whole cells, termed cell-SELEX (systematic evolution of ligands by exponential enrichment), has become an attractive method for discovering aptamers that can differentiate malignant cells from healthy normal cells.[26–28] Our group has also used this target-agnostic cell-SELEX method to identify an aptamer that preferentially binds both monocytes within a PBMC population as well as M0- and M2-like macrophages over M1-like macrophages.[29] Given these benefits, cell-SELEX holds great promise for discovering DNA aptamers that can selectively bind and deplete circulating leukemia and lymphoma cells from PBMCs at low cost prior to CAR T-cell manufacturing.

Here, in a cell-SELEX intended to identify T-cell antigen-binding aptamers, we discovered and truncated an aptamer, named tJBA8.1, that displays high-affinity binding for Jurkat T-leukemia cells. Further assays identified transferrin receptor 1 (TfR1), an iron-uptake receptor not expressed on resting immune cells but upregulated on actively dividing and cancerous cells, as the binding target of tJBA8.1. We characterized the tJBA8.1-TfR1 interaction by flow cytometry, biolayer interferometry, and competition studies, including comparison to the XQ-2d TfR1-binding aptamer reported previously by the Tan group.[30,31] We further employed tJBA8.1 in MACS to remove spiked Raji B-lymphoma cells from PBMCs with high yield and minimal impact on the healthy immune cell composition. Lastly, we study the off-target binding of tJBA8.1 and describe changes for specificity and affinity improvement. Given the broad expression of TfR1 on many cancers, including difficult to distinguish T-cell leukemias and lymphomas, we anticipate that this method could be universally used for the depletion of circulating cancer cells from patient PBMCs prior to downstream CAR T-cell manufacturing, leading to a safer, more potent, and cost-mindful therapy.

2.2 Materials and methods

2.2.1 Cell line and primary cell culture

Jurkat cell line (human T-ALL) was kindly gifted by the Jensen group in Seattle Children's Research Institute. J.RT3-T3.5 cell line (human T-ALL), Raji cell line (human B cell lymphoma), and H9 cell line (human T cell lymphoma) were purchased from ATCC. Jurkat, J.RT3-T3.5, Raji, and H9 cell lines were cultured in RPMI 1640 medium (Corning) with 10% fetal bovine serum (FBS, Life Tech). Primary human PBMCs were obtained by purchasing Leukocyte Reduction System (LRS) cones from Bloodworks Northwest, followed by density-based separation in Ficoll buffer. Positively enriched primary human T cells were gifted by Juno Therapeutics. $CD8^+$ T cell activation was done by culturing cells in 20 ng/mL recombinant human IL-2 (Miltenyi) and 0.5 ng/mL recombinant human IL-15 (Miltenyi) added to RPMI 1640 medium with 10% FBS. $CD4^+$ T cells activation was done by culturing cells in 5 ng/mL recombinant human IL-7 (Miltenyi) and 0.5 ng/mL recombinant human IL-15 (Miltenyi) spiked RPMI 1640 medium with 10% FBS. Both cell types were cultured along with CD3/CD28 Dynabeads (Invitrogen) according to the user manual and expanded up to 22 days.

2.2.2 Oligonucleotides, PCR reagents, and recombinant proteins

Customed oligonucleotides, including naïve library, primers, and individual aptamers were purchased from Integrated DNA Technology (IDT). Naïve library and individual aptamers (**Supplementary Table 2.4**) were purified by HPLC. The forward primer, FAM-5'-ATCCAGAGTGACGCAGCA-3', and reverse primer, biotin-5'-ACTAAGCCACCGTGTCCA-3', used to amplify aptamer library were both purified by standard desalting. dNTP was ordered from QIAGEN. Phusion High-Fidelity DNA polymerase was purchased from NEB. Recombinant human and murine holo-transferrin were both ordered from Sigma-Aldrich. Biotinylated recombinant human transferrin receptor 1 was purchased from ACROBiosystems (TfR-H82E5). His-tagged recombinant mouse transferrin receptor 1 was purchased from Sino Biological (50741-M07H).

2.2.3 Cell staining reagents and flow cytometry

For flow cytometry cell staining and competition studies, we used the following live/dead staining dye and antibodies: Zombie Violet (1:500 in 100ul containing 10^6 cells, BioLegend), FITC anti-human CD71 (1:100, BioLegend, CY1G4), FITC anti-human CD3 antibody (1:100, BioLegend, UCHT1), Super Bright 600 anti-human CD56 (1:100, Invitrogen, TULY56), FITC anti-human CD14 (1:100, BioLegend, M5E2), APC-Cy7 anti-human CD14 (1:200, Molecular probes, 6ID3), Super Bright 702 anti-human CD19 (1:100, Invitrogen, SJ25C), PE anti-human CD3 (1:100, BioLegend, HIT3a), and Alexa Fluor 647 streptavidin (1:500, BioLegend).

The components for making aptamer staining buffer include Dulbecco's phosphate buffered saline (DPBS) with calcium and magnesium (Corning), yeast tRNA (Invitrogen), D-glucose (Sigma-Aldrich), magnesium chloride (Fisher), and bovine serum albumin (BSA, Miltenyi). In the aptamer staining process, we used wash buffer with 1% BSA for wash steps and binding buffer for staining steps. The wash buffer was made with 500 mL DPBS (with calcium and magnesium) plus 2.5 mL 1 M $MgCl_2$ and 2.25 g D-glucose, which contains 0.137 M Na^+ and 0.0055 M Mg^{2+}. The binding buffer was made with wash buffer plus 0.1 mg/ml yeast tRNA and 1% BSA. Aptamers ordered from IDT were labeled with either FAM, Cy5, or biotin. Aptamers were annealed at 1 μM in wash buffer by heating the solution to 95 ^oC for 5 minutes and snap cold on ice for at least 15 minutes. Aptamer staining cells was done at 4 ^oC to avoid internalization. The RANL aptamer (**Supplementary Table 2.4**), an aptamer randomly picked out from the naïve library, was used as control. The readout of aptamer binding on cells was collected on Attune NxT Cytometer (Invitrogen).

2.2.4 Cell-SELEX

The experimental design of cell-SELEX used in this study are summarized in **Figure 2.1A** and **Supplementary Table 2.1**. This selection process is modified from a published protocol.[26] We started by inputting 40 nmol of naïve library. This provides us theoretically 10^{16} unique sequences. Each sequence consists of a N45 random region, flanked by 18 bases constant region. A total volume of 400 μL was used throughout the library incubation steps. In positive selection

steps, the amount of target cells indicated in **Supplementary Table 2.1** were resuspended with the library in wash buffer with 0.1 mg/mL yeast tRNA and various concentrations of FBS at 4 ^{o}C. Once the stained target cells were washed, the library was eluted from the cells by heating at 95 ^{o}C in wash buffer. The cell debris was spun down, and the supernatant was collected for negative selection. In negative selection steps, the heat-eluted library was incubated with control cells in the same staining condition as positive selection. The sequence-bound cells were removed by centrifugation, and the supernatant was collected for PCR amplification. After each selection round, we optimized the PCR cycle number required to amplify the libraries with Phusion High-Fidelity DNA polymerase, dNTP, FAM-labeled forward primer, and biotinylated reverse primer. The reverse strand of the amplified pool was captured using High Capacity Neutravidin Agarose Resin (Thermo Fisher). The forward single stranded DNA (ssDNA) was then denatured and eluted from the reverse strand using 200 mM sodium hydroxide. The eluted forward strand DNA was annealed at 1 µM after being solvent exchanged into wash buffer.[26]

2.2.5 Next generation sequencing (NGS) and sequence analysis

MiSeq System (Illumina) and MiSeq Reagent kit v2 (300 cycles) was used for NGS. The libraries were amplified using barcoded primers unique for each round of library (**Supplementary Table 2.2**). FASTAptamer v1.0.3 toolkit was used to analyze the FASTA files.[32] *FASTAptamer-count* was first used to identify top aptamers with high frequency (reads per million). *FASTAptamer-enrich* was then used to analyze the fold-enrichment of each unique sequences in adjacent rounds (later rounds over earlier rounds). MEME suite v5.2.0 Motif Discovery tool was used to predict binding motifs of round 8 top 50 aptamers base on their sequence similarities.[33] The top 50 aptamer sequences of round 8 was also used for phylogenic tree generation with FigTree toolkit v1.4.4 to map the similarities between each sequences.[34] The NUPACK web application was used to simulate aptamer structures when folded into their thermally stable secondary structures.[35]

2.2.6 Flow cytometry internalization assay and confocal imaging

The internalization of tJBA8.1 by Jurkat cells was evaluated by both flow cytometry assay as well as confocal imaging. In the flow cytometry assay, Jurkat cells were first stained with Zombie Violet dye for live cells identification. The cells were washed and spun down for aptamer staining. 100 nM Cy5-labled tJBA8.1 was diluted in binding buffer described in section 2.3. Aptamer staining took place at 4 ^{o}C for 30 minutes, followed by repeated washes. 0.25% trypsin or wash buffer with 1% BSA was then added to the cells for 5-minute incubation at 37 ^{o}C. After incubation, a 4-time trypsin volume of complete cell culture media was added to the cells to neutralize trypsin enzymatic activity. The cells were washed and fixed in wash buffer with 1% BSA and 0.2% PFA. The change in Cy5-tJBA8.1 binding on the Jurkat cell surface was evaluated on flow cytometer.

To visualize the cell compartments that tJBA8.1 binds to, Jurkat cells were stained with Cy5-lebled aptamers, FITC Phalloidin (Invitrogen), and DAPI (ThermoFisher) for confocal imaging. RANL aptamer was used as control. Prior to the staining steps, glass slides used for cell attachment were first coated with 10 µg/mL poly-D-lysine by incubating in a humidity chamber at 37 ^{o}C for 2 hours. To stain the cells, 5 million Jurkat cells were first labeled with 200 nM Cy5 aptamers in binding buffer at 4 ^{o}C for 30 minutes. Next, the cells were washed and resuspended in wash buffer to be transferred to the poly-D-lysine coated glass slides. After being set on the glass slides for 30 minutes at room temperature, the cells were settled and attached to the surface. The excess media was aspirated and replaced with 4% PFA. Fixation took place in room temperature for 10 minutes. After rinsing off the fixative, the cells were permeabilized using 0.1% Triton X-100 by 10 minutes incubation in room temperature, followed by washes. Next, FITC Phalloidin (1:100 dilution) and DAPI (300 nM) were applied to the fixed and permeated cells for 30-minute staining in room temperature. Lastly, the glass slides were mounted in polyvinyl acetate. The fluorescent images were taken using Leica SP8X confocal in the Keck Microscopy Center at the University of Washington, and were overlayed using Image J.

2.2.7 Target receptor pull-down and identification

About 85 million Jurkat cells (aptamer target cells) were used for each group. The membrane protein extraction and target purification process were modified from a previously

published method.[36] Jurkat cell pallets were first lysed with hypotonic buffer that was 10 mM Tris-HCl (pH 7.5) containing EDTA-free cOmplete Protease Inhibitor Cocktail (Roche) supplemented with 1 mM phenylmethylsulfonyl fluoride at 4 ^{o}C for 30 minutes. The cell membrane debris was washed 3 times with the same hypotonic buffer, followed by extraction with wash buffer containing 1% Triton X-100, and the same concentration of protease inhibitors. The extraction took place at 4 ^{o}C with constant rotation for 30 minutes, and 5 minutes brief sonication in ice water bath. We then used centrifugation to remove insoluble debris. The membrane extract was stored at -80 ^{o}C until next step.

Once proceeded, the extract was first "pre-cleared" with 100 nM biotin RANL incubation with 0.1 mg/ml tRNA as anionic blocker. The protein that are prone to non-specifically bind to DNA will be removed by incubating the biotin-RANL labeled protein extract with MyOne Streptavidin C1 Dynabeads (Thermo Fisher) on a magnetic rack. Along with 0.1 mg/ml salmon sperm DNA as background blocker, the "cleared" membrane protein solution was then incubated with either 100 nM biotin tJBA8.1 for 30 minutes followed by incubating with Streptavidin Dynabeads for 15 minutes, or with Streptavidin Dynabeads that was first saturated with 10x binding capacity of biotin. The Streptavidin Dynabeads were washed 5 times with cold wash buffer with 0.01% Triton X-100. The captured membrane protein was eluted in loading buffer by heating the beads at 47^{o}C for 15 minutes. The loading buffer is composed of 1x Laemmli sample buffer (containing SDS) supplemented with 4.6 M urea, 2.5% 2-mercaptoethanol, 10 mM EDTA, and 0.1% Triton X-100. After removing the Streptavidin Dynabeads from the supernatant, the protein extract was separated by electrophoresis on an 8% SDS-PAGE gel. The gel was stained with Colloidal Blue Staining Kit (Invitrogen). The excised band samples were digested, desalted, and subjected to tandem mass spectrometry (Orbitrap Elite). The data was analyzed with Proteome Discoverer 2.2 against Uniprot Human database at the Fred Hutchinson Cancer Research Proteomics Center.

2.2.8 siRNA knockdown study

Jurkat cells were nucleofected using Human T cell Nucleofector Kit (Lonza) with program settings X-001 following the manufacturer instruction. 30 pmol of TFRC1 (**Supplementary Table**

2.5) and NS siRNA (non-specific scrambled control) were used. After nucleofection, the cells were incubated for 22 hour and stained with Cy5 tJBA8.1 and FITC antihuman CD71 antibody. The aptamer staining and CD71 expression was evaluated with flow cytometry.

2.2.9 Bio-layer interferometry

Bio-layer interferometry studies were performed on the Sartorius Octet Red 96, using either streptavidin or Ni-NTA biosensing tips. The sensing tips were also purchased from Sartorius. The buffer used in these binding studies was 1% BSA, 0.1 mg/ml yeast tRNA, 0.1 mg/mL salmon sperm DNA, and 0.01% tween 20 in wash buffer. Depending on the assay orientation, the sensing tips were first loaded with biotinylated human TfR1, biotinylated aptamer, then immersed in wells containing various concentrations of aptamers for with 1000 r.p.m agitation for association. Next, the tips were transferred to wells containing only the buffer for dissociation with 1000 r.p.m agitation. Data analysis was done on the Octet Data Analysis 9.0 software.

2.2.10 Aptamer, recombinant protein and antibody competition studies

Jurkat or H9 cells were incubated with Cy5- or FAM-labeled aptamers at 25 nM with or without various fold-increased concentrations of competitor aptamers, FITC anti-human CD71 antibody or recombinant holo-transferrin proteins for 30 minutes at 4 ^{o}C. Cells were washed 2 times with wash buffer with 1% BSA and fixed in wash buffer with 1% BSA and 0.2% PFA. Changes in aptamer binding affected by the competitors was evaluated on flow cytometer.

2.2.11 Antibody and aptamer binding correlation study

To correlate the binding capacity of aptamers and antibodies base on fluorescent intensity, we used Cy5-labeled tJBA8.1 and XQ-2d at 25 nM, and FITC labeled anti-human TfR1 (CD71) antibody. The individual aptamers were co-incubated with the antibody in binding buffer

containing Jurkat cells for 30 minutes. The correlation of fluorescent intensity on single cells were measured using flow cytometry.

2.2.12 Western blotting

Western blotting was used to identify human TfR1 and HFE protein in the aptamer purified protein mixture. The aptamer targeted membrane proteins were first purified using the pull-down process described above with 100 nM biotinylated tJBA8.1 and XQ-2d. The purified protein solution was separated on 4-20% SDS-PAGE gel by applying 190V for 15 minutes and 220V until loading dye migrate close to the end of the gel. Protein bands on the gel were transferred to a PVDF membrane using 50V for 3 hours on ice. Background blocking was done by incubating the transferred PVDF membrane in TBST buffer (20mM Tris, 150mM NaCl, 0.1% tween 20 at pH 7.5) with 3% BSA at room temperature for 1 hour. Rabbit anti-human TfR1 (1:1000, D7G9X) and rabbit anti-human HFE (1:1000, EPR6750) were diluted in TBST 1% BSA and applied to separate PVDF membranes for overnight incubation at 4 ^{o}C with gentle shaking. After primary antibody incubation, the membranes were washed 3 times for 5 minutes with TBST. Secondary antibody, HRP anti-rabbit IgG (1:5000, A6154), was diluted with TBST 1% BSA for 1-hour incubation with the PVDF membranes at room temperature. The PVDF membranes were then washed 3 more times with TBST after incubation. To image the stained protein bands, SuperSignal West Pico PLUS kit (Thermo Fisher) was mixed at 1:1 to generate chemiluminescent signal on the HRP tagged protein. The membranes, while kept in the substrate, were imaged on Xenogen imager. Bright field photographs were taken using small binning, F-stop at 2, subject height set at 2.5 centimeter. The same settings were used on taking chemiluminescent images with 10-60 seconds of exposure.

2.2.13 Raji cell isolation

tJBA8.1-facilitated cell isolation was done on about 30 million Ficoll-enriched PBMCs per group mixed with cell tracker dye-stained Raji cells at different percentages. Raji cell membrane was stained by resuspending Raji cells in RPMI 1640 medium at 1 million cells per milliliter with

cell tracker dye, 1:200 diluted CM-Dil (Invitrogen). After incubated at room temperature for 30 minutes, the Raji cells were washed twice with wash buffer before being mixed with PBMCs. The mixed cells were first stained with 80 nM biotinylated tJBA8.1 in wash buffer with 0.5% BSA and 0.1 mg/ml yeast tRNA for 30 minutes. Meanwhile, 150 µL anti-biotin microbeads (Miltenyi) per group were blocked with the same buffer for 10 minutes to prevent non-specific interactions. Aptamer labeled cells were washed once and resuspended in the microbead-containing solution. After attaching the microbeads to the aptamer-labeled cells, the mixture was spun down and resuspend in wash buffer with 0.5% BSA and 0.1 mg/ml yeast tRNA.

Prior to column isolation process, the LS column (Miltenyi) was first anchored onto a separation magnet (Miltenyi) and washed once with cold wash buffer with 0.5% BSA and 0.1 mg/ml yeast tRNA. The cell mixture was then applied to the LS column, followed by washes with wash buffer and 0.5% BSA. To collect the cells that were captured in the column by tJBA8.1 targeting, we took the LS column off the magnet and flushed cells out by pushing buffer through the column with a plunger. The cell type compositions in each fraction and Raji cell depletion efficiencies were determined by antibody staining and flow cytometry.

2.2.14 Statistical analysis

Data are expressed as mean ± s.d., unless stated differently in the figure legends. Two-tailed *t*-test was used for hypothesis testing when comparing only two populations. ANOVA was used for hypothesis testing comparing more than two populations to each other. If comparisons could not be assumed independent from each population, Dunnett's, Šídák or Bonferroni correction were used to adjust the *P* values. After adjustment, difference in comparisons is considered significant if $P < 0.05$. Statistical tests were done using GraphPad Prism Software.

2.3 Results

2.3.1 Discovery of the Jurkat-Binding Aptamer 8.1 (JBA8.1) by Cell-SELEX

In an initial effort to identify aptamers that bind the human CD3 and CD28 T-cell receptors, we performed cell-SELEX using $CD3^+CD28^+$ Jurkat T-leukemia cells for positive selection and $CD3^-CD28^-$ J.RT3-T3.5 cells for negative/counter selection (**Figure 2.1A**). As the J.RT3-T3.5 cell line is a derivative mutant of the Jurkat cell line that was produced by ethyl methanesulfonate treatment and complement-activated negative selection via a CD3ε-specific OKT3 antibody,[37–39] we postulated that the shared lineage between the two cell lines would produce stringent selection and robust partitioning of desired aptamer binders. The single-stranded DNA (ssDNA) library used in cell-SELEX was comprised of a 45 bases random region flanked by two 18-bp constant regions designed for both PCR amplification between rounds and stem formation, amounting to 81 bp total. After an initial positive selection against Jurkat cells with a theoretical naive library consists of 10^{16} unique ssDNA sequences, seven additional rounds of sequential positive selection with Jurkat cells and negative selection with J.RT3-T3.5 cells were conducted with progressively increased stringency (**Supplementary Table 2.1**). Flow cytometry binding of aptamer pools from the individual SELEX rounds revealed substantial binding to both Jurkat and J.RT3-T3.5 cells starting in round 5 that plateaued by round 8 (**Figure 2.1B**). While preferential binding to Jurkat cells was observed in later rounds, it is important to acknowledge that differences in cell size and absolute number of receptors per cell may have biased binding to larger Jurkat cells. Nonetheless, we proceeded with next generation sequencing (NGS) of the ssDNA pools from all 8 rounds using the primers detailed in **Supplementary Table 2.2** to identify the enriched cell-binding aptamers.

FASTAptamer toolkit was used to analyze NGS results and calculate fold-enrichment of unique aptamer sequences over rounds of cell-SELEX.[32] Unique sequence reads were low for rounds 1-4, reflecting high aptamer pool diversity until rounds 5-8. These results are consistent with the cell-SELEX round binding results in **Figure 2.1B**, in which we observed aptamer pool binding to Jurkat cells starting in round 5. FigTree software and MEME analysis were used to generate phylogenetic trees and identify consensus motifs, respectively, for the top 50 aptamer sequences over rounds 5-8 (**Supplementary Figure 2.1**).[33,34] In round 5, top aptamer sequences were primarily characterized by one of three short motifs (Motifs 1, 2, and 3) with low individual sequence representation (<0.4%). Individual aptamer representation progressively increased in rounds 6 and 7, with top sequences representing as much as 6.3% and 10.6% of the pools, respectively. A new motif, Motif 4, also emerged during round 6 but later disappeared. By round 8, Motif 3 expanded to encompass the whole 45 bases random region and a new 40 bases motif,

Motif 5, emerged, with top aptamers belonging to each motif displaying robust tree clustering and thus high sequence similarity. Notably, the most prevalent aptamer in round 8, which belonged to Motif 3, represented 21.1% of the entire sequence pool. **Supplementary Table 2.3** lists the predicted motifs, sequences, and the round-by-round enrichment of the top 50 aptamers identified from round 8.

Nine Jurkat-binding aptamers from round 8 listed in **Supplementary Table 2.4** and named JBA8.X (where "X" is the aptamer's rank in **Supplementary Table 2.3**) were chosen for cell binding based on their representation, motif, and enrichment across rounds. None of the selected fluorescein-labeled aptamers displayed specific binding for Jurkat cells over J.RT3-T3.5 cells, indicating that the SELEX process did not enrich CD3- or CD28-binding aptamers (**Figure 2.1C**). Fluorescein-labeled JBA8.1 from Motif 3, JBA8.3, JBA8.7, and JBA8.11 from Motif 2, and JBA8.4 without a motif all displayed robust binding to both Jurkat and J.RT3-T3.5 cells compared to a random aptamer from the naïve library (RANL), with JBA8.1 distinguishing itself with greater than 2-fold higher binding than the other aptamers. JBA8.8 did not significantly bind to either cell line despite belonging to the 40 bases Motif 5, whereas JBA8.17 without a motif displayed preferential binding for J.RT3-T3.5 cells. Given these data, we speculate that our negative selection steps were ineffective due to improper refolding of eluted aptamers during the heat extraction step between positive selection and negative selection. Indeed, when we repeated the cell-SELEX process with negative selection preceding positive selection, which does not require heat extraction between selection steps, we do not observe non-specific binding of ssDNA pools to the negative selection J.RT3-T3.5 cells (data not shown). We next characterized and optimized the JBA8.1 aptamer due to its pronounced binding to Jurkat T-leukemia cells.

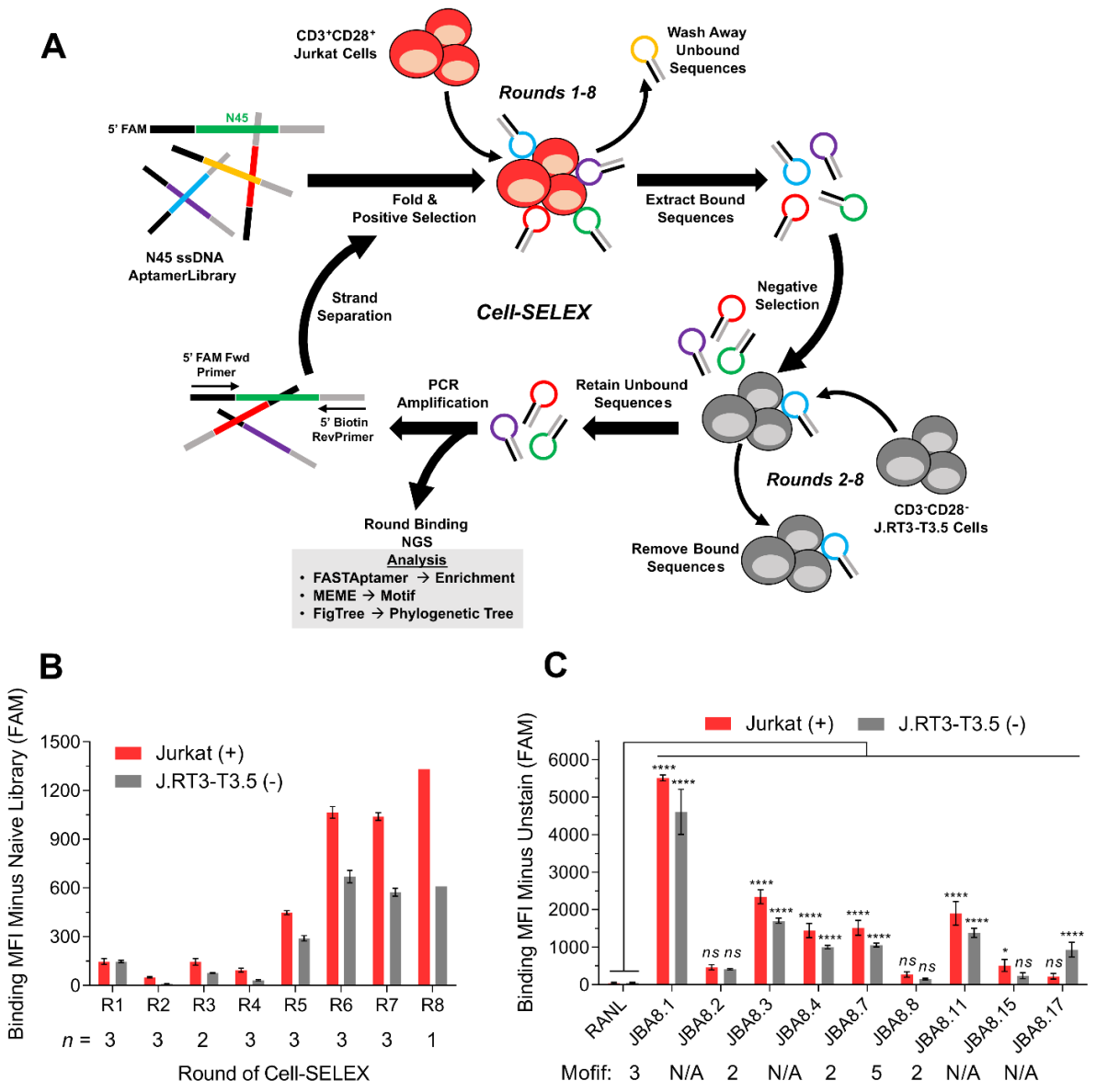

Figure 2.1. Cell-SELEX leads to the discovery of the JBA8.1 aptamer. (A) Schematic of cell-SELEX using $CD3^{+}CD28^{+}$ Jurkat cells for positive selection and $CD3^{-}CD28^{-}$ J.RT3-T3.5 cells for negative selection. (B) Binding median fluorescence intensity (MFI) of 250 nM aptamer pools from consecutive rounds of cell-SELEX to Jurkat cells and J.RT3-T3.5 cells by flow cytometry. Graph bars and error bars represent mean ± standard deviation; n = 1-3 technical replicates. Replicates vary due to some rounds having limited aptamer pool. (C) Binding MFI of 100 nM RANL and individual aptamers identified from round 8 of cell-SELEX to Jurkat cells and J.RT3-T3.5 cells by flow cytometry. Aptamers belonging to predicted motifs are indicated. Graph bars and error bars represent mean ± standard deviation; n = 3 independent experiments. ns > 0.05, *P < 0.05, ****P < 0.0001 (ordinary two-way ANOVA with Šídák correction). FAM, 6-carboxyfluorescein.

2.3.2. Truncation and Binding Affinity of the JBA8.1 Aptamer

The cost and time of oligo synthesis scales down linearly with sequence length and the resulting yield of full-length oligo exponentially decays with every additional base pair.[40] Therefore, aptamer truncation to a minimal functional sequence is imperative for downstream applications,[41,42] and secondary structure prediction algorithms can facilitate design of these truncations.[43] Using the NUPACK application to predict the minimum free energy (MFE) structure of JBA8.1,[35] we find that the structure of JBA8.1 conforms well to the intended library design, with the majority of the 45 bases Motif 3 forming a multi-hairpin structure that sits on top of a stem comprised of the partially complementary 18 bases flanking primer sequences (**Figure 2.2A**). While the stem may be important for maintaining the integrity of the Motif 3 hairpin structure, we speculated that it does not directly contribute to aptamer binding and thus could be shortened without compromising the binding affinity of the aptamer. Accordingly, we truncated the stem of tJBA8.1 sequence, removing 12 bases from the 5' constant region and all 18 bases from the 3' constant region, yielding the 51 bases long tJBA8.1 aptamer sequence (**Figure 2.2A** and **Supplementary Table 2.4**). Comparing the apparent binding affinity (K_D) of the full-length and truncated aptamer to Jurkat cells, we found that JBA8.1 has an apparent K_D of 5.5 ± 1.2 nM versus that of 10.9 ± 2.4 nM for tJBA8.1, suggesting that the truncation only has a minimal impact on target binding (**Figure 2.2B**). We thus chose the more cost-effective tJBA8.1 for further receptor identification, characterization, and application studies.

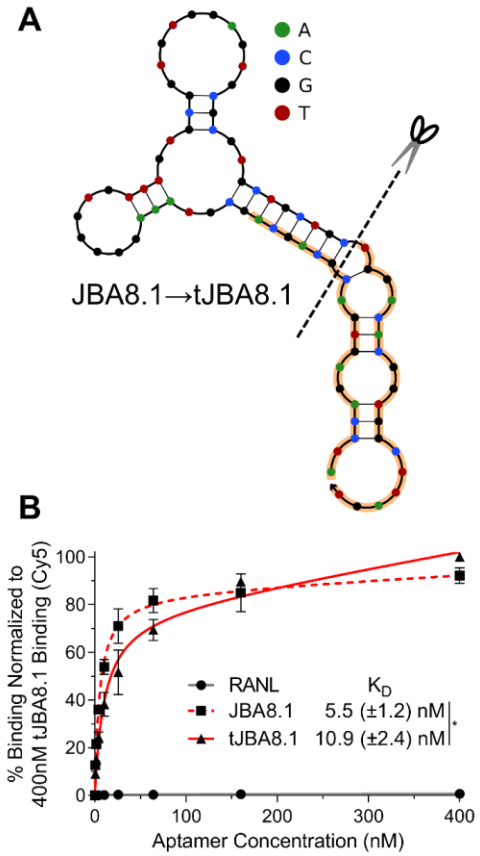

Figure 2.2. Stem truncation of JBA8.1 to tJBA8.1 minimally impacts binding affinity. (A) MFE secondary structures of JBA8.1 and its truncation (tJBA8.1), predicted using NUPACK (temperature = 4 °C; Na^+ = 137 mM; Mg^{2+} = 5.5 mM). The dashed line indicates the site of truncation, whereas the orange highlighting denotes the 18-bp flanking constant regions. (B) Flow cytometry binding curves of RANL, JBA8.1, and tJBA8.1 to Jurkat cells, normalized to 400 nM tJBA8.1 binding. The curves represent a nonlinear regression assuming one-site total binding. K_D values were calculated by averaging the individual regression values of the independent experiments. Data points and error bars, and K_D values, represent mean ± standard deviation; n = 3 independent experiments with technical duplicates. *P < 0.05 (two-sided unpaired t-test). Cy5, cyanine 5.

2.3.3. Identification and Validation of Transferrin Receptor 1 (TfR1) as a Target of tJBA8.1

To investigate the cellular compartment and type of molecule targeted by tJBA8.1, we labeled Jurkat cells with tJBA8.1 at 4 °C followed by enzymatic treatment with trypsin, a cell-impermeable serine endopeptidase that cleaves many extracellular proteins. tJBA8.1 binding was almost completely abolished after trypsin treatment (**Supplementary Figure 2.2A**), suggesting that the aptamer targets trypsin-sensitive cell membrane proteins. We further confirmed the

localization of tJBA8.1 binding on Jurkat cells by confocal microscopy, which primarily showed punctate staining of the cell membrane after incubation with tJBA8.1 at 4 °C (**Supplementary Figure 2.2B**).

Having demonstrated that tJBA8.1 binds to an extracellular membrane protein, we next adapted a reported aptamer-based pull-down assay designed for identification of target membrane receptors.[36] Briefly, cell membrane proteins extracted and solubilized from Jurkat cells were depleted for non-specific DNA-binding proteins using the RANL aptamer before incubation with biotinylated tJBA8.1. Aptamer-bound membrane proteins were then purified using streptavidin-coated magnetic beads and stratified by molecular weight via SDS-PAGE. Compared to a control sample that was purified with biotin-saturated streptavidin beads without tJBA8.1, we observed two distinct protein bands that were highly enriched by tJBA8.1 at approximately 200 kDa (band a) and 100 kDa (band b) (**Figure 2.3A**). The protein bands were extracted, digested, analyzed by mass spectrometry, and matched to the human transferrin receptor protein 1 (TfR1; also known as CD71) (**Figure 2.3B**). Specifically, peptides extracted from the higher molecular weight band (a) covered 62% of the TfR1 amino acid sequence, whereas the lower molecular weight band (b) covered 58%. The presence of two bands is consistent with the structure of TfR1, which is a homodimer composed of two disulfide-linked monomers.[44] TfR1 is a type II transmembrane glycoprotein that regulates the uptake of transferrin-bound iron needed for cellular metabolism and proliferation.[45] TfR1 is thus ubiquitously expressed at low levels on many cell types, with elevated expression on rapidly dividing cells such as activated lymphocytes and cancer cells including Jurkat cells.[46–48]

To validate that tJBA8.1 binds TfR1, we used short interfering RNA (siRNA) duplexes (**Supplementary Table 2.5**) to knockdown the expression of TfR1 encoded by the *TFRC* gene in Jurkat cells and evaluated aptamer binding. Compared to cells that were nucleofected with non-specific (NS) siRNA, cells nucleofected with TFRC siRNA had 51% reduced TfR1 expression as evaluated by anti-CD71 antibody (CD71 Ab) staining, which matched closely with the observed 49% reduction in tJBA8.1 binding (**Figure 2.3C**). We also evaluated TfR1 expression on the positive selection Jurkat cells and negative selection J.RT3-T3.5 cells used in cell-SELEX by CD71 Ab staining. In agreement with the binding profiles of the cell-SELEX aptamer pools and the individual JBA8.1 aptamer (**Figure 2.1B, C**), both cell lines robustly express TfR1

(**Supplementary Figure 2.3A**), with Jurkat cells having higher expression than J.RT3-T3.5 cells (**Supplementary Figure 2.3B**). Lastly, as TfR1 is expressed negligibly on resting T cells but is upregulated upon antigen and cytokine stimulation,[47,49] we evaluated tJBA8.1 binding to unactivated and day 3 CD3/CD28 Dynabead-activated $CD4^+$ and $CD8^+$ T cells. For both subsets, tJBA8.1 binding was low to unactivated T cells but greatly increased after Dynabead activation (**Supplementary Figure 2.4A**). Furthermore, when tracking JBA8.1 binding and TfR1 expression by CD71 Ab staining on $CD4^+$ and $CD8^+$ T cells over 7 days of Dynabead activation, we found that JBA8.1 binding kinetics correlated strongly with that of TfR1 expression (**Supplementary Figure 2.4B**). Collectively, these results confirm that TfR1 is a binding target of JBA8.1 and tJBA8.1.

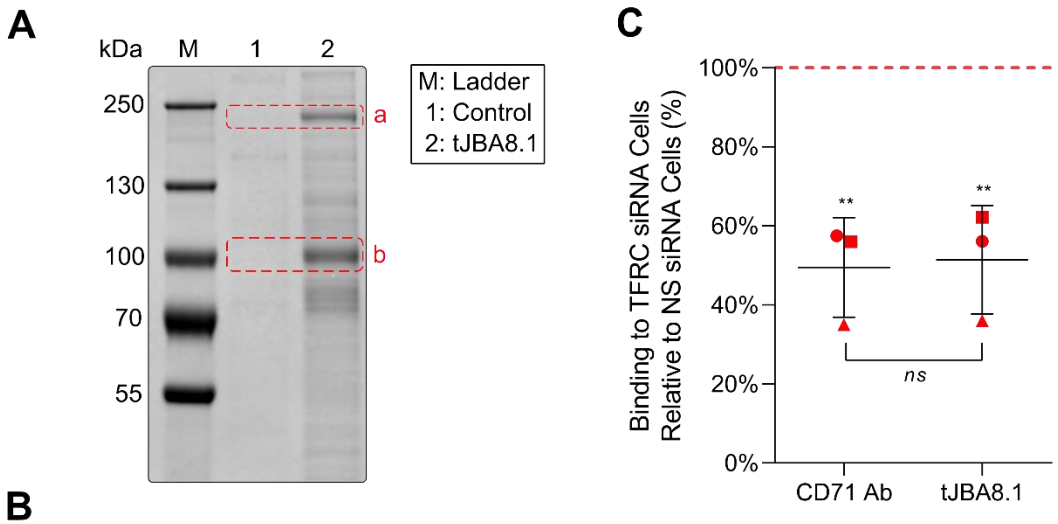

B

Band	Description	Lane 1: Peptide Coverage (Control)	Lane 2: Peptide Coverage (tJBA8.1)	Lane 1: # of Peptides (Control)	Lane 2: # of Peptides (tJBA8.1)
a	Transferrin receptor protein 1	9%	62%	4	52
b	Transferrin receptor protein 1	13%	58%	5	50

Figure 2.3. TfR1 is identified as the target of tJBA8.1. (A) Colloidal blue-stained 8% SDS-PAGE gel of Jurkat cell membrane proteins pulled down by tJBA8.1. The control lane represents proteins captured by biotin-saturated magnetic beads only. Bands a and b (dashed red boxes) from both lanes were excised for mass spectrometry analysis. (B) Summary of the protein with the highest peptide coverage and number of peptides identified in each excised band by mass spectrometry. (C) Flow cytometry analysis of FITC-labeled CD71 Ab and 25 nM Cy5-labeled tJBA8.1 binding to Jurkat cells 24 h after nucleofection with TFRC siRNA duplexes. Red, dashed horizontal line represents binding to non-specific (NS) siRNA-treated controls to which the TFRC siRNA data points were normalized. Horizontal lines and error bars represent mean ± standard deviation; n = 3 independent experiments. **P < 0.01 (significance between ligand staining on TFRC siRNA- and NS siRNA-treated cells; one-way ANOVA with Bonferroni correction). ns > 0.05

(significance between the relative CD71 Ab and tJBA8.1 staining in pairwise experiments; two-sided paired t-test). Cy5, cyanine 5; FITC, fluorescein isothiocyanate.

2.3.4. Characterization of tJBA Binding to TfR1 and Competition with Other Ligands

To better elucidate the interaction between tJBA8.1 and TfR1, we co-stained Jurkat cells with CD71 Ab (clone CY1G4) and tJBA8.1. We observed a striking positive correlation between CD71 Ab and tJBA8.1 staining, demonstrating that tJBA8.1 can bind TfR1 on cells simultaneously with the CD71 Ab (**Figure 2.4A**). As binding to cells probes steady-state behavior but not binding in real-time, we next used biolayer interferometry (BLI) to directly characterize the kinetics of tJBA8.1 binding to TfR1. We immobilized recombinant biotinylated TfR1 protein onto streptavidin BLI biosensors to avoid avidity effects from homodimeric TfR1 protein that may occur if the aptamers were immobilized instead. tJBA8.1 bound the protein with a K_D value of 25.11 ± 0.19 nM (**Figure 2.4B**), demonstrating fast and high-affinity binding kinetics (**Supplementary Table 2.6**). We also evaluated binding of His-tagged mouse recombinant TfR1 protein to immobilized tJBA8.1 by BLI, but results were negative despite positive control antibody binding, suggesting that tJBA8.1 does not target mouse TfR1 (**Supplementary Figure 2.5A and B**).

Iron is delivered intracellularly to cells via a transferrin cycle. Specifically, iron-bound transferrin (holo-Tf) binds to TfR1 for uptake, after which iron is released from transferrin under acidic endosomal pH and the resulting iron-free transferrin (apo-Tf) is recycled to the cell surface for dissociation under neutral pH.[50] As we demonstrated in **Figure 2.4A** tJBA8.1 can stain cells simultaneously with CD71 Ab (clone CY1G4), which has been previously shown to bind a TfR1 epitope distinct from that of holo-Tf,[51] we hypothesized that tJBA8.1 may compete with holo-Tf for binding to TfR1. To test this, we co-incubated Jurkat cells with a fixed concentration of labeled tJBA8.1 and varying concentrations of holo-Tf as a competitor. tJBA8.1 binding was reduced by half upon competition with just 1-fold excess of holo-Tf, confirming that tJBA8.1 and holo-Tf share proximal binding sites on TfR1 (**Figure 2.4C**). However, relative tJBA8.1 binding plateaued at 50% and did not further decrease even when holo-Tf was added at 32-fold excess, suggesting that tJBA8.1 has a transferrin- or TfR1-independent binding component to Jurkat cells. We also

conducted a similar competition assay with tJBA8.1 and the CD71 Ab (clone CY1G4) discussed previously. Compared to an anti-CD3 antibody control (CD3 Ab), the CD71 Ab did not compete off tJBA8.1 binding to Jurkat cells (**Figure 2.4D**), confirming that tJBA8.1 and the CD71 Ab (clone CY1G4) do not share an overlapping binding epitope on TfR1.

XQ-2d is a 56 bases long truncated aptamer previously discovered by the Tan group that also targets TfR1.[30,31] Aligning the variable sequence regions of tJBA8.1 and XQ-2d, we observed sequence similarity between tJBA8.1 and XQ-2d, with 21 nucleotides overlapping in their respective 45 bases and 42 bases random regions (**Supplementary Figure 2.6A**). The overlapping nucleotides are mostly found within predicted hairpin structures of each aptamer, and four of them (G17, G36, T38, and G39 in XQ-2d) were previously predicted by molecular dynamics simulations to participate in a hydrogen bond network that drives the interaction between XQ-2d and TfR1 and produces a steric clash with holo-Tf.[31] To validate the reported TfR1-binding properties of XQ-2d and compare them to tJBA8.1, we conducted the same characterization assays as we showed previously for tJBA8.1. Using flow cytometry, we observed positive correlation between CD71 Ab and XQ2d staining on Jurkat cells (**Supplementary Figure 2.6B**), and XQ-2d was found to bind Jurkat cells with an apparent K_D of 2.2 ± 0.6 nM (**Supplementary Figure 2.6C**). Compared to XQ-2d, tJBA8.1 produced a substantially higher binding signal to Jurkat cells that did not fully saturate at 400 nM, further demonstrating that tJBA8.1 may bind an additional protein expressed by Jurkat cells with lower affinity. By BLI, XQ-2d bound immobilized TfR1 with a K_D value of 14.45 ± 0.15 nM (**Supplementary Figure 2.6D**), displaying both slower association and dissociation than tJBA8.1 (**Supplementary Table 2.6**). Similar to tJBA8.1, XQ-2d binding was competed off by holo-Tf but not CD71 Ab (clone CY1G4) (**Supplementary Figure 2.6E and F**), although XQ-2d binding was more completely depleted by holo-Tf competition compared to tJBA8.1.

Given the discrepancies between tJBA8.1 and XQ-2d binding to Jurkat cells, we also evaluated holo-Tf competition with these aptamers on H9 T-lymphoma cells, which have higher TfR1 expression than Jurkat cells and exhibit more equivalent max binding signal between tJBA8.1 and XQ-2d (**Supplementary Figure 2.7A and B**). Unexpectedly, holo-Tf equivalently competed off over 90% of both tJBA8.1 and XQ-2d binding in this cell model (**Supplementary Figure 2.7C**), indicating either that H9 cells lack expression of the unidentified protein that

tJBA8.1 binds independent of TfR1 or that the higher TfR1 expression on H9 cells causes TfR1-dependent binding to overshadow TfR1-independent binding. We next tested competitive binding between tJBA8.1 and XQ-2d on Jurkat and H9 cells relative to a RANL control. We observed concentration-dependent reduction in tJBA8.1 binding with XQ-2d as a competitor, verifying that tJBA8.1 and XQ-2d do target a common epitope on TfR1 (**Supplementary Figure 2.8**). Furthermore, in agreement with the above holo-Tf competition results, only half of tJBA8.1 binding was competed off by high fold excess of XQ-2d on Jurkat cells whereas over 90% was competed off on H9 cells under the same conditions.

Besides holo-Tf, TfR1 has other natural ligands that may share binding epitopes with tJBA8.1 and XQ-2d. HFE is a major histocompatibility complex (MHC) class I-like membrane protein that is known to compete with holo-Tf at its TfR1-binding site to regulate iron uptake,[52–55] and mutation of HFE can cause iron overload that resembles hereditary hemochromatosis via hepatic hepcidin deficiency.[56–58] To ascertain whether tJBA8.1 and XQ-2d differentially bind TfR1 with respect to HFE, we performed the same membrane protein pull-down assay as before but also included western blotting to examine HFE co-precipitation, if any, with aptamer-enriched TfR1. Bands with the characteristic sizes of TfR1 were highly enriched by both tJBA8.1 and XQ-2d (**Supplementary Figure 2.9A**, bands a-c), and western blotting confirmed the presence of TfR1 in these bands (**Supplementary Figure 2.9B**). Of importance, XQ-2d uniquely enriched two protein bands, one at 35 kDa and the other slightly larger (**Supplementary Figure 2.9A**, bands d and e), and western blotting discovered the corresponding enrichment of HFE (~40 kDa) at these molecular weights (**Supplementary Figure 2.9C**). This indicates that XQ-2d co-precipitates HFE with TfR1 whereas tJBA8.1 does not, bringing attention to differences in each aptamer's interaction with TfR1. Band f, which was uniquely enriched by tJBA8.1 and may represent the other protein that tJBA8.1 binds independent of TfR1 on Jurkat cells, will be discussed in a later section. Altogether, these results demonstrate that tJBA8.1 and XQ-2d have overlapping but distinct binding sites on TfR1.

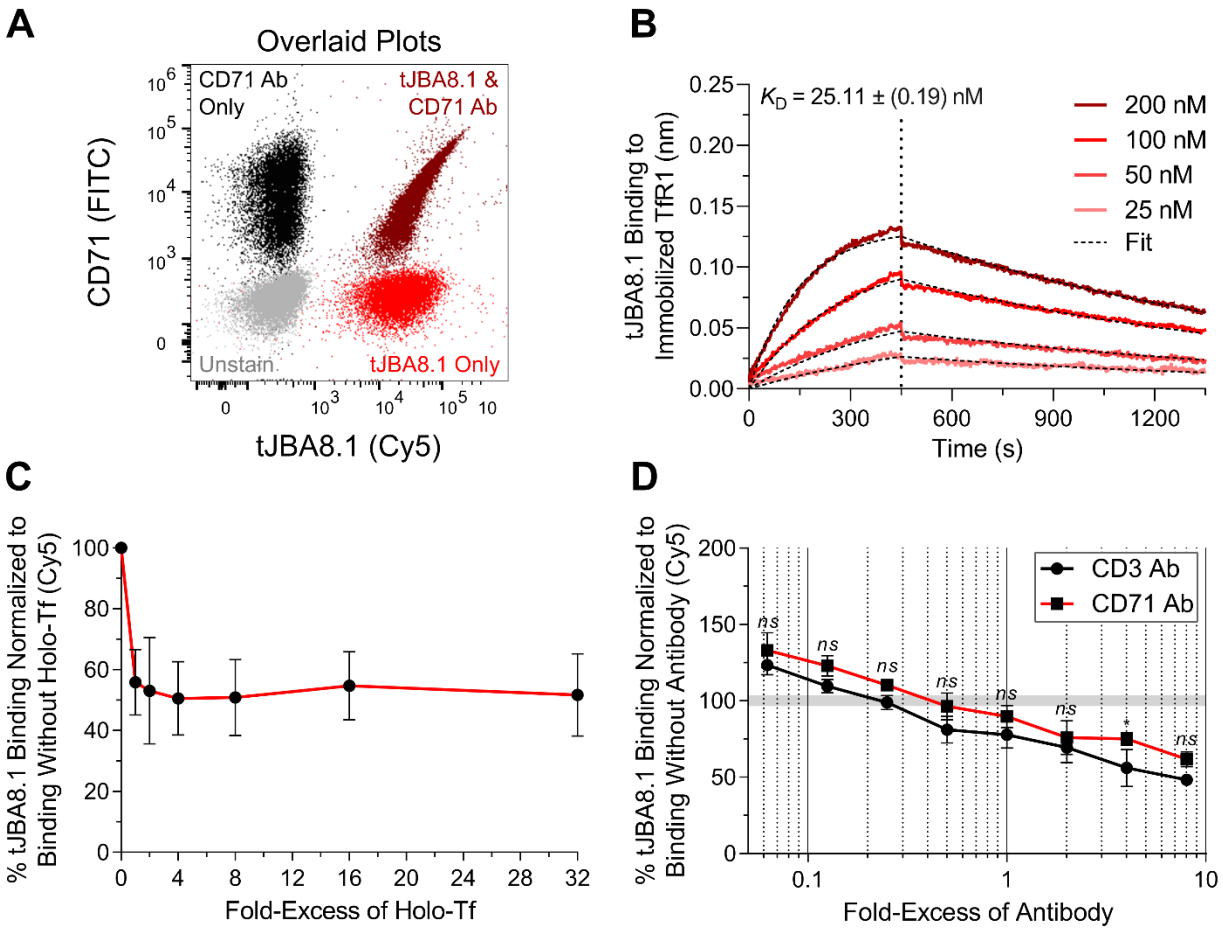

Figure 2.4. tJBA8.1 competes with holo-Tf for binding to TfR1. (A) Overlaid flow cytometry plots of unstained (grey), FITC-labeled CD71 Ab single-stained (black), 25 nM Cy5-labeled tJBA8.1 single-stained (red), and antibody and aptamer co-stained (dark red) Jurkat cells. Plots are representative of n = 2 independent experiments. (B) Association and dissociation kinetics of serially diluted FAM-labeled tJBA8.1 binding to biotinylated TfR1 immobilized on streptavidin biosensors by BLI. The association phase is illustrated from 0-450 s, whereas dissociation is shown from 450-1350 s (separated by the vertical dotted line). K_D values were calculated by performing a global fit of the multi-concentration kinetic data to a 1:1 binding model. K_D values represent mean ± standard deviation; n = 4 individual concentrations of aptamers. (C and D) Competitive binding of 25 nM Cy5-labeled tJBA8.1 with varying fold-excess of holo-Tf (C) and CD3 or CD71 Ab (D) to Jurkat cells by flow cytometry. Binding was normalized to aptamer-stained controls without holo-Tf or antibody. Data points and error bars represent mean ± standard deviation; n = 3 independent experiments. ns > 0.05, *P < 0.05 (ordinary two-way ANOVA with Šídák correction). FITC, fluorescein isothiocyanate; Cy5, cyanine 5; FAM, 6-carboxyfluorescein.

2.3.5. tJBA8.1-Mediated Depletion of B-Lymphoma Cells from PBMCs

Because TfR1 is overexpressed in many cancer types including leukemias (both lymphocytic and myeloid),[59–62] lymphomas,[63–65] and myelomas,[48] and the level of TfR1 expression marks the proliferative potential of these malignant cells,[66] we recognized that tJBA8.1 might be utilized as a malignant cell depletion agent in CAR T-cell manufacturing. Specifically, malignant cell contamination in patient PBMC products used for CAR T-cell production can be detrimental to therapy outcomes,[15,16] and a selective and universal approach for removing these circulating cancerous cells has remained elusive. We therefore developed a MACS-based approach combining biotinylated tJBA8.1 and Anti-Biotin Microbeads (Miltenyi Biotec) for selective depletion of cancerous cells from PBMCs (**Figure 2.5A**, top). We used immortalized Raji B-lymphoma cells, which robustly express TfR1 unlike healthy PBMCs that have near-background expression (**Supplementary Figure 2.10A and B**), to mimic cancers currently treated by FDA-approved CD19-directed CAR T-cell therapies. Raji cells were pre-labeled with a CM-Dil membrane dye for tracking purposes (**Supplementary Figure 2.11A**) and subsequently spiked into healthy PBMCs at low (~0.1%), medium (~1%), and high (~10%) percentages to reproduce circulating malignant cell heterogeneity found in patient leukapheresis populations.[67] The mixed cells were incubated with biotinylated tJBA8.1 and beads followed by magnetic separation on a column, and the pre-sort, depleted, and flow through fractions were analyzed by flow cytometry to detect CM-Dil$^+$ Raji cells (**Figure 2.5B** and **Supplementary Figure 2.11B and C**). Whereas pre-sort cells had on average 0.090%, 0.930%, or 10.040% CM-Dil$^+$ cells across three PBMC donors, flow through cells had only 0.016%, 0.118%, and 1.250% CM-Dil$^+$ cells on average, respectively (**Figure 2.5C**). Compared to un-spiked PBMC controls (0.011% CM-Dil$^+$), these flow through values were not statistically different, illustrating the effectiveness of tJBA8.1-mediated depletion of TfR1$^+$ cancer cells from normal PBMCs. Analyzing the depleted fractions, we observed enrichment of CM-Dil$^+$ Raji cells, as expected, although their purity scaled with the amount of spike cells and never peaked past 60% (**Figure 2.5C**). As this indicates some CM-Dil$^-$ PBMCs were depleted as well, we further examined the percentages of immune cells in the CM-Dil$^-$ pre-sort and flow through fractions to determine if the PBMC composition was being impacted by the depletion process. There were no significant changes in the percentages of CD19$^+$ B cells, CD14$^+$ monocytes, CD56$^+$ NK cells, and CD3$^+$ T cells between the pre-sort and flow through fractions (**Figure 2.5D, Supplementary Figure 2.12A and B**), suggesting that loss of CM-Dil$^-$ PBMCs in the depleted fraction was low and likely non-specific. Taken together, these data demonstrate

proof-of-concept removal of TfR1^{+} malignant cells from PBMCs using tJBA8.1, yielding healthy and uncompromised cell product that can be used in downstream CAR T-cell manufacturing with improved safety.

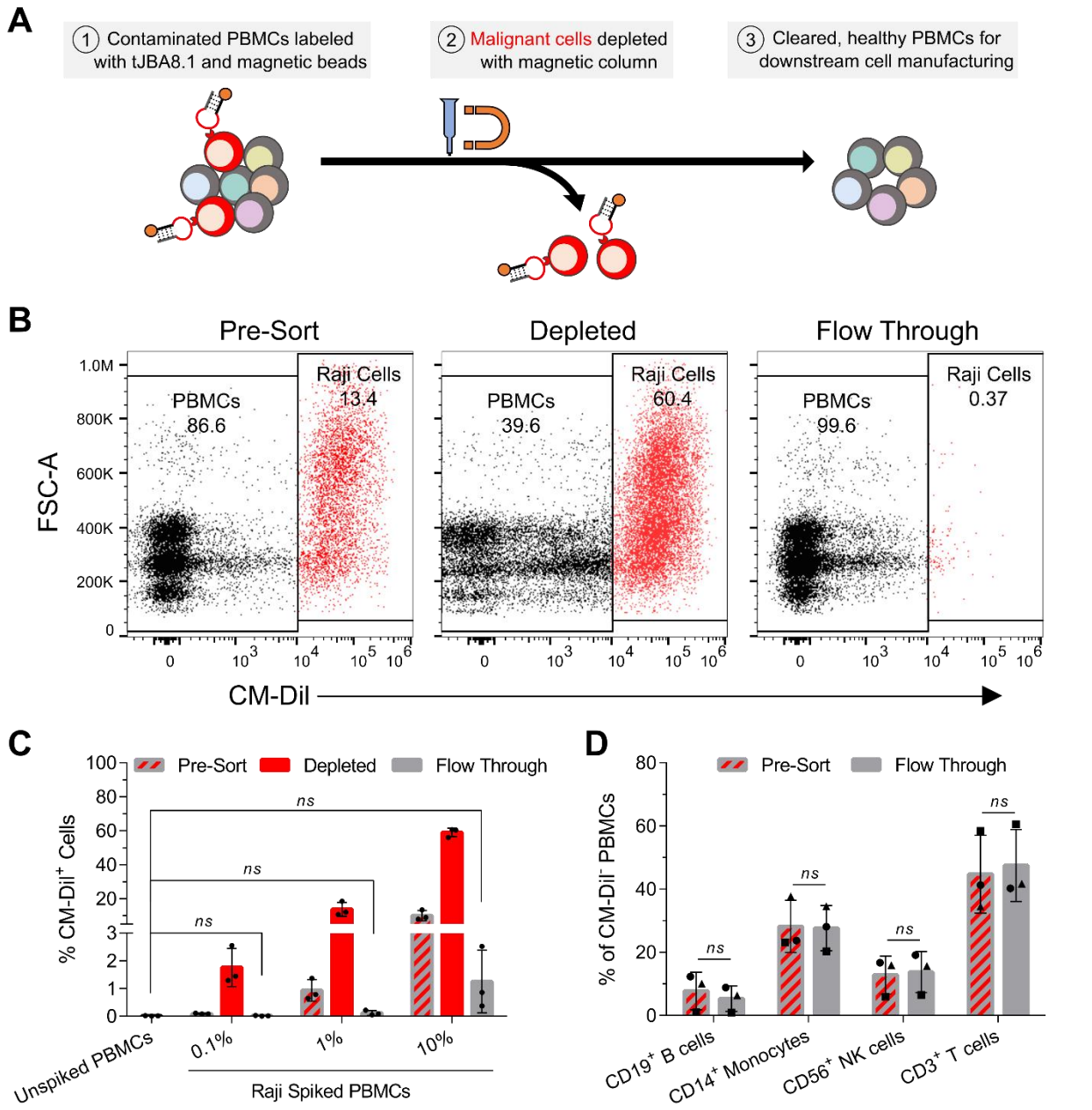

Figure 2.5. tJBA8.1 thoroughly depletes Raji B-lymphoma cells from PBMCs without compromising healthy immune cell composition. (A) Schematic of malignant cell depletion from PBMCs using tJBA8.1-mediated MACS. (B) Flow cytometry plots of CM-DiI^{+} Raji cell depletion from high (10%) Raji spiked PBMCs. The different cell fractions from the depletion process are shown. Plots for low (0.1%) and medium (1%) Raji spiked PBMCs can be found in Supplementary Figure 2.11B and C. Plots are representative of n = 3 independent experiments with different

PBMC donors. (C) Flow cytometry analysis of the percentage of CM-Dil$^+$ Raji cells in each cell fraction of the depletion process using low (0.1%), medium (1%), and high (10%) Raji spiked PBMCs. Unspiked PBMCs were included as a benchmark of complete depletion. Graph bars and error bars represent mean ± standard deviation; n = 3 independent experiments with different PBMC donors. ns > 0.05 (ordinary one-way ANOVA with Dunnett's correction). (D) Flow cytometry analysis of the healthy immune cell composition within CM-Dil$^-$ PBMCs before (pre-sort) and after (flow through) Raji depletion from high (10%) Raji spiked PBMCs. Analysis for low (0.1%) and medium (1%) Raji spiked PBMCs can be found in Supplementary Figure 2.12A,B. The circles, squares and triangles represent different PBMC donors from separate depletion studies. Graph bars and error bars represent mean ± standard deviation; n = 3 independent experiments with different PBMC donors. ns > 0.05 (paired two-way ANOVA with Šídák correction). CM-Dil, chloromethylbenzamido-1,1'-dioctadecyl-3,3,3',3'-tetramethylindocarbocyanine perchlorate.

2.3.6. Elucidation of TfR1-Independent tJBA8.1 Binding and Affinity Optimization

The previous binding and competition results with tJBA8.1 on Jurkat cells support the hypothesis that tJBA8.1 has a TfR1-independent binding component. Given that tJBA8.1 captured some PBMCs in our depletion studies, we speculated that tJBA8.1 may bind a subpopulation of PBMCs via the same TfR1-independent mechanism. To test this and better understand the nucleotides that contribute to this interaction, we revisited the individual full-length aptamers identified from cell-SELEX in **Figure 2.1C** and compared their ability to bind PBMCs. We also co-stained with a CD3 Ab to distinguish binding to CD3$^+$ T cells and other CD3$^-$ PBMCs (B cells, monocytes, etc.). While none of the aptamers bound CD3$^+$ T cells, four of them (JBA8.1, JBA8.3, JBA8.11, and JBA8.15) displayed high binding to CD3$^-$ PBMCs relative to the RANL control, with JBA8.1 having the highest binding (**Supplementary Figure 2.13A**). Using JBA8.1 and a broader antibody panel for co-staining, we found that CD14$^+$ monocytes and CD19$^+$ B cells comprised the majority of aptamer bound CD3$^-$ PBMCs (**Supplementary Figure 2.13B**). Comparing the sequences of all the individual aptamers tested, we identified a motif of five consecutive guanine bases (GGGGG or G-quintet) that was specific to JBA8.1, JBA8.3, JBA8.11, and JBA8.15 (**Supplementary Figure 2.13C**). Interestingly, only the G-quintet motif of JBA8.1 was predicted to be single-stranded, whereas the G-quintet motifs of the other three aptamers were predicted to be partially or fully double-stranded (**Supplementary Figure 2.13D**). These results establish a potential molecular and structural basis for the TfR1-independent binding of tJBA8.1.

Next, we revisited the NGS results to identify alternative Motif 3 aptamers that could have improved affinity for TfR1, which would allow us to lower the concentration of aptamer needed for effective cancer cell depletion and thereby minimize TfR1-indpendent binding. Besides JBA8.1, there were three other aptamers belonging to Motif 3 in the top 50 sequences of the round 8 cell-SELEX pool, namely JBA8.10, JBA8.26, and JBA8.45 (**Supplementary Table 2.3**). Notably, all three aptamers were single-point variants of JBA8.1 that displayed approximately 20-fold enrichment in round 8, which was significantly greater than the 6.9-fold round 8 enrichment for JBA8.1. We selected JBA8.26 for further characterization given that it had the highest fold enrichment of the three aptamers. Analyzing the predicted MFE secondary structure of JBA8.26, we noticed that JBA8.26 has an extended stem region compared to JBA8.1, owing to a T→C mutation that induces complementary base pairing (**Supplementary Figure 2.14A**). Interestingly, this base pairing contracts the central hairpin of the aptamer and increases the distance between the two outbranching hairpins. We theorized that these predicted changes would increase the structural stability of JBA8.26 relative to JBA8.1 and alter its binding interaction with TfR1, elevating its affinity. Confirming this, JBA8.26 bound H9 cells with an apparent K_D of 3.3 ± 0.6 nM, which was comparable to that of XQ-2d (2.2 ± 0.2 nM) and a near 8-fold improvement compared to tJBA8.1 (25.6 ± 13.0 nM) (**Supplementary Figure 2.14B**). Using BLI, JBA8.26 was found to bind immobilized TfR1 with a K_D of 6.87 ± 0.04 nM (**Supplementary Figure 2.14C**), which was the highest affinity observed amongst the aptamers we tested. Specifically, JBA8.26 bound TfR1 with a 2- to 3-fold faster association rate than those of tJBA8.1 and XQ-2d and a dissociation rate nearly 2-fold slower than that of tJBA8.1 (**Supplementary Table 2.6**). Given these upgraded TfR1-binding kinetics, we predict that JBA8.26 and its future truncations will increase the partitioning efficiency of our cancer cell depletion strategy.

2.4 Discussion

As expensive, living drugs that often serve as the final barrier between severely ill cancer patients and terminal disease, CAR T cells require stringent manufacturing to maximize their safety and efficacy. Autologous T-cell isolation is the first crucial step in the manufacturing of CAR T cells, and the composition of these isolated cells can heavily dictate successful therapy formulation and patient outcomes. Surprisingly, there is no standardized procedure for isolating T

cells in clinical CAR T-cell manufacturing. Some companies use elutriation to enrich lymphocytes from patient leukapheresis products based on size and density.[10,12,76] While cost-effective, this approach is unable to discriminate healthy T cells from cancerous B and T lymphocytes, allowing malignant cells to contaminate and exhaust CAR T cells in-production prior to patient infusion.[15] In rare cases, these malignant cells can even be transduced to express the CAR, inadvertently creating a cancer resistant to therapy.[16] To minimize contaminating cells, other companies use immunomagnetic approaches to isolate T cells. However, these strategies are costly, requiring biologically produced antibodies and Fabs, and these labeling reagents often remain bound to T cells after isolation. Furthermore, they do not distinguish between healthy and neoplastic T cells, making autologous CAR T-cell production challenging for patients with T-cell malignancies.[20,21] Accordingly, an inexpensive approach that actively removes cancerous cells from patient PBMCs while leaving healthy T cells untouched would be of high value to CAR T-cell manufacturing and safety.

DNA aptamers are well-suited to address this unmet manufacturing need. As low-cost, synthetic ligands generated by SELEX, aptamers can be selected for affinity-based recognition and capture of specific cell types. Demonstrating this, our lab has previously discovered DNA aptamers that selectively bind $CD8^+$ T cells and $CD14^+$ monocytes within PBMCs, and we showed that the former aptamer could robustly isolate pure $CD8^+$ T cells for downstream production of CAR T cells.[25,29] Here, we expand this work and report the discovery of a nanomolar-affinity DNA aptamer, named tJBA8.1, that binds the iron importer TfR1 overexpressed by cancer cells but not expressed by healthy PBMCs. In proof-of-concept MACS-based depletion studies, tJBA8.1 was capable of efficiently removing Raji B-lymphoma cells spiked into PBMCs at various concentrations, yielding uncontaminated, label-free PBMCs. Importantly, the composition of healthy immune cells was unaltered by the depletion steps, showing the precise partitioning afforded by tJBA8.1. This work provides a straightforward, cost-effective approach for selectively removing malignant cells before CAR T-cell production, enabling safer and more reproducible manufacturing of this precious therapy.

Comprehensive validation and characterization of aptamer binding to their cognate receptors is a necessary step to their widespread recognition and use. For tJBA8.1, we conducted many assays to both validate its binding to TfR1 and further understand its binding site on the

receptor, especially within the context of other TfR1 ligands. Notably, tJBA8.1 binding to $TfR1^+$ cells was competed off by both iron-bearing transferrin and another TfR1-binding aptamer described in the literature, XQ-2d,[30,31] indicating that tJBA8.1 shares overlapping binding epitopes on TfR1 with these ligands. Intriguingly, in pull-down assays using cell membrane proteins, tJBA8.1 failed to co-precipitate HFE, another natural TfR1 ligand that is co-expressed on the cell surface, while XQ-2d could. This establishes a key difference in TfR1 binding between tJBA8.1 and XQ-2d, hinting that their binding interfaces spread over multiple regions on the receptor, some of which overlap between the two aptamers while others are unique. Indeed, molecular dynamics simulations predicted that XQ-2d binds to TfR1 at two regions,[31] and only the nucleotides involved in binding to one region overlap strongly with the tJBA8.1 sequence. However, as these are deductions from circumstantial evidence and predictive models, x-ray crystallography or cryogenic electron microscopy will be key to defining the interaction of tJBA8.1 and XQ-2d with TfR1.[77–79] Evaluating aptamer binding to transferrin receptor 2 (TfR2), a hepatic-localized homolog of TfR1 that shares 66% similarity in its ectodomain with TfR1, may also shed light on binding differences between tJBA8.1 and XQ-2d.[80]

Although this aptamer-based depletion system has shown promise, it is important to acknowledge that our studies were conducted on immortalized cancer cell lines and healthy donor PBMCs, which is an idealized model compared to real-world patient samples that have gone through multiple lines of therapy. TfR1 expression on patient-derived malignant cells is likely not as robust as it is on *ex vivo* cultured cancer cells, and expression will vary with cancer type, disease stage, and patient history. Validating that tJBA8.1 binds to malignant cells within an array of patient samples will thus be imperative to this system's translation, and the aptamer affinity improvements detailed at the end of this study (JBA8.26) will be important for increasing the depletion system's sensitivity to lower levels of TfR1 expression. Also unexplored in this study is the effect of malignant cell depletion on CAR T-cell differentiation, exhaustion, and expansion during manufacturing. Early expression of differentiation and exhaustion markers on CAR T cells prior to patient infusion is associated with remission induction failure,[82] and poor CAR T-cell expansion can prevent reaching target doses needed for therapy.[83] Removing malignant cell contamination prior to CAR T-cell manufacturing should theoretically prevent uncontrolled differentiation and exhaustion of CAR T cells *ex vivo* and thus improve their expansion, but further testing will be needed to verify these claims.

While we used B-lymphoma cells in our depletion studies to mimic cancers currently treated by commercial CAR T-cell therapies, we anticipate the depletion strategy described here will have a greater impact on the treatment of T-cell malignancies. Presently, autologous CAR T-cell manufacturing for treating T-cell leukemias and lymphomas is impractical since malignant T cells are often found in the peripheral blood of patients with these diseases and immunoaffinity purification approaches that target common T-cell antigens are unable to distinguish normal T cells from these malignant T cells.[84–86] To circumvent these challenges, CAR NK cells or allogeneic CAR T cells can be used for treatment,[87,88] but the former is difficult to manufacture at a clinical scale whereas the latter requires gene editing to prevent fatal graft-versus-host-disease and likely has limited persistence due to host-versus-graft effects. For these reasons, CAR T-cell manufacturing for T-cell malignancies would serve to benefit the most from the depletion strategy developed here, as it would allow selective harvesting of healthy autologous T cells that are otherwise unattainable. Furthermore, as T-lineage leukemias and lymphomas have been shown to have greater TfR1 expression and positivity than B-lineage counterparts,[60,62,65] these cancers should be especially amenable to tJBA8.1 recognition and capture.

In the future, the aptamer-based malignant cell depletion strategy described here could be adapted to affinity chromatography approaches, eliminating cell processing steps associated with MACS.[89,90] Chemical conjugation of aptamers to chromatography solid supports will also realize a fully-synthetic, low-cost cell depletion system, unlike the anti-biotin coupling used here that relies on expensive antibodies. As contaminating myeloid cells also inhibit the production of CAR T cells,[91] tJBA8.1 could be applied in combination with the monocyte-binding aptamer described above to elegantly deplete malignant cells and monocytes from patient PBMC concentrates in a single processing step.[29] Besides cell isolation, we foresee other applications of tJBA8.1 within CAR T-cell manufacturing. Our group previously used cationic comb polymers and polymer-lytic peptide conjugates (VIPER) for non-viral gene delivery to T cells, and low uptake was one of the limiting barriers to activated T-cell transfection.[92,93] Of relevance, we show in this work that activated T cells have upregulated TfR1 expression and high tJBA8.1 binding, and TfR1 is well known to be rapidly internalized upon ligand binding via clathrin-mediated endocytosis.[50] Comb polymer and VIPER formulations could thus be decorated with tJBA8.1 to enhance their binding to activated T cells via TfR1, improving their uptake for T-cell transfection. Outside of CAR T-cell therapy, TfR1 targeting with tJBA8.1 could have implications in the detection of circulating

tumor cells and the delivery of drugs across the blood-brain barrier,[94,95] paving the way for tJBA8.1-based diagnostics and therapeutics.

2.5 Acknowledgment

This work was supported by a sponsored research agreement from Juno Therapeutics, a Bristol-Myers Squibb company. Over the course of this work, Ian Cardle was supported by a National Science Foundation Graduate Research Fellowship under Grant No. DGE-1762114 and by the National Cancer Institute of the National Institutes of Health under Award No. 5T32CA080416-19. We thank Dr. Chris Ramsborg, Dr. Allison Bianchi, Dr. Julie Shi, and Calvin Chan from Juno Therapeutics for their valuable discussion and suggestions. We acknowledge support from the NIH under Grant No. S10 OD016240 to the W. M. Keck Microscopy Center that originally funded the Leica SP8X confocal microscope used in our studies, and we thank Keck Center manager Dr. Nathaniel Peters for his assistance. We are also grateful to Dr. Philip Gafken and Lisa Jones from the Fred Hutchinson Cancer Research Center for preparing and processing our mass spectrometry samples.

2.6 References

1. Maude, S. L. *et al.* Tisagenlecleucel in Children and Young Adults with B-Cell Lymphoblastic Leukemia. *N. Engl. J. Med.* **378**, 439–448 (2018).

2. Schuster, S. J. *et al.* Tisagenlecleucel in Adult Relapsed or Refractory Diffuse Large B-Cell Lymphoma. *N. Engl. J. Med.* **380**, 45–56 (2018).

3. Neelapu, S. S. *et al.* Axicabtagene Ciloleucel CAR T-Cell Therapy in Refractory Large B-Cell Lymphoma. *N. Engl. J. Med.* **377**, 2531–2544 (2017).

4. Locke, F. L. *et al.* Long-term safety and activity of axicabtagene ciloleucel in refractory large B-cell lymphoma (ZUMA-1): a single-arm, multicentre, phase 1-2 trial. *Lancet Oncol.* **20**, 31–42 (2019).

5. Wang, M. *et al.* KTE-X19 CAR T-Cell Therapy in Relapsed or Refractory Mantle-Cell Lymphoma. *N. Engl. J. Med.* (2020) doi:10.1056/nejmoa1914347.

6. Abramson, J. S. *et al.* Lisocabtagene maraleucel for patients with relapsed or refractory large B-cell lymphomas (TRANSCEND NHL 001): a multicentre seamless design study. *Lancet (London, England)* **396**, 839–852 (2020).

7. Munshi, N. C. *et al.* Idecabtagene Vicleucel in Relapsed and Refractory Multiple Myeloma. *N. Engl. J. Med.* (2021) doi:10.1056/nejmoa2024850.

8. Vormittag, P., Gunn, R., Ghorashian, S. & Veraitch, F. S. A guide to manufacturing CAR T cell therapies. *Current Opinion in Biotechnology* (2018) doi:10.1016/j.copbio.2018.01.025.

9. Cardle, I. I., Cheng, E. L., Jensen, M. C. & Pun, S. H. Biomaterials in chimeric antigen receptor T-cell process development. *Acc. Chem. Res.* (2020) doi:10.1021/acs.accounts.0c00335.

10. Powell, D. J. *et al.* Efficient clinical-scale enrichment of lymphocytes for use in adoptive immunotherapy using a modified counterflow centrifugal elutriation program. *Cytotherapy* **11**, 923–935 (2009).

11. Maude, S. L. *et al.* Chimeric Antigen Receptor T Cells for Sustained Remissions in Leukemia. *N. Engl. J. Med.* **371**, 1507–1517 (2014).

12. Levine, B. L., Miskin, J., Wonnacott, K. & Keir, C. Global Manufacturing of CAR T Cell Therapy. *Mol. Ther. - Methods Clin. Dev.* **4**, 92–101 (2017).

13. Iyer, R. K., Bowles, P. A., Kim, H. & Dulgar-Tulloch, A. Industrializing Autologous Adoptive Immunotherapies: Manufacturing Advances and Challenges. *Front. Med.* **5**, 150 (2018).

14. Raje, N. *et al.* Anti-BCMA CAR T-Cell Therapy bb2121 in Relapsed or Refractory

Multiple Myeloma. *N. Engl. J. Med.* **380**, 1726–1737 (2019).

15. Hoffmann, J.-M. *et al.* Differences in Expansion Potential of Naive Chimeric Antigen Receptor T Cells from Healthy Donors and Untreated Chronic Lymphocytic Leukemia Patients. *Frontiers in Immunology* vol. 8 1956 (2018).

16. Ruella, M. *et al.* Induction of resistance to chimeric antigen receptor T cell therapy by transduction of a single leukemic B cell. *Nat. Med.* (2018) doi:10.1038/s41591-018-0201-9.

17. Miltenyi, S., Müller, W., Weichel, W. & Radbruch, A. High gradient magnetic cell separation with MACS. *Cytometry* **11**, 231–238 (1990).

18. Stemberger, C. *et al.* Novel serial positive enrichment technology enables clinical multiparameter cell sorting. *PLoS One* (2012) doi:10.1371/journal.pone.0035798.

19. Teoh, J. *et al.* Lisocabtagene Maraleucel (liso-cel) Manufacturing Process Control and Robustness across CD19+ Hematological Malignancies. *Blood* **134**, 593 (2019).

20. Alcantara, M., Tesio, M., June, C. H. & Houot, R. CAR T-cells for T-cell malignancies: challenges in distinguishing between therapeutic, normal, and neoplastic T-cells. *Leukemia* **32**, 2307–2315 (2018).

21. Fleischer, L. C., Spencer, H. T. & Raikar, S. S. Targeting T cell malignancies using CAR-based immunotherapy: challenges and potential solutions. *J. Hematol. Oncol.* **12**, 141 (2019).

22. Zhou, J. & Rossi, J. Aptamers as targeted therapeutics: current potential and challenges. *Nat. Rev. Drug Discov.* **16**, 440 (2017).

23. Walter, J. G., Stahl, F. & Scheper, T. Aptamers as affinity ligands for downstream processing. *Engineering in Life Sciences* (2012) doi:10.1002/elsc.201100197.

24. Chen, Y. Y. Cell fishing with DNA aptamers. *Nat. Biomed. Eng.* **3**, 757–758 (2019).

25. Kacherovsky, N. *et al.* Traceless aptamer-mediated isolation of CD8+ T cells for chimeric antigen receptor T-cell therapy. *Nat. Biomed. Eng.* (2019) doi:10.1038/s41551-019-0411-6.

26. Sefah, K., Shangguan, D., Xiong, X., O'Donoghue, M. B. & Tan, W. Development of DNA aptamers using cell-selex. *Nat. Protoc.* (2010) doi:10.1038/nprot.2010.66.

27. Shangguan, D. *et al.* Identification of Liver Cancer-Specific Aptamers Using Whole Live Cells. *Anal. Chem.* **80**, 721–728 (2008).

28. Li, W.-M., Zhou, L.-L., Zheng, M. & Fang, J. Selection of Metastatic Breast Cancer Cell-Specific Aptamers for the Capture of CTCs with a Metastatic Phenotype by Cell-SELEX. *Mol. Ther. - Nucleic Acids* **12**, 707–717 (2018).

29. Sylvestre, M. *et al.* Identification of a DNA Aptamer That Binds to Human Monocytes and Macrophages. *Bioconjug. Chem.* **31**, 1899–1907 (2020).

30. Wu, X. *et al.* DNA Aptamer Selected against Pancreatic Ductal Adenocarcinoma for In vivo Imaging and Clinical Tissue Recognition. *Theranostics* **5**, 985–994 (2015).

31. Wu, X. *et al.* Elucidation and structural modeling of cd71 as a molecular target for cell-specific aptamer binding. *J. Am. Chem. Soc.* (2019) doi:10.1021/jacs.9b03720.

32. Alam, K. K., Chang, J. L. & Burke, D. H. FASTAptamer: A bioinformatic toolkit for high-throughput sequence analysis of combinatorial selections. *Mol. Ther. - Nucleic Acids* **4**, (2015).

33. Bailey, T. L. *et al.* MEME Suite: Tools for motif discovery and searching. *Nucleic Acids Res.* (2009) doi:10.1093/nar/gkp335.

34. Rambaut, A. FigTree-version 1.4. 3, a graphical viewer of phylogenetic trees. *Computer program distributed by the author, website: http://tree.bio.ed.ac.uk/software/figtree* (2016).

35. Zadeh, J. N. *et al.* NUPACK: Analysis and design of nucleic acid systems. *J. Comput. Chem.* (2011) doi:10.1002/jcc.21596.

36. Shangguan, D. *et al.* Cell-specific aptamer probes for membrane protein elucidation in cancer cells. *J. Proteome Res.* (2008) doi:10.1021/pr700894d.

37. Weiss, A. & Stobo, J. D. Requirement for the coexpression of T3 and the T cell antigen receptor on a malignant human T cell line. *J. Exp. Med.* **160**, 1284–1299 (1984).

38. Ohashi, P. S. *et al.* Reconstitution of an active surface T3/T-cell antigen receptor by DNA transfer. *Nature* **316**, 606–609 (1985).

39. Dong, Z. M., Jackson, L. & Murphy, J. W. Mechanisms for induction of L-selectin loss from T lymphocytes by a cryptococcal polysaccharide, glucuronoxylomannan. *Infect. Immun.* **67**, 220–229 (1999).

40. Kosuri, S. & Church, G. M. Large-scale de novo DNA synthesis: technologies and applications. *Nat. Methods* **11**, 499–507 (2014).

41. Lyu, Y. *et al.* Generating Cell Targeting Aptamers for Nanotheranostics Using Cell-SELEX. *Theranostics* **6**, 1440–1452 (2016).

42. Wang, G. *et al.* Selection and characterization of DNA aptamer against glucagon receptor by cell-SELEX. *Sci. Rep.* **7**, 7179 (2017).

43. Shangguan, D., Tang, Z., Mallikaratchy, P., Xiao, Z. & Tan, W. Optimization and Modifications of Aptamers Selected from Live Cancer Cell Lines. *ChemBioChem* **8**, 603–606 (2007).

44. Montemiglio, L. C. *et al.* Cryo-EM structure of the human ferritin–transferrin receptor 1 complex. *Nat. Commun.* (2019) doi:10.1038/s41467-019-09098-w.

45. Tortorella, S. & Karagiannis, T. C. Transferrin receptor-mediated endocytosis: A useful target for cancer therapy. *Journal of Membrane Biology* (2014) doi:10.1007/s00232-014-9637-0.

46. Gatter, K. C., Brown, G., Trowbridge, I. S., Woolston, R. E. & Mason, D. Y. Transferrin receptors in human tissues: their distribution and possible clinical relevance. *J. Clin. Pathol.* **36**, 539–545 (1983).

47. Caruso, A. *et al.* Flow cytometric analysis of activation markers on stimulated T cells and their correlation with cell proliferation. *Cytometry* (1997) doi:10.1002/(SICI)1097-0320(19970101)27:1<71::AID-CYTO9>3.0.CO;2-O.

48. Yeh, C.-J. G., Taylor, C. G. & Faulka, W. P. Transferrin Binding by Peripheral Blood Mononuclear Cells in Human Lymphomas, Myelomas and Leukemias. *Vox Sang.* **46**, 217–223 (1984).

49. Motamedi, M., Xu, L. & Elahi, S. Correlation of transferrin receptor (CD71) with Ki67 expression on stimulated human and mouse T cells: The kinetics of expression of T cell activation markers. *J. Immunol. Methods* (2016) doi:10.1016/j.jim.2016.08.002.

50. Mayle, K. M., Le, A. M. & Kamei, D. T. The intracellular trafficking pathway of transferrin. *Biochimica et Biophysica Acta - General Subjects* (2012) doi:10.1016/j.bbagen.2011.09.009.

51. Boumsell, L., Bensussan, A. & Kadouche, J. Anti-CD71 monoclonal antibodies and uses thereof for treating malignant tumor cells. (2013).

52. Bennett, M. J., Lebrón, J. A. & Bjorkman, P. J. Crystal structure of the hereditary haemochromatosis protein HFE complexed with transferrin receptor. *Nature* (2000) doi:10.1038/47417.

53. Cheng, Y., Zak, O., Aisen, P., Harrison, S. C. & Walz, T. Structure of the Human Transferrin Receptor-Transferrin Complex. *Cell* **116**, 565–576 (2004).

54. Feder, J. N. *et al.* The hemochromatosis gene product complexes with the transferrin receptor and lowers its affinity for ligand binding. *Proc. Natl. Acad. Sci.* **95**, 1472–1477 (1998).

55. Waheed, A. *et al.* Regulation of transferrin-mediated iron uptake by HFE, the protein defective in hereditary hemochromatosis. *Proc. Natl. Acad. Sci.* **99**, 3117–3122 (2002).

56. Feder, J. N. *et al.* A novel MHC class I–like gene is mutated in patients with hereditary haemochromatosis. *Nat. Genet.* **13**, 399–408 (1996).

57. Schmidt, P. J., Toran, P. T., Giannetti, A. M., Bjorkman, P. J. & Andrews, N. C. The

Transferrin Receptor Modulates Hfe-Dependent Regulation of Hepcidin Expression. *Cell Metab.* **7**, 205–214 (2008).

58. Vujic Spasic, M. Molecular basis of HFE-hemochromatosis. *Front. Pharmacol.* **5**, 42 (2014).

59. Scott, C. S., Ramsden, W., Limbert, H. J., Master, P. S. & Roberts, B. E. Membrane transferrin receptor (TfR) and nuclear proliferation-associated Ki-67 expression in hemopoietic malignancies. *Leukemia* **2**, 438–442 (1988).

60. Płoszyńska, A. *et al.* Cytometric evaluation of transferrin receptor 1 (CD71) in childhood acute lymphoblastic leukemia. *Folia Histochem. Cytobiol.* **50**, 304–311 (2012).

61. Liu, Q. *et al.* Significance of CD71 expression by flow cytometry in diagnosis of acute leukemia. *Leuk. Lymphoma* **55**, 892–898 (2014).

62. Hagag, A. A., Badraia, I. M., Abdelmageed, M. M., Hablas, N. M. & Nosair, S. M. E. H. and N. A. Prognostic Value of Transferrin Receptor-1 (CD71) Expression in Acute Lymphoblastic Leukemia. *Endocrine, Metabolic & Immune Disorders - Drug Targets* vol. 18 610–617 (2018).

63. Habeshaw, J. A., Lister, T. A., Stansfeld, A. G. & Greaves, M. F. Correlation of transferrin receptor expression with histological class and outcome in non-Hodgkin lymphoma. *Lancet* **321**, 498–501 (1983).

64. Jeffrey Medeiros, L., Picker, L. J., Horning, S. J. & Warnke, R. A. Transferrin receptor expression by non-hodgkin's lymphomas. Correlation with morphologic grade and survival. *Cancer* **61**, 1844–1851 (1988).

65. Das Gupta, A. & Shah, V. I. Correlation of transferrin receptor expression with histologic grade and immunophenotype in chronic lymphocytic leukemia and non-Hodgkin's lymphoma. *Hematol. Pathol.* **4**, 37–41 (1990).

66. Kozlowski, R., Reilly, I. A. G., Sowter, D., Robins, R. A. & Russell, N. H. Transferrin receptor expression on AML blasts is related to their proliferative potential. *Br. J. Haematol.* **69**, 275–280 (1988).

67. Allen, E. S. *et al.* Autologous lymphapheresis for the production of chimeric antigen receptor T cells. *Transfusion* **57**, 1133–1141 (2017).

68. Armas, P., Nasif, S. & Calcaterra, N. B. Cellular nucleic acid binding protein binds G-rich single-stranded nucleic acids and may function as a nucleic acid chaperone. *J. Cell. Biochem.* **103**, 1013–1036 (2008).

69. Benhalevy, D. *et al.* The Human CCHC-type Zinc Finger Nucleic Acid-Binding Protein Binds G-Rich Elements in Target mRNA Coding Sequences and Promotes Translation. *Cell Rep.* **18**, 2979–2990 (2017).

70. David, A. P. *et al.* CNBP controls transcription by unfolding DNA G-quadruplex structures. *Nucleic Acids Res.* **47**, 7901–7913 (2019).

71. Kikin, O., D'Antonio, L. & Bagga, P. S. QGRS Mapper: a web-based server for predicting G-quadruplexes in nucleotide sequences. *Nucleic Acids Res.* **34**, W676–W682 (2006).

72. Lee, E., Lee, T. A., Yoo, H. J., Lee, S. & Park, B. CNBP controls tumor cell biology by regulating tumor-promoting gene expression. *Mol. Carcinog.* **58**, 1492–1501 (2019).

73. Liu, H. *et al.* Alternative splicing analysis in human monocytes and macrophages reveals MBNL1 as major regulator. *Nucleic Acids Res.* **46**, 6069–6086 (2018).

74. Hovanessian, A. G. *et al.* The Cell-Surface-Expressed Nucleolin Is Associated with the Actin Cytoskeleton. *Exp. Cell Res.* **261**, 312–328 (2000).

75. Bates, P. J., Kahlon, J. B., Thomas, S. D., Trent, J. O. & Miller, D. M. Antiproliferative Activity of G-rich Oligonucleotides Correlates with Protein Binding*. *J. Biol. Chem.* **274**, 26369–26377 (1999).

76. Stroncek, D. F. *et al.* Elutriated lymphocytes for manufacturing chimeric antigen receptor T cells. *J. Transl. Med.* **15**, 59 (2017).

77. Padmanabhan, K., Padmanabhan, K. P., Ferrara, J. D., Sadler, J. E. & Tulinsky, A. The structure of alpha-thrombin inhibited by a 15-mer single-stranded DNA aptamer. *J. Biol. Chem.* **268**, 17651–17654 (1993).

78. Zhang, K. *et al.* Cryo-EM structure of a 40 kDa SAM-IV riboswitch RNA at 3.7 Å resolution. *Nat. Commun.* **10**, 5511 (2019).

79. Ruigrok, V. J. B. *et al.* Characterization of aptamer-protein complexes by X-ray crystallography and alternative approaches. *Int. J. Mol. Sci.* **13**, 10537–10552 (2012).

80. Worthen, C. & Enns, C. The role of hepatic transferrin receptor 2 in the regulation of iron homeostasis in the body . *Frontiers in Pharmacology* vol. 5 34 (2014).

81. Ren, S. *et al.* The RNA/DNA-binding protein PSF relocates to cell membrane and contributes cells' sensitivity to antitumor drug, doxorubicin. *Cytom. Part A* **85**, 231–241 (2014).

82. Finney, O. C. *et al.* CD19 CAR T cell product and disease attributes predict leukemia remission durability. *J. Clin. Invest.* **129**, 2123–2132 (2019).

83. Bersenev, A. CAR-T cell manufacturing: time to put it in gear. *Transfusion* **57**, 1104–1106 (2017).

84. Brada, M. *et al.* Circulating lymphoma cells in patients with B & T non-Hodgkin's lymphoma detected by immunoglobulin and T-cell receptor gene rearrangement. *Br. J. Cancer* **56**, 147–152 (1987).

85. Marks, D. I. *et al.* T-cell acute lymphoblastic leukemia in adults: clinical features, immunophenotype, cytogenetics, and outcome from the large randomized prospective trial (UKALL XII/ECOG 2993). *Blood* **114**, 5136–5145 (2009).

86. Asnafi, V. *et al.* Analysis of TCR, pTα, and RAG-1 in T-acute lymphoblastic leukemias improves understanding of early human T-lymphoid lineage commitment. *Blood* **101**, 2693–2703 (2003).

87. Cooper, M. L. *et al.* An "off-the-shelf" fratricide-resistant CAR-T for the treatment of T cell hematologic malignancies. *Leukemia* (2018) doi:10.1038/s41375-018-0065-5.

88. Xu, Y. *et al.* 2B4 costimulatory domain enhancing cytotoxic ability of anti-CD5 chimeric antigen receptor engineered natural killer cells against T cell malignancies. *J. Hematol. Oncol.* **12**, 49 (2019).

89. Kumar, A. & Srivastava, A. Cell separation using cryogel-based affinity chromatography. *Nat. Protoc.* (2010) doi:10.1038/nprot.2010.135.

90. Mohr, F. *et al.* Efficient immunoaffinity chromatography of lymphocytes directly from whole blood. *Sci. Rep.* **8**, 16731 (2018).

91. Stroncek, D. F. *et al.* Myeloid cells in peripheral blood mononuclear cell concentrates inhibit the expansion of chimeric antigen receptor T cells. *Cytotherapy* **18**, 893–901 (2016).

92. Olden, B. R., Cheng, Y., Yu, J. L. & Pun, S. H. Cationic polymers for non-viral gene delivery to human T cells. *J. Control. Release* **282**, 140–147 (2018).

93. Olden, B. R., Cheng, E., Cheng, Y. & Pun, S. H. Identifying key barriers in cationic polymer gene delivery to human T cells. *Biomater. Sci.* (2019) doi:10.1039/C8BM01262H.

94. Biglione, C. *et al.* Optimizing Circulating Tumor Cells' Capture Efficiency of Magnetic Nanogels by Transferrin Decoration. *Polymers (Basel).* **10**, 174 (2018).

95. Li, X. *et al.* Enhanced in Vivo Blood–Brain Barrier Penetration by Circular Tau–Transferrin Receptor Bifunctional Aptamer for Tauopathy Therapy. *J. Am. Chem. Soc.* **142**, 3862–3872 (2020).

2.7 Supplementary information

Supplementary Table 2.1. Experimental conditions used in rounds of cell-SELEX.

SELEX Round	Positive Selection (Jurkat)	Negative Selection (J.RT3-T3.5)	Aptamer Pool (μM)	FBS (%)	Time (min)	# of Washes
1	10^7 Cells	-	14	-	60	3
2	5×10^6 Cells	10^7 Cells	0.5	-	60	3
3	4×10^6 Cells	10^7 Cells	0.5	-	60	3
4	2×10^6 Cells	10^7 Cells	0.5	5	45	4
5	1×10^6 Cells	10^7 Cells	0.5	5	45	4
6	1×10^6 Cells	10^7 Cells	0.5	10	45	5
7	1×10^6 Cells	10^7 Cells	0.5	10	30	5
8	1×10^6 Cells	10^7 Cells	0.5	20	30	6

Supplementary Table 2.2. Primers used for next generation sequencing (NGS) of naive library (NL) and cell-SELEX rounds 1-8. The NL and Rounds 7-8 were sequenced initially, followed by Rounds 1-6 in a separate run. Accordingly, there is some overlap in the barcoded reverse primers used between the separate runs.

Primer Name	SELEX Round	Sequence	Barcode (in red)
Aptamer_F	NL, 1-8	AATGATACGGCGACCACCGAGATCTACACCGAGGAGATAC CACTAAGCCACCGTGTCCA	
Aptamer_R_77	NL	CAAGCAGAAGACGGCATACGAGATGCAATTCGACAGACCG TCGATCCAGAGTGACGCAGCA	CGAATTGC
Aptamer_R_79	1	CAAGCAGAAGACGGCATACGAGATTCGATTAAACAGACCG TCGATCCAGAGTGACGCAGCA	TTAATCGA
Aptamer_R_80	2	CAAGCAGAAGACGGCATACGAGATGAATGGACACAGACCG TCGATCCAGAGTGACGCAGCA	GTCCATTC
Aptamer_R_81	3	CAAGCAGAAGACGGCATACGAGATAGAATCAGACAGACCG TCGATCCAGAGTGACGCAGCA	CTGATTCT
Aptamer_R_82	4	CAAGCAGAAGACGGCATACGAGATAACTGCCAACAGACCG TCGATCCAGAGTGACGCAGCA	TGGCAGTT
Aptamer_R_83	5	CAAGCAGAAGACGGCATACGAGATAAGTAACGACAGACCG TCGATCCAGAGTGACGCAGCA	CGTTACTT
Aptamer_R_84	6	CAAGCAGAAGACGGCATACGAGATACTCAATGACAGACCG TCGATCCAGAGTGACGCAGCA	CATTGAGT
Aptamer_R_78	7	CAAGCAGAAGACGGCATACGAGATCAAGAGGTACAGACCG TCGATCCAGAGTGACGCAGCA	ACCTCTTG

Aptamer_R_79	8	CAAGCAGAAGACGGCATACGAGATTCGATTAAACAGACCG TCGATCCAGAGTGACGCAGCA	TTAATCGA

Supplementary Table 2.3. Enrichment of top 50 Round 8 (R8) aptamer sequences between rounds of cell-SELEX. Fold enrichment is calculated by dividing the reads per million (RPM) of the sequence from a round by the value of the former round.

				Fold Enrichment		
R8 Rank	**% Rep.**	**Motif**	**Random Region Sequence**	**R8/R7**	**R7/R6**	**R6/R5**
1	21.08	3	GCGTAAAGGGGGTGTTTGTGCGGTGTGGAGTGCGCGTGCTGCTGC	6.9	7.8	19.5
2	11.15		ATCCGGGAGAGTCGTTGTGTTGAGGTCCGCCCCTGCTCGCCCGCG	11.1	20.3	
3	6.41	2	GGGGCCGCGGATGCAAACGCCCGATAGGGGGACGGCACTGGAGCT	0.6	4.1	89.4
4	5.59		ACCCAAACCACCAGCCGGGGATGCAAACACCGCACAGGGAACGGC	1.3	6.7	104.6
5	5.07		AAGCGGTTTTCGGGTTCGGGTCTGGGGGTTGGGTTGTCGGCACTA	0.8	15.9	
6	4.61		ACAGACAGCTGCGCCGCCGGGAGGGCACCCGGACGGGCTGGGCGG	1.7	0.4	55.1
7	4.01	2	ACCACAGATGCAAATGCGCGAGAGCGGGACGGTTTGCTAGGCTCA	0.7	5.3	80.8
8	3.88	5	GTGGGCCAAATGGATTGGATTAGGGTTGGGCCGCCCGGGAGGGGT	0.6	28.2	51.4
9	3.29	1	AGGCGCTAGACGCAATCCCGCAAGCGGAGCCGGATTCCCTAGTGG	0.7	2.0	13.9
10	3.17	3	GCATAAAGGGGGTGTTTGTGCGGTGTGGAGTGCGCGTGCTGCTGC	20.1	17.4	
11	2.88	2	GCCGGTCGCAGATGCAAATGCCCGACAGGGGGACGCGGGCTGCCA	0.6	4.4	65.7
12	2.70	2	CAGATGCAAATGCCTGACCAGGGAACTGCGACTGGATGGCTCTTG	1.0	5.3	60.4
13	2.26	1	ATCACAGGGCTACAAGGTGCTAAACGTAAACTAGCAAGAGAACTA	0.8	1.8	20.1
14	1.82	2	GATGCAAATGCTCGAGAGAGGACCGGCGGCACTGGTGAACGTAGG	1.0	5.6	70.8
15	1.55		CTCTCGGGGGGTAGGTGGGAAGGGGGCCGCCCCCTGGGTTAGGCT	2.4	9.8	
16	1.18	2	AGCGGGGATGCAAACACCCGAAAGGGGAACGGGAGCTGCGTCAAG	1.7	1.1	73.4
17	0.93		AGGTGGCTGTGGGCGGATGGTGGGCTCGCGTGGGCGGCCACCTGA	0.9	0.9	12.4
18	0.90		ACGTTATCCCCTTTACGGGGTCCTAGAGCCCCGTGAGTGCTCACG	1.0	1.7	19.4
19	0.83		TCGGTGTTTATGGTGTCTGTCGGTGCGTACTCGGGGCTTCACTAG	0.8	9.9	15.3
20	0.69	2	TTGGAGGTGGCGGATGCAAACGCTAGACAGAGGCACCAGCTCCAA	0.8	3.9	
21	0.64		GACTGCTGTGCCACCGGGAGTGCCTTCAGCGCCGTACGGTCTGCT	1.2	0.2	31.9
22	0.63	1	ACGCAGCAAGGTGCTAAACGCAATCCCGGATTCTCGTGCGTCAAG	1.3	1.2	18.3
23	0.49	2	GATGCAAATGCCCGAATGGGGGACGGCGGACACGGGGTGTGCCGA	0.6	4.4	
24	0.43		TACGGCTTATGCTCAGAGGGGCTGTGGGCCGAGGGGAGCGTCGCG	0.9	1.2	9.5
25	0.35		TGTAAGCCGAATGTTGGTGCTTGGGTAGGCGCCATTGTGAGCTCG	0.8	3.2	12.8
26	0.33	3	GCGTAAAGGGGGTGTTTGTGCGGTGTGGAGTGCGCGCGCTGCTGC	22.3		
27	0.25		CTGTGGGGTCACATTGGGGGACGGGACCGTGCGTGAGATCTAAGA	2.6	12.6	

28	0.21		GGGTTCCGGATGTGGTGGGGCTTAGGGGGGTTTCACTGCTAGCGT	0.5	5.2	
29	0.19		AAGGTTGCCATACCACCGGGAGCGTTCGAGTACGGCCTGTCGCGC	0.6	0.5	23.3
30	0.18	1	AGGGGTACAAGGTGTTAAACGTAAATTCTGCGCGGAGGGGAACTT	0.8	1.5	11.0
31	0.16		GACGCAGCAGTGCCATCGGGGGGGATTTCCTTGTACGACGTCACC	0.6	0.8	16.0
32	0.15		GTGCCATCGGGAGGCGCGAGTCCGTACGACGTCATTTGGCAAAAC	0.8	0.8	19.3
33	0.14		AAAAGAAGCGACCGAGACCACGGATGCAAACGCCCAGGCGGGGAA	0.7	2.8	
34	0.13	1	CTGTGGCGTAATTCTGGTCGGCGGTCACGTGCGTGAGAGCTGGGG	3.7	10.7	
35	0.11	1	AGGTGTTAAACGCTAACGCCAGTTATCTTAAAGAAAGTAAACGAC	0.5	1.3	7.5
36	0.11		TCAAGGGGTTACACGAAAAGATAGGCTTTCACGCTAGTGGGCTTG	0.6	1.3	7.5
37	0.10		GTGGTATGGTCTAAGAGCCGTCTGGCGAGTCGGTGGGAGTAGCGA	0.7	1.5	6.4
38	0.09	2	CAGATGCAAATGCCTGACCAGGGAACTGCGACTGGATGGCTCTTT	1.5	6.8	
39	0.09		CGAAAATTTCAAGCTTTATGCTCTAGCGCAGCGCCTCGTACCCCT	1.8	1.5	
40	0.08		GGTGAAGGGCAGTGGTTTGCTGTGGTGGGCGCCCGTGAGCGTTGC	2.2	6.1	
41	0.08		GGGAGTTCGGGCATGATTTGCCCTGGGGGGCACGGGAAGGTACCG	1.0	7.7	2.7
42	0.08	1	CGCACCAAGGCGTTAGACGGAATGGATTTGGAACTTCATGCGAAG	0.4	1.3	6.4
43	0.08		GTTGGGCTAAGCGGAGGATGGTAATGGTGCTTGGGCAGGCGCTCA	0.8	2.5	11.3
44	0.07	2	CAGATGCAAATGCCTGACCAGGGAACTGCGACTTGATGGCTCTTG	1.5	5.8	
45	0.07	3	GCGCAAAGGGGGTGTTTGTGCGGTGTGGAGTGCGCGTGCTGCTGC	20.6		
46	0.07		GTGCCATCGGGAAGGTGTTGACCTGTACGACGTCATAGGATGGAC	1.2	1.0	
47	0.07		GGGGTGTAGGGTGGGGTAGTGGGAACATTGCGTAAAGTGTAGCTC	0.9	6.2	
48	0.06		ACTGTTTGTACGGAGTTAGGGTGTGCCTTTATTGCGCGGGGGGGA	5.6		
49	0.06		TCATTGGAGTGGGTAGGGGTGTTTGTGCGGGATGCGGTGGCTAGG	3.4	5.4	
50	0.06	5	GTTGGCCAAATGGATTGGATTAGGGTTGGGCCGCCCGGGAGGGGT	1.0		

Supplementary Table 2.4. Sequences of aptamers used in experiments. Aptamers were modified on their 5'-end with either 6-FAM, Cy5, or biotin-hexa-ethyleneglycol depending on the assay. The exact modifications are specified in the figures and captions. For 5' modification of tJBA8.1 with 6-FAM, a thymidine nucleotide was added at the 5' end to prevent fluorescence quenching by guanosine. Underlined nucleotides represent constant regions. Red text represents nucleotides that were deleted to make the truncated tJBA8.1 aptamer, and blue text represents nucleotides that were substituted to create either point variants of tJBA8.1 or JBA8.26.

Name	Sequence
RANL	5'-ATCCAGAGTGACGCAGCAAATTCCAAACTCGAGTAAGCGTAGAGCCTCTCATCGCCTCAATA ATGGACACGGTGGCTTAGT-3'
JBA8.1	5'-ATCCAGAGTGACGCAGCAGCGTAAAGGGGGTGTTTGTGCGGTGTGGAGTGCGCGTGCTGCTG CTGGACACGGTGGCTTAGT-3'
JBA8.2	5'-ATCCAGAGTGACGCAGCAATCCGGGAGAGTCGTTGTGTTGAGGTCCGCCCCTGCTCGCCCGCG TGGACACGGTGGCTTAGT-3'
JBA8.3	5'-ATCCAGAGTGACGCAGCAGGGGCCGCGGATGCAAACGCCCGATAGGGGGACGGCACTGGAGC TTGGACACGGTGGCTTAGT-3'
JBA8.4	5'-ATCCAGAGTGACGCAGCAACCCAAACCACCAGCCGGGGATGCAAACACCGCACAGGGAACGG CTGGACACGGTGGCTTAGT-3'
JBA8.7	5'-ATCCAGAGTGACGCAGCAACCACAGATGCAAATGCGCGAGAGCGGGACGGTTTGCTAGGCTCA TGGACACGGTGGCTTAGT-3'
JBA8.8	5'-ATCCAGAGTGACGCAGCAGTGGGCCAAATGGATTGGATTAGGGTTGGGCCGCCCGGGAGGGG TTGGACACGGTGGCTTAGT-3'
JBA8.11	5'-ATCCAGAGTGACGCAGCAGCCGGTCGCAGATGCAAATGCCCGACAGGGGGACGCGGGCTGCC ATGGACACGGTGGCTTAGT-3'
JBA8.15	5'-ATCCAGAGTGACGCAGCACTCTCGGGGGGTAGGTGGGAAGGGGGCCGCCCCCTGGGTTAGGC TTGGACACGGTGGCTTAGT-3'
JBA8.17	5'-ATCCAGAGTGACGCAGCAAGGTGGCTGTGGGCGGATGGTGGGCTCGCGTGGGCGGCCACCTG ATGGACACGGTGGCTTAGT-3'
tJBA8.1	5'-GCAGCAGCGTAAAGGGGGTGTTTGTGCGGTGTGGAGTGCGCGTGCTGCTGC-3'
XQ-2d	5'-ACTCATAGGGTTAGGGGCTGCTGGCCAGATACTCAGATGGTAGGGTTACTATGAGC-3'
tJBA8.1 GGAGG	5'-GCAGCAGCGTAAAGGAGGTGTTTGTGCGGTGTGGAGTGCGCGTGCTGCTGC-3'
tJBA8.1 GGGAG	5'-GCAGCAGCGTAAAGGGAGTGTTTGTGCGGTGTGGAGTGCGCGTGCTGCTGC-3'
tJBA8.1 GGGGC	5'-GCAGCAGCGTAAAGGGGCTGTTTGTGCGGTGTGGAGTGCGCGTGCTGCTGC-3'
JBA8.26	5'-ATCCAGAGTGACGCAGCAGCGTAAAGGGGGTGTTTGTGCGGTGTGGAGTGCGCGCGCTGCTG CTGGACACGGTGGCTTAGT-3'

Supplementary Table 2.5. siRNA duplexes used for transferrin receptor 1 (TfR1) knockdown.

Name	Sequence
hs.Ri.TFRC.13.1-SEQ1	5'-rCrArGrUrUrCrArGrArArUrGrArUrGrGrArUrCrArArGrCTA-3'
hs.Ri.TFRC.13.1-SEQ2	5'-rUrArGrCrUrUrGrArUrCrCrArUrCrArUrUrCrUrGrArArCrUrGrCrC-3'

Supplementary Table 2.6. Bio-layer interferometry (BLI) measured affinity kinetics of tJBA8.1, XQ-2d, and JBA8.26 aptamer binding to immobilized TfR1 protein. Data are mean ± standard deviation; *n* = 4-5 individual aptamer concentrations. Values were calculated by performing a global fit of the multi-concentration kinetic data in Figure 4B, Figure S6D, and Figure S15C to a 1:1 binding model. The ratio between the dissociation rate constant (K_{dis}) and the association rate constant (K_{on}) gives the equilibrium dissociation constant (K_D). The goodness of fit was evaluated by a reduced chi-square (χ^2) and a R^2 value approaching 1.

Aptamer	K_D (nM)	K_{on} ($nM^{-1}s^{-1}$) × 10^{-5}	K_{dis} (s^{-1}) × 10^{-4}	Full χ^2	Full R^2
tJBA8.1	25.11 (±0.19)	3.05 (±0.02)	7.66 (±0.03)	0.0402	0.9928
XQ-2d	14.45 (±0.15)	2.06 (±0.02)	2.97 (±0.02)	0.1272	0.9939
JBA8.26	6.87 (±0.04)	6.24 (±0.03)	4.29 (±0.02)	0.0439	0.9968

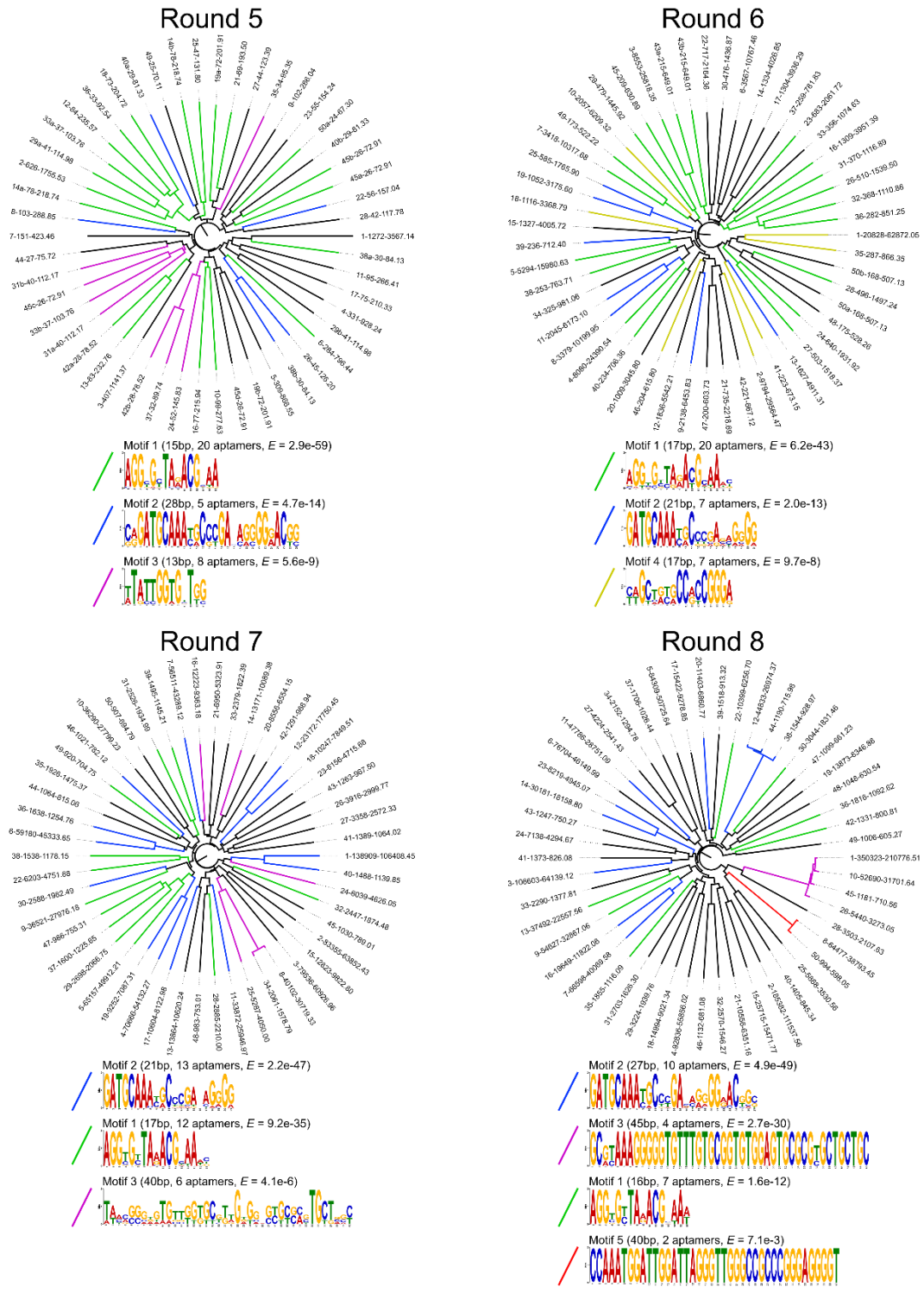

Supplementary Figure 2.1. Phylogenetic trees of the top 50 aptamers from rounds 5-8 of Jurkat cell-SELEX and emerging consensus motifs. Phylogenetic trees were generated with FigTree software (http://tree.bio.ed.ac.uk/software/figtree/), and statistically significant binding motifs were predicted using MEME analysis (MEME-suite.org). Phylogenetic trees are colored to denote

aptamers belonging to identified motifs. Branch labels denote the aptamer rank followed by raw reads and reads per million.

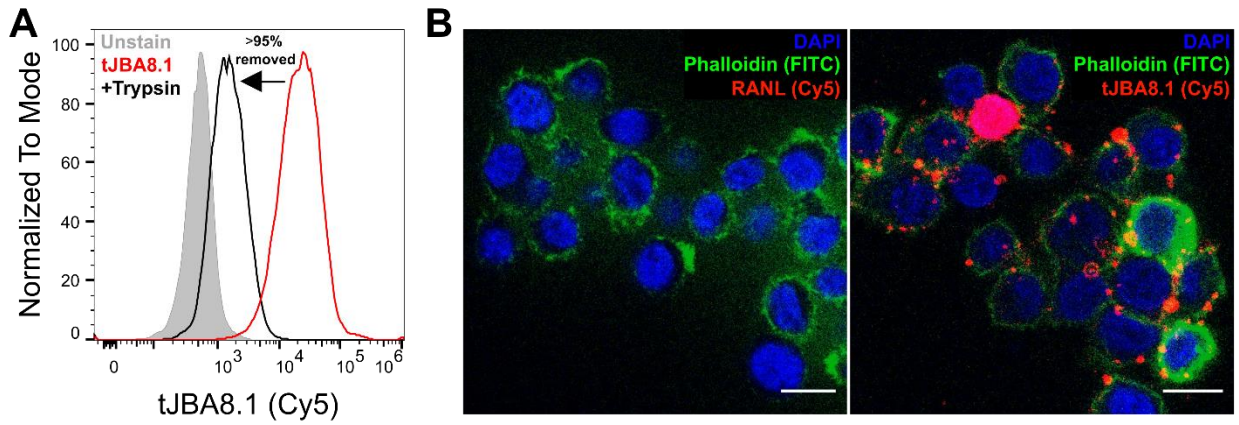

Supplementary Figure 2.2. tJBA8.1 targets membrane-bound proteins on Jurkat cells. (A) Flow cytometry histograms of 100 nM Cy5-labeled tJBA8.1 binding to Jurkat cells with and without trypsin treatment. Histograms are representative of *n* = 1 independent experiment with technical triplicates. (B) Subcellular localization of 200 nM Cy5-labeled RANL (left) and tJBA8.1 (right) binding to Jurkat cells at 4 °C by confocal microscopy imaging. Phalloidin recognizes F-actin, which primarily localizes to the cell membrane in Jurkat cells. Scale bars = 10 μm. Cy5, cyanine 5; DAPI, 4′,6-diamidino-2-phenylindole; FITC, fluorescein isothiocyanate.

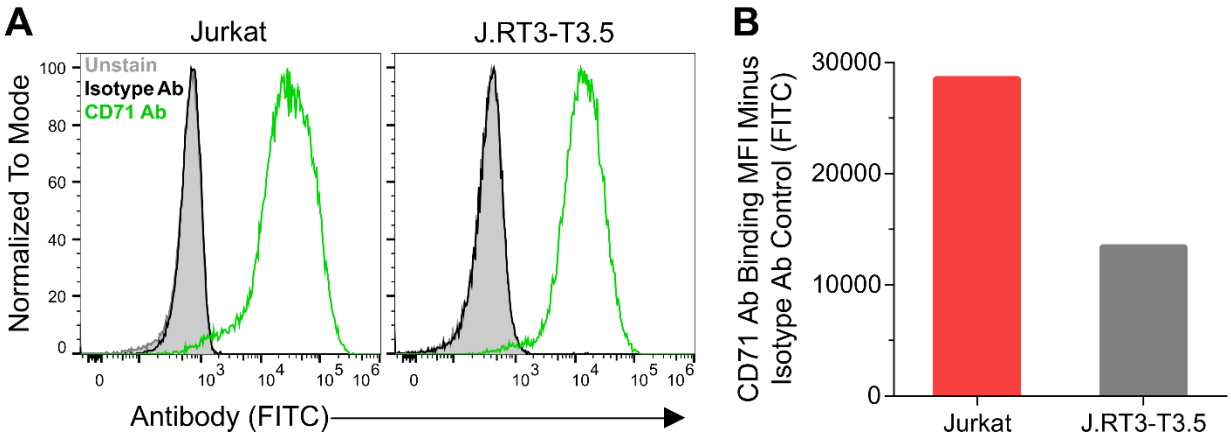

Supplementary Figure 2.3. Jurkat and J.RT3-T3.5 cells robustly and differentially express TfR1. (A) Flow cytometry histograms of FITC-labeled anti-CD71 antibody (CD71 Ab) binding to Jurkat and J.RT3-T3.5 cells. A FITC-labeled anti-CD14 antibody was used as an isotype control (Isotype Ab). Histograms are representative of *n* = 1 independent experiment. (B) Corresponding median fluorescence intensity (MFI) of CD71 Ab binding to Jurkat and J.RT3-T3.5 cells minus Isotype Ab binding. Data are representative of *n* = 1 independent experiment. FITC, fluorescein isothiocyanate.

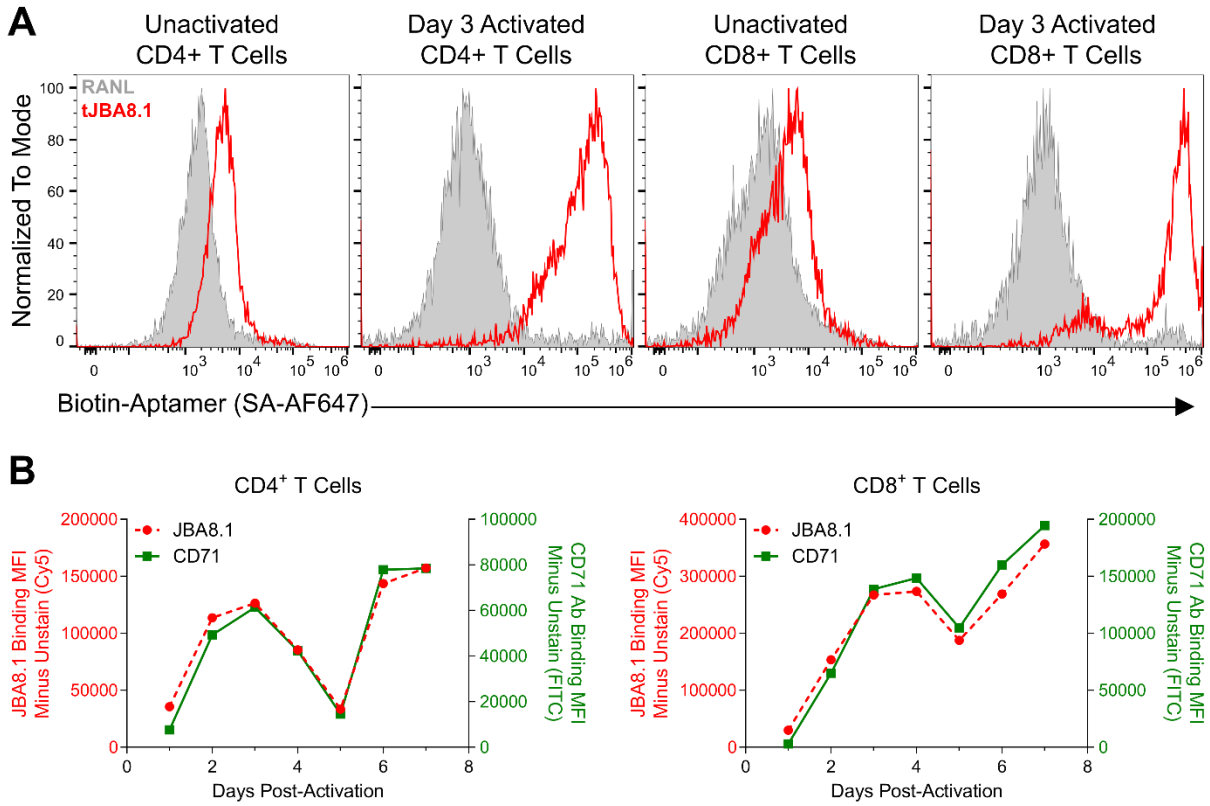

Supplementary Figure 2.4. JBA8.1 and tJBA8.1 binding correlates with TfR1 upregulation on activated $CD4^+$ and $CD8^+$ T cells. (A) Flow cytometry histograms of 100 nM biotinylated RANL and tJBA8.1 binding to unactivated and day 3 CD3/CD28 Dynabead-activated $CD4^+$ and $CD8^+$ T cells. Histograms are representative of n = 2 independent experiment. (B) MFI of 25nM Cy5-labeled JBA8.1 (red, left y-axis) and FITC-labeled CD71 Ab (green, right y-axis) binding to $CD4^+$ and $CD8^+$ T cells over 7 days of CD3/CD28 Dynabead activation by flow cytometry. Data are representative of n = 1 independent experiment carried out on each day of activation. SA-AF647, streptavidin Alexa Fluor 647; Cy5, cyanine 5; FITC, fluorescein isothiocyanate.

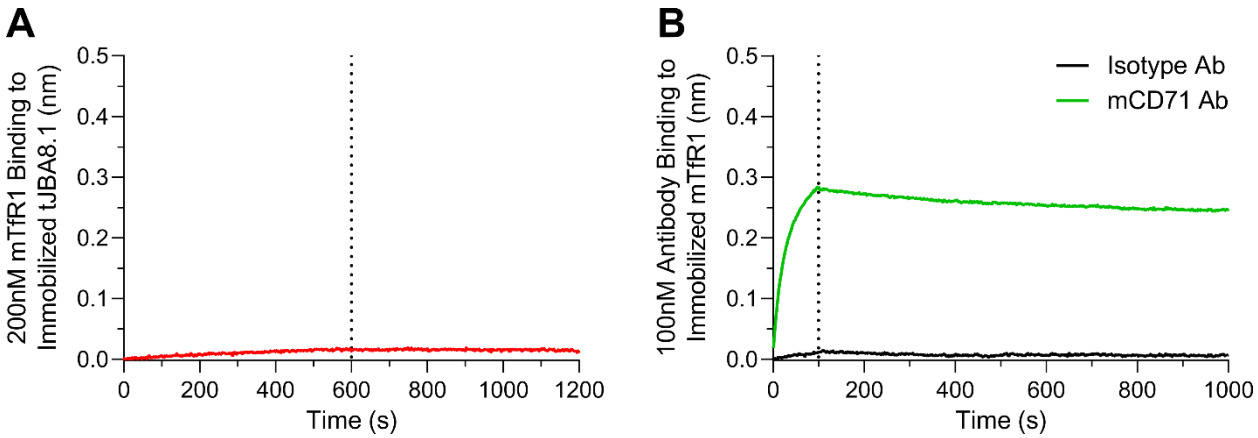

Supplementary Figure 2.5. tJBA8.1 does not bind mouse TfR1. (A) Association and dissociation kinetics of 200 nM His-tagged mouse TfR1 (mTfR1) protein binding to biotinylated tJBA8.1 immobilized on streptavidin biosensors by BLI. The association phase is illustrated from 0-600 s, whereas dissociation is shown from 600-1200 s (separated by the vertical dotted line). Data are representative of n = 1 independent experiment with one individual concentration of mTFR1. (B) Positive control binding of 100 nM FITC-labeled anti-mCD71 antibody (mCD71 Ab) to his-tagged mTfR1 immobilized on nickel-charged tris-nitriloacetic acid biosensors by BLI. A FITC-labeled anti-mCD3e antibody was used as an isotype control (Isotype Ab). The association phase is illustrated from 0-100 s, whereas dissociation is shown from 100-1000 s (separated by the vertical dotted line). Data are representative of n = 1 independent experiment with one individual concentration of antibody.

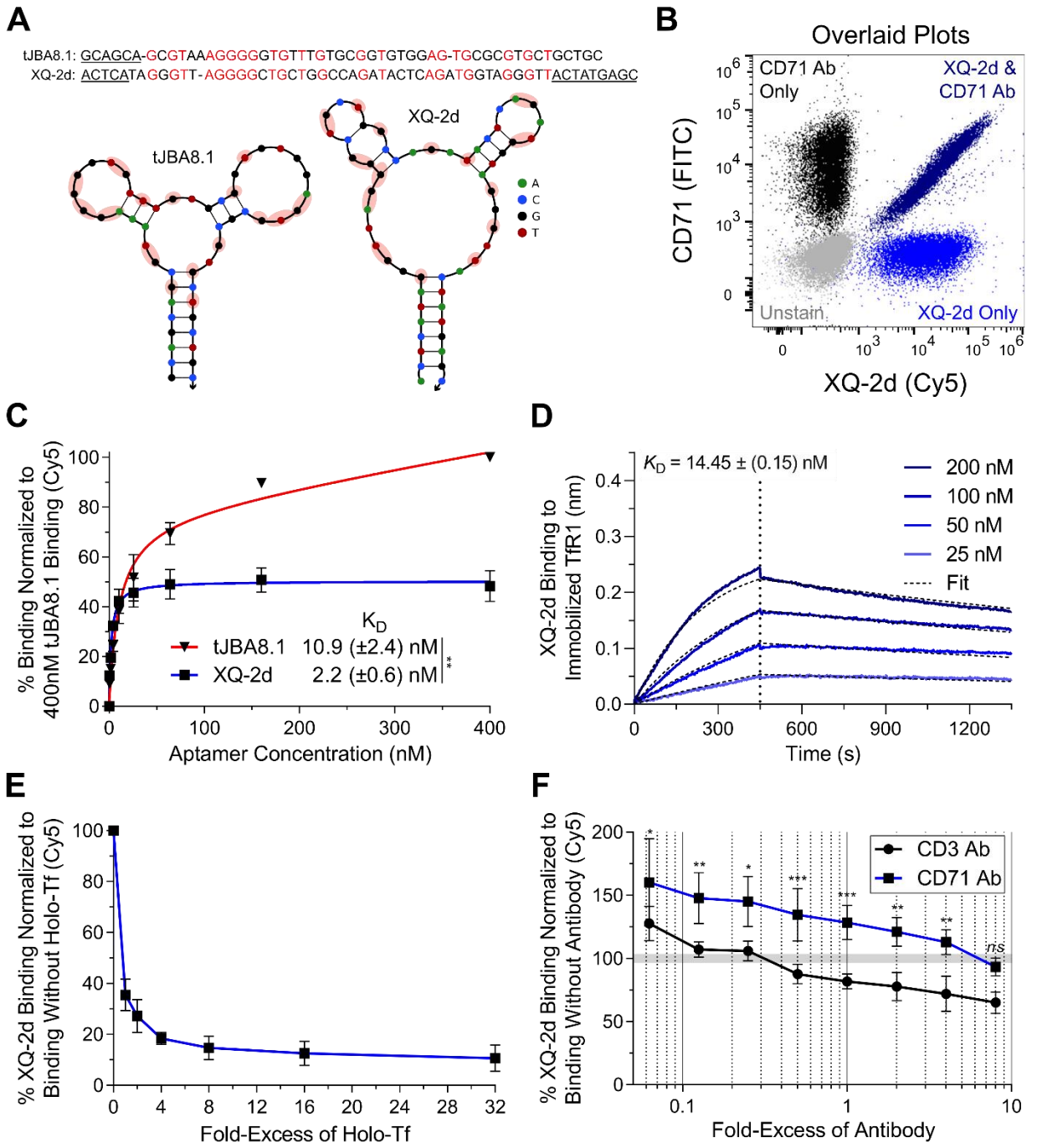

Supplementary Figure 2.6. XQ-2d competes with holo-Tf for binding to TfR1. (A) Sequence alignment and MFE structure comparison of tJBA8.1 and XQ-2d. MFE structures were predicted using NUPACK (temperature = 4 °C; Na^+ = 137 mM; Mg^{2+} = 5.5 mM). Red font and highlighting indicate overlapping nucleotides between the two aptamers. Dashes in sequence alignment represent single gap introductions and underlined nucleotides denote constant regions. (B) Overlaid flow cytometry plots of unstained (grey), FITC-labeled CD71 Ab single-stained (black), 25 nM Cy5-labeled XQ-2d single-stained (blue), and antibody and aptamer co-stained (dark blue) Jurkat cells. Plots are representative of $n = 2$ independent experiments. (C) Flow cytometry binding curves of Cy5-labeled tJBA8.1 and XQ-2d to Jurkat cells, normalized to 400 nM tJBA8.1 binding.

The binding curve for tJBA8.1 is the same as the one in **Figure 2B**. The curves represent a nonlinear regression assuming one-site total binding. K_D values were calculated by averaging the individual regression values of the independent experiments. Data points and error bars, and K_D values, represent mean ± standard deviation; *n* = 3 independent experiments with technical duplicates. ***P* < 0.01 (two-sided unpaired t-test). (D) Association and dissociation kinetics of serially diluted FAM-labeled XQ-2d binding to biotinylated TfR1 immobilized on streptavidin biosensors by BLI. The association phase is illustrated from 0-450 s, whereas dissociation is shown from 450-1350 s (separated by the vertical dotted line). K_D values were calculated by performing a global fit of the multi-concentration kinetic data to a 1:1 binding model. K_D values represent mean ± standard deviation; *n* = 4 individual concentrations of aptamers. (E and F) Competitive binding of 25 nM Cy5-labeled XQ-2d with varying fold-excess of holo-Tf (E) and CD3 or CD71 Ab (F) to Jurkat cells by flow cytometry. Binding was normalized to aptamer-stained controls without holo-Tf or antibody. Data points and error bars represent mean ± standard deviation; *n* = 3 independent experiments. *ns* > 0.05, **P* < 0.05, ***P* < 0.01, ****P* < 0.001 (ordinary two-way ANOVA with Šídák correction). FITC, fluorescein isothiocyanate; Cy5, cyanine 5; FAM, 6-carboxyfluorescein.

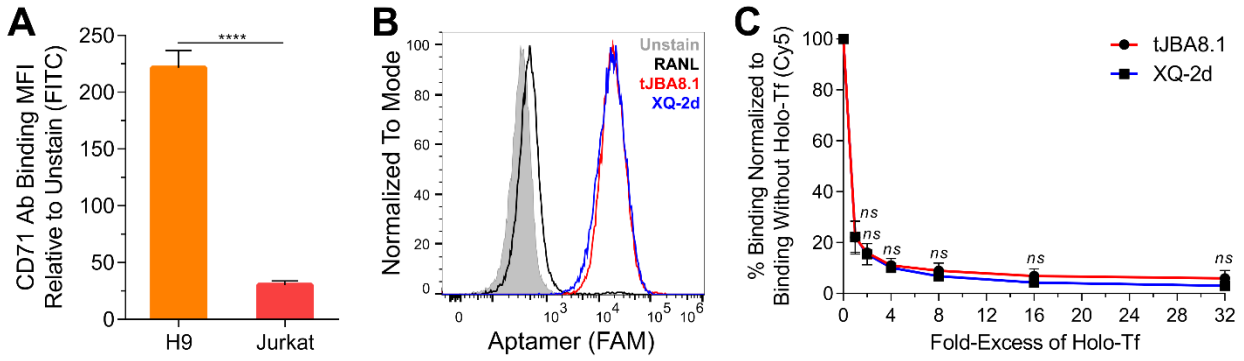

Supplementary Figure 2.7. tJBA8.1 binds TfR1^{hi} H9 cells solely through TfR1. (A) Flow cytometry MFI of FITC-labeled CD71 Ab binding to H9 and Jurkat cells relative to unstained controls. Graph bars and error bars represent mean ± standard deviation; *n* = 3 independent experiments. *****P* < 0.0001 (two-sided unpaired t-test). (B) Flow cytometry histograms of 160 nM FAM-labeled RANL, tJBA8.1, and XQ-2d binding to H9 cells. Histograms are representative of *n* = 1 independent experiment. (C) Competitive binding of 25 nM Cy5-labeled tJBA8.1 and XQ-2d with varying fold-excess of holo-transferrin (holo-Tf) to H9 cells by flow cytometry. Binding was normalized to aptamer-stained controls without holo-Tf. Data points and error bars represent mean ± standard deviation; *n* = 3 independent experiments. *ns* > 0.05 (ordinary two-way ANOVA with Šídák correction). FITC, fluorescein isothiocyanate; FAM, 6-carboxyfluorescein; Cy5, cyanine 5.

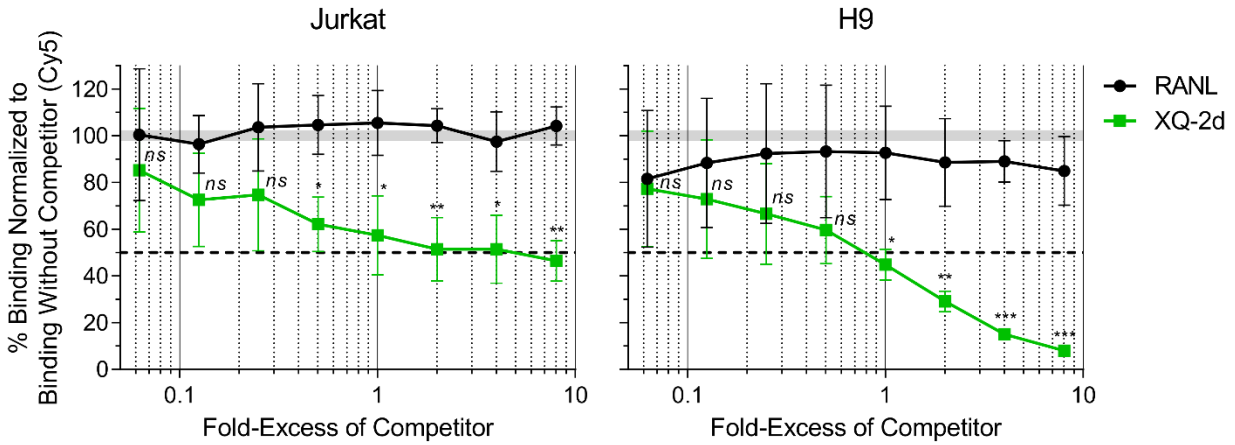

Supplementary Figure 2.8. tJBA8.1 and XQ-2d share a common binding epitope on TfR1. Competitive binding of 25 nM Cy5-labeled tJBA8.1 with varying fold-excess of FAM-labeled RANL and XQ-2d on Jurkat and H9 cells by flow cytometry. Binding was normalized to tJBA8.1-stained controls without competitor. Data points and error bars represent mean ± standard deviation; $n = 3$ independent experiments. *ns* > 0.05, *P < 0.05, **P < 0.01, ***P < 0.001 (ordinary two-way ANOVA with Šídák correction). Cy5, cyanine 5; FAM, 6-carboxyfluorescein.

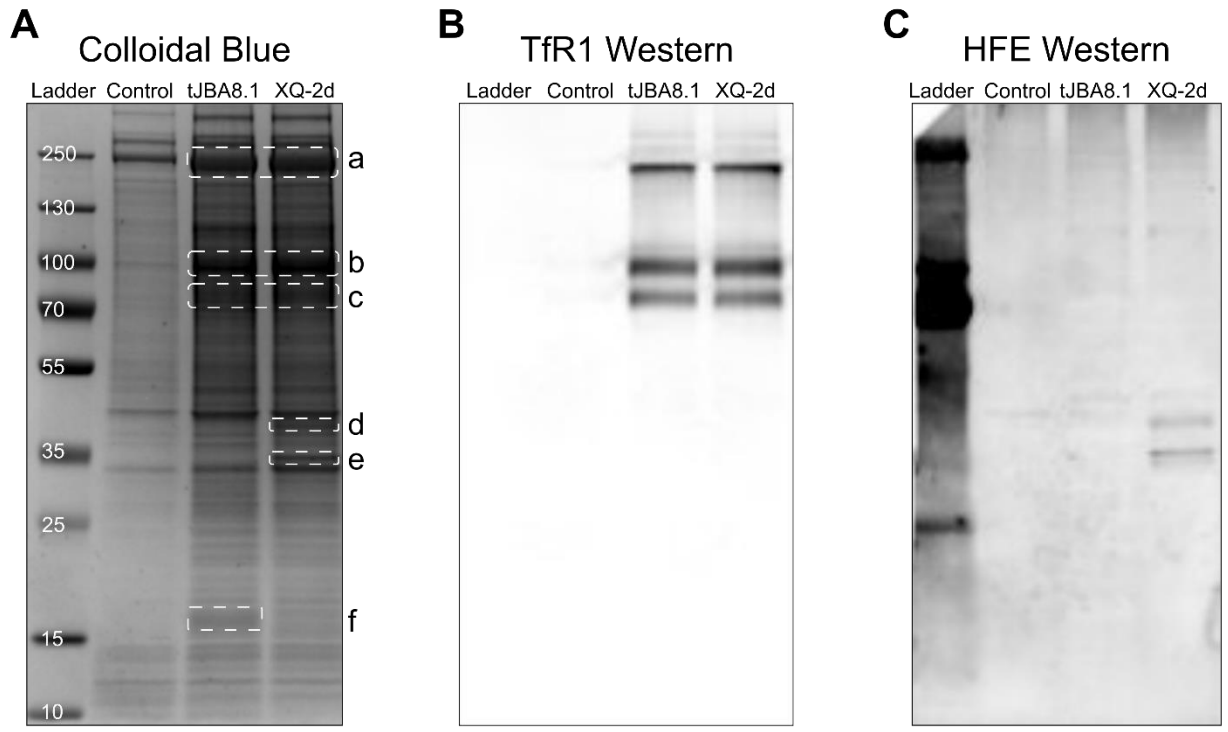

Supplementary Figure 2.9. tJBA8.1 and XQ-2d differentially bind TfR1 with respect to HFE. (A-C) Colloidal blue-stained 4-20% SDS-PAGE gel of Jurkat cell membrane proteins pulled down by tJBA8.1 and XQ-2d (A) and corresponding western blots staining for TfR1 (B) and HFE (C). The control lanes represent proteins captured by biotin-saturated magnetic beads only. Dashed white boxes on SDS-PAGE gel designate prominently enriched proteins, most of which were

identified by western blotting (bands a-e). Band f is identified by mass spectrometry in **Figures S14A**.

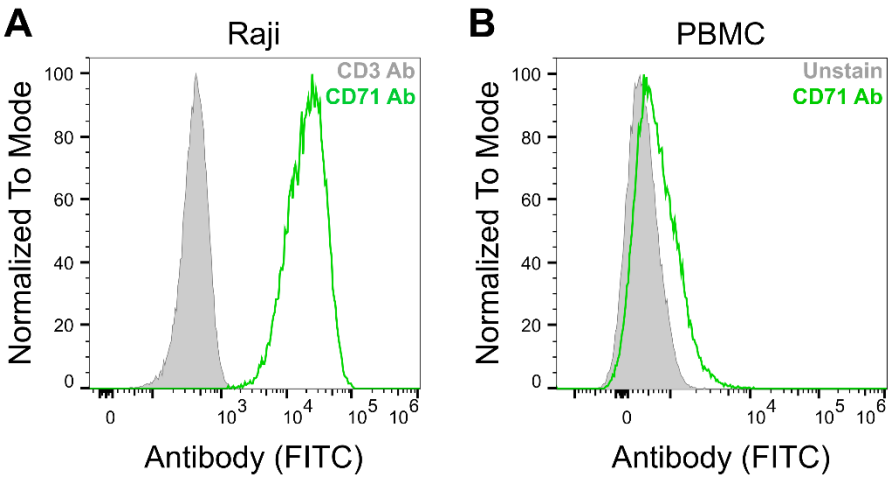

Supplementary Figure 2.10. TfR1 expression distinguishes Raji B-lymphoma cells from healthy PBMCs. (A and B) Flow cytometry histograms of FITC-labeled CD71 Ab binding to Raji cells (A) and healthy donor PBMCs (B). For Raji cells, a FITC-labeled anti-CD3 antibody (CD3 Ab) was used as a negative/isotype control. Histograms are representative of *n* = 1 independent experiment. FITC, fluorescein isothiocyanate.

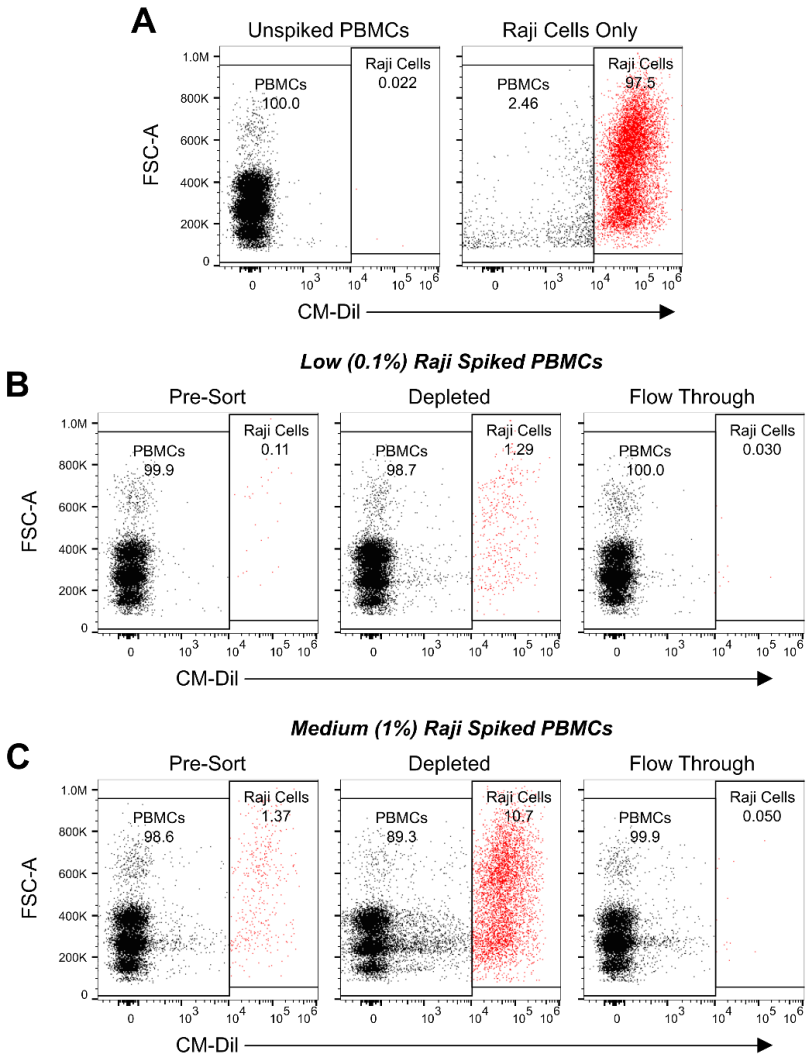

Supplementary Figure 2.11. tJBA8.1 efficiently depletes Raji cells from PBMCs even at low spiked percentages. (A) Flow cytometry plots demonstrating gating strategy for tracking CM-DiI-labeled Raji cells in depletion studies. CM-DiI^{-} unspiked PBMCs and CM-DiI^{+} Raji cells are shown. Plots are representative of n = 3 independent experiments with different PBMC donors. (B and C) Flow cytometry plots of CM-DiI^{+} Raji cell depletion from low (0.1%) (B) and medium (1%) (C) Raji spiked PBMCs. The different cell fractions from the depletion process are shown. Plots are representative of n = 3 independent experiments with different PBMC donors. CM-DiI, chloromethylbenzamido-1,1'-dioctadecyl-3,3,3',3'-tetramethylindocarbocyanine perchlorate.

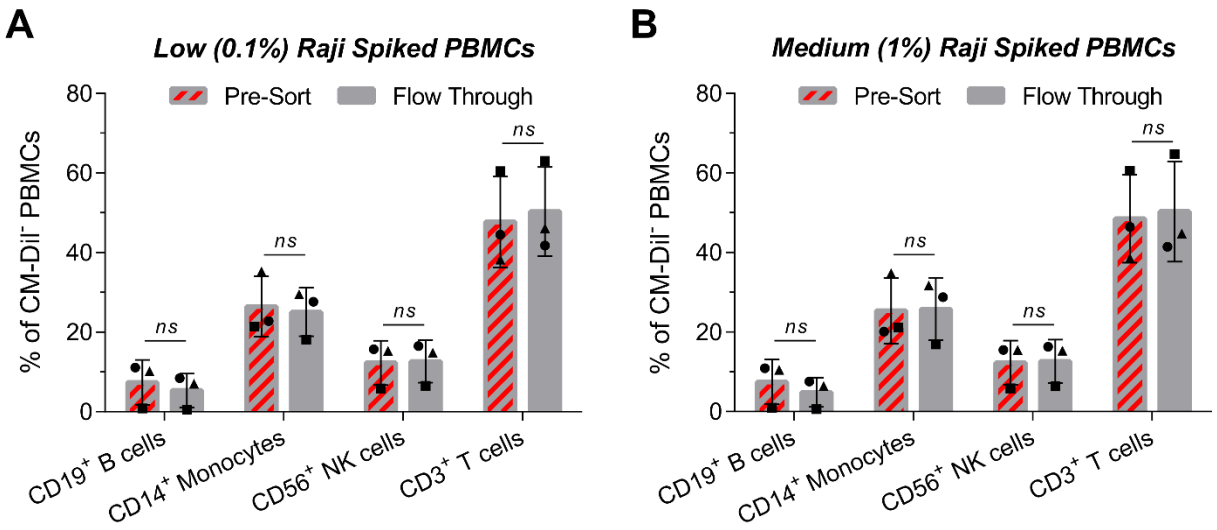

Supplementary Figure 2.12. tJBA8.1-mediated depletion of Raji cells from low and medium spiked PBMCs does not affect the healthy immune cell composition. (A and B) Flow cytometry analysis of the healthy immune cell composition within CM-Dil$^-$ PBMCs before (pre-sort) and after (flow through) Raji depletion from low (0.1%) (A) and medium (1%) (B) Raji spiked PBMCs. The circles, squares and triangles represent different PBMC donors from separate depletion studies. Graph bars and error bars represent mean ± standard deviation; n = 3 independent experiments with different PBMC donors. *ns* > 0.05 (paired two-way ANOVA with Šídák correction). CM-Dil, chloromethylbenzamido-1,1'-dioctadecyl-3,3,3',3'-tetramethylindocarbocyanine perchlorate.

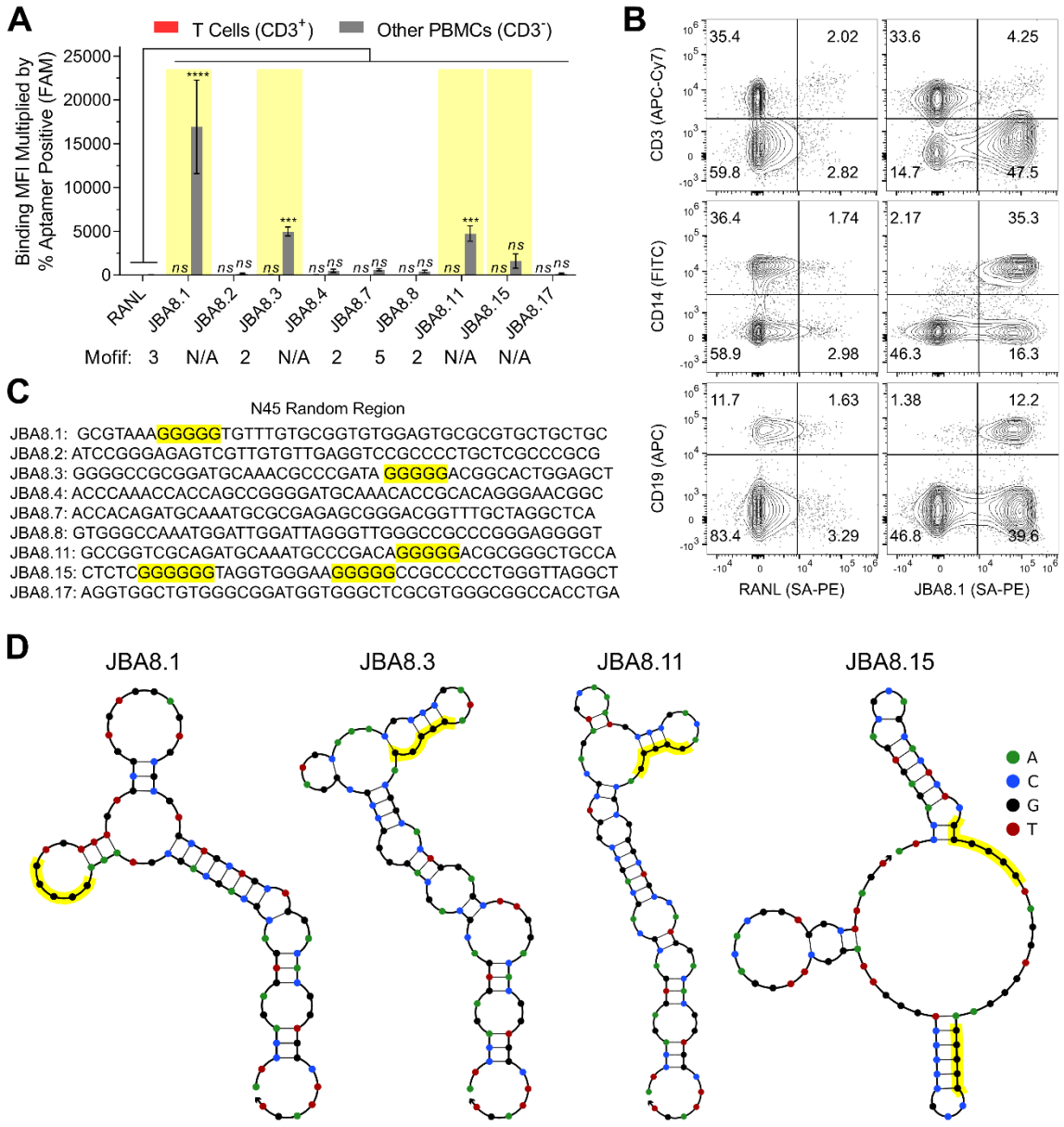

Supplementary Figure 2.13. TfR1-independent binding of tJBA8.1 to PBMCs is likely caused by a G-quintet motif. (A) Binding MFI multiplied by percent positivity of 100 nM RANL and individual aptamers identified from round 8 of cell-SELEX to $CD3^+$ and $CD3^-$ PBMCs by flow cytometry. Aptamers belonging to predicted motifs are indicated. Graph bars and error bars represent mean ± standard deviation; $n = 3$ independent experiments with the same PBMC donor. *ns* > 0.05, ***$P < 0.001$, ****$P < 0.0001$ (ordinary two-way ANOVA with Šídák correction). (B) Flow cytometry plots of PBMCs co-stained with APC-Cy7-labeled CD3, FITC-labeled CD14, and APC-labeled CD19 antibodies and 100 nM biotinylated RANL and JBA8.1 aptamers. Plots are representative of $n = 1$ independent experiment. (C) Random region sequences of individual aptamers identified from round 8 of cell-SELEX. Yellow highlighting indicates G-quintet motifs. (D) MFE structures of JBA8.1, JBA8.3, JBA8.11, and JBA8.15, predicted using NUPACK (temperature = 4 °C; Na^+ = 137 mM; Mg^{2+} = 5.5 mM). Yellow highlighting indicates G-quintet

motifs. FAM, 6-carboxyfluorescein; APC-Cy7, allophycocyanin-cyanine 7; FITC, fluorescein isothiocyanate; APC, allophycocyanin; SA-PE, streptavidin–phycoerythrin.

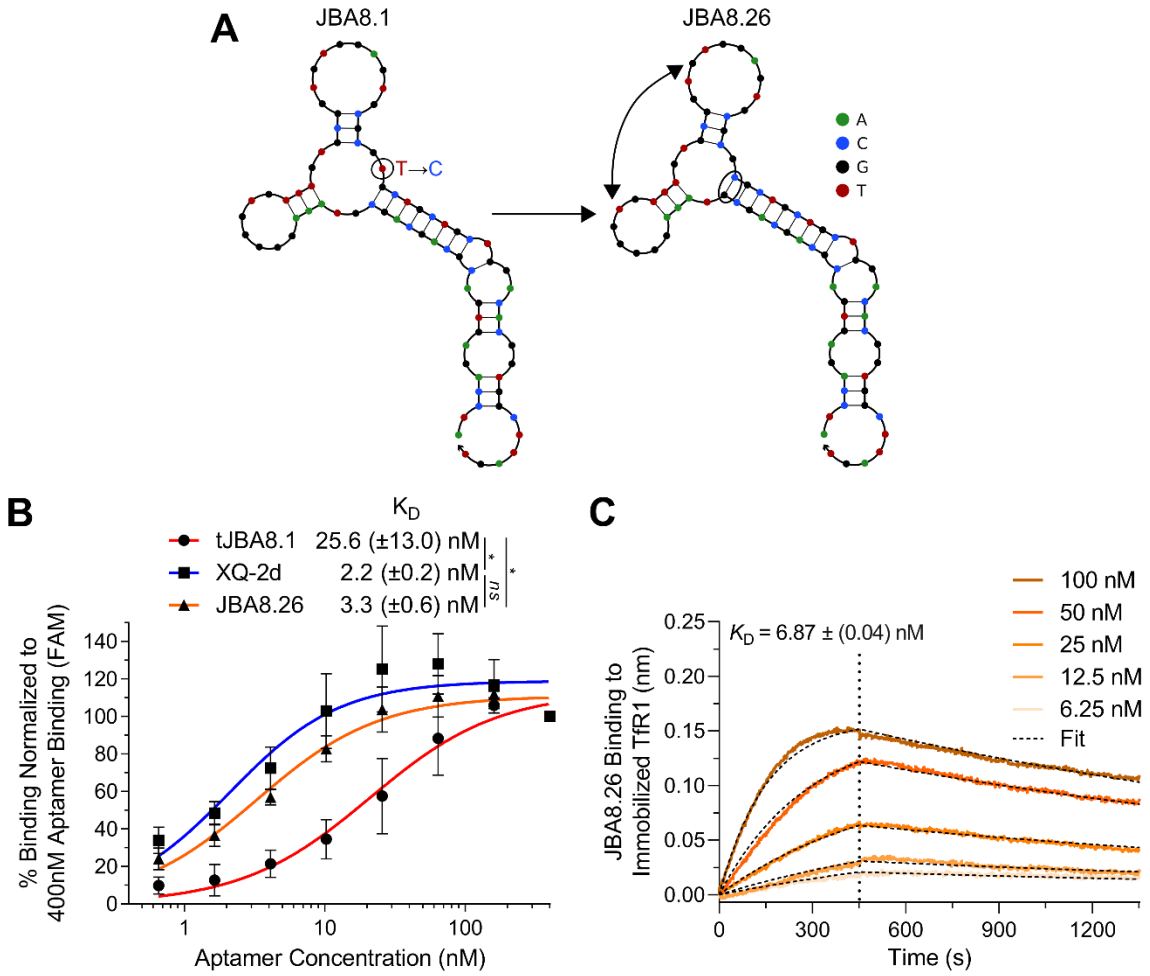

Supplementary Figure 2.14. JBA8.26 is a higher affinity point variant of JBA8.1. (A) MFE structure of JBA8.1 and JBA8.26, predicted using NUPACK (temperature = 4 °C; Na^+ = 137 mM; Mg^{2+} = 5.5 mM). Circles indicate T→C point mutation from original JBA8.1 sequence and subsequent base pairing. The bidirectional arrows call attention to the increased distance between the outbranching hairpins in the JBA8.26 structure. (B) Flow cytometry binding curves of FAM-labeled tJBA8.1, XQ-2d, and JBA8.26 to H9 cells, normalized to 400 nM aptamer binding. The curves represent a nonlinear regression assuming one-site specific binding with Hill slope. K_D values were calculated by averaging the individual regression values of the independent experiments. Data points and error bars, and K_D values, represent mean ± standard deviation; *n* = 3 independent experiments. *ns* > 0.05, **P* < 0.05 (ordinary one-way ANOVA with Tukey correction). (C) Association and dissociation kinetics of serially diluted FAM-labeled JBA8.26 binding to biotinylated TfR1 immobilized on streptavidin biosensors by BLI. The association phase is illustrated from 0-450 s, whereas dissociation is shown from 450-1350 s (separated by the vertical dotted line). K_D values were calculated by performing a global fit of the multi-concentration kinetic data to a 1:1 binding model. K_D values represent mean ± standard deviation; *n* = 5 individual concentrations of aptamers. FAM, 6-carboxyfluorescein.

Chapter 3. Aptamer based traceless multiplexed isolation system for rapid cell purification

Emmeline L. Cheng, Nataly Kacherovsky, Suzie H. Pun

Abstract

Isolation systems that purify cells without masking their receptors with purification agents are necessary in biomedical fields such as cell signaling pathways research and are desirable for clinical adoptive cell therapies. Reported traceless cell isolation methods using engineered antigen binding fragments or aptamers have been limited to processing a single cell type at a time. There remains an unmet need for cell isolation processes that rapidly sort for multiple targets cell types. Here, we utilized two aptamers along with their designated complementary strands (antidotes) to tracelessly isolate two cell types from a mixed cell population with one aptamer labeling step and two sequential cell elution steps with antidotes. We engineered a CD71-binding aptamer (rvCD71apt) and antidote pair to be used simultaneously with our previously-reported traceless purification approach using CD8 aptamer (rvCD8apt) and its antidote. We verified the compatibility of the two aptamer displacement mechanisms by flow cytometry, and the feasibility of incorporating rvCD71apt with a magnetic solid state. We then combined rvCD71apt with rvCD8apt to respectively isolate activated $CD4^+$ T cells and resting $CD8^+$ cells by eluting these target cells into separate fractions with orthogonal strand displacements. This is the first demonstration of isolating different cell types using two aptamers and antidotes at the same time. Potentially, different or more aptamers can be included into this traceless multiplexed isolation system for diverse applications with shortened operation time and lower production cost.

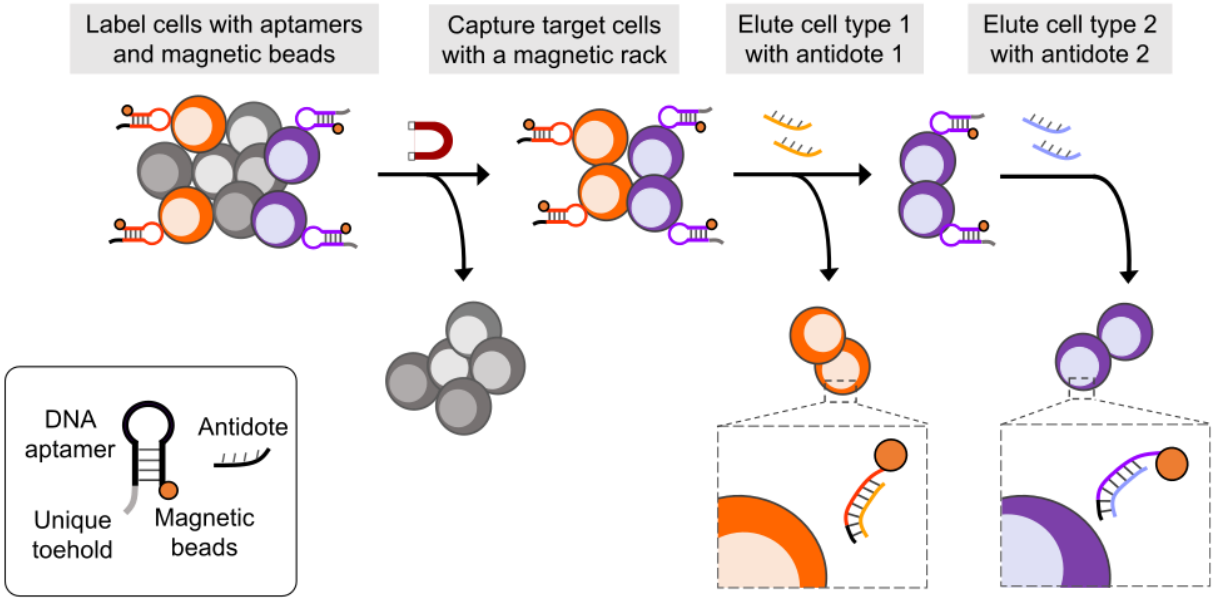

Scheme 3.1. Dual selection workflow.

3.1 Introduction

Immunoaffinity-based cell isolation methods are effective ways to purify specific cell types and include fluorescent-activated cell sorting (FACS)[1], magnetic cell separation[2], and cell affinity chromatography[3,4]. In contrast to separation methods based on physical differences (e.g., size, density) between cells that often result in lower isolation resolution[5,6], immunoaffinity-based methods rely on labeling cell surface proteins with antibodies or antibody fragments to differentiate between cell populations. The labeled cells are then separated from non-labeled cells using solid supports such as magnetic beads or agarose resins. In positive selection strategies, the desired cells are directly labeled for isolation, whereas in negative selection strategies, the undesired cells are labeled for removal from the desired cells. Positive selections usually result in high purity of target cells[7,8] but with certain surface proteins still bound by the ligands and solid supports. Negative selections rely on a panel of antibodies and result in residue-free target cell products but often with reduced purity and yield dependent on sample variability.[9,10] Since the antibodies and solid supports used for isolation can potentially induce unwanted immunogenicity[11], block cell signaling pathways[12], and impact cell proliferation[13], it is desirable for cell therapy applications such as stem cell transplantation[14] and adoptive T cell therapy[15,16] that the isolated

target cells are free of cell labeling materials. Thus, our group and others have focused on developing positive isolation strategies that employ removable selection agents.[17]

Fab-Streptamer is a "quasi-traceless" protein-based isolation system using modified Fabs (antigen binding fragments) that have lower binding affinity to targets when applied as monovalent form and have higher affinity as multivalent complexes. Fabs fused with Strep-Tag peptides[18,19] will form tetramers in the presence of Strep-Tactin[20], a mutated streptavidin, through non-covalent interaction. The interaction between Fab-Strep-Tag and Strep-Tactin is reversable upon competition with high affinity D-biotin for Strep-Tactin binding. Upon release from Strep-Tactin, the monovalent Fab has reduced affinity for target and will then separate from the target spontaneously. This technology has been used to purify proteins[21], as well as to isolate cells in clinical adoptive cell therapy manufacturing[4,22–24]. However, D-biotin is a universal target releasing agent in this system. Isolating multiple cell types with Fab-Streptamer is therefore a time-consuming process that requires repeated staining and dissociating steps for different targets.

Gao and coworkers developed a DNA nanotechnology method for reversible antibody labeling and sorting of targets by functionalizing antibodies with DNA oligonucleotides consisting of a toehold for on-demand displacement and a targeting probe for anchoring onto the solid state.[25] Multiple targets can be captured using an antibody cocktail with subsets subsequently recovered by sequence-dependent strand displacement initiated at the toehold domain to detach antibodies from solid supports. This approach has been applied to isolate multiple immune cell types from mouse splenocytes with high purity.[26] This elegant approach allows fast sequential isolation of multiple cell types with a single staining step, but the end product still bound by antibodies. In addition, antibodies are a relatively costly and thermosensitive reagent.

Aptamers are short, folded single-stranded DNA or RNA oligonucleotides that bind to a wide range of targets including cell surface protein receptors. Typically selected from *in vitro* library screening, aptamers have comparable affinity and specificity, but have the benefits of reversible binding, lower production cost, faster and more consistent manufacturing process compared to their protein counterparts, antibodies.[27–29] Aptamer binding can be reversed either by universal reagents, such as DNases, ion chelators, and competitors,[30–32] or by complementary nucleic acid strands, also called antidotes. When the antidote anneals to portions of the aptamer, part of the folded aptamer may be displaced, losing its structure essential for binding. This unique

characteristic of aptamers has been utilized in various applications. For example, the Ch-9.3t RNA aptamer which serves as an anticoagulant by targeting factor IXa, can be neutralized using a modified RNA antidote complementary to its loop structure.[33] Another example is E07, an EGFR targeting RNA aptamer that was incorporated into FACS and MACS (magnetic-activated cell sorting) systems to isolate $EGFR^+$ epidermoid carcinoma cells. These $EGFR^+$ target cells were incubated with E07 antidote for aptamer removal, and were suitable for downstream studies on EGFR-related pathways.[34] One can also design highly effective antidotes by implementing an overhang sequence, also referred to as a toehold, on either the 5'- or 3'-end of the aptamer. With the assistance of toehold-initiated annealing, the strand displacement rate constant can be significantly increased.[35,36] For example, we previously developed a CD8 receptor-binding aptamer, A3t, with an 8 nucleotides (nt) toehold for isolating $CD8^+$ T cells from PBMCs. With 20 minutes of incubation using antidote at room temperature, over 90% of the DNA aptamer is removed from cells. The isolated $CD8^+$ T cells are free of labeling materials and are ideal for manufacturing adoptive cell therapeutic products.[16]

The goal of this study is to demonstrate isolation of multiple cell types from a single selection process by using multiple aptamers paired with their antidotes. To achieve this goal, we introduced different DNA toeholds into two targeting aptamers so that two cell types can be captured together upon aptamers binding and then sequentially eluted with antidotes. Aptamers tolerate sequence modifications at the regions not essential for receptor binding. We first modified an existing CD71-binding aptamer, JBA8.1, to carry a suitable toehold and a displaceable stem structure for antidote annealing and branch migration. The new variant was named as rvCD71apt (reversible CD71 aptamer). The corresponding antidote was optimized to achieve robust strand displacement. When immobilized on magnetic beads, the rvCD71apt/antidote pair separate cells from bulk-stimulated PBMCs into different fractions based on their CD71 expression level. We next combined rvCD71apt with a previously reported CD8 aptamer used for cell isolation, A3t (renamed as rvCD8apt, reversible CD8 aptamer)[16], as a traceless multiplex cell sorting system for purifying activated $CD4^+$ T cells and resting $CD8^+$ cells. In the future, this isolation system can be expanded to incorporate different and/or more aptamers and antidote pairs and applied to various types of solid supports for diverse applications.

3.2 Materials and methods

3.2.1 Cell preparation

Jurkat cell (human T-ALL) culture was maintained in RPMI 1640 media (Corning) supplemented with 10% FBS (fetal bovine serum, Life Tech). Primary human PBMCs were Ficoll-enriched from apheresis product purchased from Bloodworks Northwest. $CD4^+$ T cell and $CD8^+$ T cell subsets were isolated from PBMCs using negative cell isolation kits (Miltenyi) to obtain cells without antibody and magnetic bead labeling. T cells were stimulated with recombinant cytokines (Miltenyi) and CD3/CD28 stimulation Dynabeads (Invitrogen) on day 0. $CD4^+$ T cell culture media was consisted of RPMI 1640 media with 10% FBS, 5 ng/mL IL-7, and 0.5 ng/mL IL-15. Whereas CD8+ T cell culture media was consisted of RPMI 1640 media with 10% FBS, 20 ng/mL IL-2, and 0.5 ng/mL IL-15. Unless stated otherwise, the stimulation beads were removed by pipetting cells with p1000 tips and separated on a magnetic rack on day 9. The cells were kept in the complete culture media containing cytokines for expansion until day 21. For bulk-stimulated PBMCs, the T cell fraction in PBMCs was used to calculate the amount of stimulation beads and cytokine needed.

3.2.2 Flow cytometry and staining reagents

The following live/dead staining dye and antibodies were used for staining cells: Zombie Violet (1:500 in 100 µl containing 10^6 cells, BioLegend), FITC-antihuman CD71 (1:100, BioLegend, CY1G4), Super Bright 702-antihuman CD56 (1:100, Invitrogen, TULY56), APC-Cy7-antihuman CD14 (1:200, Molecular probes, 6ID3), Super Bright 600-antihuman CD19 (1:100, Invitrogen, SJ25C1), PE-antihuman CD3 (1:100, BioLegend, HIT3a), APC-antihuman CD8a (1:100, BioLegend, RPA-T8), FITC-antihuman CD8a (1:100, BioLegend, RPA-T8), APC-Cy7-antihuman CD4 (1:100, BioLegend, RPA-TA), FITC-streptavidin (1:500, BioLegend), Alexa Fluor 647-streptavidin (1:500, BioLegend), and PE-streptavidin (1:500, BioLegend).

In the aptamer staining process, wash buffer and binding buffer were used for washes and staining. Wash buffer, which contains 137 mM Na^+ and 5.5 mM Mg^{2+}, was made with 500 mL DPBS (with calcium and magnesium, Corning) plus 2.5 mL1 M $MgCl_2$ (Fisher) and 2.25 g D-

glucose (Sigma-Aldrich). Binding buffer was made of wash buffer supplemented with 0.1 mg/mL yeast tRNA (Invitrogen) and 1% BSA (Miltenyi), unless stated otherwise. Aptamers were labeled with either FAM fluorophore (6-carboxyfluorescein) or biotin. To anneal aptamers, the DNA was adjusted to 1 µM in wash buffer and heated at 95 ^{o}C for 5 minutes followed by snap chilling on ice for at least 15 minutes. The cell staining process was kept at 4 ^{o}C to avoid aptamer internalization. RAN aptamer, a sequence that does not bind to any target cell types in this study, was used as control. The cell-associated fluorescence from aptamer binding was analyzed with an Attune NxT cytometer (Invitrogen).

3.2.3 Oligonucleotide design

The customed oligonucleotides used in this study, including aptamers and antidotes were ordered from Integrated DNA Technology (IDT). Modifications of JBA8.1 was done partially with NUPACK web application for simulating aptamer and antidote-annealed aptamer structures when sequences folded into their thermally stable structures.[37] The parameter settings for simulating annealed aptamer structures were 137 mM Na^{+} and 5.5 mM Mg^{2+}, and temperature at 4 ^{o}C. The settings for antidote annealing were the same cation concentrations, with temperature at 25 ^{o}C.

3.2.4 Antidote displacement

The cells were stained with targeting aptamers, and then washed with wash buffer to remove unbound aptamers. Based on the previously optimized aptamer displacement conditions,[16] we used 100x concentration of antidotes (e.g., applying 100 nM antidote to cells stained with 1 nM aptamer) for incubations at room temperature for 10-20 minutes.[16] The antidotes were first heated at 37 ^{o}C in water bath for 5 minutes, and then applied to the aptamer-stained cells. After washing off the displaced DNA strands, the remaining aptamer binding was evaluated by flow cytometry.

3.2.5 rvCD71apt aptamer cell sorting with MACS

Bulk-stimulated PBMCs were used in the rvCD71apt MACS (Miltenyi) cell sorting studies. Cells were activated using the method described in section 3.2.1 on day 0. The CD3/CD28 stimulation beads were removed on day 3 by a magnetic rack. 50 million stimulated PBMCs were first applied to an LS column (Miltenyi) anchored on a magnetic separator (Miltenyi) to remove cells with residual stimulation beads. The resulting cells were stained with 1 mL 40 nM biotinylated aptamer in wash buffer with 0.5% BSA and 1 mg/mL tRNA for 30 minutes at 4 ^{o}C. After staining, the cells were washed and labeled with 150 µL anti-biotin Microbeads (Miltenyi) in the same buffer with 15 minutes incubation at 4 ^{o}C. 30 µL of anti-biotin Microbead stock solution was used for every 10 million total cells. The labeled cells were spun down and resuspended in buffer to remove excess beads. In the meantime, an LS column was rinsed with wash buffer containing 0.5% BSA and 1 mg/mL tRNA to reduce non-specific interactions. After the labeled cells were applied to the column for isolation, the column was washed 3 times with wash buffer containing 0.5% BSA. 1 mL of 4 µM pre-warmed antidote (100x) was then applied to the column. An initial 600 µL of antidote solution was passed through the column and the remaining volume was trapped in the column with a Luer lock plug. The antidote solution was incubated in the column for 10 minutes at room temperature, after which the plug was removed, and the column was washed 3 times for cell collection. The remaining cells that were not eluted by antidote displacement, was collected by taking the LS column off the magnetic separator and flushed with wash buffer with a plunger. The CD71 expression and cell type of the isolated cells in each fraction were evaluated by antibody staining and flow cytometry.

3.2.6 Removing un-eluted cells with dextran sulfate

Activated $CD4^{+}$ T cells were isolated and cultured using the method described in section 3.2.1. Resting $CD8^{+}$ T cells were isolated using the method described section 3.2.1. Both cell types were first stained with Zombie Violet live/dead staining dye, followed by 60 nM biotinylated rvCD71apt or 5 nM biotinylated rvCD8apt labeling (0.2 million cells in 100 µL binding buffer) for 20 minutes at 4 ^{o}C. The surface bound biotinylated aptamer was then labeled with secondary staining, streptavidin-AF647, at 4 ^{o}C for 15 minutes. The cells were washed and incubated in dextran sulfate (6.5-10 kDa, Sigma Aldrich) dissolved in wash buffer with 0.5% BSA at 0, 0.16, 0.31, 0.63, 1.25, 2.5, 5, 10, and 12 mM at room temperature for 20 min, with or without 6 µM

rvCD71apt antidote or 0.5 μM rvCD8apt antidote. The cells were washed, fixed with wash buffer with 1% BSA and 0.1% PFA (paraformaldehyde), and then analyzed by flow cytometry. The AF647 fluorescence associated with cells due to aptamer binding was normalized to the control group without dextran sulfate and the antidotes.

3.2.7 Traceless multiplexed cell isolation with serial antidote elution

About 45-50 million pre-sort cells consisting of activated $CD4^+$ T cells and PBMCs were washed with DPBS and 0.5% BSA and resuspended in 900 μL binding buffer. In this mixed cell population, the $CD4^+CD71^+$ cells (activated $CD4^+$ T cells) are rvCD71apt target cells, while the $CD8^+$ cells (mostly resting $CD8^+$ T cells) are rvCD8apt target cells. This mixed population was pre-cleared using 1 mg MyOne Streptavidin C1 Dynabeads (Invitrogen) to remove non-specific binding cells by incubation at room temperature for 20 minutes, followed by bead removal using a magnetic rack (MagRack 6, GE). The cleared cells were set on ice during beads preparation. To prepare the isolation beads, 0.64 mg Dynabeads were washed and resuspended in 640 μL wash buffer with 0.5% BSA and 0.1 mg/mL yeast tRNA. The beads were incubated in the buffer for at least 20 minutes at 4 ^oC to reduce non-specific interaction. 0.6 mg Dynabeads were transferred into 500 μL of 60 nM biotinylated rvCD71apt in wash buffer with 0.5% BSA and 0.1 mg/mL yeast tRNA. The remaining 0.04 mg Dynabeads were transferred into 500 μL of 5 nM biotinylated rvCD8apt in the same buffer. These streptavidin beads were incubated with the biotinylated aptamers for 15 minutes at 4 ^oC for aptamer immobilization to take place. The aptamer-labeled beads were washed and resuspended in 50 μL wash buffer with 0.5% BSA and 0.1 mg/mL yeast tRNA.

To isolate the target cells, the aptamer-beads were incubated with the cleared cells for 30 minutes at 4 ^oC and separated on the magnetic rack. The cell-aptamer-bead complex was applied to the magnetic rack to isolate the bead-labeled target cells. The unbound cells were removed by gentle washing. The rvCD71apt antidote (1 mL of 6 μM) in wash buffer with 0.5% BSA was pre-heated at 37 ^oC, and then applied to the cell-aptamer-bead complex. The solution was incubated at room temperature for 20 minutes on rotation to displace rvCD71apt. The beads were then thoroughly washed to collect the activated $CD4^+$ T cells. Next, 10 mM dextran sulfate was applied

for 20 min at room temperature to wash off the un-eluted activated $CD4^+$ T cells. After rinsing dextran sulfate off the cells with wash buffer 0.5% BSA, the solution of 0.5 μM rvCD8apt antidote in 1 mL wash buffer containing 0.5% BSA was applied for 15 minutes at room temperature and then collected with through washing. The remaining cells were collected along with the magnetic beads. All incubations were done in DNA lo-bind tubes (Fisher) on rotation. The washing steps implemented between each incubation procedure were done by using wash buffer and 0.5% BSA. The cell compositions collected in each step were evaluated by flow cytometry after staining with human CD71, CD4, and CD8 antibodies.

The purity of target cells collected in the antidote elution steps is the percentage of cells within the population gates. rvCD71apt target cells were gated on $CD4^+CD71^+$ cells. rvCD8apt target cells were gated on $CD8^+$ cells. The yield of the target cells is defined as the target cell number counted in the antidote elution steps divided by total target cell number counted in the pre-clearing, antidote elution, dextran sulfate wash steps, as well as the number of cells that were not captured by the aptamers and were not eluted by the antidotes.

3.2.8 Statistical analysis

Data are shown as mean ± s.d of 3 biological replicates unless stated otherwise. Two-tailed unpaired t test was used to compare two populations. If there were more than two populations, one-way ANOVA was used to test the hypothesis. Tukey's test was used for multiple comparison in which every mean was compared to every other means. If $P < 0.05$ after adjustments, the difference is considered significant. Graphing and statistical analysis was performed on GraphPad Prism 6 for Windows, version 6.01.

3.3 Results

3.3.1 Modification of CD71-binding aptamer to achieve multiplexed cell sorting

In order to isolate two cell populations from a single aptamer-based selection procedure, we need two aptamers that can be specifically reversed by their antidote sequences. We selected two previously reported aptamers from our group: JBA8.1, a CD71 (also called transferrin receptor

1)-binding aptamer, and A3t, a CD8 receptor-binding aptamer.[16] To elute target cells from these individual aptamers, we require complementary strands (antidotes) that specifically reverse the folded structure of corresponding aptamer sequences. JBA8.1, however, shares overlapped sequences in its stem structure with A3t, renamed to rvCD8apt (reversible CD8 aptamer) for this work (**Supplementary Figure 3.1A**). Therefore, the rvCD8apt antidote is expected to interfere with JBA8.1 by annealing near its 3'-end (**Supplementary Figure 3.1B**). We confirmed that rvCD8apt antidote reverses binding of both rvCD8apt (**Supplementary Figure 3.1C**) and JBA8.1 (**Supplementary Figure 3.1D**) to their receptors using flow cytometry with apheresis cells containing the target cells of both aptamers. According to the 2-dimentional DNA structure simulations and flow cytometry results, the crucial binding structure of JBA8.1 is susceptible to the annealing of a 14 nt sequence (GGACACGGTGGCTT) near its 3'-end to the rvCD8apt antidote. Therefore, we made distinctive changes in the stem region of JBA8.1, which was highly similar to the one of rvCD8apt, by mutating 17 bases (**Figure 3.1A, red**). Changing these sequences also de-stabilized the overall structure of JBA8.1 by increasing the free energy of DNA folding from -27.08 kcal/mol to -22.71 kcal/mol which is expected to increase the possibility of branch migration. Toehold annealing is an effective way to initiate strand displacement of oligonucleotides in a controlled manner.[35,38,39] To implement a toehold domain, we removed the 5'- and 3'-overhang sequences, and added an 8 nt unique toehold to the 3'-end of the JBA8.1 (**Figure 3.1A, blue**). This new variant was named rvCD71apt (reversible CD71 aptamer). Compared to JBA8.1, rvCD71apt showed higher binding affinity to CD71 expressing Jurkat cells, with apparent K_D around 35.2 nM (**Figure 3.1B**). More importantly, rvCD71apt is resistant to rvCD8apt antidote annealing. When treated with 100x molar excess rvCD8apt antidote, rvCD71apt binding showed no significant difference in binding to $CD71^+$ Jurkat cells compared to the control group without antidote incubation (**Figure 3.1C**).

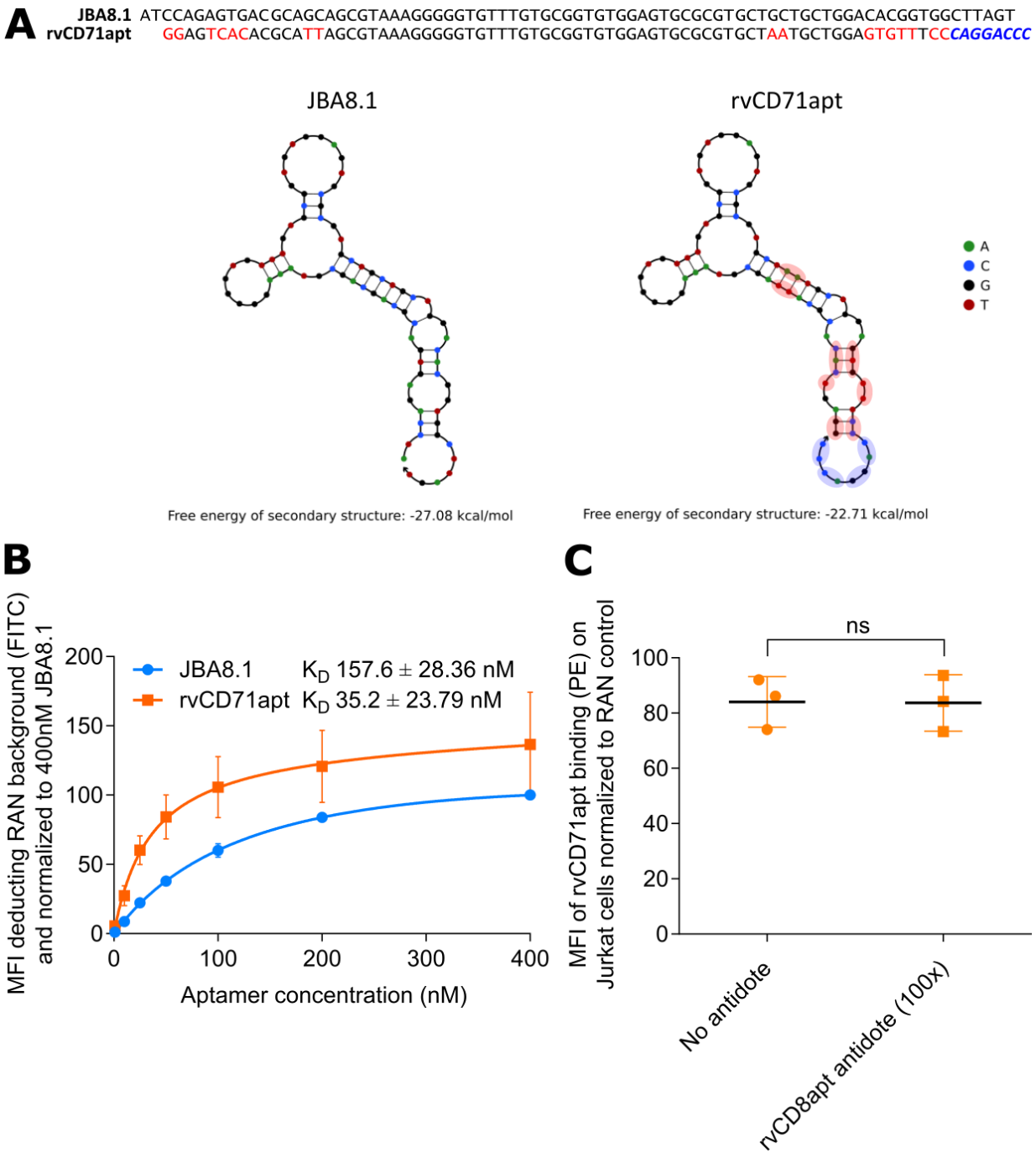

Figure 3.1. rvCD71apt design. (A) JBA8.1 sequence modification. Red font color on the sequence and red shading on the 2-dimentional structure indicate the changed sequences. Blue font color and blue shading indicate the added toehold. (B) Flow cytometry binding study using Jurkat cells. Aptamers were modified with biotin and labeled with secondary Streptavidin FITC staining. Data are shown as mean ± s.d., n = 3. (C) Flow cytometry binding study of rvCD71apt with or without the presence of rvCD8apt antidote. Jurkat cells were stained with 20 nM rvCD71apt, followed by Streptavidin PE labeling, and 2 μM (100x) rvCD8apt antidote incubation at room temperature. Data are shown as mean ± s.d., n = 3, ns (two-tailed unpaired t-test, P = 0.9659). Each point

represents one independent biological repeat. MFI: median fluorescence intensity; FITC: fluorescein isothiocyanate; PE: phycoerythrin.

3.3.2 Optimization of antidote and toehold sequence for rvCD71apt

Next, we optimized the rvCD71apt system for reversibility by testing different antidotes and different G-C content in the aptamer toehold sequences. Antidotes with various lengths (21, 28, 33, and 51 nt) were designed for branch migration from the toehold placed on the 3'-end to various sites on rvCD71apt (**Figure 3.2A, Supplementary Table 3.1**). We labeled Jurkat cells with rvCD71apt and then incubated labeled cells with antidote (100x aptamer) at room temperature. The 33 nt antidote, which theoretically reaches the branched loop, showed the highest displacement with 71.9% aptamer binding reduction. Interestingly, the 51 nt antidote, which has 18 extra bases on top of the 33 nt antidote sequence, only showed 44.5% reduction on aptamer binding fluorescent intensity (**Figure 3.2A**). Although longer antidote strands have lower theoretical binding free energies[35], the 51 nt antidote might be blocked by steric hindrance on the protein-aptamer complex. Potential conformational changes[40] in CD71 protein or in rvCD71apt itself are also factors that are unaccounted by the 2-dimentional DNA structure simulation.

We next explored the impact of G-C content in the aptamer toehold sequence on strand displacement efficacy. Toeholds with higher G-C content favor faster annealing rate of complementary strands due to their lower binding free energy.[35] We designed three rvCD71apt sequences containing 8 nt toeholds with different G-C content (**Figure 3.2B)** and tested the aptamers for binding to Jurkat cells followed by antidote-mediated reversal using their corresponding 33 nt antidotes. Unexpectedly, we did not observe better strand displacement from the cells using higher G-C content toeholds (**Figure 3.2C)**. It is likely that the incubation time, antidote concentration, and temperature we applied in this experiment was sufficient for maximum antidote annealing to take place, negating any effect from the G-C pairs. In addition, swapping out different toehold sequences did not alter the binding of rvCD71apt significantly when staining cells with a fixed concentration at 20 nM. However, as rvCD71apt with 1 and 3 GC in the toehold sequence showed lower mean binding fluorescence intensity than rvCD71apt with 6 GC toehold (**Figure 3.2D**), we continued the study using rvCD71apt with the 6 GC toehold as shown in **Figure 3.1A**.

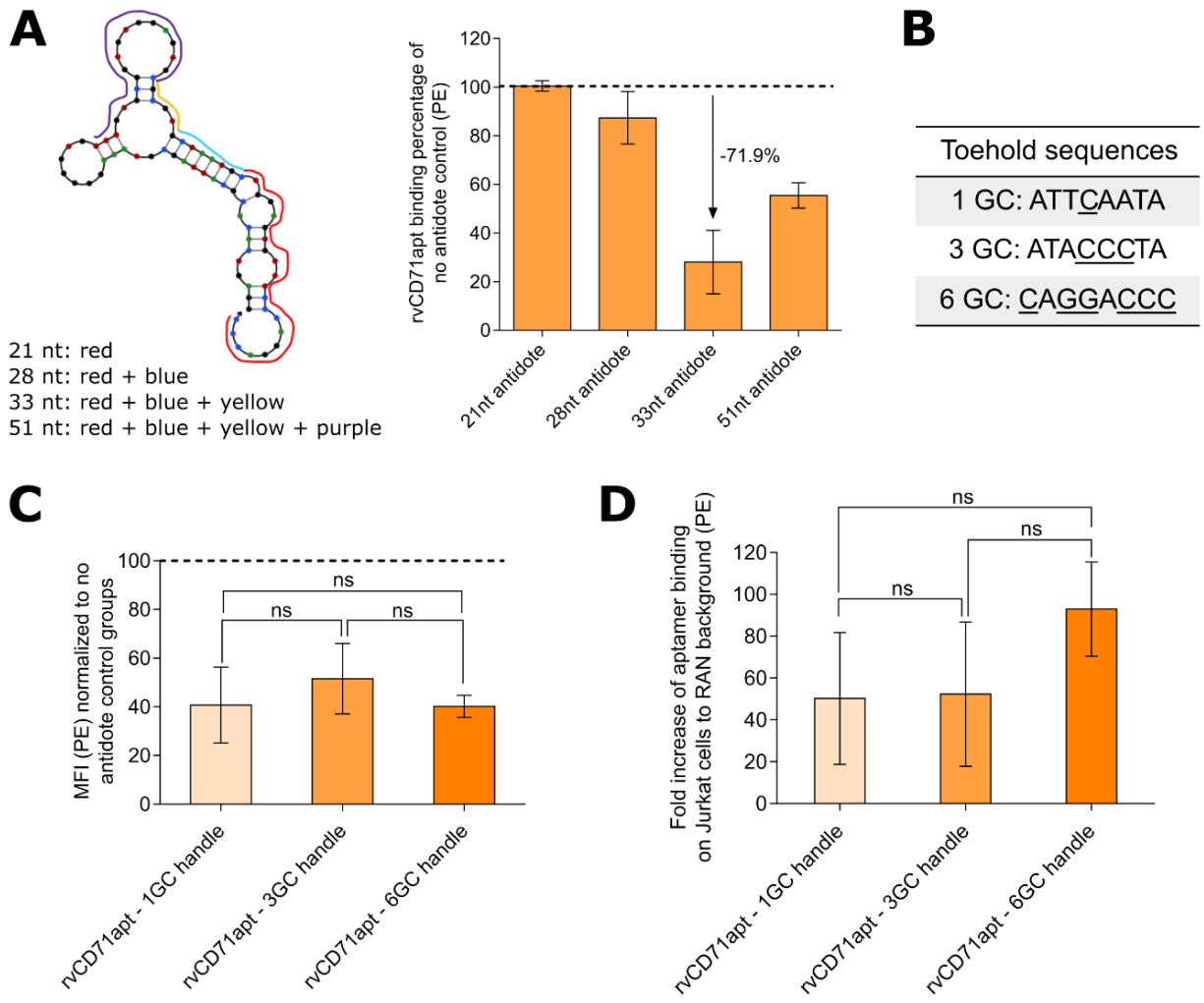

Figure 3.2. rvCD71apt toehold and antidote optimization evaluated by flow cytometry. (A) Jurkat cells were stained with 20 nM of rvCD71apt and displaced with 2 µM (100x) antidotes with lengths of 21, 28, 33, 51 nt. Dotted line indicates 100% aptamer binding without antidote incubation. Data are shown as mean ± s.d., n = 3. (B) Toehold sequences with various G-C contents were designed and placed at the 3' end of rvCD71apt. (C) 2 µM of the corresponding 33 nt antidotes were applied to Jurkat cells labeled with 20 nM rvCD71apt carrying various G-C content toeholds. Dotted line indicates 100% aptamer binding without antidote incubation. Data are shown as mean ± s.d., n = 3, ns (one-way ANOVA with Tukey's test, $P > 0.05$). (D) Normalized MFI value of rvCD71apt containing different toeholds binding to Jurkat cells. Data are shown as mean ± s.d., n = 3, ns (one-way ANOVA with Tukey's test, $P > 0.05$). MFI: median fluorescence intensity; PE: phycoerythrin; nt: nucleotides.

3.3.3 Compatibility of rvCD71apt and rvCD8apt aptamer/antidote

The compatibility between rvCD71apt, rvCD8apt, and their corresponding antidote sequences is crucial for isolating target cells at high purity with sequential elution. We evaluated

sequence-specific displacement by the two antidotes using flow cytometry. We previously demonstrated that rvCD8apt with its antidote can be used for traceless isolation of $CD8^+$ T cells.[16] rvCD71apt targets CD71 receptor, which is expressed by proliferating, activated T cells but not by resting T cells.[41] rvCD71apt binds with high affinity to both activated $CD4^+$ and $CD8^+$ T cells, with apparent K_D around 28.5 nM and 35 nM, respectively (**Figure 3.3A and 3.3B**). Therefore, we evaluated sequence-specific antidote displacement by staining a mixed population containing activated $CD4^+$ T cells and resting $CD8^+$ T cells with 20 nM rvCD71apt and 5 nM rvCD8apt, followed by antidote displacement. We used 20 nM rvCD71apt, a concentration close to its apparent K_D, to ensure sufficient labeling on activated $CD4^+$ T cells while avoiding non-specific binding. 5 nM rvCD8apt was used in this staining procedure since it was previously shown to be adequate in a cell isolation procedure.[16] Application of a single antidote specifically reduced binding of the target aptamer without affecting the other aptamer sequence. Application of both antidotes simultaneously successfully removed binding of both aptamers from their target cells. These results show that the rvCD71apt antidote and rvCD8apt antidote can target their respective aptamer without interfering the other aptamer sequence. It is also encouraging that the two antidotes showed complementary displacement without non-specific annealing even when incubated at high concentration in the same well (2 µM rvCD71apt antidote; 0.5 µM rvCD8apt antidote) (**Figure 3.3C**).

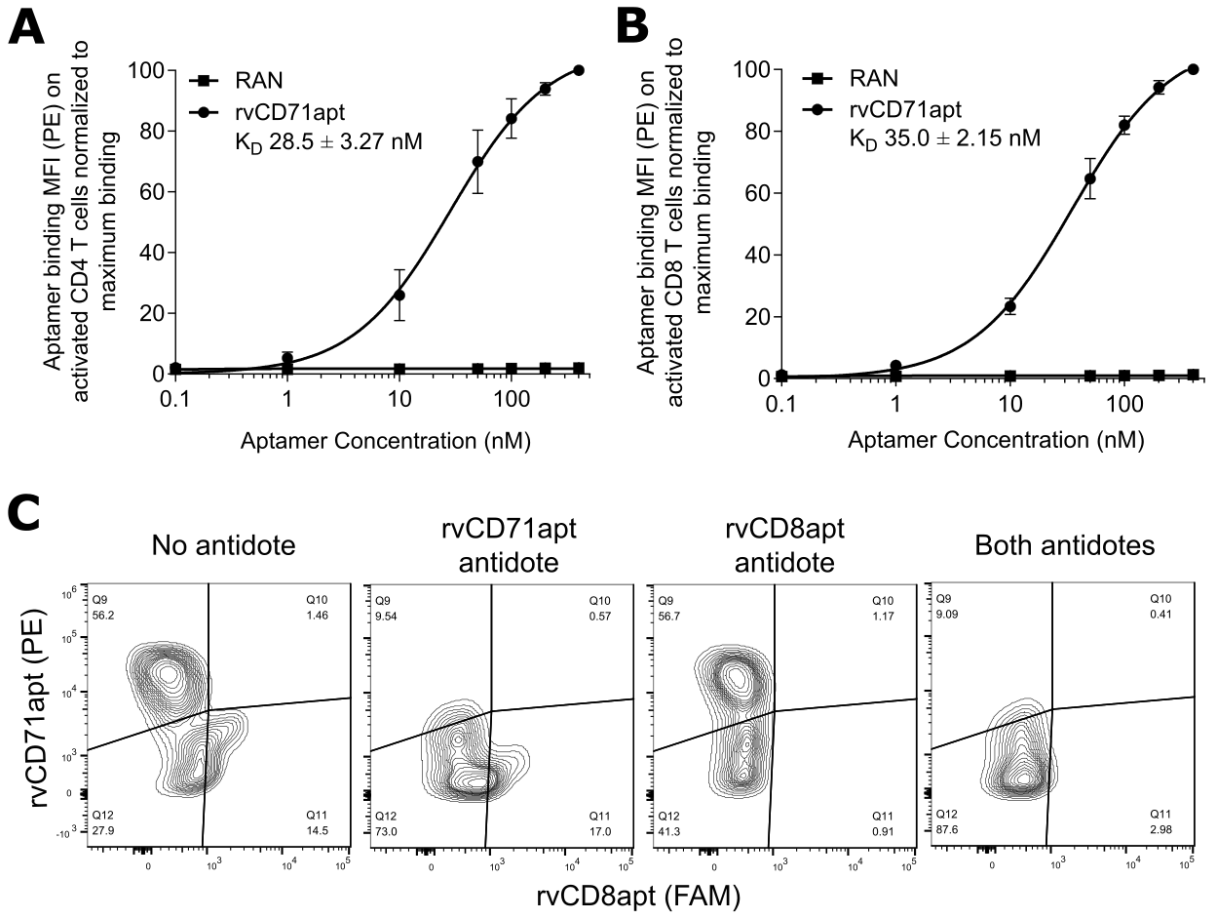

Figure 3.3. Antidote-specific reversal of aptamer binding. rvCD71apt binding on (A) activated $CD4^+$ T cells and (B) $CD8^+$ T cells using biotinylated aptamers followed by streptavidin-PE staining. Data are shown as mean ± s.d., n = 3. (C) Evaluation of antidote-specific removal of bound aptamer. $CD4^+$ T cells and resting $CD8^+$ T cells were mixed together and stained with both 20 nM PE-labeled rvCD71apt and 5 nM FAM-labeled rvCD8apt (left-most panel). Application of rvCD71apt antidote (second panel from left) or rvCD8apt antidote (third panel from left) selectively reduces aptamer labeling in target cells. Application of both antidotes reduces binding in both populations (right-most panel). Streptavidin-PE was used as secondary staining. 100-fold excess antidote were incubated with stained cells. MFI: median fluorescence intensity; FAM: 6-carboxyfluorescein; PE: phycoerythrin.

3.3.4 rvCD71apt and antidote separates PBMCs into cell populations base on CD71 expression level

We incorporated rvCD71apt and its antidote into the MACS® system (Miltenyi) cell isolation, which utilizes superparamagnetic particles to anchor ligand-labeled cells in a column applied with magnetic field. We previously used MACS with aptamer labeling for isolating $CD8^+$ T cells at

high purity.[16] Therefore, we chose this system to test the feasibility of cell isolation with rvCD71apt.

To generate cells for sorting, we treated bulk PBMCs with cytokines and CD3/CD28 stimulation beads for 3 days. On day 3, the cells were first washed to remove stimulation beads (named pre-sort fraction). During this stimulation process, the fraction of non-T cell (i.e., NK cells, B cells, and monocytes) populations reduced while the T cells preferentially proliferated, resulting in 83% T cells in the total pre-sort population (**Supplementary Figure 3.2A**). All of the stimulated PBMC populations express CD71 receptor to varying levels, with NK cells showing the lowest CD71 expression (**Supplementary Figure 3.2B**). The stimulated PBMCs were stained with biotinylated rvCD71apt, labeled with magnetic anti-biotin Microbeads (Miltenyi), and applied to the magnetic MACS column for separation. As expected, we saw NK cells enrichment in the fraction that was not captured by the column (named flow through fraction) due to their lower CD71 expression (**Supplementary Figure 3.2A**). The cells that were retained in the column were then incubated with rvCD71apt antidote at 100x aptamer concentration. A population of cells were released from the column upon antidote treatment (named antidote elution fraction). The rest of the cells not eluted by antidote incubation were flushed out of the column with buffer (named flush fraction). Strikingly, we found over 2 orders of magnitude difference in CD71 expression measured by fluorescent intensity on flow cytometry between the sorted cell fractions. The cells in the flow through fraction expressed the lowest CD71 which led to insufficient physical support to counter the gravity flow of washes. The cells that were retained in the column despite antidote elution showed the highest CD71 expression. The cells being eluted from the column with antidote displacement had intermediate CD71 expression (**Supplementary Figure 3.2C**).

3.3.5 An aptamer-based multiplexed system for traceless cell selection

The amount of cells left retained in the MACS column after antidote treatment led us to consider using a different isolation method (**Supplementary Figure 3.2D**), in which the strand displacement step takes place in a rotating enclosed solution rather than a static state. Other groups have previously reported use of the micrometer-sized superparamagnetic Dynabeads® (Invitrogen) for fluorescent bead[25] and cell[26] sorting that relies on effective DNA gate strand displacements.

Therefore, we tested multiplexed cell isolation using MyOne Streptavidin C1 Dynabeads (Invitrogen) labeled with rvCD71apt and rvCD8apt aptamers (**Figure 3.4A**). Biotinylated rvCD71apt and biotinylated rvCD8apt were first incubated with the Streptavidin Dynabeads to generate rvCD71apt-labeled and rvCD8apt-labeled solid supports. The aptamer-functionalized beads were then applied to a mixed cell population (i.e., pre-sort fraction) that consisted of activated $CD4^+$ T cell-spiked PBMCs with a goal of using rvCD71apt and rvCD8apt to isolate activated $CD4^+$ T cells and $CD8^+$ T cells, respectively. The labeled target cells were applied to a magnetic Eppendorf tube rack (MagRack 6, GE), such that target cells were retained on the side of the tube due to magnetic force, while the un-labeled or un-sufficiently anchored cells were washed away (i.e., not captured fraction). Activated $CD4^+$ T cells were eluted first with rvCD71apt antidote incubation (i.e., rvCD71apt antidote elution fraction). Next, the excess DNA and un-eluted activated $CD4^+$ T cells were rinsed away using dextran sulfate solution, a anionic polysaccharide commonly used to reduce both non-specific background (at low concentrations) and targeted aptamer binding (at high concentrations) (**Supplementary Figure 3.3A and 3.3B**).[42,43] rvCD8apt antidote was then applied to the column for $CD8^+$ T cell elution (i.e., rvCD8apt antidote elution fraction). Lastly, the remaining bead-labeled cells were collected by resuspending with buffer (i.e., not eluted fraction). We collected cells from each fraction to be stained for antibody staining to determine cell phenotype (**Figure 3.4B**). rvCD71apt target cells were gated as $CD4^+CD71^+$. rvCD8apt target cells were gated as $CD8^+$ cells. We found that rvCD71apt antidote eluted activated $CD4^+$ T cells at high purity of 93.3% and rvCD8apt antidote eluted $CD8^+$ cells at 84.6% purity (**Figure 3.4C**). These results demonstrated that aptamer-specific antidote elution can be used to isolate multiple cell types in a sequential and traceless manner.

In contrast to the MACS system, we effectively eluted most of the target cells from the aptamer-functionalized Dynabeads (**Supplementary Figure 3.4**). However, despite the high purity and effective collection of traceless activated $CD4^+$ T cells and $CD8^+$ cells (mostly resting $CD8^+$ T cells) sorted by this method, we noticed that a significant fraction of target cells was not retained by the magnetic beads (not captured fraction in **Figure 3.4B** and **Supplementary Figure 3.4**). Unlike the insufficient antidote displacement issue we observed with the MACS system (**Supplementary Figure 3.2D)**, cells were not anchored securely by the Dynabeads MyOne Streptavidin C1 and GE MagRack 6 system. Consequently, the yield of target cells isolated from antidote elution was only 49.7% of total $CD4^+CD71^+$ cells and 25.7% for $CD8^+$ cells (**Figure**

3.4D). This is likely due to insufficient strength afforded by the magnetic separation since we have titrated and applied excessive aptamer and streptavidin beads to saturate the binding events in each staining step. However, only less than 1% of the input target cells remained attached on the Dynabeads after antidote displacement (**Supplementary Figure 3.4**). We attribute the efficient recovery to the free-floating state of cells and beads during the elution steps, which likely makes aptamers more accessible to the antidote sequences.

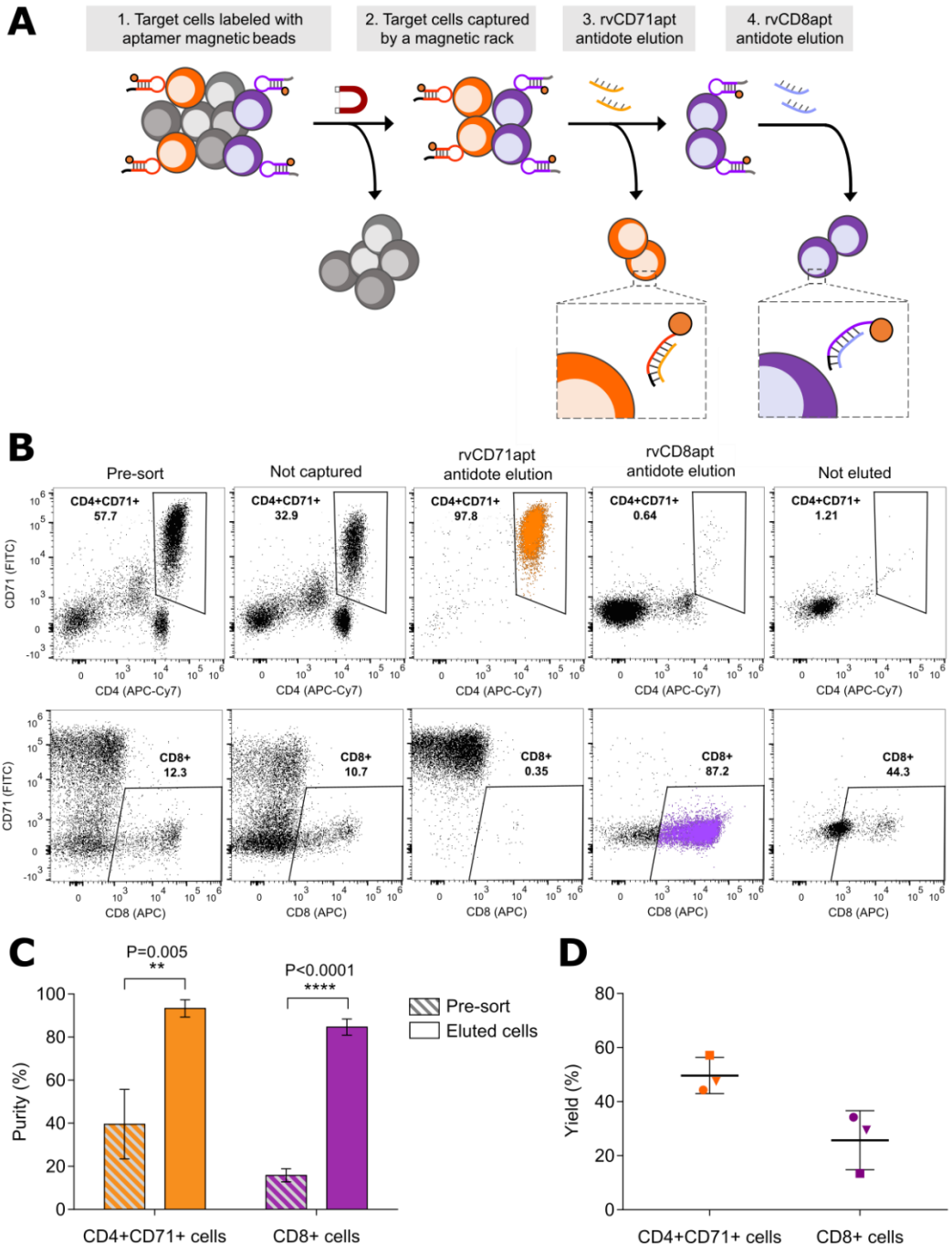

Figure 3.4. Multiplexed cell isolation using aptamer antidote elution. (A) Simplified schematic of aptamer labeling and 2-step antidote elution. (B) Representative flow cytometry plots of isolated cells in different fractions stained with CD4, CD8, and CD71 antibodies. rvCD71apt target cells were gated as $CD4^+CD71^+$ cells. rvCD8apt target cells were gated as $CD8^+$ cells. (C) Purity of target cells in the pre-sort and eluted fractions. Data are shown as mean ± s.d., n = 3 (two-tailed unpaired t test). (D) Yield of target cells in the eluted fractions. Data are shown as mean ± s.d., n = 3 (two-tailed unpaired t test). FITC: fluorescein isothiocyanate; APC: allophycocyanin; APC-Cy7: allophycocyanin-Cy7.

3.4 Discussion

The most common strategy for traceless cell isolation is by negative selection, which requires a full panel of staining reagents for capturing undesired cells and often results in insufficient yield and purity.[9,10,17] There is therefore significant interest in developing removable affinity agents, including both recombinant proteins and synthetic oligonucleotides. Cell sorting systems using Strep-Tag and Strep-Tactin complexes can achieve cell purity over 90%[22,23,44], with yields between 10-60%[22] when used to isolate cell types that require multiple marker labeling such as memory T cells[22] and regulatory T cells[44]. MACS-based cell isolation method using a single aptamer and antidote pair to purify $CD8^+$ T cells[16] and $EGFR^+$ cell line[34] has been reported to provide high isolation purity of around 95%. In this work, we demonstrate a new isolation method using two pairs of aptamers and antidotes as cell type-releasing DNA gates[25,26] to isolate two cell types without repeated staining and sorting steps. By serially eluting cells captured by the superparamagnetic beads, we isolated activated $CD4^+$ T cells and $CD8^+$ cells with 85-93% purity.

Non-specific cell binding to the solid support is a potential factor in reduced purity. Dynabeads are superparamagnetic beads coated with polystyrene, and polystyrene has been reported to non-specifically bind to cells.[45,46] Another potential factor that might cause reduced purity is unintentional physical removal of captured cells from the Dynabeads by pipetting or by charge repulsion due to the application of anionic reagents like DNA strands. This is a concern especially in the $CD8^+$ cell elution step, which occurs after CD71 antidote elution, since any un-eluted $CD71^+$ cells would have less aptamer binding and be retained less securely by the beads. Since there was only a small amount of $CD71^+$ (<1%) cells observed in the rvCD8apt antidote elution fraction, the remaining $CD8^-$ cells contamination likely comes from non-specific association with the beads, despite our inclusion of following components to reduce non-specific cell adsorption: pre-clearing,

dextran sulfate rinse, and anionic blockers. A more inert surface coating with less interaction with the cell surface, such as poly (ethylene glycol) or zwitterionic polymers, could help improve cell purity from this method.[47]

In the process of developing the multiplexed cell isolation method, we also noticed the varying yield of target cells between different donors. The choice of magnetic beads and magnets directly impacted the immobilization of cells on the side of the tubes during washing steps. On the other hand, the expression level of target receptors, CD71 and CD8 protein, dictates the amount of beads attached to the cell surface. Since receptor expression is a donor-dependent and uncontrollable factor, the use of stronger magnets or different bead sizes are points of future optimization.

3.5 Conclusion

In this study, we demonstrated the feasibility of aptamer-based, traceless isolation of two target cell types from a single selection procedure. We first modified a reported CD71 aptamer, rvCD71apt, so that it is suitable for cell retention on the solid supports and independent antidote elution of the bound targets. We also optimized the antidote for this aptamer that could trigger rapid and efficient strand displacement to reverse target binding. We demonstrated that rvCD71apt could separate $CD71^+$ cells in PBMCs according to their CD71 expression level. We then combined rvCD71apt with rvCD8 apt and demonstrated traceless serial elution of activated $CD4^+$ T cells (rvCD71apt target) and resting $CD8^+$ cells (rvCD8apt target) from mixed cell populations. The two antidote elution steps successfully displaced most target cells captured on the Dynabeads through strand displacement with 93% and 85% mean target cells purity. Theoretically, this approach can be scaled up for isolation of even more cell populations with the development of additional orthogonal aptamer-antidote pairs. Another potential direction is immobilization of aptamers into chromatography systems that can further shorten the processing duration by eliminating the time required for the magnets to anchor the magnetic beads. As long as the aptamers and antidotes are designed properly as demonstrated in this study, the multiplexed isolation system could be versatile for a wide range of applications and different setups.

3.6 Acknowledgements

This research is supported by Juno Therapeutics (a Bristol Myers Squibb company). We thank Dr. Julie Shi (Juno Therapeutics) for coordinating and providing apheresis cells. We also thank Ian I. Cardle for his helpful discussions on cell isolation.

3.7 References

1. Bonner, W. A., Hulett, H. R., Sweet, R. G. & Herzenberg, L. A. Fluorescence Activated Cell Sorting. *Rev. Sci. Instrum.* **43**, 404–409 (1972).

2. Thiel, A., Scheffold, A. & Radbruch, A. Immunomagnetic cell sorting-pushing the limits. *Immunotechnology* (1998) doi:10.1016/S1380-2933(98)00010-4.

3. Kumar, A. & Srivastava, A. Cell separation using cryogel-based affinity chromatography. *Nat. Protoc.* (2010) doi:10.1038/nprot.2010.135.

4. Mohr, F., Przibilla, S., Leonhardt, F., Stemberger, C., Dreher, S., Müller, T. R., Fräßle, S. P., Schmidt, G. P., Kiene, M.-L., Stadler, H. & Busch, D. H. Efficient immunoaffinity chromatography of lymphocytes directly from whole blood. *Sci. Rep.* **8**, 16731 (2018).

5. Timonen, T. & Saksela, E. Isolation of human NK cells by density gradient centrifugation. *J. Immunol. Methods* (1980) doi:10.1016/0022-1759(80)90133-7.

6. Chen, K., Amontree, J., Varillas, J., Zhang, J., George, T. J. & Fan, Z. H. Incorporation of lateral microfiltration with immunoaffinity for enhancing the capture efficiency of rare cells. *Sci. Rep.* (2020) doi:10.1038/s41598-020-71041-7.

7. Marek, R., Caruso, M., Rostami, A., Grinspan, J. B. & Sarma, J. Das. Magnetic cell sorting: A fast and effective method of concurrent isolation of high purity viable astrocytes and microglia from neonatal mouse brain tissue. *J. Neurosci. Methods* (2008) doi:10.1016/j.jneumeth.2008.08.016.

8. Øren, A., Husebø, C., Iversen, A. C. & Austgulen, R. A comparative study of immunomagnetic methods used for separation of human natural killer cells from peripheral blood. *J. Immunol. Methods* (2005) doi:10.1016/j.jim.2005.04.022.

9. Tondreau, T., Lagneaux, L., Dejeneffe, M., Delforge, A., Massy, M., Mortier, C. & Bron, D. Isolation of BM mesenchymal stem cells by plastic adhesion or negative selection: phenotype, proliferation kinetics and differentiation potential. *Cytotherapy* **6**, 372–379 (2004).

10. Lyons, P. A., Koukoulaki, M., Hatton, A., Doggett, K., Woffendin, H. B., Chaudhry, A. N. & Smith, K. G. C. Microarray analysis of human leucocyte subsets: The advantages of positive selection and rapid purification. *BMC Genomics* (2007) doi:10.1186/1471-2164-8-64.

11. Harding, F. A., Stickler, M. M., Razo, J. & DuBridge, R. The immunogenicity of humanized and fully human antibodies. *MAbs* (2010) doi:10.4161/mabs.2.3.11641.

12. Elkord, E., Williams, P. E., Kynaston, H. & Rowbottom, A. W. Human monocyte isolation methods influence cytokine production from in vitro generated dendritic cells. *Immunology* (2005) doi:10.1111/j.1365-2567.2004.02076.x.

13. Laghmouchi, A., Hoogstraten, C., Falkenburg, J. H. F. & Jedema, I. Long-term in vitro persistence of magnetic properties after magnetic bead-based cell separation of T cells. *Scand. J. Immunol.* (2020) doi:10.1111/sji.12924.

14. Zhu, B. & Murthy, S. K. Stem cell separation technologies. *Current Opinion in Chemical Engineering* (2013) doi:10.1016/j.coche.2012.11.002.

15. Ying, Z., Huang, X. F., Xiang, X., Liu, Y., Kang, X., Song, Y., Guo, X., Liu, H., Ding, N., Zhang, T., Duan, P., Lin, Y., Zheng, W., Wang, X., Lin, N., Tu, M., Xie, Y., Zhang, C., Liu, W., Deng, L., Gao, S., Ping, L., Wang, X., Zhou, N., Zhang, J., Wang, Y., Lin, S., Mamuti, M., Yu, X., Fang, L., Wang, S., Song, H., Wang, G., Jones, L., Zhu, J. & Chen, S. Y. A safe and potent anti-CD19 CAR T cell therapy. *Nat. Med.* (2019) doi:10.1038/s41591-019-0421-7.

16. Kacherovsky, N., Cardle, I. I., Cheng, E. L., Yu, J. L., Baldwin, M. L., Salipante, S. J., Jensen, M. C. & Pun, S. H. Traceless aptamer-mediated isolation of CD8+ T cells for chimeric antigen receptor T-cell therapy. *Nat. Biomed. Eng.* (2019) doi:10.1038/s41551-019-0411-6.

17. Cardle, I. I., Cheng, E. L., Jensen, M. C. & Pun, S. H. Biomaterials in chimeric antigen receptor T-cell process development. *Acc. Chem. Res.* (2020) doi:10.1021/acs.accounts.0c00335.

18. Schmidt, T. G. M. & Skerra, A. The random peptide library-assisted engineering of a c-terminal affinity peptide, useful for the detection and purification of a functional ig Fv fragment. *Protein Eng. Des. Sel.* (1993) doi:10.1093/protein/6.1.109.

19. Schmidt, T. G. M., Koepke, J., Frank, R. & Skerra, A. Molecular interaction between the strep-tag affinity peptide and its cognate target, streptavidin. *J. Mol. Biol.* (1996) doi:10.1006/jmbi.1996.0061.

20. Korndorfer, I. P. Improved affinity of engineered streptavidin for the Strep-tag II peptide is due to a fixed open conformation of the lid-like loop at the binding site. *Protein Sci.* (2002) doi:10.1110/ps.4150102.

21. Schmidt, T. G. M. & Skerra, A. The Strep-tag system for one-step purification and high-affinity detection or capturing of proteins. *Nat. Protoc.* (2007) doi:10.1038/nprot.2007.209.

22. Stemberger, C., Dreher, S., Tschulik, C., Piossek, C., Bet, J., Yamamoto, T. N., Schiemann, M., Neuenhahn, M., Martin, K., Schlapschy, M., Skerra, A., Schmidt, T., Edinger, M., Riddell, S. R., Germeroth, L. & Busch, D. H. Novel serial positive enrichment technology enables clinical multiparameter cell sorting. *PLoS One* (2012) doi:10.1371/journal.pone.0035798.

23. Neudorfer, J., Schmidt, B., Huster, K. M., Anderl, F., Schiemann, M., Holzapfel, G., Schmidt, T., Germeroth, L., Wagner, H., Peschel, C., Busch, D. H. & Bernhard, H. Reversible HLA multimers (Streptamers) for the isolation of human cytotoxic T lymphocytes functionally active against tumor- and virus-derived antigens. *J. Immunol. Methods* (2007) doi:10.1016/j.jim.2007.01.001.

24. Odendahl, M., Grigoleit, G. U., Bönig, H., Neuenhahn, M., Albrecht, J., Anderl, F., Germeroth, L., Schmitz, M., Bornhäuser, M., Einsele, H., Seifried, E., Busch, D. H. & Tonn, T. Clinical-scale isolation of 'minimally manipulated' cytomegalovirus-specific donor lymphocytes for the treatment of refractory cytomegalovirus disease. *Cytotherapy*

(2014) doi:10.1016/j.jcyt.2014.05.023.

25. Probst, C. E., Zrazhevskiy, P. & Gao, X. Rapid multitarget immunomagnetic separation through programmable DNA linker displacement. *J. Am. Chem. Soc.* (2011) doi:10.1021/ja2072324.

26. Dahotre, S. N., Chang, Y. M., Wieland, A., Stammen, S. R. & Kwong, G. A. Individually addressable and dynamic DNA gates for multiplexed cell sorting. *Proc. Natl. Acad. Sci. U. S. A.* (2018) doi:10.1073/pnas.1714820115.

27. Tuerk, C. & Gold, L. Systematic evolution of ligands by exponential enrichment: RNA ligands to bacteriophage T4 DNA polymerase. *Science (80-.).* (1990) doi:10.1126/science.2200121.

28. Ellington, A. D. & Szostak, J. W. In vitro selection of RNA molecules that bind specific ligands. *Nature* (1990) doi:10.1038/346818a0.

29. Zhou, J. & Rossi, J. Aptamers as targeted therapeutics: Current potential and challenges. *Nature Reviews Drug Discovery* (2017) doi:10.1038/nrd.2016.199.

30. Walter, J. G., Stahl, F. & Scheper, T. Aptamers as affinity ligands for downstream processing. *Engineering in Life Sciences* (2012) doi:10.1002/elsc.201100197.

31. Li, L., Chen, X., Cui, C., Pan, X., Li, X., Yazd, H. S., Wu, Q., Qiu, L., Li, J. & Tan, W. Aptamer Displacement Reaction from Live-Cell Surfaces and Its Applications. *J. Am. Chem. Soc.* (2019) doi:10.1021/jacs.9b07191.

32. Chen, Y., Tyagi, D., Lyu, M., Carrier, A. J., Nganou, C., Youden, B., Wang, W., Cui, S., Servos, M., Oakes, K., He, S. & Zhang, X. Regenerative nanooctopus based on multivalent-aptamer-functionalized magnetic microparticles for effective cell capture in whole blood. *Anal. Chem.* (2019) doi:10.1021/acs.analchem.8b05432.

33. Rusconi, C. P., Roberts, J. D., Pitoc, G. A., Nimjee, S. M., White, R. R., Quick, G., Scardino, E., Fay, W. P. & Sullenger, B. A. Antidote-mediated control of an anticoagulant aptamer in vivo. *Nat. Biotechnol.* (2004) doi:10.1038/nbt1023.

34. Gray, B. P., Requena, M. D., Nichols, M. D. & Sullenger, B. A. Aptamers as Reversible Sorting Ligands for Preparation of Cells in Their Native State. *Cell Chem. Biol.* (2020) doi:10.1016/j.chembiol.2019.12.004.

35. Zhang, D. Y. & Winfree, E. Control of DNA strand displacement kinetics using toehold exchange. *J. Am. Chem. Soc.* (2009) doi:10.1021/ja906987s.

36. Zhang, D. Y. & Seelig, G. Dynamic DNA nanotechnology using strand-displacement reactions. *Nat. Chem.* (2011) doi:10.1038/nchem.957.

37. Zadeh, J. N., Steenberg, C. D., Bois, J. S., Wolfe, B. R., Pierce, M. B., Khan, A. R., Dirks, R. M. & Pierce, N. A. NUPACK: Analysis and design of nucleic acid systems. *J. Comput. Chem.* (2011) doi:10.1002/jcc.21596.

38. Yang, X., Tang, Y., Traynor, S. M. & Li, F. Regulation of DNA Strand Displacement Using an Allosteric DNA Toehold. *J. Am. Chem. Soc.* (2016) doi:10.1021/jacs.6b08794.

39. Hao, Y., Li, J., Li, Q., Zhang, L., Shi, J., Zhang, X., Aldalbahi, A., Wang, L., Fan, C. & Wang, F. Programmable Live-Cell CRISPR Imaging with Toehold-Switch-Mediated Strand Displacement. *Angew. Chemie - Int. Ed.* (2020) doi:10.1002/anie.202009062.

40. Gelinas, A. D., Davies, D. R. & Janjic, N. Embracing proteins: Structural themes in aptamer-protein complexes. *Current Opinion in Structural Biology* (2016) doi:10.1016/j.sbi.2016.01.009.

41. Motamedi, M., Xu, L. & Elahi, S. Correlation of transferrin receptor (CD71) with Ki67 expression on stimulated human and mouse T cells: The kinetics of expression of T cell activation markers. *J. Immunol. Methods* (2016) doi:10.1016/j.jim.2016.08.002.

42. Gold, L., Ayers, D., Bertino, J., Bock, C., Bock, A., Brody, E. N., Carter, J., Dalby, A. B., Eaton, B. E., Fitzwater, T., Flather, D., Forbes, A., Foreman, T., Fowler, C., Gawande, B., Goss, M., Gunn, M., Gupta, S., Halladay, D., Heil, J., Heilig, J., Hicke, B., Husar, G., Janjic, N., Jarvis, T., Jennings, S., Katilius, E., Keeney, T. R., Kim, N., Koch, T. H., Kraemer, S., Kroiss, L., Le, N., Levine, D., Lindsey, W., Lollo, B., Mayfield, W., Mehan, M., Mehler, R., Nelson, S. K., Nelson, M., Nieuwlandt, D., Nikrad, M., Ochsner, U., Ostroff, R. M., Otis, M., Parker, T., Pietrasiewicz, S., Resnicow, D. I., Rohloff, J., Sanders, G., Sattin, S., Schneider, D., Singer, B., Stanton, M., Sterkel, A., Stewart, A., Stratford, S., Vaught, J. D., Vrkljan, M., Walker, J. J., Watrobka, M., Waugh, S., Weiss, A., Wilcox, S. K., Wolfson, A., Wolk, S. K., Zhang, C. & Zichi, D. Aptamer-based multiplexed proteomic technology for biomarker discovery. *PLoS One* (2010) doi:10.1371/journal.pone.0015004.

43. Yoon, J. W., Jang, I. H., Heo, S. C., Kwon, Y. W., Choi, E. J., Bae, K.-H., Suh, D.-S., Kim, S.-C., Han, S., Haam, S., Jung, J., Kim, K., Ryu, S. H. & Kim, J. H. Isolation of Foreign Material-Free Endothelial Progenitor Cells Using CD31 Aptamer and Therapeutic Application for Ischemic Injury. *PLoS One* **10**, e0131785 (2015).

44. Mohr, F., Fischer, J. C., Nikolaus, M., Stemberger, C., Dreher, S., Verschoor, A., Haas, T., Poeck, H. & Busch, D. H. Minimally manipulated murine regulatory T cells purified by reversible Fab Multimers are potent suppressors for adoptive T-cell therapy. *Eur. J. Immunol.* (2017) doi:10.1002/eji.201747137.

45. Jackson, C. J., Garbett, P. K., Nissen, B. & Schrieber, L. Binding of human endothelium to Ulex europaeus I-coated Dynabeads: application to the isolation of microvascular endothelium. *J. Cell Sci.* (1990) doi:10.1242/jcs.96.2.257.

46. Janssen, W. E. & Rios, A. M. Non-specific cell binding characteristics of para-magnetic polystyrene microspheres used for antibody-mediated cell selection. *J. Immunol. Methods* (1989) doi:10.1016/0022-1759(89)90173-7.

47. Chen, L., Yan, C. & Zheng, Z. Functional polymer surfaces for controlling cell behaviors. *Materials Today* (2018) doi:10.1016/j.mattod.2017.07.002.

3.8 Supplementary information

Supplementary Table 3.1. Dual selection aptamer and antidote sequences. The underlined sequences are the toehold structures.

Name	Sequence
RAN	5'- ATCCAGAGTGACGCAGCAAATTCCAAACTCGAGTAAGCGTAGAGCCTCTCATCGCCTCAATAATGGA CACGGTGGCTTAGT -3'
JBA8.1	5'- ATCCAGAGTGACGCAGCAGCGTAAAGGGGGTGTTTGTGCGGTGTGGAGTGCGCGTGCTGCTGCTG GACACGGTGGCTTAGT -3'
rvCD71apt	5'- GGAGTCACACGCATTAGCGTAAAGGGGGTGTTTGTGCGGTGTGGAGTGCGCGTGCTAATGCTGGAG TGTTTCCCAGGACCC -3'
rvCD8apt	5'- CCAGAGTGACGCAGCAACAGAGGTGTAGAAGTACACGTGAACAAGCTTGAAATTGTCTCTGACAGAG GTGGACACGGTGGCTTTTAGT -3'
rvCD71apt antidote (21 nt)	5'- GGGTCCTGGGAAACACTCCAG -3'
rvCD71apt antidote (28 nt)	5'- GGGTCCTGGGAAACACTCCAGCATTAGC -3'
rvCD71apt antidote (33 nt)	5'- GGGTCCTGGGAAACACTCCAGCATTAGCACGCG -3'
rvCD71apt antidote (51 nt)	5'- GGGTCCTGGGAAACACTCCAGCATTAGCACGCGCACTCCACACCGCACAAA -3'
rvCD8apt antidote	5'- ACTAAAAGCCACCGTGTCCACCTCTGTCAGAGACAA -3'

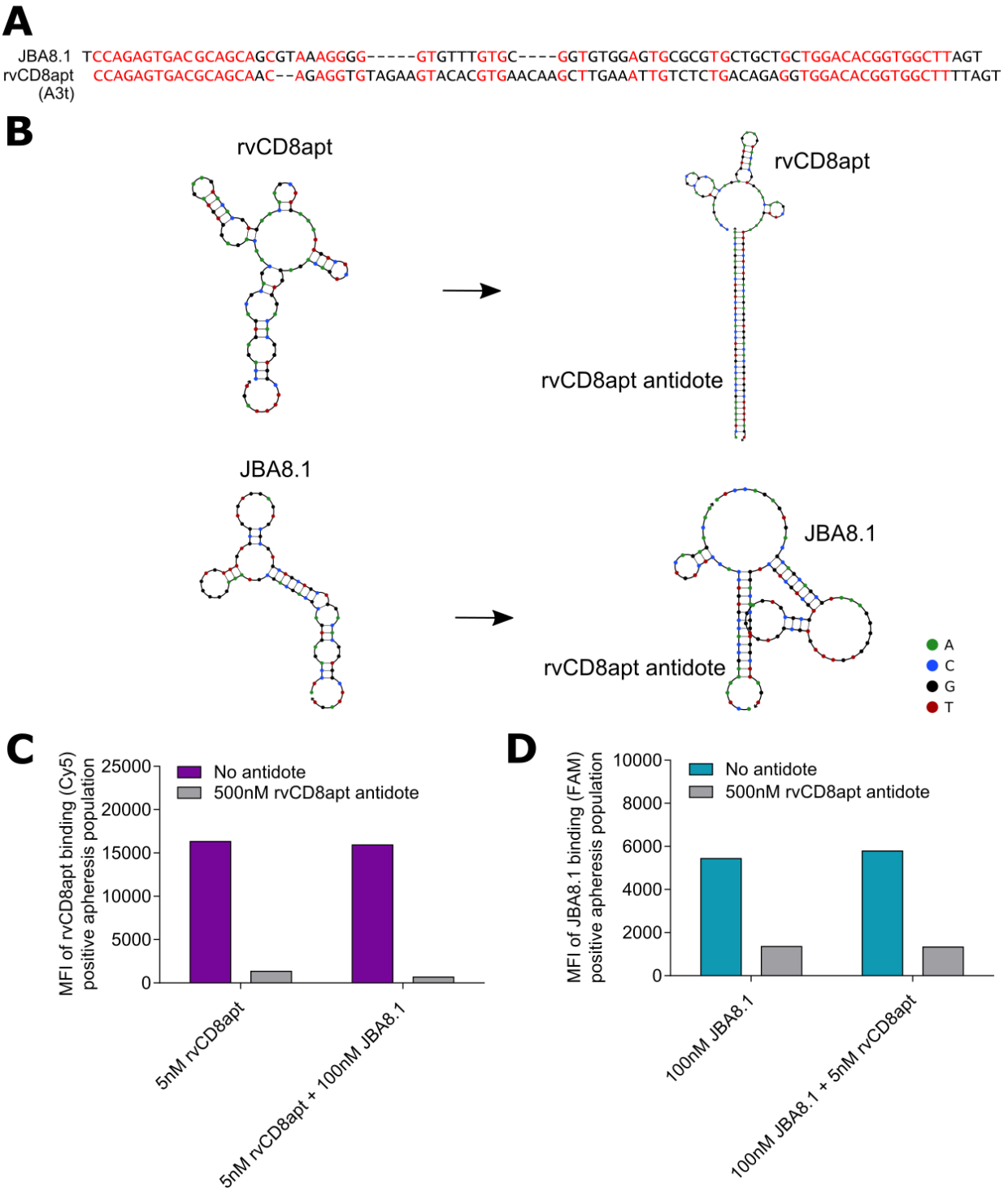

Supplementary Figure 3.1. JBA8.1 sequence overlapped with rvCD8apt led to strand displacement by rvCD8apt antidote. (A) Sequence alignment of JBA8.1 and rvCD8apt. Overlapping sequences are marked in red. (B) NUPACK 2-dimentional structure prediction of JBA8.1 aptamer and rvCD8apt aptamer at 4°C (left), and the predicted structures when aptamers are incubated with rvCD8apt antidote at 25°C. NUPACK settings: Na^+ = 137 mM; Mg^{2+} = 5.5 mM.

Strand displacement of (C) rvCD8apt and (D) JBA8.1 evaluated with flow cytometry by staining apheresis cells with individual or combined aptamers at 4°C for 30 minutes. Strand displacement took place at 25°C for 10 minutes. MFI: median fluorescent intensity; Cy5: Cyanine 5; FAM: 6-carboxyfluorescein.

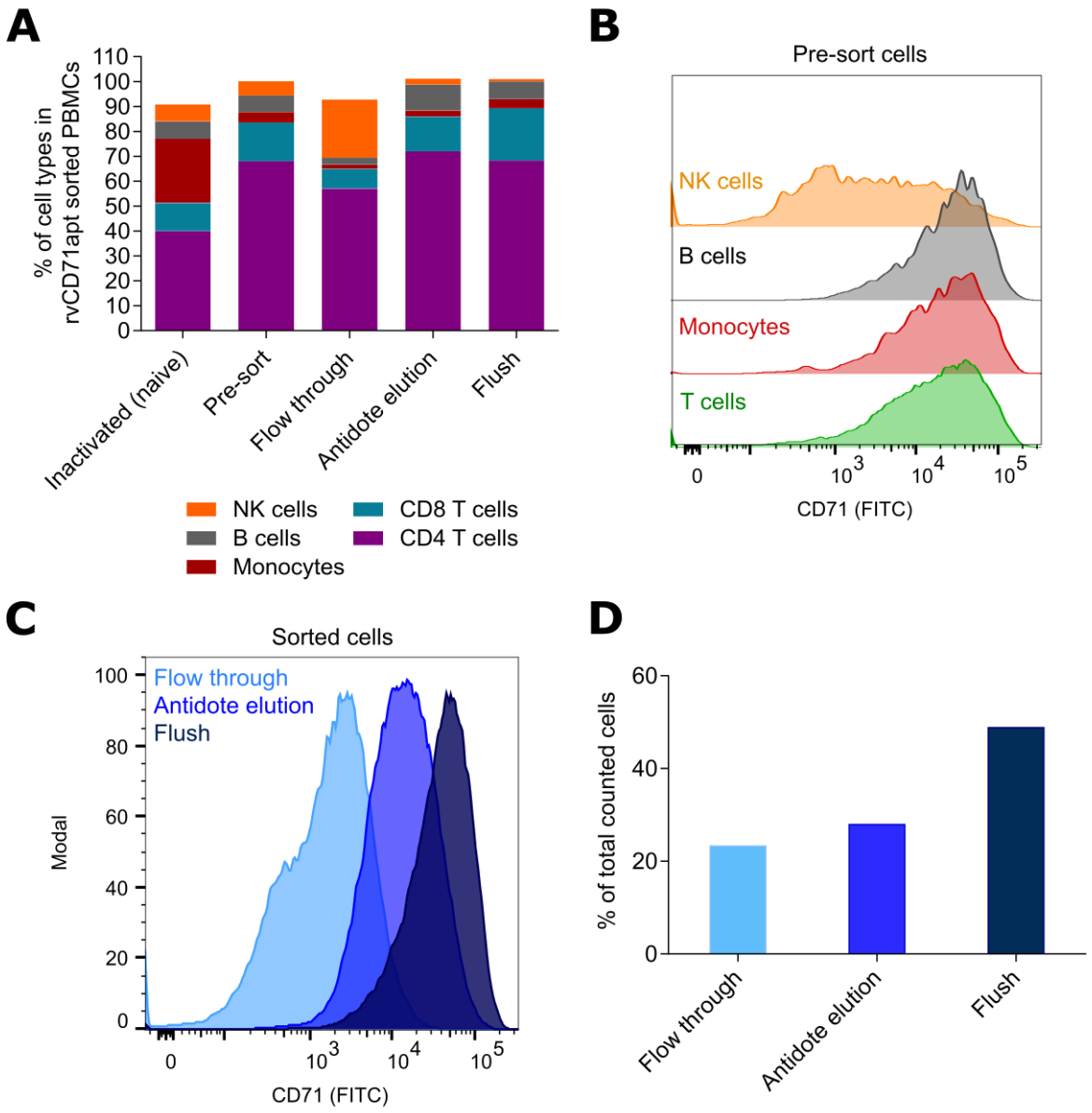

Supplementary Figure 3.2. Sorting bulk stimulated PBMCs with rvCD71apt. (A) Percentage of PBMC compositions in the inactivated, pre-sort, and sorted cell fractions measured by flow cytometry. NK cells were gated on $CD3^{-}CD56^{+}$ population. B cells were gated on $CD3^{mid}CD19^{+}$ population. Monocytes were gated on $CD14^{+}$ population. CD4 T cells were gated on $CD3^{+}CD8^{-}$ population. CD8 T cells were gated on $CD3^{+}CD8^{+}$ population. (B) Flow cytometry evaluation of CD71 expression on PBMCs bulk stimulated with IL-7, IL-15, IL-2 cytokines and CD3/CD28

activation beads. (C) CD71 expression on the sorted cells in flow through, antidote elution, and flush fractions measured by flow cytometry. (D) Percentages of total cell count found in flow through, antidote elution, and flush fractions. Figures were generated with results from 1 biological repeat. FITC: fluorescein isothiocyanate.

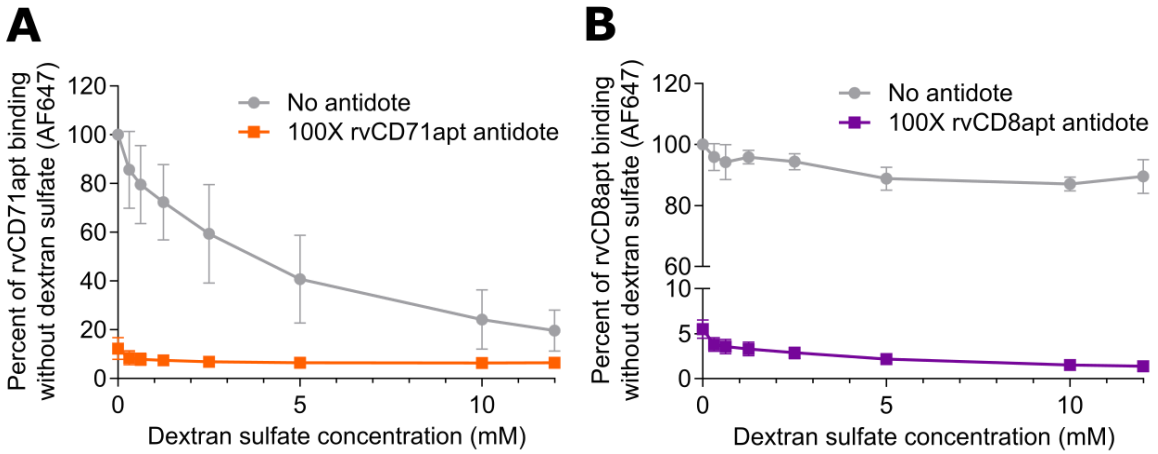

Supplementary Figure 3.3. Flow cytometry evaluation of dextran sulfate impacting aptamer binding. (A) $CD4^+$ T cells were activated using IL-7 cytokines, IL-15 cytokines, and CD3/CD28 activation beads. The activated $CD4^+$ T cells were stained with 60 nM biotinylated rvCD71apt before exposed to various concentrations of dextran sulfate with or without 6 µM rvCD71apt antidote. rvCD71apt binding was evaluated using Streptavidin AF647 as secondary staining. Data are shown as mean ± s.d., $n = 3$. (B) $CD8^+$ T cells were stained with 5 nM biotinylated rvCD8apt before exposed to various concentrations of dextran sulfate with or without 500 nM rvCD8apt antidote. rvCD8apt binding was evaluated using Streptavidin AF647 as secondary staining. Data are shown as mean ± s.d., $n = 3$. AF647: Alexa Fluor 647.

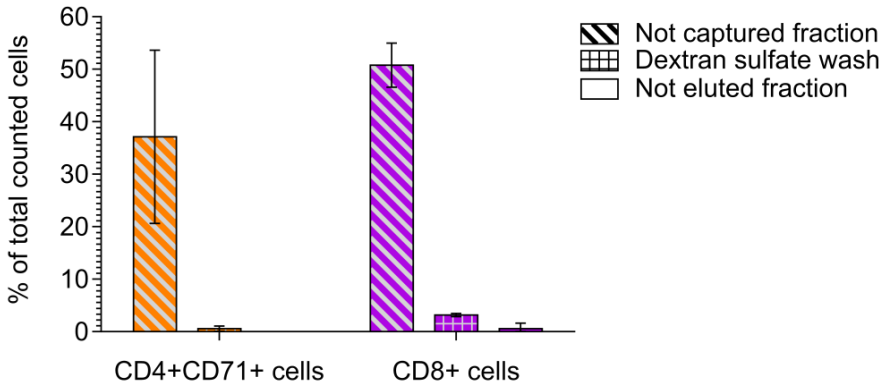

Supplementary Figure 3.4. Percentage of the target cells counted in different fractions divided by the total cell counts in all fractions combined in the traceless multiplexed isolation system. Data are shown as mean ± s.d., $n = 3$.

Chapter 4. Towards identification of $CD4^+$ T cell-binding ligand for cell isolation

Emmeline L. Cheng, Abigail A. O'Connor, Nataly Kacherovsky, Suzie H. Pun

Abstract

$CD8^+$ T cells (CD8 T cells) are crucial to successful CAR T cell therapies due to their cancer call-targeted lytic functions. Although recent studies have also highlighted the importance of $CD4^+$ T cells (CD4 T cells) providing these cytotoxic T cells survival signals. Therefore, some companies manufacture the CAR T cell products with defined 1:1 CD4:CD8 T cell ratio. However, this refined procedure requires additional isolation steps to purify both T cell subgroups. The current T cell isolation process uses antibody targeting. Labeling cells with these biological reagents are costly and irreversible. Since isolating T cells without labeling residue is desired for patient safety, novel targeting ligands that are easy to use, removable, and inexpensive is needed for CAR T cell manufacturing. Aptamers, also called "chemical antibodies", are economically friendly alternatives that offer reversible target specificity due to their binding structure being dictated by Watson-Crick base-paring. Our group has developed a CD8 protein binding aptamer (A3t) suitable for traceless isolating $CD8^+$ T cells from PBMCs (peripheral blood mononuclear cells) using MACS system. $CD8^+$ T cells were first retained in the magnetic column by A3t binding. A3t-designated complementary strands were then used to elute the cells from the A3t aptamer and beads. To expand this technology, a $CD4^+$ T cell-binding aptamer with different sequence can be used on white blood cells (PBMCs or apheresis product) along with A3t aptamer. The CD4 aptamer binding can be reversed by its corresponding complementary strand. Hence, we can traceless isolate both $CD4^+$ and $CD8^+$ T cells from the same specimen using just one magnetic column with a single staining step. This isolation method greatly reduces the time, expanse, and amount of PBMCs or apheresis cells required for traceless isolating both subtypes of T cells for CAR T cell engineering. Prior to performing aptamer selection, we first tested three reported CD4 binding DNA aptamers. But none of them were found specifically bind to CD4-expressing T cells and T cell line. Therefore, we sought to identify novel aptamers that bind to CD4 protein with versions of cell-SELEX. Advantages and potential drawbacks of each selection attempts were

discussed. Ultimately, we aim to use the discovered CD4 aptamer on reversable $CD4^+$ T cell isolation.

4.1 Introduction

4.1.1 CAR T cell products with well-defined $CD4^+$ and $CD8^+$ cells ratio improves patient prognosis

CAR T cell therapies consist of two major T cell subtypes, $CD8^+$ cytotoxic T cells ($CD8^+$ T cells) and $CD4^+$ helper T cells ($CD4^+$ T cells). $CD8^+$ T cells have drawn major attention due to their lytic function against cancer cells and positive correlation with patient prognosis when found infiltrating solid tumors.[1,2] However, recent discoveries spotlight the importance of CD4 T^+ cells providing cell signals in CAR T cell therapies. In a mouse model study, intrapleurally administered mesothelin targeting CAR T cells to treat pleural malignancies (primary and metastatic pleural mesothelioma) were found to have long-term functional T cell persistence when having higher CD4/CD8 ratio in the intratumoral environment and elevated CD28-depandant $CD4^+$ T cell activation.[3] Researchers tested an approved CD19 CAR T cell product with a well-defined 1:1 $CD4^+$ and $CD8^+$ T cells ratio in mouse model baring Raji B cell lymphoma tumor and demonstrated that the $CD4^+$ CAR T cells, especially their IL-2 production, enhances the survival, proliferation, and function of $CD8^+$ CAR T cells. This study highlights the syngeneic effect of $CD4^+$ CAR T cells, especially their IL-2 production, may enhance the survival, proliferation, and function of $CD8^+$ CAR T cells.[4] In clinical settings, a striking 94% (27/29) remission rate was observed in a clinical trial using 1:1 ratio of $CD4^+$ and $CD8^+$ CD19 CAR T cells against B-ALL malignancy in adults.[5] The feasibility of this improved CAR T cell product was verified on other relapse and/or refractory blood cancer patients, such as children and young adults with B-ALL[6] and adults with B-cell non-Hodgkin's lymphoma.[7] However, producing T cells at a specified ratio is challenging from a manufacturing standpoint because patients that have gone through therapies, such as lymphodepletion treatment, often have reduced T cells and varied CD4/CD8 T cell ratios. As a result, it becomes necessary to produce $CD4^+$ and $CD8^+$ T cells separately during the activation, transduction, and expansion steps. After expanding cell numbers to required dosages, the cells are mixed at 1:1 for patient infusion to ensure the consistent cell compositions across each patient (**Figure 1.1**).

4.1.2 Aptamers are suitable for tracelessly isolating $CD4^+$ and $CD8^+$ T cells

Currently, the cell isolation materials used to isolate $CD4^+$ and $CD8^+$ T cells are antibodies and magnetic beads. The residue of these materials on the final CAR T cell product needs to be below a certain level to be approved by FDA.[8] If antibody-based positive selection is used for isolating these T cells, the resulting CAR T cell product will contain irremovable labeling materials. If negative selection with an antibody panel labeling non-target cells is used for the process, the resulting target cell purity can vary between patients. Moreover, the labeled non-target cells are also prohibited from additional isolations. Both methods are costly because of the use of antibodies, which are biological reagents. As the current price tags of approved CAR T cell therapies are high as 475,000 USD (Kymriah)[9], and 373,000 USD (Yescarta and Tecartus)[9,10] per dose, an economically friendly isolation method that can easily remove labeling antigen and beads from the $CD4^+$ and $CD8^+$ T cell surface is needed. As we discussed in previous chapters, aptamers are attractive alternatives to antibodies because they are cheaper, faster, and more consistent to produce. They also have reversable binding structure, and similar binding affinity to antibodies.[11]

In chapter 2, we used tJBA8.1 aptamer (a CD71 protein-binding aptamer) to positively isolate $CD71^+$ Raji cells from PBMCs using MACS system. In a published study reporting A3t (a CD8 aptamer), we further showed controlled release of $CD8^+$ target cells from the MACS column is feasible with some modifications on the aptamers and using complementary strands (antidotes). These acquired $CD8^+$ T cells were cleared of the manufacturing materials.[12] In chapter 3, we combined two different aptamers in one staining step, and demonstrated aptamer sequence-specific reverse binding with their antidotes. In this chapter, we work toward identifying novel CD4 receptor binding aptamers. We aim to ultimately use the discovered CD4 aptamer along with the A3t CD8 aptamer[12] for traceless multiplexed cell selection with antidotes to collect label-free $CD4^+$ and $CD8^+$ T cells from a single column.

4.1.3 Parameters of Cell-SELEX for enriching desired protein binders

As mentioned in the previous chapters, we use cell-SELEX to develop aptamers with desired targeting property. The choice of target cells for positive selection and control cells for negative selection have major impact on the binder enrichment. The two cell types should have different molecular expression level of the target of interest but similar expression of other surface proteins to reduce undesired background binding.[13,14] The similarity of these two cell types, along with the number of cells and their incubation time with aptamer libraries, all contribute to the selection stringency. Some polyanionic blockers were used to reduce non-specific binding of aptamers, including yeast tRNA, salmon sperm DNA, BSA, and FBS. These nucleotide and protein blockers have been reported to assist development of high affinity aptamers.[15,16] By controlling the stringency of aptamer selection, we can increase the evolution stress throughout each selection round. Last, we kept the temperature of the SELEX process at 4 ^{o}C to avoid aptamer internalization occurs. This way, we are more likely to discover aptamers that binds to cell surface instead of intracellular proteins.

4.1.4 Advanced SELEX strategies for enriching high affinity target binders

To enrich aptamers with high affinity and specificity binding, we incorporated several advanced strategies on top of the general SELEX method mentioned in the previous paragraph. These methods include competitive SELEX, complementary strand neutralization, SOMAmer (Slow Off-rate Modified Aptamer) SELEX, ligand-guided SELEX, and protein/cell combination SELEX. Competitive SELEX combined with cell-SELEX has been used to develop CD8 protein binding aptamer with nano-molar K_D less than 20 nM.[12] The competition step in this process was done by staining PBMCs with aptamer library, followed by traceless isolation of T cells using MACS kit. This method helps eliminate background binding sequences toward non-T cells in the mixed cell population.

Using complementary strands to block certain variable regions is another method we used to deplete non-specific binders. This requires early-on sequencing of round libraries and binding studies to identify the undesired sequences that were not depleted in the negative selection step. The complementary strands used to neutralize these undesired sequences were doped-in to the library pool when it was annealed, thus, preventing their three-dimensional structures from

forming. Therefore, the blocked sequences will be washed off in the positive selection step due to their lack of binding motifs.

Ligand-guided selection (LIGS) is a SELEX process that includes competition steps using existing binding ligands.[17] While cell-SELEX utilizes natural cellular protein instead of recombinant protein as the selection target, it requires addition receptor identification process for the developed ligand since the binding target of the aptamer can be any molecules exist on or within the cells. In theory, performing LIGS eliminates the need of receptor identification because it utilizes existing ligands to elute the receptor-bound sequences in selection rounds. For example, Zumrut et al. applied CD3 antibody binding to compete CD3 receptor-bound sequences from CD3 receptor in a cell-SELEX that identified a TCR-CD3 complex-binding aptamer.[18] However, one foreseeable drawback of this method is developing aptamers with lower binding affinity. This can be improved by post-selection modifications such as multimerizing the aptamers.[19,20]

Next, some chemically modified "protein-like" bases have been reported to promote successful SELEX against several targets with repeatedly failed selection attempts using natural DNA aptamers. These bases include benzyl-dU, isobutyl-dU, tryptamino-dU, and more, which carries structures similar to amino acid side chains. The aptamers composed of these building blocks are called SOMAmers. By mimicking amino acid side chains, SOMAmers have enhanced hydrophobic interactions with proteins that natural DNA aptamers are lack of.[21] This increased chemical diversity was reported to expand the target epitopes could be recognized by aptamers.[22] Among these modified nucleic acids, tryptamino-dU (TrpdU) has led to some successful aptamer identification on "difficult" targets expressed on T cells, including 4-1BB, and CTLA-4.[23]

Our last strategy for selecting CD4 protein binding aptamers combines protein-SELEX with cell-SELEX. As mentioned in previous paragraphs, these two types of aptamer selection methods have different advantages. Protein-SELEX narrows down the binding target to a single type of recombinant protein which eliminates the possibility of selecting for sequences bind to other receptors, whereas Cell-SELEX yields aptamers that binds to protein in their natural state. Therefore, we switched back-and-forth between protein-SELEX and cell-SELEX strategies in order to enrich aptamers that binds to the native state of our protein of choice, CD4 receptor. Theoretically, we could reduce the chance of selecting for aptamers that binds to other proteins on

the cell surface, to the purification tags on recombinant proteins, and to possible mutations on the recombinant proteins.[24]

In this chapter, we first evaluated the potential of using published CD4 binders on primary $CD4^+$ T cells or CD4-expressing cancer cells. We then explored different cell-SELEX methods combining some or all of the strategies mentioned above to identify CD4-binding aptamers.

4.2 Materials and methods

4.2.1 Cell preparation and culture maintenance

Jurkat cell line (human T-ALL) was gifted by the Jensen lab (Seattle Children's Research Institute). J.RT3-T3.5 cell line (human T-ALL) was purchased from ATCC. $CD4^+$ T cells (positively selected) used in SELEX A and B, and all the $CD8^+$ T cells (positively selected), apheresis, T cells, and T cell-depleted apheresis were provided by Juno Therapeutics. $CD4^+$ T cells used in the rest of the SELEX, were isolated from PBMCs using CD4 T cell negative selection kit (Miltenyi). The PBMCs were prepared by Ficoll-enriching apheresis product purchased from Bloodworks Northwest.

All cell culture was maintained in RPMI 1640 medium (Corning) with 10% FBS (Life Tech). The $CD4^+$ T cells used in SELEX A and B were rested in IL-2 spiked cell media overnight prior to selection for removing the cell-freezing reagent, DMSO. In the later SELEXes, $CD4^+$ T cells were either rested in cytokine-free cell media or being repeatedly washed with buffer to remove DMSO prior to selection. To prepare activated T cells, we used recombinant cytokines (Miltenyi) and CD3/CD28 stimulation Dynabeads (Thermo Fisher). IL-7 and IL-15 were used on $CD4^+$ T cells, while IL-2 and IL-15 were used in $CD8^+$ T cell culture media, along with the stimulation beads supplemented on day 0. On day 9, the stimulation beads were removed by pipetting cells with p1000 tips and separation on a magnetic rack. Activated $CD4^+$ and $CD8^+$ T cell culture was kept in the complete culture media containing cytokines for expansion until day 21.

4.2.2 Cell staining and flow cytometry

The following live/dead stain and antibodies were used for staining cells: Zombie Violet (1:500 in 100ul containing 10^6 cells, BioLegend), PE-antihuman CD3 (1:100, BioLegend, HIT3a), FITC-antihuman CD3 antibody (1:100, BioLegend, UCHT1), biotin-antihuman CD3 antibody (1:11, Miltenyi, OKT3), biotin-antihuman CD4 antibody (1:250, Miltenyi, REA623), polyclonal Alexa Fluor 700-antihuman CD4 antibody (R&D system, FAB8165N), APC-Cy7-antihuman CD4 (1:100, BioLegend, RPA-TA), APC-antihuman CD4 antibody (1:100, BioLegend, B234854), biotin-antihuman CD8 antibody (1:250, Miltenyi, REA734), FITC-antihuman CD8a (1:100, BioLegend, RPA-T8), APC-Cy7-antihuman CD14 (1:200, Molecular probes, 6ID3), Super Bright 702-antihuman CD19 (1:100, eBioscience, SJ25C1), Super Bright 600-antihuman CD56 (1:100, eBioscience, TULY56), polyclonal HRP-Anti-fluorescein antibody (1:2000, Abcam, ab6656), APC-anti-fluorescein antibody (1:100, Biolegend, FIT-22), and Alexa Fluor 647-streptavidin (1:500, BioLegend). Aptamers were ordered from IDT, with FAM, Cy5, or biotin labeled on the 5'-end.

Wash buffer and binding buffer were used for washes and staining in the aptamer binding studies. Wash buffer was made with 500 ml DPBS (with calcium and magnesium, Corning) plus 2.5 ml 1M $MgCl_2$ (Fisher) and 2.25g D-glucose (Sigma-Aldrich), which contains 0.137M Na^+ and 0.0055M Mg^{2+}. Binding buffer was made of wash buffer supplemented with 0.1 mg/ml yeast tRNA (Invitrogen) and 1% BSA (Miltenyi). The cell staining process was kept at 4 ^oC to avoid internalization. RAN aptamer, a binder that does not bind to any cell types used in this study, was used as control. The fluorescence readout of aptamer binding was collected using Attune NxT cytometer (Invitrogen).

4.2.3 Aptamer binding study using protein-coated well plates

The buffer used for washes in this study was wash buffer (section 4.2.2) with 0.5% BSA and 0.01% tween 20. The blocking buffer consisted of wash buffer with 5% BSA, 0.1 mg/mL tRNA, 0.1 mg/mL salmon sperm DNA, and 0.01% tween 20. The binding buffer used to dilute aptamer library was wash buffer with 2% BSA, 0.1 mg/mL tRNA, 0.1 mg/mL salmon sperm DNA, and 0.01% tween 20.

Nunc MaxiSorp flat-bottom 96 well plate was coated with His-tagged and Fc-tagged recombinant human CD4 protein (Sino) at 5 µg/mL and 8 µg/mL in DPBS, respectively, by incubation overnight at 4 ^{o}C. Next day, the plate was washed 3 times by filling the wells with buffer, flicking over the sink, and patting the plate on a paper towel to remove the liquid in the wells. The wells were then blocked by incubating with blocking buffer at room temperature for 1.5 hours. After which the solution was removed, and the FAM-labeled aptamer libraries were added to each well at 250 nM in binding buffer. The solution was incubated at room temperature for 30 minutes. The wells were washed 4 times and stained with antiFITC-HRP (1:2000 dilution) in wash buffer for 1 hour at room temperature. The wells were washed 4 more times before incubation with HRP substrate (3,3',5,5'-tetramethylbenzidine and hydrogen peroxide mixed at 1:1) for 5-30 minutes until desired color develops. Equal volume of 2M sulfuric acid was added to the wells to stop the color development. Within 30 minutes after the reaction was stopped, the absorbance at 450 nm and reference at 550 nm was tested on a plate reader (Infinite 200 Pro, Tecan).

4.2.4 Traditional cell-SELEX

The experimental design of cell-SELEX with un-modified DNA bases used are summarized in **Figure 4.2A, 4.3A, 4.4A**, **4.5A, 4.6A,** and **4.8A**. The general cell-SELEX process was adapted from a published protocol.[25] For cell-SELEX using un-modified DNA bases, we purchased a naïve library contains sequences with N52 variable region flanked by 18 bases constant region from IDT. This provides us theoretically 10^{16} unique sequences in the starting naïve library. A total volume of 400µL was used throughout all library incubation steps. The key factors account for evolution stress, such as target cell numbers, incubation time, blocker concentration, are indicated in **Figure 4.2A, 4.3A, 4.4A**, **4.5A, 4.6A, 4.7A,** and **4.8A.** Most selections, except for the competitive steps, took place at 4^{o}C to avoid cell internalization. To elute the sequences from target cells, the cells were heated at 95^{o}C in wash buffer. The cell debris was then spun down, and the supernatant was collected. After each selection round, we optimized the PCR cycles to amplify the libraries with Phusion High-Fidelity DNA polymerase (NEB), dNTP (QIAGEN), FAM labeled forward primer, and biotinylated reverse primer (IDT). The reverse strand of the amplified pool was removed using High Capacity Neutravidin Agarose Resin

(Thermo Fisher). The forward single stranded DNA (ssDNA) was eluted from the resin using sodium hydroxide and can be annealed after solvent exchanged into wash buffer at 1μM.[25]

4.2.5 Competitive cell-SELEX

In competitive cell-SELEX, aptamer pools were first incubated with a mixed cell population. Target cells were then isolated from these aptamer-stained populations using the one or combined following methods. The competitive selection steps were done either using the Magnetic-Activated Cell Sorting (MACS) systems by Miltenyi or Fluorescence-Activated Cell Sorting (FACS) method on Canto II flow cytometer (BD) hosted in Department of Pathology at the University of Washington. Commercialized kits were used to stain cells in MACS methods including Pan T cell kit, biotin-antihuman CD8 antibody, biotin-antihuman CD4 antibody, anti-biotin Microbeads, and CD4 T cell negative selection kit, which were purchased from Miltenyi. For the FACS process, APC-antihuman CD4 was used to separate $CD4^{hi}$ cells.

4.2.6 Complementary strand annealing

In one of the competitive cell-SELEX strategies, we used complementary strands to neutralize known undesired sequences (**Figure 4.5**). The complementary strands target these variable regions were order from IDT without any labels. Prior to aptamer pool annealing, the complementary strands were added to the pool according to the sequence percentages indicated in **Supplementary Table 4.1**. The wash buffer containing aptamer pool and complementary strands was heated at 95^{o}C for 5 minutes on a heating block. We then moved the heating block from heat source to the bench top. The solution will cool down slowly to room temperature in about 2.5 hour. The annealed pool was then either kept on ice or stored at -20^{o}C until selection.

4.2.7 Ligand-guided cell-SELEX

The ligand-guided selection method was implemented in the SELEX right after 3 rounds of selection using complementary strand annealing (**Figure 4.5A**). In each round, the negative

selection on $CD8^+$ T cells were first used to remove undesired sequences, and then positive selection with $CD4^+$ T cells. After positive selection, polyclonal antihuman CD4 antibody (R&D system, FAB8165N) staining was used to elute the CD4 receptor-bound sequences instead of heating. Higher concentrations of CD4 antibody were applied in earlier rounds to compete more aptamer sequences off from the target cells. Lower concentrations of CD4 antibody were applied in later rounds to avoid undesired sequences being eluted by non-specific interaction of the antibodies (**Figure 4.6A**).

4.2.8 SOMAmer cell-SELEX

We used a naïve library with sequences contain a N40 variable region flanked by 20 bases-long constant regions for SOMAmer SELEX. Biotinylated forward primer and FAM-labeled reverse primer used for amplification were ordered from IDT. The SOMAmer selection process (**Figure 4.7B**) was mostly the same as competitive cell-SELEX described in section 4.2.3 and 4.2.4. Different from the traditional SELEX, SOMAmer SELEX requires an additional primer extension step. At the end of each selection round, the library pool was amplified by PCR with optimized cycle number. The PCR product was incubated with Dynabeads MyOne Streptavidin C1 beads, on which the biotinylated forward strands were immobilized. The reverse strands were removed by sodium hydroxide incubation. The Streptavidin beads containing the forward strands were washed and mixed with FAM-labeled reverse primer, dATP, dCTP, dGTP (QIAGEN), and TrpdU (TriLink). The reverse primers were annealed onto the forward strands at 95 ^oC for 5 minutes followed by 60 ^oC for 1 minute. After annealing, we added the KOD polymerase and let primer extension proceed for 6-8 hours at 68 ^oC. The reverse strands containing TrpdU were collected by sodium hydroxide incubation. The SOMAmer reverse strands were desalted and resuspended in wash buffer for the next round of selection.

4.2.9 Protein/cell combination SELEX

In the protein/cell SELEX strategy, His-tagged and Fc-tagged recombinant human CD4 protein (Sino) were immobilized onto nickel or protein G beads (Invitrogen), respectively, for

positive selection. Bare nickel or protein G beads were used for negative selection in the first 4 rounds. The used of different recombinant protein and beads were switched back-and-forth to avoid selecting for Hig tag or Fc tag binding aptamers. Round 5 through round 7 selections were done by using either primary T cells or Fc-tagged recombinant protein to increase the chance to enriching sequence that bind to both recombinant and natural CD4 protein. In the last round, HEK293T cells were used for negative selection to reduce non-specific binding aptamers. The resulting sequence pool was split in half for two separate positive selections on $CD4^+$ T cells and $CD8^+$ T cells. This final round was designed to identify the $CD8^+$ T cell-binding sequences to be ruled out later in the NGS analysis process. The binding condition for selection rounds on recombinant proteins were done at room temperature, whereas the selection rounds using cells were done at 4 ^oC.

4.2.10 NGS and sequence analysis

MiSeq System (Illumina) and MiSeq Reagent kit v2 (300 cycles) was used for NGS. The libraries were amplified using barcoded primers unique for each round library. FASTAptamer v1.0.3 toolkit was used to analyze the FASTA files.[26] FASTAptamer-count was first used to identify top aptamers with the highest frequency (high count). FASTAptamer-enrich was then used to analyze the fold-enrichment of each unique sequences in adjacent rounds (later over earlier rounds). MEME suite v5.2.0 Motif Discovery tool was used to predict binding motifs of top aptamers in final rounds base on their sequence similarities.[27] A certain number of top aptamer sequences of final rounds were used for phylogenic tree generation with FigTree toolkit v1.4.4 to compare the similarities between each sequences.[28] The NUPACK web application was used to simulate aptamers folding into their thermally stable secondary structures.[29]

4.3 Results and discussion

4.3.1 Binding studies using reported CD4 binding aptamers have been unsuccessful

We first tested three DNA aptamers that was reported to target CD4 protein. 1-62 aptamer was developed through a hybrid SELEX using $CD4^+$ Karpas 299 cell line and recombinant CD4

protein as enrichment targets.[30] This aptamer was reported to have apparent K_D 1.59 nM on Karpas 299 cells. The authors applied 1-62 aptamer to inhibiting viral entry to these cells by blocking gp-120 and CD4 receptor interactions. We tested 1-62 aptamer binding on primary $CD4^+$ T cells in PBS-based buffer with highest aptamer concentration at 250 nM. At first glance, 1-62 aptamer showed slight increased staining on $CD4^+$ T cells comparing to RAN aptamer. However, increased binding was also observed on $CD4^-$ T cells (likely to be CD8 T cells, **Figure 4.1A**). Thus, we did not apply 1-62 aptamer on traceless cell isolation due to its low affinity on primary CD4 T cells and off-target binding to other immune cells. Zhu et al. converted a reported RNA CD4 aptamer to its DNA homolog for siRNA delivery. The original RNA aptamer was enriched by recombinant CD4 protein immobilized beads and was tested to have sub-nanomolar apparent K_D on transfected murine T cell line expressing human CD4 receptor.[31] The converted DNA CD4 aptamer was combined with HIV-1 protease siRNA to specifically deliver siRNA into acute T cell leukemia cell line forced-expressing CD4 receptor. Significant reduction of HIV-1 protease mRNA expression was achieved by using 100 nM and 200 nM of DNA-siRNA chimera.[32] We tested this DNA CD4 aptamer binding at 100 nM on Jurkat cells which express CD4 receptor (**Figure 4.1B**). However, we did not see relative increased staining using this aptamer over the control aptamer (**Figure 4.1B**). Fellows et al. reported a DNA aptamer that binds to recombinant CD4 receptor immobilized beads with K_D~2.93 nM. This aptamer, U26, was developed through crossover-SELEX by switching the enrichment target between recombinant CD4 protein and CD4 expressing human lymphoma cell line for 6 rounds. The U26 aptamer was applied to lateral-flow strip test as a CD4 expression monitoring system for HIV infection.[24] Unfortunately, we did not see U26 binding on primary $CD4^+$ T cells comparing to either A3t (CD8 aptamer) or unstained cells (**Figure 4.1C**). All the above SELEX processes were done on either recombinant CD4 protein or cancer cell lines expressing CD4 receptor. We have yet come across an aptamer that is specific to CD4 receptor expressed on healthy primary $CD4^+$ T cells. Therefore, we tried various versions of SELEX aiming at enriching CD4 aptamers in this chapter.

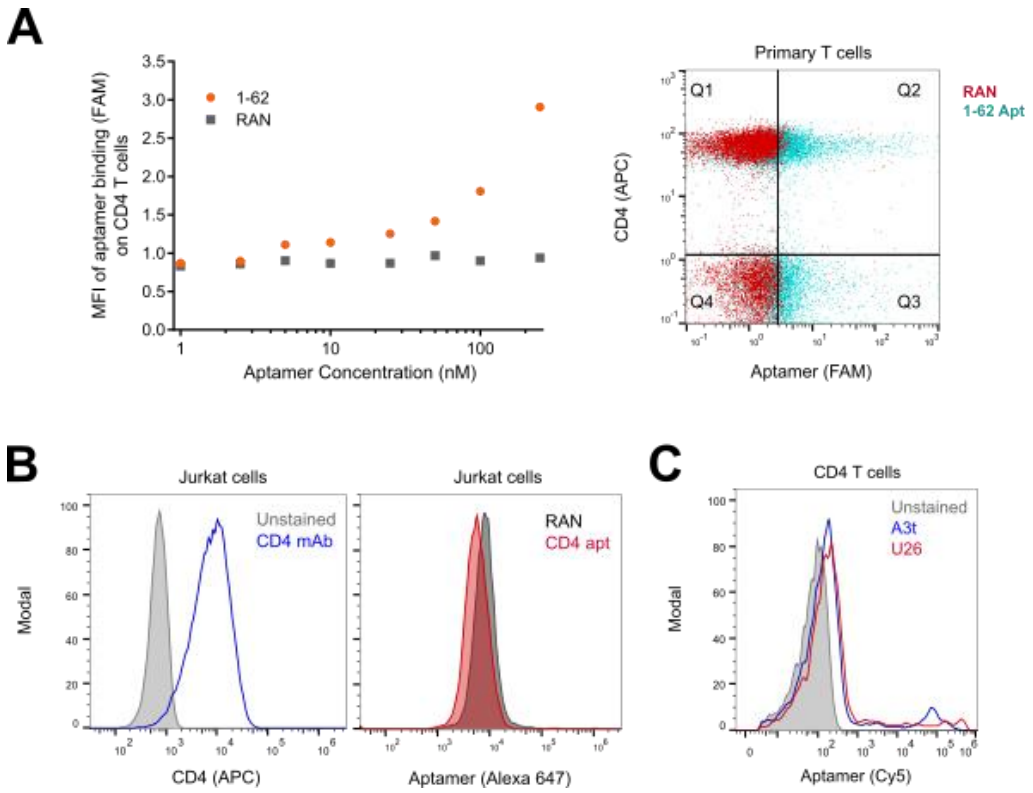

Figure 4.1. Validating reported CD4 binding aptamers on CD4 expressing T cells and cell lines. (A) Flow cytometry binding curves of aptamers and CD4 antibody co-staining on T cells. MFI was collected by gating on $CD4^+$ cells stained at several concentrations. Pseudo-color dot plot was the co-staining result using CD4-APC antibody and 250 nM 1-62 aptamer. (B) Flow cytometry binding study on Jurkat cells. CD4 expression was verified by CD4-APC antibody (left). Biotinylated aptamer single stain was done on Jurkat cells without antibody staining with 100 nM Zhu CD4 aptamer and RAN aptamer, followed by streptavidin Alexa 647 secondary staining (right). (C) 500 nM aptamer-Cy5 staining on CD4 T cells. MFI: median fluorescent intensity; FAM: carboxylfluorescein; APC: allophycocyanin; Cy5: cyanine 5.

4.3.2 Combinational cell-SELEX - combining traditional cell-SELEX with competitive SELEX

The input naïve library (purchased from IDT) provides 10^{16} unique sequences. Each sequence has a N52 randomized variable region, flanked by two 18-mer constant region for PCR amplification. We started our cell-SELEX attempt by mostly using CD4 T cells (strategy A) or PBMC with a T cell isolation step (strategy B) as positive selections. The two strategies utilize different methods to eliminate background binding on non-T cells in leukapheresis, namely NK cells, monocytes, B cells, and granulocytes (**Figure 4.2A**). The target cells were pre-incubated in IL-2 cytokine spiked cell media (20 ng/ml) before selection to sufficiently remove DMSO freezing

reagent. In strategy A, we used T cell-depleted apheresis to reduce background binders. At the same time, we consistently used $CD4^+$ T cells to enrich CD4 protein binders and competitive cell-SELEX in the last round. In strategy B, we used competitive SELEX starting from early rounds to enrich T cell binders more stringently by depleting non-T cell binders at the same time. $CD4^+$ T cells were used as target cells only in the last round. J.RT3-T3.5 cells, which are $CD3^-$ and $CD28^-$, were used as counter selection cells. Both strategies yielded a final round pool that binds to $CD4^+$ T cells more than counter selection cells (**Figure 4.2B and C**). We sequenced the rounds from both strategies with next generation sequencing (NGS). Through sequence analysis with FASTAptamer tool kit,[26] we found a couple of overlapping high count aptamers in the top 30 aptamers in strategy A and B final pool. One of the overlapped sequences is a previously reported CD8 aptamer (**Supplementary Figure 4.1**, shaded in yellow). The top 50 sequences in the final round library of strategy A and B were analyzed separately using FigTree software.[33] Although neither libraries have highly diversified clusters, strategy A showed slightly more distinct structural enrichment. This was verified on MEME suite[27] that a 41-mer long motif was identified within the 52-mer variable region (**Supplementary Figure 4.1**). Therefore, we selected a few high-count sequences from strategy A, including one other overlapped sequence, A1 (**Supplementary Figure 4.1**, shaded in red). A1 was the only aptamer that binds to CD4 T cells in these selections (**Figure 4.2D**) and was later used as T-ALL drug delivery targeting ligand. However, we observed an incubation-dependent binding pattern of A1 on $CD4^+$ T cells (**Figure 5.3A, B, and C**; see chapter 5 for detailed binding characterization of A1). In order to exclude the incubation-dependent binding pattern, we adjusted our protocol in the next two strategies (C and D) to using cells only briefly incubated in culture media for 2 hours or were repeatedly washed prior to selection.

A

		Positive selection				Negative selection		
Round #	Library	Cell type and #	Time	Washes	Protein blocker	Cell type and #	Time	Protein blocker
1	13.7uM	30 million T cells	1h	3x	0.1% BSA	None	1h	0.1% BSA
2	500nM	10 million CD4+ T cells	1h	3x	0.1% BSA	10 million J.RT3-T3.5	1h	0.1% BSA
3	500nM	5 million CD4+ T cells	0.5h	3x	1% BSA	10 million J.RT3-T3.5	0.5h	1% BSA
4	250nM	5 million CD4+ T cells	0.5h	3x	1% BSA	10 million T cell depleted apheresis	0.5h	1% BSA
5	250nM	2.5 million CD4+ T cells	0.5h	4x	2% BSA	10 million T cell depleted apheresis	0.5h	2% BSA
6	250nM	2.5 million CD4+ T cells	0.5h	4x	5% FBS	10 million T cell depleted apheresis	0.5h	5% FBS
7	250nM	2.5 million CD4+ T cells	0.5h	4x	5% FBS	10 million T cell depleted apheresis	0.5h	5% FBS
8	250nM	5 million PBMCs and T cell isolation	0.5h	4x	5% FBS	None	0.5h	5% FBS
Strategy B								
4	250nM	10 million PBMCs and T cell isolation	0.5h	3x	1% BSA	10 million J.RT3-T3.5	0.5h	1% BSA
5	250nM	10 million PBMCs and T cell isolation	0.5h	4x	1% BSA	10 million J.RT3-T3.5	0.5h	1% BSA
6	250nM	2.5 million CD4+ T cells	0.5h	4x	1% BSA	10 million J.RT3-T3.5	0.5h	1% BSA

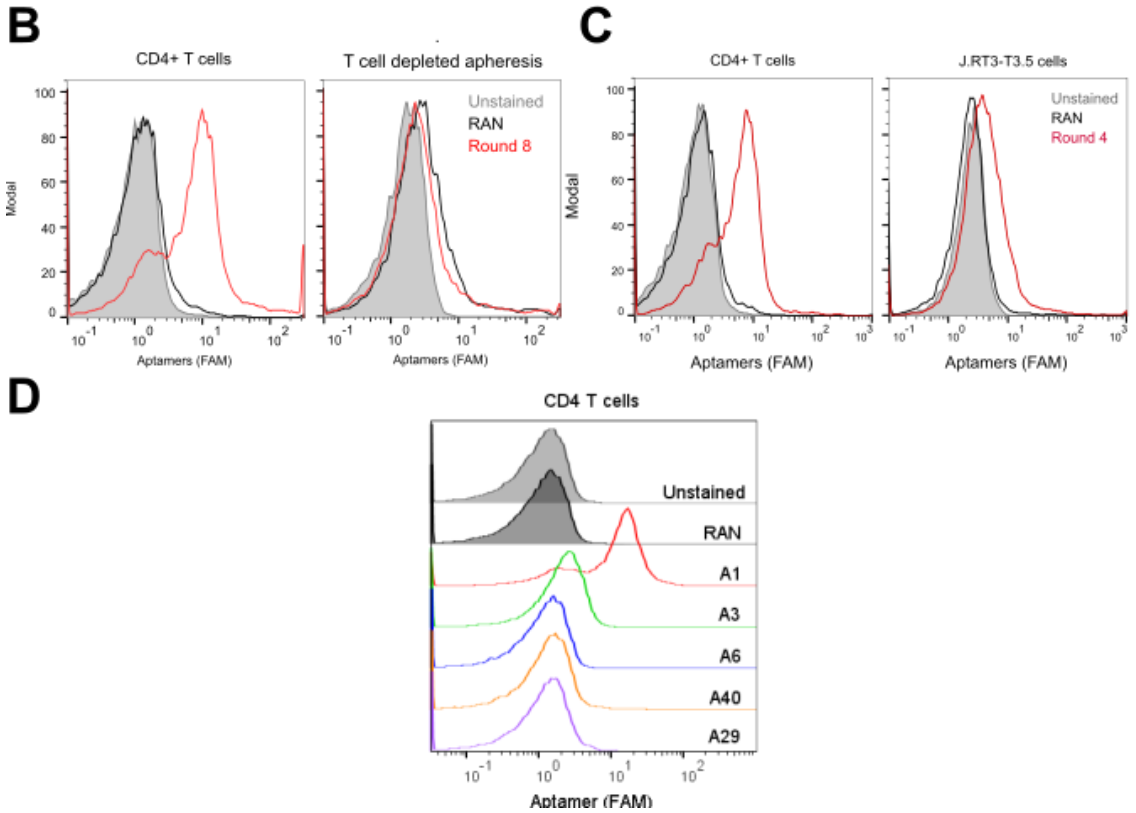

Figure 4.2. Combinational cell-SELEX strategy A and B experimental design and final round binding results. (A) First three rounds of selection were done using T cells and $CD4^+$ T cells as target; J.RT3-T3.5 as control cells. Selection branched out to strategy A and strategy B starting round 4. (Strategy A also showed in Figure 5.1) (B) Final round binding of strategy A using 250 nM aptamers. (Data same as Figure 5.2A) (C) Final round binding of strategy B using 200 nM aptamers. (D) Aptamer selected from strategy A binding on IL-2 media-incubated $CD4^+$ T cells at 250 nM. (Data same as Figure 5.2B) FAM: carboxylfluorescein.

Next, we used primary immune cells without cytokine pre-incubation in combinational cell-SELEX strategies C and D. Since there were CD8 aptamer sequences identified in strategy A and B (**Supplementary Figure 4.1**, shaded in yellow), we implemented $CD8^+$ T cell depletion either on T cells or PBMCs starting from round 2 (**Figure 4.3A**). However, despite depleting the non-target cells with CD8 antibody along or in combination with pan T cell isolation cocktail from round 2 to round 5, we still enriched libraries that preferentially bind to $CD8^+$ T cells (**Figure 4.3B**). A potential cause is the CD8 antibody might have competed off CD8 binding sequences in the process. Since the counter selection cell types used were mostly T cell-depleted apheresis, the competed-off CD8-binding sequences were, therefore, not depleted in the negative selection.

A

		Positive selection				Negative selection		
Round #	Library	Cell type and #	Time	Washes	Protein blocker	Cell type and #	Time	Protein blocker
1	13.7uM	10 million CD4+ T cells	1h	3x	0.1% BSA	None	1h	0.1% BSA
2	500nM	10 million T cells and isolation with CD8 mAb	1h	3x	0.5% BSA	10 million CD8 T cells	1h	0.5% BSA
3	500nM	10 million PBMCs and traceless isolation of CD4 T cells (CD8 mAb spiked T cell isolation kit)	0.5h	3x	0.5% BSA	10 million T cell depleted apheresis	0.5h	0.5% BSA
4	250nM	10 million PBMCs and traceless isolation of CD4 T cells (CD8 mAb spiked T cell isolation kit)	0.5h	4x	1% BSA	10 million T cell depleted apheresis	0.5h	1% BSA
5	250nM	5 million PBMCs and traceless isolation of CD4 T cells (CD8 mAb spiked T cell isolation kit)	0.5h	4x	1% BSA	10 million T cell depleted apheresis	0.5h	1% BSA

B

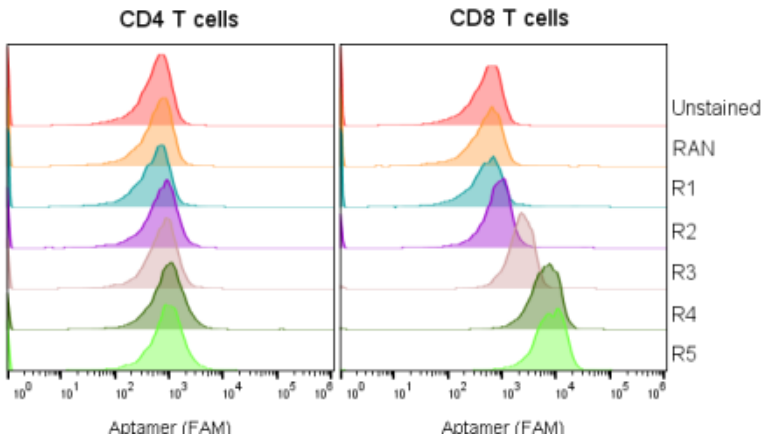

Figure 4.3. Combinational cell-SELEX strategy C (A) experimental design and (B) 250 nM round library binding study on flow cytometer. FAM: carboxylfluorescein.

In strategy D, we used $CD4^+$ T cells as target and $CD8^+$ T cells as control for the most rounds. In round 5, we performed negative selection on $CD8^+$ T cells first and split the library into 3 for different competitive positive selections, in which PBMCs were stained with libraries and were purified using CD4 antibody or T cell isolation cocktail spiked with CD8 antibody and sorted by FACS or MACS (**Figure 4.4A**). Through flow cytometry binding studies, we saw little enrichment throughout round 1 to 4, except for round 3 showing seemingly higher binding on CD8 T cells. With the competitive selection methods used in round 5 (R5), all R5 libraries had increased binding on CD4 T cells (**Figure 4.4B**). Although we also saw R5 library binding to CD8 T cells (**Figure 4.4B**), no known CD8 binders were found in the top 19 sequences in the R5 pools (list of sequences not shown). Interestingly, the A1 aptamer that we identified in strategy A was also found in the top 5 sequences of R5a, R5b, and R5c (#2 in a, #5 in b, #4 in c), despite the incubation steps were minimized. We first selected a few top sequences, namely 1a, 3a, 4a, 5a, 7a, and 8a, which carry highly representative motifs and are diverse from each other (**Supplementary Figure 4.2**). These aptamers were labeled with FAM for testing binding on $CD4^+$ and $CD8^+$ T cells. 5a, 7a, and 8a showed overall higher binding on both cell types than other sequences. However, there was only little to no preferential binding observed (**Figure 4.4C**). We ran the same binding study using biotinylated sequences with streptavidin Alexa 647 secondary staining for a stronger fluorescent signal on flow cytometer. However, the binding was not improved except for 5a. Both 7a and 8a binding were affected by biotinylation. We tested two more additional sequences, 13a and 22a, in the same study, but did not observe any targeted binding (**Figure 4.4D**). We took a closer look at FAM-7a and biotin-5a since they showed higher binding on both $CD4^+$ and $CD8^+$ T cells. We evaluated the specificity of these aptamers to primary T cells by co-staining PBMCs with aptamers and CD3 antibody. However, we found that FAM-7a binds more to the non-T cell fraction than T cells, whereas biotin-5a binds to all cell types (**Figure 4.4E**). Despite using refined experimental designs, we did not identify new CD4 T cell binders using strategy C and D.

A

Round #	Library	Positive selection: Cell type and #	Time	Washes	Protein blocker	Negative selection: Cell type and #	Time	Protein blocker
1	13.7uM	10 million CD4+ T cells	1h	3x	0.1% BSA	None	1h	0.1% BSA
2	500nM	5 million CD4+ T cells	1h	4x	0.1% BSA	10 million CD8 T cells	1h	0.1% BSA
3	250nM	5 million CD4+ T cells	0.5h	4x	0.1% BSA	10 million CD8 T cells	0.5h	0.1% BSA
4	250nM	5 million CD4+ T cells	0.5h	4x	1% BSA	20 million CD8 T cells	0.5h	1% BSA
5	250nM	**a.** 5 million PBMCs and FACS with CD4 mAb	0.5h	4x	1% BSA	20 million CD8 T cells (before positive selections)	0.5h	1% BSA
		b. 5 million PBMCs and traceless isolation of CD4 T cells (CD8 mAb spiked T cell isolation kit)						
		c. 5 million PBMCs and MACS with CD4 mAb						

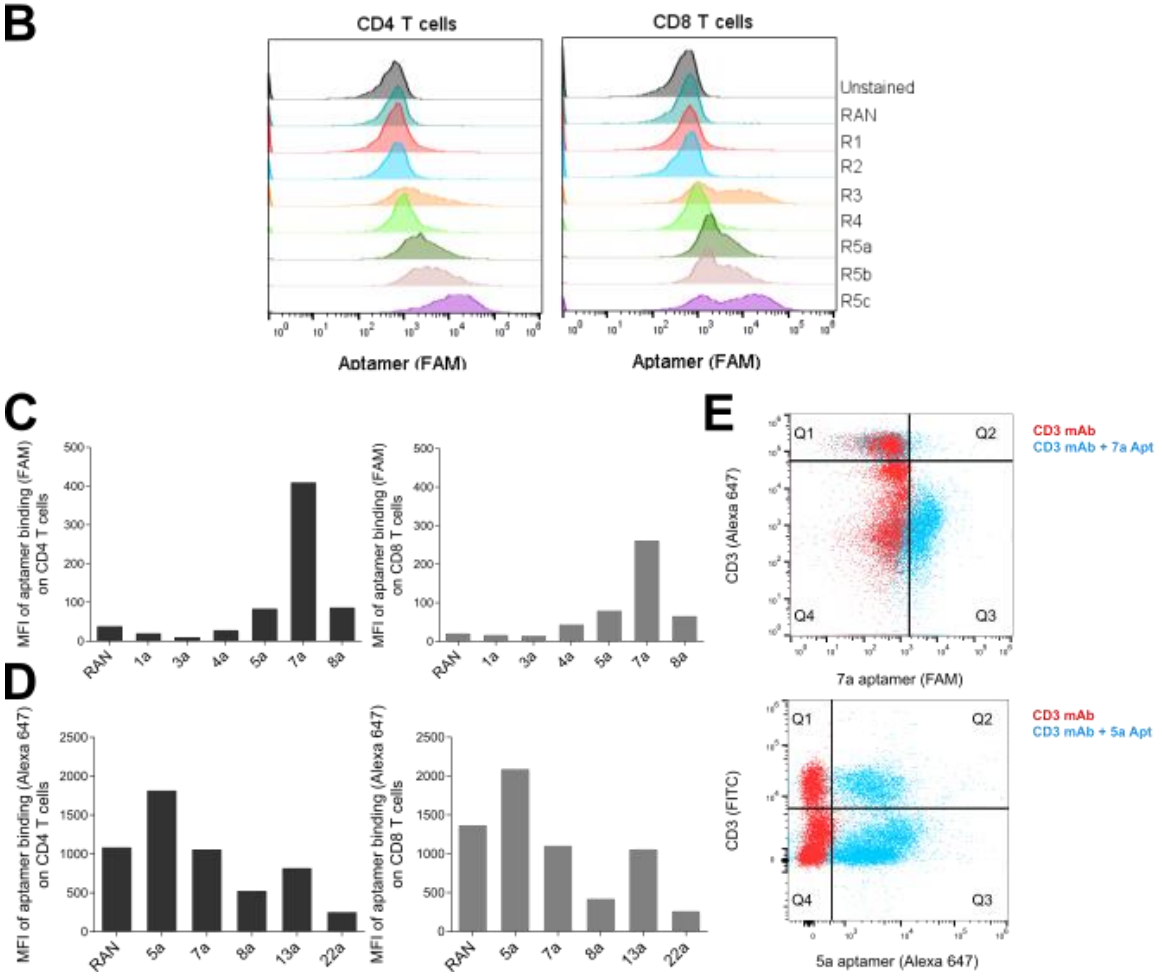

Figure 4.4. Combinational cell-SELEX strategy D (A) SELEX experimental design; (B) round binding study using 250 nM libraries staining $CD4^+$ and $CD8^+$ T cells; (C) 250 nM of selected aptamers labeled with FAM binding on $CD4^+$ and $CD8^+$ T cells; (D) 250 nM of the selected aptamers labeled with biotin followed by streptavidin Alexa 647 secondary staining on $CD4^+$ and $CD8^+$ T cells; (E) 250 nM FAM-7a and biotin-5a aptamers co-stained with CD3 antibody on PBMCs. MFI: median fluorescent intensity; FAM: carboxylfluorescein; FITC: fluorescein isothiocyanate.

4.3.3 Blocking non-binders with complementary strands

Since we discovered a couple of non-specific binders in the round 5a, 5b, and 5c libraries from strategy D, we proceeded to the next selection with these undesired aptamers neutralized by complementary strands annealing. We chose R5c library for round 6 selection because of its higher binding on CD4 T cells (**Figure 4.4B**). We used the strands that complement the variable region on the undesired aptamers tested in 4.3.2 section, in addition to A1 and TCBA3 (full-length A3t) that both discovered using the same source of naïve library lot. The individual complementary strands were added to the annealing solution using concentrations calculated based on R5c sequencing result (**Supplementary Table 4.1**) prior to the annealing process. These complementary strands, in theory, anneals to their corresponding aptamer variable regions composed of 35.63% of the total R5c sequences. The same concentration of each complementary strands calculated for the 125 nM library was applied throughout round 6 to 9 (**Figure 4.5A**). In round 9, competitive SELEX with CD4 antibody isolating CD4 T cells from PBMCs was used to increase stringency and to avoid eluting CD8 binder. We observed slower progressing enrichment comparing to the other combinational cell-SELEX. However, the enrichment of CD8 binding sequences were still more than CD4 binding sequences (**Figure 4.5B)**. It is possible the round libraries changed so much between rounds that the complementary strand concentration needs to be adjusted accordingly which requires pool sequencing and binding studies before every round.

A

		Positive selection					Negative selection		
Round #	Library	Cell type and #	Time	Washes	Nucleotide blocker	Protein blocker	Cell type and #	Time	Protein blocker
6	111nM	2 million CD4+ T cells	0.5h	4x	0.1mg/ml tRNA, 0.1mg/ml salmon sperm DNA, and complementary strands	1% BSA	20 million CD8 T cells	0.5h each	1% BSA
7	125nM	2 million CD4+ T cells					20 million CD8 T cells x2		
8	125nM	2 million CD4+ T cells					20 million CD8 T cells x2		
9	125nM	4.3 million PBMCs and MACS with CD4 mAb					20 million CD8 T cells x2		

B

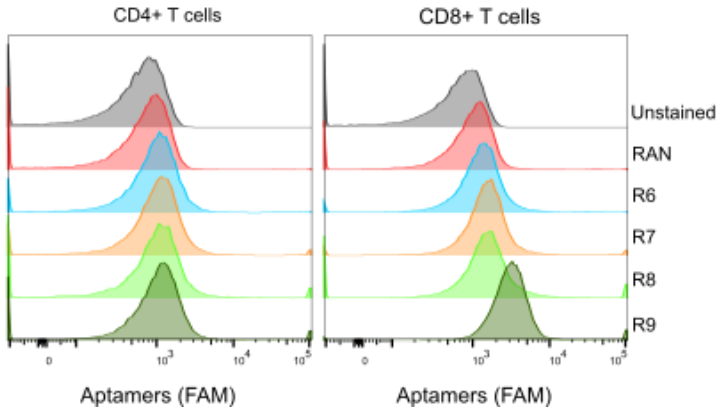

Figure 4.5. Combinational cell-SELEX with complementary strand blocking. (A) Round 6 to 9 selection with R5c library. (B) 125 nM library round binding on $CD4^+$ and $CD8^+$ T cells. FAM: carboxylfluorescein.

4.3.4 Ligand-guided cell-SELEX

Cell-SELEX in combination of complementary strand blocking yield aptamer round libraries that bind to both $CD4^+$ T cells and $CD8^+$ T cells at varying degrees. We decided to continue strategy D using round 8 library for more selections and incorporating an antibody competition step for sequence elution since round 8 library has less binding to $CD8^+$ T cells (**Figure 4.5B**). In general, this process is similar to the traditional cell-SELEX, except for eluting the sequences from the cells after positive selections. Higher concentration of polyclonal human CD4 antibody was used in the earlier rounds to elute more sequences from the target cells, hence has lower selection stringency. Lower concentration of the same antibody was used in the later rounds to avoid eluting sequences by non-specific interaction and provide higher selection stringency (**Figure 4.6A**). The binding study using the newly generated round 9 through round 11 libraries suggests that antibody competition did not enrich the sequences that bind to CD4 protein on the $CD4^+$ T cell surface. In addition, the parasitic sequences that bind to $CD8^+$ T cells persisted

(**Figure 4.6B**). It is important to note that we cannot control the non-specific interaction of the CD4 antibodies to other cell surface proteins since it is impossible to wash off excess antibodies during the elution steps. The only way to control background binding is by reducing antibody input. Since CD4 protein-binding sequences were not being eluted by the antibodies, a different antibody with higher affinity might be necessary for effective competition.

A

		Negative selection				Positive selection				
Round #	Library	Cell type and #	Time	Nucleotide blocker	Protein blocker	Cell type and #	Time	Washes	Nucleotide blocker	Protein blocker
9	125nM	20 million CD8+ T cells	0.5h	0.1mg/ml tRNA	1% BSA	2 millionCD4+ T cells	0.5h	4	0.1mg/ml tRNA, 0.1mg/ml salmon sperm DNA	1% BSA
10			0.5h				0.5h	5		
11			0.75h				0.75h	5		

	Antibody competition		
Round #	Antibody concentration	Time	Blockers
9	41.6nM	0.5h	1% BSA
10	13.16nM		
11	4.2nM		

B

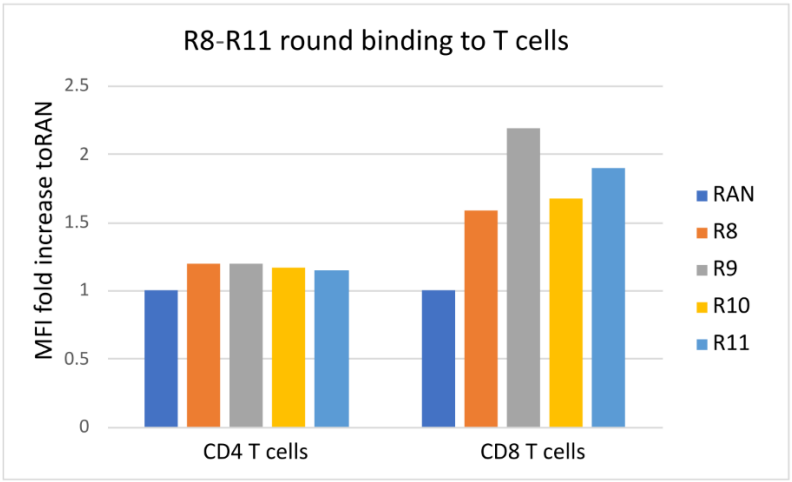

Figure 4.6. LIGS cell-SELEX with anti-human CD4 antibody. (A) Round 9 to 11 selection strategy. (B) 125 nM FAM-labeled library round binding on $CD4^+$ and $CD8^+$ T cells. FAM: carboxylfluorescein.

4.3.5 SOMAmer cell-SELEX

After completing the above selection strategies, we concluded that CD4 receptor is a difficult target to select for aptamer binders. Here, we implemented an artificial base reported to improve the interaction between nucleotides and proteins. The artificial base, 5-tryptaminocarbonyl-dU (TrpdU), is a modified uridine carrying a tryptamino side chain. This hydrophobic side chain is similar to tryptophan and could expand the possible binding mechanism between aptamers and proteins. DNA aptamers incorporated with these modified bases, also called SOMAmers, have shown slower dissociation rate to target due to the additional hydrophobic interactions.[23] Similar to strategy D, we use $CD4^+$ T cells as target cells and $CD8^+$ T cells as control cells in most rounds in this SELEX. Starting round 4, we reverse the selection order by doing negative selection before positive selection to further decrease the aptamer concentration incubated with target cells. Competitive SELEX on apheresis cells (containing PBMCs and granulocytes) were used in round 5 and round 6 with $CD4^+$ T cell negative selection kit. Different concentrations of salmon sperm DNA, and along with yeast tRNA at constant concentration, was used in the selections to decrease non-specific anionic interaction of aptamers. However, after 6 rounds of selection, where we usually see libraries enrichment, there was no enrichment on either cell types. Although it will further increase the cost, incorporating additional modifications might be beneficial for CD4 binder selections.

A

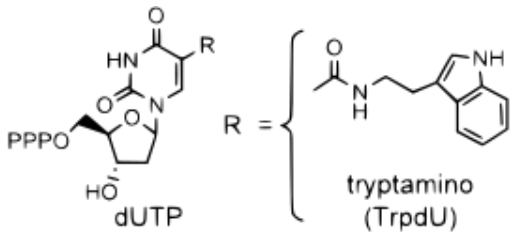

B

		Positive selection					Negative selection		
Round #	Library	Cell type and #	Time	Washes	Nucleotide blocker	Protein blocker	Cell type and #	Time	Protein blocker
1	13.7uM	30 million CD4+ T cells	1h	3x	None	0.1% BSA	None	1h	0.1% BSA
2	500nM	10 million CD4+ T cells	1h	3x	0.1mg/ml tRNA	0.5% BSA	10 million CD8 T cells	1h	0.5% BSA
3	500nM	5 million CD4+ T cells	0.5h	3x	0.1mg/ml tRNA	1% BSA	10 million CD8 T cells x2	0.5h each	1% BSA
4	250nM	2.5 million CD4+ T cells	0.5h	3x	0.1mg/ml tRNA, 0.02mg/ml salmon sperm DNA	1% BSA	10 million CD8 T cells x2 (negative selection first)	0.5h each	1% BSA
5	250nM	25 million apheresis cells and traceless selection of CD4 T cells	0.5h	4x	0.1mg/ml tRNA, 0.05mg/ml salmon sperm DNA	1% BSA	10 million CD8 T cells x3 (negative selection first)	0.5h each	1% BSA
6	250nM	12.5 million apheresis cells and traceless selection of CD4 T cells	0.5h	4x	0.1mg/ml tRNA, 0.08mg/ml salmon sperm DNA	1% BSA	10 million CD8 T cells x5 (negative selection first)	0.5h each	1% BSA

C

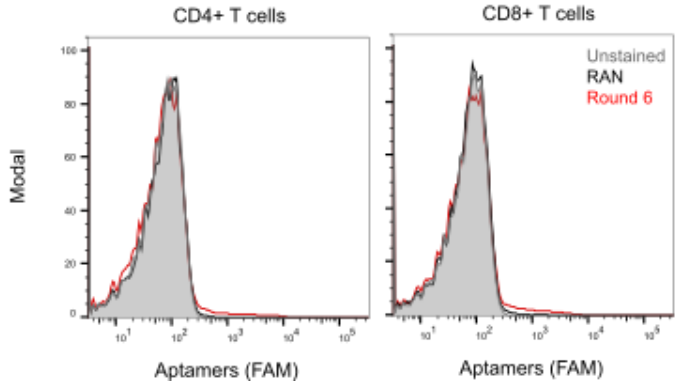

Figure 4.7. SOMAmer combinational cell-SELEX. (A) Chemical structure of TrpdU. Scheme adopted from ref. [23]. (B) Experimental design of combinational cell-SELEX. (C) 250 nM final round library binding on $CD4^+$ and $CD8^+$ T cells.

4.3.6 Protein/cell combination SELEX

As indicated in **Figure 4.8A**, the first 7 rounds of protein/cell SELEX consist of 5 selections on recombinant protein and 5 selections on primary cells. We first tested binding of round 4 to round 6 libraries on recombinant CD4 proteins. Encouragingly, all 3 libraries showed binding on recombinant CD4 proteins with both Hig-tag and Fc-tag (**Figure 4.8B**). We further tested round 6 and round 7 library binding on PBMCs. When we gated on the T cells in PBMCs, we observed a higher binding of aptamer libraries compared to gating on non-T cell fraction (**Figure 4.8C**). If we gate on different T cell subsets and look at $CD4^+$ T cells and $CD8^+$ T cells

separately, both libraries showed more binding on $CD8^+$ T cells. This, again, proofed that parasitic sequences in the libraries are challenging to remove. However, a small increased binding of library binding to $CD4^+$ T cells persisted (**Figure 4.8D**). Which indicates some high affinity $CD4^+$ T cell-binding sequences might exist in those libraries despite there might be a high abundance of $CD8^+$ T cell-binding sequences. Therefore, we performed another round of selection on cells (round 8), in which human embryonic kidney cells that has been used for isogenic cell-SELEX, HEL293T cells[34], was used for negative selection. Both T cell subsets were used for positive selection. By performing positive selection on undesired targeting cell type, we aim at amplifying the undesired sequences so we can remove them later on through NGS analysis.[35]

A

		Negative selection				Positive selection				
Round #	Library	Target and concentration	Time	Nucleotide blocker	Protein blocker	Target and concentration	Time	Washes	Nucleotide blocker	Protein blocker
1	1000ul 10uM (10nmol)	X	X	X	X	100nM (100pmole) CD4-His on 50ul Ni Dynabeads	1h	4	0.1mg/ml tRNA	0.1% BSA
2	300ul 500nM (150pmol)	50ul Ni beads	1h	0.1mg/ml tRNA	0.25% BSA	20nM (6pmole) CD4-His on 10ul NiDynabeads	1h	4	0.1mg/ml tRNA	0.25% BSA
3	300ul 500nM (150pmol)	100ul Protein G beads	0.5h	0.1mg/ml tRNA	0.5% BSA	20nM (6pmole) CD4-Fc on 20ul Protein G beads	0.5h	4	0.1mg/ml tRNA	0.5% BSA
4	300ul 250nM (75pmol)	50ul Ni beads	0.5h	0.1mg/ml tRNA	1% BSA	10nM (3pmole) CD4-His on 5ul Ni beads	0.5h	5	0.1mg/ml tRNA	1% BSA
5	300ul 250nM (75pmol)	X	X	X	X	5 million CD4 T cells	0.5h	5	0.1mg/ml tRNA, 0.1mg/ml salmon sperm DNA	1% BSA
6	300ul 250nM (75pmol)	5 million CD8 T cells	0.5h	0.1mg/ml tRNA, 0.1mg/ml salmon sperm DNA	2% BSA	5 million CD4 T cells	0.5h	5	0.1mg/ml tRNA, 0.1mg/ml salmon sperm DNA	2% BSA
7	300ul 250nM (75pmol)	100ul Protein G beads	0.5h	0.1mg/ml tRNA, 0.1mg/ml salmon sperm DNA	2% BSA	20nM (6pmol) CD4-Fc on 20ul Protein G beads	0.5h	5	0.1mg/ml tRNA, 0.1mg/ml salmon sperm DNA	2% BSA
8	300ul 100nM (30pmol)	5 million HEK293T cells	0.5h	0.1mg/ml tRNA, 0.1mg/ml salmon sperm DNA	2% BSA	1 million CD4 T cells	0.5h	6	0.1mg/ml tRNA, 0.1mg/ml salmon sperm DNA	2% BSA
						1 million CD8 T cells	0.5h	6	0.1mg/ml tRNA, 0.1mg/ml salmon sperm DNA	2% BSA

B

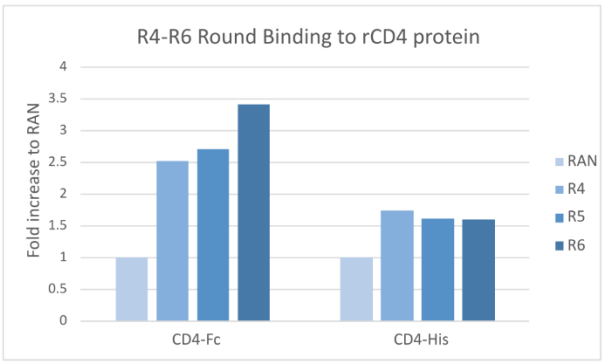

C

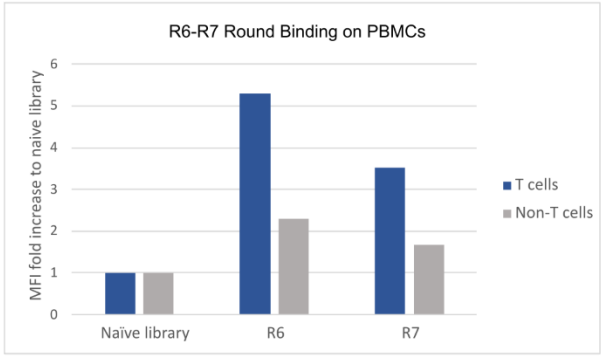

D

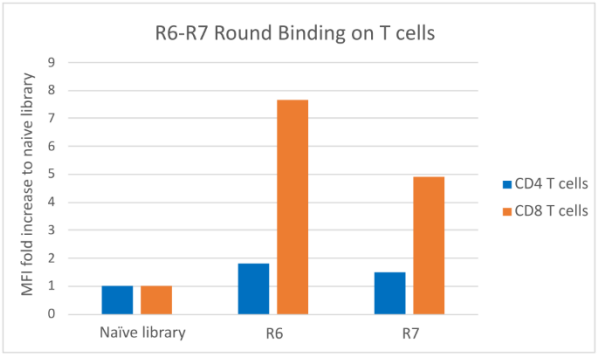

Figure 4.8. Protein/cell SELEX. (A) Selection strategy for round 1 through 8 using His-tagged and Fc-tagged recombinant human CD4 proteins and primary T cells. (B) Colorimetric round binding study by staining recombinant CD4 proteins with 250 nM R4-6 libraries. (C) 250 nM FAM-labeled libraries binding on PBMCs, followed by antiFITC APC and antihuman CD3 antibody staining. T cells were gated on $CD3^+$ cells, whereas non-T cells were gated on $CD3^-$ cells. (D) 250 nM FAM-labeled library round binding on PBMCs, followed by antiFITC-APC secondary staining, antihuman CD4 staining, and antihuman CD3 staining. $CD4^+$ T cells were gated on $CD3^+CD4^+$ cells, whereas $CD8^+$ T cells were gated on $CD3^+CD4^-$ cells. FAM: carboxylfluorescein; APC: allophycocyanin; FITC: fluorescein.

Three potential CD4 protein-binding aptamers were selected from this SELEX strategy (**Figure 4.9A**). We chose these sequences with the following reasons. First, they have high representation in the R8(CD4) library. Secondly, most of them were enriched in sequence count from round 6 to round 7, of which the library binding to $CD8^+$ T cells decreased (**Figure 4.8D**). Lastly, they show higher sequence count in R8(CD4) over R8(CD8). The selected aptamers, aptamer #1, #2, and #3, were first tested on $CD4^+$ T cells along with low concentration dextran sulfate, an anionic blocker commonly used to reduce background binding[36], incubation. While all three sequences showed high binding to $CD4^+$ T cells without dextran sulfate blocking, only aptamer #1 retains binding on about 13% of the $CD4^+$ T cell population with dextran sulfate blocking (**Figure 4.9B**). When incubated with PBMCs, aptamer #1 also showed low level of binding on monocytes, but no binding on $CD8^+$ T cells, B cells, and NK cells when incubated along with dextran sulfate (**Figure 4.9C**). It is encouraging that aptamer #1 binds to a subset of $CD4^+$ T cells and shows low to none binding on other cell types in PBMCs. However, this binding characteristic also suggests the target protein of aptamer #1 is not CD4 receptor. Further evaluation of aptamer 1 binding on PBMCs from different donors, as well as receptor identification with pull-down assay are needed for characterization.

A

	Variable Region Sequence	Top 4 rankings	Enrichment R7/R6	Enrichment R8(CD4)/R8(CD8)
#1	TGTGTTCTGATGTTGAGAACTTCATACATGTTACTGTCATACCCTCTCAATT	R5, R6, R7, R8(CD4)	1.354	3.453
#2	CCCACCGTATTTAACCCCCGACTCTTTTCCTCGTTCACTCTGTATCTCTGGA	R7, R8(CD4)	2.708	1.727
#3	TGCTACGGTGTTGCGTCCTCTATATATCCTCGGAAGTATAAATGCGGCTTTT	R8(CD4)	NA	5.181

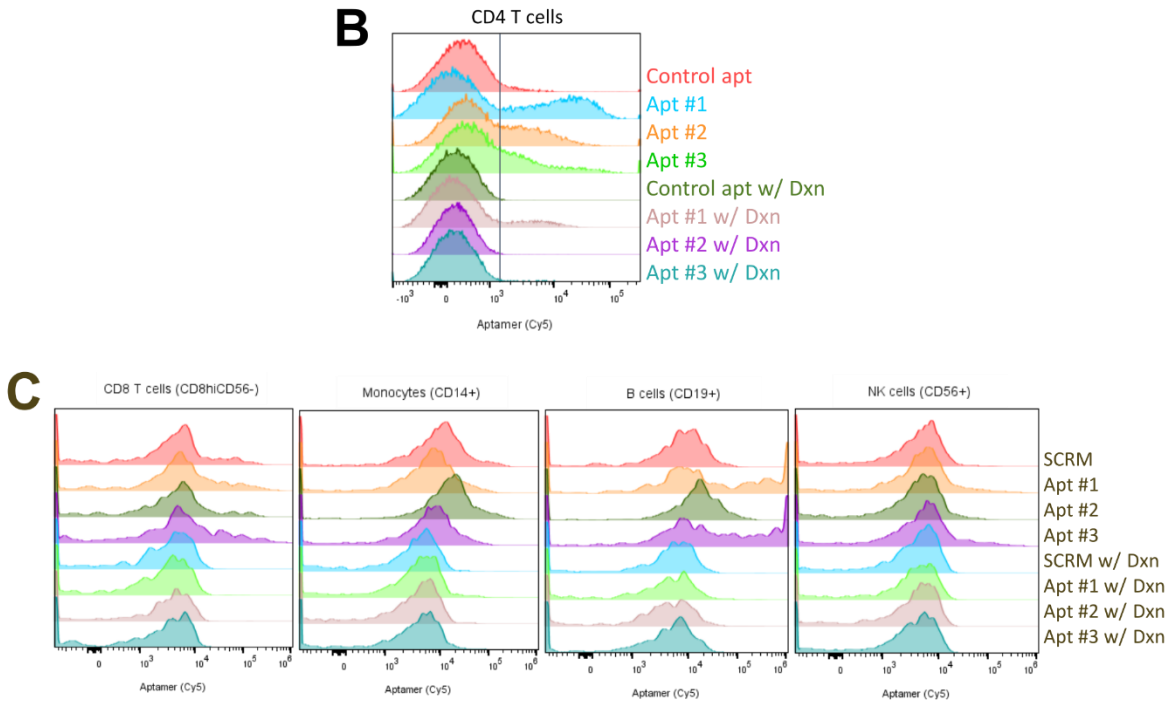

Figure 4.9. Novel sequences developed through protein/cell SELEX. (A) 3 sequences identified through protein/cell SELEX. (B) Cy5-labled aptamer #1, #2, and #3 binding on $CD4^+$ T cells with or without 0.2mM dextran sulfate as anionic blocker. A CD8 protein-binding aptamer was used as control. (C) Cy5-labled aptamer #1, #2, and #3 binding on $CD8^+$ T cells (PBMCs gated on $CD8^{hi}CD56^-$ cells), monocytes (PBMCs gated on $CD14^+$ cells), B cells (PBMCs gated on $CD19^+$ cells), and NK cells (PBMCs gated on $CD56^+$ cells) with or without 0.2mM dextran sulfate as anionic blocker.

4.4 Conclusion

To conclude, we reported 4 different combinational cell-SELEX using natural DNA library, a non-binder targeted blocking method, an antibody elution method, a SOMAmer combinational cell-SELEX, and a protein/cell SELEX used to discover CD4 protein binding aptamers. Despite the selection design has been consistently targeting $CD4^+$ T cell binders and depleting $CD8^+$ T cell or non-T cell binders, we still enriched non-binding, non-specific binding, and $CD8^+$ T cell binding

libraries in the end. A1, the only aptamer that shows high binding to $CD4^+$ T cells discovered through traditional cell-SELEX, also binds to some other cell types (see chapter 5). Another aptamer sequence discovered through protein/cell SELEX only showed low binding to a subset of $CD4^+$ T cells. To our experience, it is easier to select aptamers to target CD8 than CD4 protein. Both aptamers discovered in this chapter require further characterization and receptor identification. Recommendations for future $CD4^+$ T cell SELEX attempts are summarized in chapter 6.

4.5 Acknowledgements

This research was supported by Juno Therapeutics (a Bristol Myers Squibb company). We thank Dr. Julie Shi (Juno) for coordinating and providing apheresis cells and primary T cells. We thank Dr. Stephan Salipante for collecting and processing the NGS data.

Abigail A. O'Connor carried out the combinational cell-SELEX with complementary strands, ligand-guided selection, and protein/cell SELEX. She also generated SOMAmer single stranded DNA for selection, while Emmeline L. Cheng designed the experiments.

4.6 References

1. Farhood, B., Najafi, M. & Mortezaee, K. CD8+ cytotoxic T lymphocytes in cancer immunotherapy: A review. *Journal of Cellular Physiology* (2019) doi:10.1002/jcp.27782.

2. Gooden, M. J. M., De Bock, G. H., Leffers, N., Daemen, T. & Nijman, H. W. The prognostic influence of tumour-infiltrating lymphocytes in cancer: A systematic review with meta-analysis. *British Journal of Cancer* (2011) doi:10.1038/bjc.2011.189.

3. Adusumilli, P. S. *et al.* Regional delivery of mesothelin-targeted CAR T cell therapy generates potent and long-lasting CD4-dependent tumor immunity. *Sci. Transl. Med.* (2014) doi:10.1126/scitranslmed.3010162.

4. Sommermeyer, D. *et al.* Chimeric antigen receptor-modified T cells derived from defined CD8+ and CD4+ subsets confer superior antitumor reactivity in vivo. *Leukemia* (2016) doi:10.1038/leu.2015.247.

5. Turtle, C. J. *et al.* CD19 CAR-T cells of defined CD4+:CD8+ composition in adult B cell ALL patients. *J. Clin. Invest.* (2016) doi:10.1172/JCI85309.

6. Gardner, R. A. *et al.* Intent-to-treat leukemia remission by CD19 CAR T cells of defined formulation and dose in children and young adults. *Blood* (2017) doi:10.1182/blood-2017-02-769208.

7. Turtle, C. J. *et al.* Immunotherapy of non-Hodgkin's lymphoma with a defined ratio of CD8+ and CD4+ CD19-specific chimeric antigen receptor-modified T cells. *Sci. Transl. Med.* (2016) doi:10.1126/scitranslmed.aaf8621.

8. Wang, X. & Rivière, I. Clinical manufacturing of CAR T cells: Foundation of a promising therapy. *Molecular Therapy - Oncolytics* (2016) doi:10.1038/mto.2016.15.

9. Yip, A. & Webster, R. M. The market for chimeric antigen receptor T cell therapies. *Nat. Rev. Drug Discov.* (2018) doi:10.1038/nrd.2017.266.

10. Voelker, R. CAR-T Therapy Is Approved for Mantle Cell Lymphoma. *JAMA* **324**, 832 (2020).

11. Zhou, J. & Rossi, J. Aptamers as targeted therapeutics: Current potential and challenges. *Nature Reviews Drug Discovery* (2017) doi:10.1038/nrd.2016.199.

12. Kacherovsky, N. *et al.* Traceless aptamer-mediated isolation of CD8+ T cells for chimeric antigen receptor T-cell therapy. *Nat. Biomed. Eng.* (2019) doi:10.1038/s41551-019-0411-6.

13. Shangguan, D. *et al.* Aptamers evolved from live cells as effective molecular probes for cancer study. *Proc. Natl. Acad. Sci. U. S. A.* (2006) doi:10.1073/pnas.0602615103.

14. Wu, X. *et al.* A PD-L1 aptamer selected by loss-gain cell-SELEX conjugated with paclitaxel for treating triple-negative breast cancer. *Med. Sci. Monit.* (2020) doi:10.12659/MSM.925583.

15. Wang, J. *et al.* In Vitro Selection of a DNA Aptamer by Cell-SELEX as a Molecular

Probe for Cervical Cancer Recognition and Imaging. *J. Mol. Evol.* (2019) doi:10.1007/s00239-019-9886-8.

16. Civit, L. *et al.* Systematic evaluation of cell-SELEX enriched aptamers binding to breast cancer cells. *Biochimie* (2018) doi:10.1016/j.biochi.2017.10.007.

17. Zumrut, H. E., Ara, M. N., Fraile, M., Maio, G. & Mallikaratchy, P. Ligand-Guided Selection of Target-Specific Aptamers: A Screening Technology for Identifying Specific Aptamers Against Cell-Surface Proteins. *Nucleic Acid Ther.* **26**, 190–198 (2016).

18. Zumrut, H. E. *et al.* Ligand-guided selection of aptamers against T-cell Receptor-cluster of differentiation 3 (TCR-CD3) expressed on Jurkat.E6 cells. *Anal. Biochem.* (2016) doi:10.1016/j.ab.2016.08.007.

19. Hasegawa, H., Taira, K. I., Sode, K. & Ikebukuro, K. Improvement of aptamer affinity by dimerization. *Sensors* (2008) doi:10.3390/s8021090.

20. Mallikaratchy, P. R. *et al.* A multivalent DNA aptamer specific for the B-cell receptor on human lymphoma and leukemia. *Nucleic Acids Res.* (2011) doi:10.1093/nar/gkq996.

21. Rohloff, J. C. *et al.* Nucleic acid ligands with protein-like side chains: Modified aptamers and their use as diagnostic and therapeutic agents. *Molecular Therapy - Nucleic Acids* (2014) doi:10.1038/mtna.2014.49.

22. Gawande, B. N. *et al.* Selection of DNA aptamers with two modified bases. *Proc. Natl. Acad. Sci. U. S. A.* (2017) doi:10.1073/pnas.1615475114.

23. Gold, L. *et al.* Aptamer-based multiplexed proteomic technology for biomarker discovery. *PLoS One* (2010) doi:10.1371/journal.pone.0015004.

24. Fellows, T. *et al.* Gold nanoparticle-streptavidin conjugates for rapid and efficient screening of aptamer function in lateral flow sensors using novel CD4-binding aptamers identified through Crossover-SELEX. *Analyst* (2020) doi:10.1039/d0an00634c.

25. Sefah, K., Shangguan, D., Xiong, X., O'Donoghue, M. B. & Tan, W. Development of DNA aptamers using cell-selex. *Nat. Protoc.* (2010) doi:10.1038/nprot.2010.66.

26. Alam, K. K., Chang, J. L. & Burke, D. H. FASTAptamer: A bioinformatic toolkit for high-throughput sequence analysis of combinatorial selections. *Mol. Ther. - Nucleic Acids* **4**, (2015).

27. Bailey, T. L. *et al.* MEME Suite: Tools for motif discovery and searching. *Nucleic Acids Res.* (2009) doi:10.1093/nar/gkp335.

28. McWilliam, H. *et al.* Analysis Tool Web Services from the EMBL-EBI. *Nucleic Acids Res.* (2013) doi:10.1093/nar/gkt376.

29. Zadeh, J. N. *et al.* NUPACK: Analysis and design of nucleic acid systems. *J. Comput. Chem.* (2011) doi:10.1002/jcc.21596.

30. Zhao, N., Pei, S. N., Parekh, P., Salazar, E. & Zu, Y. Blocking interaction of viral gp120 and CD4-expressing T cells by single-stranded DNA aptamers. *Int. J. Biochem. Cell Biol.* (2014) doi:10.1016/j.biocel.2014.03.008.

31. Davis, K. A., Lin, Y., Abrams, B. & Jayasena, S. D. Staining of cell surface human CD4 with 2'-F-pyrimidine-containing RNA aptamers for flow cytometry. *Nucleic Acids Res.* (1998) doi:10.1093/nar/26.17.3915.

32. Zhu, Q., Shibata, T., Kabashima, T. & Kai, M. Inhibition of HIV-1 protease expression in T cells owing to DNA aptamer-mediated specific delivery of siRNA. *Eur. J. Med. Chem.* **56**, 396–399 (2012).

33. Caroli, J., Taccioli, C., De La Fuente, A., Serafini, P. & Bicciato, S. APTANI: A computational tool to select aptamers through sequence-structure motif analysis of HT-SELEX data. *Bioinformatics* (2016) doi:10.1093/bioinformatics/btv545.

34. Takahashi, M., Sakota, E. & Nakamura, Y. The efficient cell-SELEX strategy, Icell-SELEX, using isogenic cell lines for selection and counter-selection to generate RNA aptamers to cell surface proteins. *Biochimie* (2016) doi:10.1016/j.biochi.2016.09.018.

35. Bakhtiari, H., Palizban, A. A., Khanahmad, H. & Mofid, M. R. Novel Approach to Overcome Defects of Cell-SELEX in Developing Aptamers against Aspartate β-Hydroxylase. *ACS Omega* (2021) doi:10.1021/acsomega.1c00876.

36. Yoon, J. W. *et al.* Isolation of Foreign Material-Free Endothelial Progenitor Cells Using CD31 Aptamer and Therapeutic Application for Ischemic Injury. *PLoS One* **10**, e0131785 (2015).

4.6 Supplementary information

Supplemental Table 4.1. Complementary strands used in cell-SELEX in section 4.2.3.

Name	Variable region sequence (5' → 3')	RPM% in 5c	Binding
1a (3b, 2c)	TGTCTACGCAGTTGAACATCAAAACTACAACGAGTAACTCTCCAGTTCCTCC	9.8%	No binding
1a complementary strand	GGAGGAACTGGAGAGTTACTCGTTGTAGTTTTGATGTTCAACTGCGTAGACA		
3a (6b,1c)	CGCAGCACAGGGATTGAGCCGATTTGAGGCGTTGTTGTGGGCCCATGAGTGG	10.6%	No binding
3a complementary strand	CCACTCATGGGCCCACAACAACGCCTCAAATCGGCTCAATCCCTGTGCTGCG		
4a (14b, 10c)	AACCTGACTCAAAAGCTTAGGTCTACGCACGATCAGAGGAGTAACTCTAATT	0.8%	No binding
4a complementary strand	AATTAGAGTTACTCCTCTGATCGTGCGTAGACCTAAGCTTTTGAGTCAGGTT		
5a (1b, 3c)	CGCAGCAGTGGGCCAAATGGATTGGATTAGGGTTGGGCCGCCCGGGAGGGGT	6.7%	None-specific
5a complementary strand	ACCCCTCCCGGGCGGCCCAACCCTAATCCAATCCATTTGGCCCACTGCTGCG		
7a (11b, 6c)	GACCTCCACACGCGGAACGAGGGCGTGTTTCGACATACAATTCAACACACTA	1.7%	None-specific
7a complementary strand	TAGTGTGTTGAATTGTATGTCGAAACACGCCCTCGTTCCGCGTGTGGAGGTC		
8a (18b, 9c)	CGCAGCAGCTTGGGAAAGACCACCCTTGAATGTCTGTAAGTGGCAAGAACCC	1.1%	No binding
8a complementary strand	GGGTTCTTGCCACTTACAGACATTCAAGGGTGGTCTTTCCCAAGCTGCTGCG		
13a (4b, 7c)	ACGCAGCAAGCGGTTTTCGGGTTCGGGTCTGGGGGTTGGGTTGTCGGCACTA	1.6%	No binding
13a complementary strand	TAGTGCCGACAACCCAACCCCCAGACCCGAACCCGAAAACCGCTTGCTGCGT		
22a (12c)	ACGCTGGTCCAAAAGCCGAGTGACACAAGATGCTCCGGTCTCTCGCAGGTGA	0.7%	No binding
22a complementary strand	TCACCTGCGAGAGACCGGAGCATCTTGTGTCACTCGGCTTTTGGACCAGCGT		
A1	TAGTCAAGGCGATAGACGAAAAACATTGTTTTCCTGGAAGGCCCAGAATCTG	2.6%	Cytokine treated CD4 T cells
A1 complementary strand	CAGATTCTGGGCCTTCCAGGAAAACAATGTTTTTCGTCTATCGCCTTGACTA		
TCBA3	ACAGAGGTGTAGAAGTACACGTGAACAAGCTTGAAATTGTCTCTGACAGAGG	0.03%	CD8 T cells
TCBA3 complementary strand	CCTCTGTCAGAGACAATTTCAAGCTTGTTCACGTGTACTTCTACACCTCTGT		

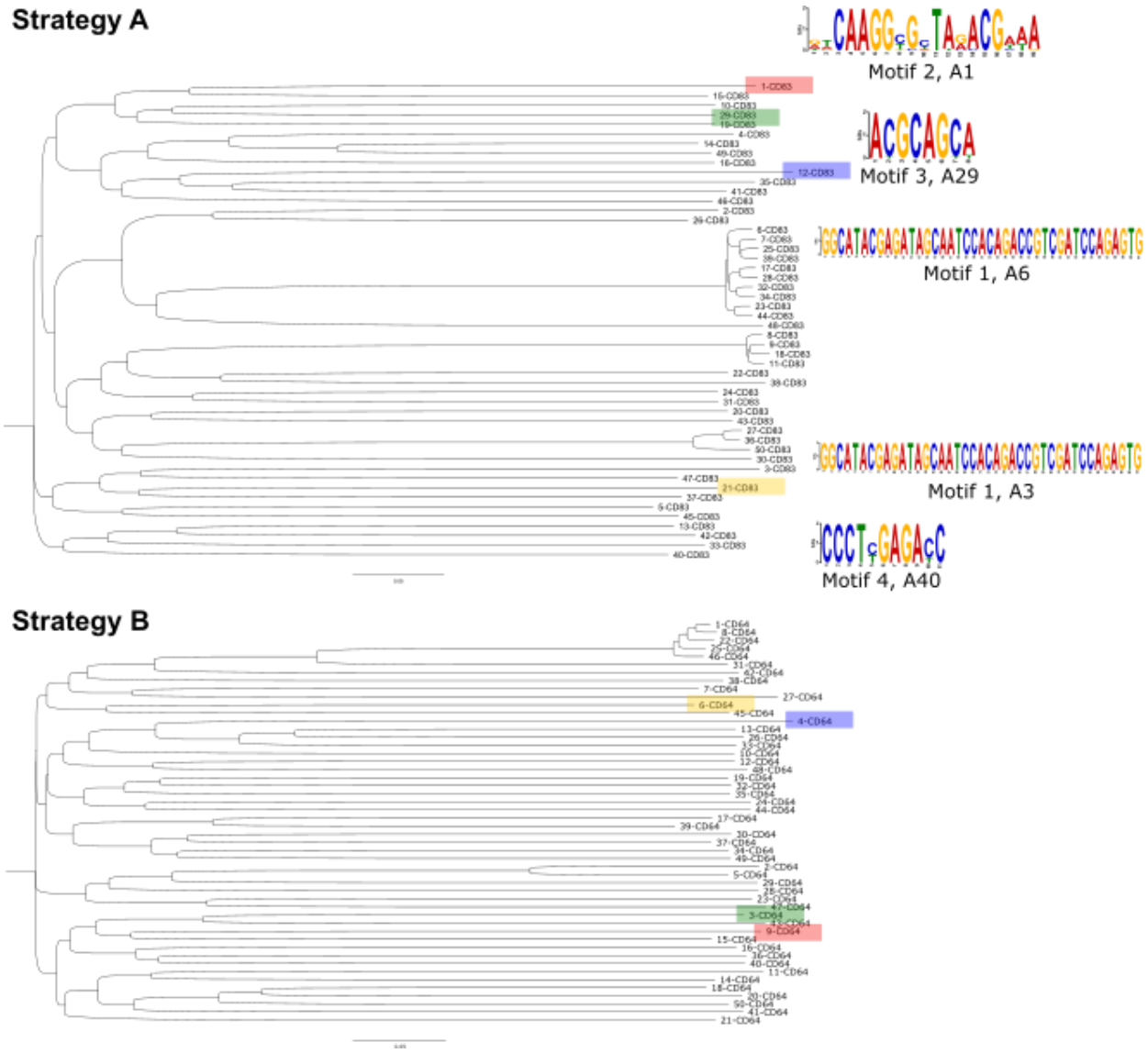

Supplemental Figure 4.1. Phylogenic tree analysis of top 50 sequences from strategy A (top) and B (bottom) final round libraries. Overlapped sequences found in the top 30 aptamers were shaded in colors. The same sequences were shaded with the same color. In strategy A, selected sequences and their predicted motifs are labeled near the location of each sequence on the phylogenic tree. MEME software predicted motifs of selected aptamer were generated using the top 50 sequences from strategy A.

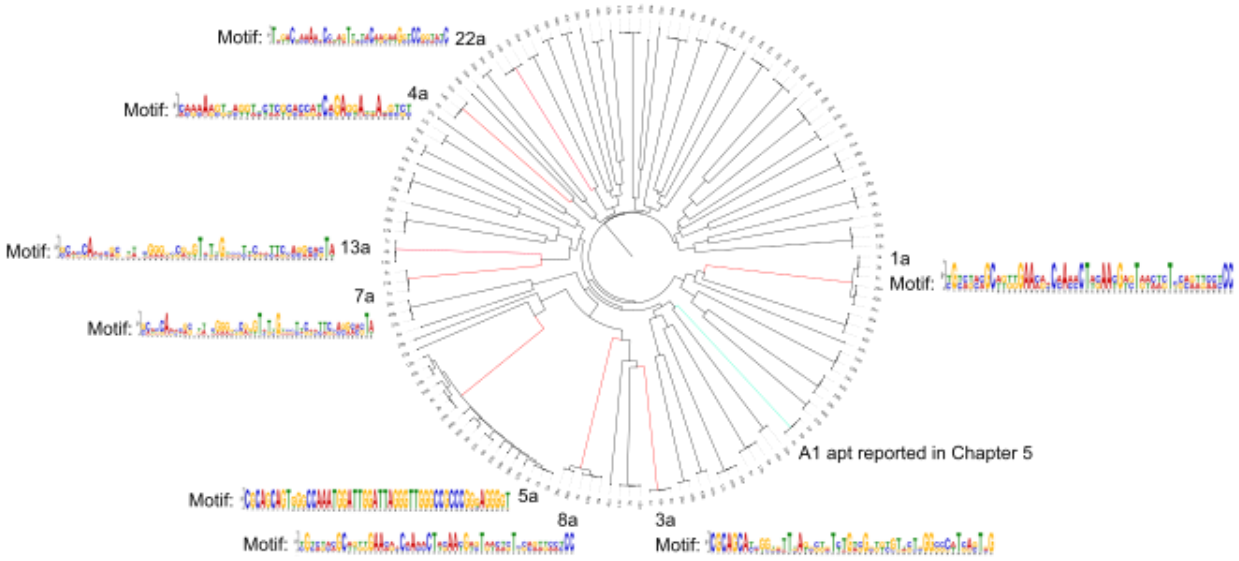

Supplemental Figure 4.2. Phylogenic tree analysis and MEME motif predictions using top 50 sequences from strategy C round 5a, b, c combined. Highlighted aptamers were selected for binding studies on target cells.

Chapter 5. Toward drug delivery to T leukemic cells with a novel aptamer

Emmeline L. Cheng, Nataly Kacherovsky, Albert Yen, Stephen J. Salipante, Suzie H. Pun

Abstract

The initial treatments for patients with first-time T cell acute lymphoblastic leukemia (T-ALL) occurrence has shown satisfactory in tumor reduction. However, the high relapse rate (20% in pediatrics, 40% in adults) of this disease and the limited available treatment remain a concern. Only one regiment, Nelarabine, is approved by FDA for treating relapse T-ALL thus far. Although this treatment could lead to severe side effects due to its non-selective cytotoxicity. In this study, we discovered a novel DNA aptamer, A1, across two independent cell-SELEX attempts. On healthy T cells, A1 aptamer showed high binding affinity (apparent K_D ~0.04nM) but had low saturated binding and targeted binding on other peripheral blood mononuclear cell types (PBMCs). On J.RT3-T3.5 T-ALL cell line, we saw targeted binding of A1 as well. Therefore, we designed a T-ALL targeted drug delivery system using A1 aptamer through two strategies: 1) directly conjugating one toxin molecule per aptamer bridged with a cleavable linker, or 2) complexing multiple toxin molecules with each folded aptamer. The structure of A1 was modified for improved stability for prolonged treatments on cells using aptamer-monomethylauristatin E (MMAE) drug conjugates. The new variant, tA1, has similar degree of binding on J.RT3-T3.5 cells compare to A1. We conjugated tA1 to MMAE toxin bridged with a valine-citrulline (Val-Cit, vc) dipeptide linker and tested this platform on both J.RT3-T3.5 cells and healthy T cells. This toxin-linker construct has shown cytotoxicity on several solid tumor cell lines. Although the initial potency tests showed promising results of tA1-targeted killing J.RT3-T3.5 cells but not healthy T cells, this cell-inhibiting effect was not consistent across different biological repeats. Therefore, we also used A1 carrying more than one doxorubicin (dox) through intercalation for cytotoxicity assays on J.RT3-T3.5 cells. So far, our results indicate aptamer-dox is more potent than aptamer-vc-MMAE but has much higher killing background. We will continue to optimize the treatment conditions to reduce background cytotoxicity of aptamer-dox complexes.

5.1 Introduction

5.1.1 T cell acute lymphoblastic leukemia has high relapse rate and limited available treatments

Acute lymphoblastic leukemia (ALL) is the second most common acute leukemia in adults. Over 6500 cases occur each year in the United States. About 25% of these cases are originated from malignant T cells.[1] 20% of the pediatric and 40% of adult T-ALL patients will relapse,[2] most of them occur within 2- years after diagnosis.[3] The long-term survival rate for the relapse T-ALL patients is less than 25%.[3] Yet, the only FDA-approved treatment for T-ALL is an anti-metabolite, Nelarabine, which non-selectively inhibits DNA synthesis in all cell types.[4] While only a portion of patients showing tumor reduction response, Nelarabine treatment could lead to severe side effects including neurotoxicity.[4,5]

5.1.2 Targeted therapies for T-ALL

Development of T-ALL targeted treatments have been lagging compared to the ones for B-ALL. Most monoclonal antibody treatments for ALL, such as CD20, CD22 and CD19 antibodies, are more effective inhibiting malignant B cells than T cells. CD52, a general ALL marker, has been targeted by antibody treatment on both B cell- and T-ALL patients; however, it has only shown low activity and with significant side effects.[6,7] In terms of adoptive cell therapies, while the treatment outcome for B-ALL has been largely improved by CAR T cell therapies, they are less feasible for treating T-ALL.[5] The treatment efficacy is compromised due to the overlapping biological markers between cancerous T cells and therapeutic CAR T cells. In the CAR T cell manufacturing process, it is also challenging to isolate healthy T cells without getting malignant T cell contamination for the same reason.[5,8] Alternative treatments that effectively deliver bioactive reagents to cancerous T cells is needed.

5.1.3 Intracellular deposit of toxins in circulating tumors using targeting ligands

Antibody-drug conjugate (ADC) is a type of drug delivery platform that usually consists of a targeting ligand for binding to cancer cells, a toxin for cell inhibition, and in some cases, a peptide

linker that bridges the ligand and the toxin together to promote toxin release inside the cells.[9] For example, brentuximab vedotin, a ADC consists of a CD30 antibody, a valine-citrulline (Val-Cit, vc) linker, and a monomethyl auristatin E (MMAE).[10] The anti-CD30 antibody is used to target several lymphatic tumors, as CD30 expression is low on most normal tissue except for activated T cells and B cells, and is higher on lymphoma cells.[10] Once the delivery platform is being internalized upon antibody binding, and trafficked to endosomes and lysosomes, the Val-Cit linker will be hydrolyzed by proteases, mainly by cathepsin B which is most active in the endosomal environment around pH 4.5-5.5.[11–13] Thereafter, MMAE is released and diffuse into cytosol, where it blocks tubulin polymerization and leads cells to apoptotic cell death.[14] This MMAE delivery platform is promising for targeted drug delivery to leukemic T cells as a derivative of MMAE has been tested on T cell ALL cell line that showed high potency.[15] More importantly, cathepsin B has been reported to over-express in some cancer cells which could increase the cell killing selectivity of the platform.[16]

5.1.4 Current progress of aptamer-drug conjugates and complexes

Aptamers are single stranded DNA or RNA. These "chemical antibodies" have similar affinity range (K_D within pM-nM range) as protein antibodies.[17] Their flexibility for chemical modification on bases makes it easy to improve the stability or to immobilize cargos. This is only one of the many advantages comparing to antibodies that are usually harder to modify without compromising their protein structure.[18] Aptamers have small size which makes them easier to penetrate deep tissues, such as solid tumors, than macromolecule antibodies.[19] The aptamers that are composed of natural nucleotide bases are considered non-immunogenic which makes them a safer component to use for *in vivo* drug delivery than antibodies.[20]

Anticancer chemotherapy or immunosuppressive drugs, such as methotrexate, maytansinoid, paclitaxel, camptothecin, and more, have been directly conjugated onto either DNA or RNA aptamers for drug delivery to a wide range of cancer cell lines, including pancreatic cancer, and chronic myelogenous leukemia.[23–25] More refined designs have gone beyond cell type targeting as they also control cargo release inside the cells with protease-sensitive linkers. Groups have shown Val-Cit dipeptide, discussed in the 5.1.3 section, is effective for depositing MMAE

into prostate,[26] colon,[27] and pancreatic[28] cancer cell cytosol when conjugated with aptamers. The targeting aptamers used in these studies range from sub-nanomolar to a couple hundred nanomolar K_D which is considered the same as the affinity range of the antibodies, therefore, is suitable for drug delivery.[26–28]

Another way to deliver chemotherapy agent is through intercalation of anthracycline in the DNA base pairing structure of aptamers. For example, Taghdisi et al. demonstrated selective inhibition of an acute T cell leukemia cell line by using PTK7 binding aptamer that non-covalently complexed with daunorubicin.[21] Other similar platform designs include using doxorubicin for DNA intercelation.[22] This platform is simple and fast to generate, although the drug cargo can be relatively unstable because it is not covalently linked with the targeting ligand.

In this study, we designed two drug delivery systems consists of a high affinity aptamer that has preferential binding on leukemic T cells, a Val-Cit dipeptide linker, and a MMAE toxin (Scheme 5.1), as well as an aptamer-doxorubicin complex for cancer-targeted doxorubicin (dox) delivery. The leukemic T cell targeting aptamer, A1, was developed using a combination of traditional cell-SELEX and competitive cell-SELEX that was designated for selecting $CD4^+$ T cell targeting ligands.[29,30] While A1 showed high affinity (K_D~0.04 nM) to resting $CD4^+$ T cells, it only has low saturated binding on these cells. Encouragingly, A1 has a high staining on J.RT3-T3.5 T-acute lymphoblastic leukemia cells. For that reason, we selected A1 as our malignant T cell targeting ligand. In this chapter, we demonstrated the feasibility of using A1 variants to generate different drug delivery platforms to inhibit J.RT3-T3.5 leukemic cells, as well as discussing the challenges of these systems.

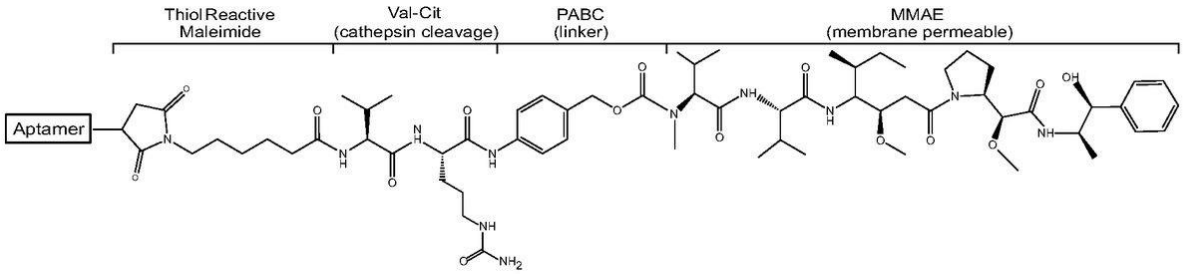

Scheme 5.1. The aptamer-drug conjugate construct used in this study. (Reproduced from ref. 26)

5.2 Materials and methods

5.2.1 Cells and culture maintenance reagents

Jurkat cell line (human T-ALL) was kindly gifted by the Jensen lab (Seattle Children's Research Institute). J.RT3-T3.5 cell line (human T-ALL), and H9 cell line (human T cell lymphoma) were purchased from ATCC. $CD4^+$ T cells (positively selected) used in the first SELEX, and the $CD8^+$ T cells (positively selected) used in both selections, apheresis cells, mixed T cells, and T cell-depleted apheresis fraction were provided by Juno Therapeutics. $CD4^+$ T cells used in the second SELEX were isolated from PBMCs using $CD4^+$ T cell negative selection kit (Miltenyi). The PBMCs were prepared by Ficoll-enriching apheresis product purchased from Bloodworks Northwest.

All cell culture was maintained in RPMI 1640 medium (Corning) with 10% FBS (Life Tech). The $CD4^+$ T cells used in SELEX, binding study, and internalization study were either rested in IL-2 (20 ng/ml) spiked cell media overnight, rested in cytokine-free cell media for a few hours, or gone through repeated washes to remove DMSO. To prepare activated T cells, we used recombinant cytokines (Miltenyi) and CD3/CD28 stimulation Dynabeads (Thermo Fisher). IL-7 (5 ng/ml) and IL-15 (0.5 ng/ml) were used on $CD4^+$ T cells, while IL-2 (20 ng/ml) and IL-15 (0.5 ng/ml) were used on $CD8^+$ T cell culture media, along with the stimulation beads supplemented on day 0. On day 9, the stimulation beads were removed by pipetting cells with p1000 tips and separated on a magnetic rack. Activated $CD4^+$ and $CD8^+$ T cell culture was kept in the complete culture media containing cytokines for expansion until day 21.

5.2.2 Cell staining and flow cytometry

We used wash buffer with 1% BSA for washes and binding buffer for staining. Wash buffer was made with 500 ml DPBS (with calcium and magnesium) plus 2.5 mL 1M $MgCl_2$ and 2.25 g D-glucose, which contains 137mM Na^+ and 5.5mM Mg^{2+}. The binding buffer was wash buffer supplemented with 0.1 mg/ml yeast tRNA and 1% BSA. Aptamers ordered from IDT were labeled with FAM, Cy5, or biotin. Aptamers were annealed at 1µM in wash buffer by heating the solution to 95 ^oC for 5 minutes and snap cold on ice for at least 15 minutes. Aptamer staining on cell was

done at 4 ^{o}C to avoid internalization. The RAN aptamer was used as control, which was a sequence randomly picked out from the naïve library. The readout of aptamer binding on cells was collected on Attune NxT (Invitrogen).

For flow cytometry and FACS cell staining, we used the following live/dead stain and antibodies: Zombie Violet (1:500 in 100ul containing 10^6 cells, BioLegend), APC-antihuman CD4 antibody (1:100, BioLegend, B234854), and Alexa Fluor 647-streptavidin (1:500, BioLegend).

5.2.3 Combinational cell-SELEX

The experimental design of combinational cell-SELEX was summarized in **Figure 5.1**, and **Supplementary Figure 5.4A**. These processes were adapted from a published protocol.[29] In brief, we purchased a naïve library containing unique sequences with N52 variable region flanked by 18 bases constant region from IDT. This provides us theoretically 10^{16} unique sequences in the starting naïve library. A total volume of 400 µL was used throughout all aptamer library incubation steps. The key factors account for evolution stress, such as target cell numbers, incubation time, blocker concentration, are indicated in **Figure 5.1B** and **Supplementary Figure 5.2A.** Most selections, except for the competitive selection steps, took place at 4 ^{o}C to avoid cell internalization. To elute the sequences from target cells, the cells were heating at 95 ^{o}C in wash buffer. The cell debris was then spun down, and the supernatant was collected for the next steps. Aptamer pools were separated from control cells by centrifugations. After each selection round, we optimized the PCR cycles to amplify the libraries with Phusion High-Fidelity DNA polymerase (NEB), dNTP (QIAGEN), FAM labeled forward primer, and biotinylated reverse primer (IDT). The reverse strands of amplified pools were removed using High Capacity Neutravidin Agarose Resin (Thermo Fisher). The forward single stranded DNA (ssDNA) was eluted from the resin by sodium hydroxide incubation and can be annealed after solvent exchanged into wash buffer at 1µM.[29]

In the competitive SELEX steps, aptamer pools were first incubated with PBMCs, a mixed cell population. Target cells were then isolated from these aptamer-stained populations either by Magnetic-Activated Cell Sorting (MACS) system with commercialized Pan T cell Kit (Miltenyi) or by Fluorescence-Activated Cell Sorting (FACS) method to purify cells with $CD4^{hi}$ expression

on Canto II flow cytometer (BD) hosted in the Department of Pathology at University of Washington.

5.2.4 NGS and sequence analysis

MiSeq System (Illumina) and MiSeq Reagent kit v2 (300 cycles) were used for NGS. The libraries were amplified using barcoded primers unique for each round library. FASTAptamer v1.0.3 toolkit was used to analyze the FASTA files.[31] *FASTAptamer-count* was first used to identify top aptamers with the highest frequency (highest count). *FASTAptamer-enrich* was then used to analyze the fold-enrichment of each unique sequences in adjacent rounds (later over earlier rounds). MEME suite v5.2.0 Motif Discovery tool was used to predict binding motifs of the top 50 aptamers in round 8 (R8) base on their sequence similarities.[32] The top 50 aptamer sequences of R8 were also used for phylogenic tree generation with FigTree toolkit v1.4.4 to map out the similarities between each sequences.[33] The NUPACK web application was used to simulate aptamers folding into their thermally stable secondary structures.[34]

5.2.5 Target receptor identification with natural DNA aptamers

About 100 to 200 million J.RT3-T3.5 cells or activated $CD4^+$ T cells (both are A1 target cells) were used for each group. The membrane protein extraction and target purification process were modified from a previously published method.[35] The target cells were first lysed with hypotonic buffer that was 10 mM Tris-HCl (pH 7.5) containing EDTA-free cOmplete Protease Inhibitor Cocktail (Roche) supplemented with 1mM PMSF at 4 ^oC for 30 minutes. The cell membrane debris was washed 3 times with the same hypotonic buffer, followed by extraction using wash buffer containing 0.1% tween 20, and the same concentration of protease inhibitors. The extraction took place at 4 ^oC with constant rotation for 30 minutes, and 5 minutes brief sonication in an ice water bath. We then used centrifugation to remove insoluble debris. The extracted membrane protein was stored at -80 ^oC until next step.

Once proceeded, the extract was first “pre-cleared” with 100nM biotin-RAN incubation along with 0.1mg/ml tRNA as background blocker. The proteins prone to non-specifically binding

to DNA will be removed by incubating the biotin-RAN labeled protein extract with MyOne Streptavidin C1 Dynabeads (Thermo Fisher) on a magnetic stand. Along with 0.1 mg/ml salmon sperm DNA as background blocker, the "cleared" membrane protein solution was then incubated with 100nM biotinylated aptamers (A1 or A3t, the control aptamer) for 30 minutes followed by Streptavidin Dynabeads for 15 minutes, or with Streptavidin Dynabeads that was first saturated with 10x binding capacity of biotin. The Streptavidin Dynabeads were washed 5 times with cold wash buffer with 0.02% tween 20. The proteins were eluted off into the gel loading buffer by heating the beads at 47 ^{o}C for 15 minutes. The loading buffer was composed of 1x Laemmli sample buffer (containing SDS), 4.6M urea, 2.5% 2-mercatoethanol, 10mM EDTA, and 0.02% tween 20. After removing the Streptavidin Dynabeads from the supernatant, the protein extract was separated using either 8% or 4-20% SDS-PAGE.

The gel was stained with either Colloidal Blue Staining Kit (Invitrogen) or SilverQuest Staining Kit (Invitrogen). The excised bands were digested, desalted, and subjected to tandem mass spectrometry (Orbitrap Elite). The data was analyzed with Proteome Discoverer 2.2 and compared with the Uniprot Human database at the Fred Hutchinson Cancer Research Proteomics Center.

5.2.6 Target receptor identification with bromodeoxyuridine-labeled aptamers

About 70 to 100 million J.RT3-T3.5 cells were used for each group. The cells were washed 3 times with wash buffer and set on ice until use. One of the control groups used only streptavidin beads for enrichment. The cells used in this group were exposed to UV light before being lysed. Another control group used A1 labeling without UV crosslinking. The cells used in this group were exposed with UV light first, before stained with 50 nM biotinylated BrdU-A1 (with modification on hairpin loop or 3' overhang mixed at 1:1) and binding buffer. Whereas the experimental group cells were stained with biotinylated BrdU-A1 first, washed, and exposed to UV light. UV exposures for 20 minutes were done by plating the cells in a 6-well plate in a thin layer of wash buffer (1 millimeter), with the UV-C LED light bulbs (peak wavelength 280 nm, 175mW/m^2, LED supply) set on top, 2 centimeters from the liquid surface and with no barriers in between.

Similar to section 5.2.5, cells were then lysed with hypotonic buffer that was 10 mM Tris-HCl (pH 7.5) containing EDTA-free cOmplete Protease Inhibitor Cocktail (Roche) supplemented with 1mM PMSF at 4 ^{o}C for 30 minutes. The cell membrane debris was washed 3 times with the same hypotonic buffer, followed by extraction using wash buffer containing 0.1% tween 20, and the same concentration of protease inhibitors. The extraction took place at 4 ^{o}C with constant rotation for 30 minutes, and 5 minutes brief sonication in an ice water bath. The insoluble debris was removed by centrifugation. The membrane extract was stored at -80 ^{o}C until next step.

0.5 mg per group MyOne Streptavidin C1 Dynabeads (Thermo Fisher) was used to enrich the biotinylated aptamer-labeled protein. The streptavidin magnetic beads used in the control group with no aptamer, was blocked with 50 nmole biotin in wash buffer for 15 minutes at 4 ^{o}C. The cell membrane protein lysate generated for all groups were incubated with the streptavidin magnetic beads along with 0.1 mg/mL salmon sperm DNA for 30 minutes at 4 ^{o}C. The magnetic beads were collected on a magnetic rack and washed with cold DPBS with 0.05% tween 20 three times, followed by DPBS with 0.05% tween 20 and 10 mM EDTA twice. The proteins were eluted off into gel loading buffer by heating the beads at 47^{o}C for 15 minutes. The loading buffer was composed of 1x Laemmli sample buffer (containing SDS), 4.6M urea, 2.5% 2-mercatoethanol, 10mM EDTA, and 0.02% tween 20. After removing the Streptavidin Dynabeads from the supernatant, the protein extract was separated using either 4-20% SDS-PAGE and stained with SilverQuest Silver Staining Kit (Invitrogen).

5.2.7 Confocal imaging aptamer internalization by cells

The target cells were incubated with 5nM Cy5-labeled aptamers at 37 ^{o}C for 20 minutes. The cells were washed and dropped onto pre-coated coverslips. The pre-coating was done by incubating the coverslips with 10 µg/mL poly-D-lysine at 37 ^{o}C for 2 hours. The cells were attached onto the coverslips by centrifugation at 2000 r.p.m. for 10 minutes. We fixed the cells by incubating them with 4% PFA for 10 minutes at room temperature. After permeabilized with 0.1% Triton X-100, the cells were then stained with FITC-Phalloidin and DAPI for 30 minutes at room temperature. Last, we mounted the coverslips on microscope slides with 10 µl PVA. Confocal images were taken on Leica DMI6000 microscope, and each staining was merged using Image J.

5.2.8 Aptamer modification with NUPACK

The aptamer modification was done partially with the help of NUPACK. As mentioned in section 5.2.4, NUPACK is a web application that simulates secondary structures of aptamers with certain ion concentration and temperature. The settings for the annealed aptamer secondary structures were 137 mM Na^+ and 5.5 mM Mg^{2+}, and temperature at 4 ^oC. The settings for simulating antidote annealing were the same cation concentrations, and temperature at 25 ^oC.

5.2.9 Generating aptamer-drug conjugates

Aptamers with the 5'-end modified to carry a thiol group were used for conjugation. Triethylammonium acetate (TEAA) was incorporated in the solvent during conjugation and HPLC as a charge-reducing reagent.[36] The conjugation protocol was adapted from published literature.[26,28] About 3 nmole of aptamers were first reduced with 0.5 ml of 50mM tri(2-carboxyethyl)phosphine hydrochloride (TCEP) in 0.5M TEAA. The reduction took place by heating the solution at 70 ^oC for 3 minutes and let sit in room temperature for 57 minutes. TCEP was removed from the aptamer solution with 10k cut-off spin column (Millipore Sigma). 30 nmole of MC-Val-Cit-PAB-MMAE was added to the reduced thiol-aptamer in DPBS with 2mM EDTA. Conjugation took place at 4 ^oC overnight. After removing unconjugated MC-Val-Cit-PAB-MMAE with 10k cut-off spin column, the conjugation efficiency was evaluated by using HPLC.

5.2.10 Testing conjugation efficiency with HPLC

The unconjugated aptamers were reduced with TCEP following the method described in section 5.2.9 to improve peak resolution. Drug conjugated aptamers were heated at 68 ^oC for 5 minutes before HPLC injections to prevent secondary structures. WATERS XBridge Oligonucleotide BEH C18 silica column (130 Å, 2.5 µm) was used to separate the conjugated and unconjugated aptamers. We used 0.1M TEAA in water as solvent A, and ACN as solvent B. 35 µL of 0.2-1 µM aptamer was sampled depending on the availability of aptamers.

At a constant flow rate of 1 mL/minute, we started the separation with HPLC by running 80% solution A and 20% solution B through the column for 5 minutes. Solution B was increased to 95% between 6 to 20 minutes. Lastly, the solvent composition was kept the same for another 2 minutes for cleaning purpose.

5.2.11 Generating aptamer-drug complexes

Annealed 1 µM aptamers were incubated with 10 µM doxorubicin for 2 hours at room temperature, after which, the excess doxorubicin was removed using Amicon Ultron-0.5 centrifuge filters (10k molecular weight cut off, Millipore Sigma). After filtering, aptamer concentrations were adjusted to 1 µM by measuring DNA absorbance (NanoDrop, Thermo Scientific). The free doxorubicin that was not intercalated by DNA was measured using fluorescence excitation at 480 nm and emission at 600 nm on a plate reader (Tecan). The total doxorubicin was measured using absorbance at 480 nm.

5.2.12 Cell viability assays

Aptamer-vc-MMAE conjugates were first annealed by heating at 68 ^{o}C for 5 minutes and snap chilled on ice for at least 10 minutes. J.RT3-T3.5 cells, activated CD4 T cells, and activated CD8 T cells were plated at 50,000 cells per ml in 48 well plates. These target cells were incubated with unconjugated drug, and tA1- and RAN-vc-MMAE conjugates at 4 ^{o}C for 1 hour at various concentrations in binding buffer. The cells were washed, resuspended in the appropriate complete culture media described in section 5.2.1, and cultured for 72 or 96 hours. Cells were cultured with constant shaking to prevent cells from settling at the bottom of the well plates.

To test cytotoxicity of aptamer-doxorubicin complex, the A1 and RAN aptamer-drug complexes were applied to J.RT3-T3.5 cells, seeded at 50,000 cells per ml in 96 well plates, for 15 minutes incubation at 37 ^{o}C. The cells were washed twice and incubated in RPMI 10% FBS for 48 or 96 hours. Cells were cultured with constant shaking to prevent cells from settling at the bottom of the well plates.

CellTiter 96 AQueous Non-radioactive Cell Proliferation Assay kit (Promega) was used to test cell viability. The MTS and PMS solution were dissolved and mixed according to the manufacturer manual. At the end of cell culture, 20 µL of MTS/PMS solution was added to each 100 µL of cell culture media. OD_{490} (with OD_{650} as reference) was collected on Tecan infinite M200 pro. Cell viability was determined by first subtracting the OD_{490} of each group with a blank group with no cells and normalizing to the un-treated control group as 100% viability.

5.3 Results and discussion

5.3.1 First cell-SELEX attempt

Cell-SELEX is an *in vitro* panning process has been used to enrich aptamers that bind to certain cell membrane targets from a randomized sequence library.[29] In this study, we used a combination of traditional cell-SELEX and competitive SELEX, which is conducted by libraries binding to a mixed cell populations and followed by isolating the target cells (**Figure 5.1A**). These combined SELEX strategies has been used to develop aptamers that targets $CD8^+$ cytotoxic T cells ($CD8^+$ T cells) with high affinity binding.[30] The top aptamer discovered in this study, A1, was selected through two unrelated SELEX attempts that were aimed at evolving $CD4^+$ helper T cell ($CD4^+$ T cells) binding aptamer. In the first attempt, $CD4^+$ T cells were used as target cells in most rounds, while T cell depleted apheresis cells were used as control cells in most rounds (**Figure 5.1B**).

A

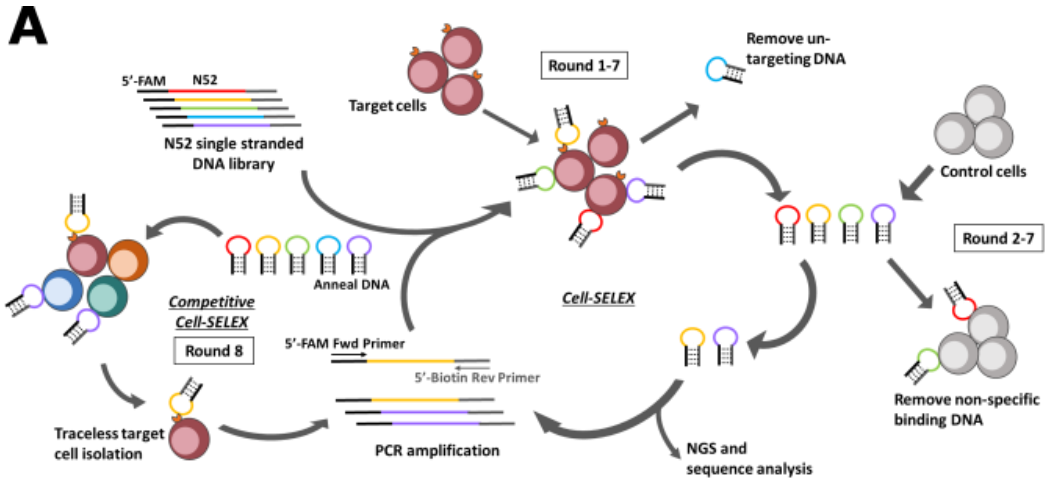

B

		Positive selection				Negative selection		
Round #	Library	Cell type and #	Time	Washes	Protein blocker	Cell type and #	Time	Protein blocker
1	14mM	30 million T cells	1h	3x	0.1% BSA	None	1h	0.1% BSA
2	500nM	10 million CD4+ T cells	1h	3x	0.1% BSA	10 million J.RT3-T3.5	1h	0.1% BSA
3	500nM	5 million CD4+ T cells	0.5h	3x	1% BSA	10 million J.RT3-T3.5	0.5h	1% BSA
4	250nM	5 million CD4+ T cells	0.5h	3x	1% BSA	10 million T cell depleted apheresis	0.5h	1% BSA
5	250nM	2.5 million CD4+ T cells	0.5h	4x	2% BSA	10 million T cell depleted apheresis	0.5h	2% BSA
6	250nM	2.5 million CD4+ T cells	0.5h	4x	5% FBS	10 million T cell depleted apheresis	0.5h	5% FBS
7	250nM	2.5 million CD4+ T cells	0.5h	4x	5% FBS	10 million T cell depleted apheresis	0.5h	5% FBS
8	250nM	5 million PBMC and T cell isolation	0.5h	4x	5% FBS	None	0.5h	5% FBS

Figure 5.1. Selection process of A1. (A) Simplified schematic of combinational cell-SELEX. (B) Detailed conditions used in the combinational cell-SELEX.

In this SELEX attempt, the $CD4^+$ T cells were cultured in IL-2 cytokine containing RPMI media overnight before selection to ensure the removal of cell-freezing reagent. After 8 rounds of selection, the round 8 (R8) library showed increased binding to $CD4^+$ T cells but no binding to T cell depleted apheresis (**Figure 5.2A**). This indicates the enrichment of the DNA sequences that bind to target cells over repeated selections. After observing increased binding to target cells, we sequenced round 1-8 DNA libraries with next generation sequencing (NGS). Potential target cell binders were selected from the final round based on their abondance in the sequence pool, their predicted binding motifs, and the diversity of sequences. The abundance and enrichment of unique sequences were generated using FASTAptamer.[31] 50 aptamer sequences with the highest counts were used for motif prediction and phylogenic tree generation (**Supplementary Figure 5.1**). Four different binding motifs were discovered using MEME toolkit.[32] After generating phylogenic tree

with the FigTree software,[37] we picked out five aptamers with high count and high enrichment from the final pool on different branches of the phylogenic tree to ensure sequence diversity between those candidates. The selected aptamers, A1, A3, A6, A29, and A40 (numbered by their abundance rank in the last round), have different predicted binding motifs identified with MEME toolkit (A1 with motif 2; A3 and A6 with motif 1; A29 with motif 3; A40 with motif 4). Despite the high representation of motif 1, A3 and A6, along with A29 and A40, did not show binding on target cells, while A1 showed binding to most, but not all, $CD4^+$ T cells that were cultured in media containing IL-2 cytokine (**Figure 5.2B**).

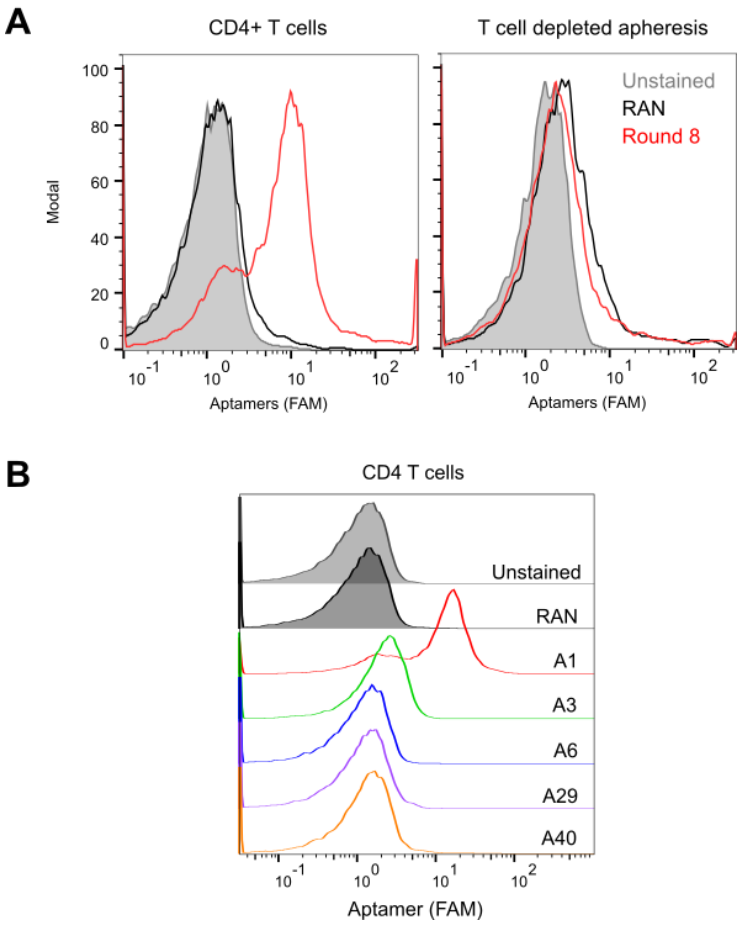

Figure 5.2. Binding studies of the final round library pool and selected aptamer candidates. (A) Final round pool binding on target cells ($CD4^+$ T cells that were rested in cytokine media) and control cells (T cell depleted apheresis) on flow cytometer. (B) Flow cytometry binding study on target cells by aptamer candidates selected base on sequence analysis. FAM: carboxyfluorescein.

5.3.2 Incubation-dependent binding and second cell-SELEX attempt

We evaluated the affinity of A1 binding to its target cells using flow cytometry. The apparent K_D of A1 binding to cryopreserved $CD4^+$ T cells that were used after thawing without culturing, cultured in RPMI media, and cultured in RPMI media with 10% FBS, was 0.04±0.033 nM, 0.31±0.086 nM and 0.60±0.684 nM, respectively (**Figure 5.3A, B, and C**). The binding affinity lies in a range similar to antibodies, which is pM-nM K_D. Interestingly, the saturated A1 binding to cells without prior incubation steps was only a third of the incubated cells. The increased saturated binding was not dependent on the cytokine inclusion since the apparent K_D and maximum fluorescent intensity did not change much between the two conditions. If we look at the time-course changes of this binding pattern, the change initiated about 4 hours after incubating cells in RPMI 10% FBS and reached maximum binding at around 15 hours (**Supplementary Figure 5.2A and B**). This incubation-dependent binding led us thinking the target protein of A1 might not be CD4 receptor. We ran a binding experiment of A1 on different leukemia and lymphoma T cell lines that express various level of CD4 receptor. A1 binds to J.RT3-T3.5 cell most, to Jurkat cells the second, to H9 cells the least. The CD4 protein expression level was the highest on H9 cells and the lowest on J.RT3-T3.5 cells (**Figure 5.3D**). We also looked at A1 binding to PBMCs. Unfortunately, A1 shows low to medium binding to a subset of $CD8^+$ T cells, NK cells, and B cells (**Supplementary Figure 5.3**), which rules out the possibility of using A1 for $CD4^+$ T cell targeted applications.

To improve our SELEX strategy for selecting $CD4^+$ T cell binders, we conducted a second combinational cell-SELEX process using resting $CD4^+$ T cells without overnight incubation as target cells and resting $CD8^+$ T cells as control cells. In the final round, we used FACS to purify T cells from PBMCs as a competition selection round (**Supplementary Figure 5.4A**). Despite minimizing the cell incubation step, we still enriched A1 at high abundance (**Supplementary Figure 5.4B**, highlighted in orange). Other top sequences identified in the second SELEX showed either no binding or no specific binding to target cells (discussed in chapter 4).

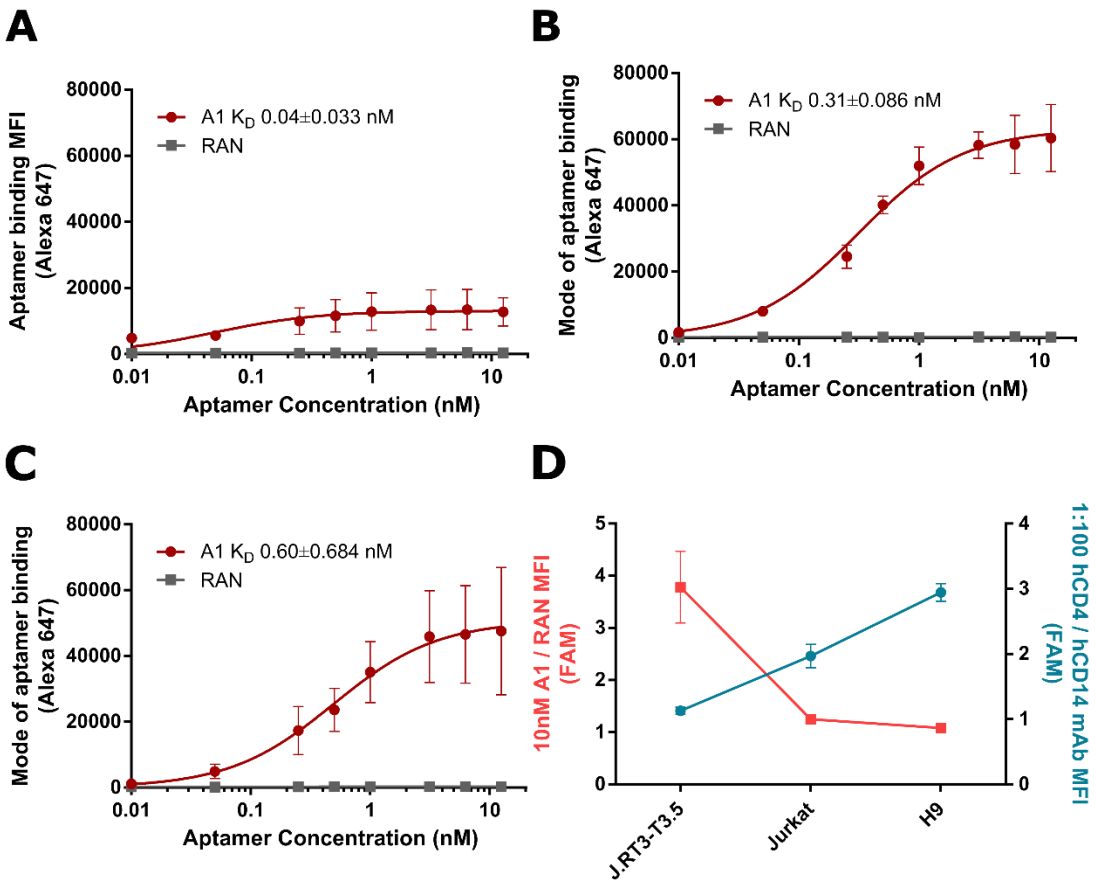

Figure 5.3. A1 binding to target cell types tested with flow cytometry. (A) Binding curve of A1 targeting to CD4$^+$ T cells without incubation. (B) Binding curve of A1 targeting CD4$^+$ T cells pre-incubated in RPMI 10% FBS media. (C) Binding curve of A1 targeting CD4$^+$ T cells pre-incubated in RPMI 10% FBS media with IL-2 cytokine. (D) 10 nM A1 binding to leukemia and lymphoma cell lines. MFI: median fluorescent intensity.

5.3.3 A1 binding to malignant T cells and internalized by target cells

To evaluate the potential drug delivery applications of A1, we tested its binding to a couple of malignant T cell lines, including J.RT3-T3.5 and Jurkat T-ALL, and H9 lymphoma cell lines. A1 showed highest binding to J.RT3-T3.5 cells, moderate binding on Jurkat cells, and the least binding to H9 cells (**Figure 5.3D**). We proceeded with J.RT3-T3.5 as our drug delivery target cells since there was a 4-fold increased A1 binding comparing to RAN control.

After identifying the cells that bind A1, we conducted receptor identification by purifying the membrane proteins labeled with A1 from activated CD4$^+$ T cells and J.RT3-T3.5 cells

(**Supplementary Figure 5.5A and B**). Several potential targets were identified with mass spectrometry. However, the identified peptide sequences only received low score on the peptide quantity, and the percentage coverage of the full-length protein (**Supplementary Figure 5.5C**). We picked Na^+/K^+ ATPase subunit alpha 1, integrin beta-2 (CD18), and leukosialin (CD43) for further evaluation due to their higher overall identification score as well as the consistency of identification across two cell types. We co-stained antibodies targeting these proteins with A1 to observe the labeling fluorescent intensity between the two ligands. However, we did not see a linear correlation between the binding of antibodies and A1, indicating the two ligands are not binding to the same protein (**Supplementary Figure 5.5D**). We also tried implementing photosensitive analogue bromodeoxyuridine (BrdU, **Supplementary Table 5.1**) and UV crosslinking to secure A1 attachment with the bound target protein.[38,39] The two modifications on A1 with BrdU showed no impact on aptamer binding (**Supplementary Figure 5.6A**). Therefore, we mixed A1 with different modifications at 1:1 ratio for receptor identification. We had two control groups, one with bare beads for enrichment and one with A1-attached beads for enrichment but without UV crosslinking, implemented to sort out the background binding proteins that were not enriched by UV crosslinked A1. However, we did not observe an increased protein collection in the UV exposed experimental group compared to the control groups (**Supplementary Figure 5.6B**). This indicates the UV crosslinking was not successful. Either putting more BrdU analogues on the same aptamer sequence or using a more sensitive photoreactive analogue is needed.

Regardless of what the protein targets of A1 are, they are quickly internalized by its target cells. We observed red punctate after 20 minutes of incubating Cy5-labeled A1 with IL-2 treated $CD4^+$ T cells (**Figure 5.4**). The same morphology was not seen when using Cy5-labeled RAN aptamer. Since we established that A1 goes through receptor mediated internalization, we further modified A1 to apply it on drug delivery system that traffics through endocytosis pathways.[40]

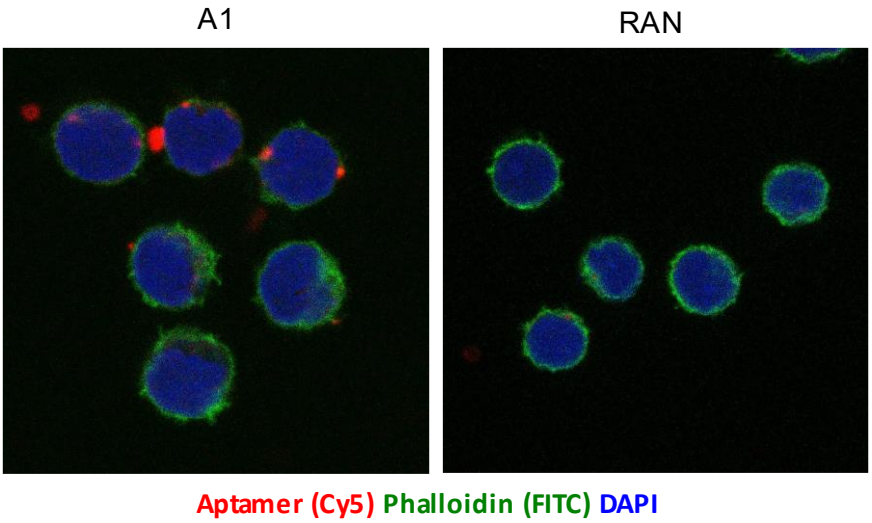

Figure 5.4. Aptamer internalization evaluated with confocal microscopy. IL-2 media incubated $CD4^+$ T cells were fixed after 20 min of incubation with A1 and RAN at 37 ^oC. Aptamers were labeled with Cy5. Actin filaments were labeled with Phalloidin. Nuclei were labeled with DAPI. Cy5: Cyanine 5; FITC: Fluorescein isothiocyanate; DAPI: 4′,6-diamidino-2-phenylindole.

5.3.4 Modification of A1 for improved stability

In order to truncate A1 to potentially reduce the cost of production, we started by identifying the essential sequences contributing to A1 binding to antigens. The secondary structure generated by NUPACK indicated A1 consists of a stem with 2 loops and 2 over-hang strands, and a major branched loop with 3 hairpins (**Figure 5.5A**, bottom). The stem structure is mostly made up by the constant region sequences, whereas the branched loop and hairpins are made up by the variable region of the aptamer. The predicted motif of A1 (motif #2, **Supplementary Figure 5.1**) is located on the hairpin closest to the 5'-end. To identify which hairpin or stem contains the actual binding motif, we truncated and replaced parts of the sequences with thymins to remove the secondary structures one by one. A1-a consists all the hairpins but not the stem. A1-b has the first and third hairpins counting from the 5'-end. A1-c has the first and second hairpins. A1-d has the second and third hairpins (**Figure 5.5A**, bottom). We tested binding of all these versions of A1 on $CD4^+$ T cells. It was verified through flow cytometry that A1 requires all of its 2-dimensional structures for maximum binding (**Figure 5.5A**, top). Even removing the stem, which is the farther-most away from the predicted motif, compromised A1 binding by 60%. When we removed one of the hairpins, the binding signal dropped by 20-fold comparing to the full length A1. It is possible that the tertiary structure of A1 involves interaction between multiple secondary structures. With this information,

we redesigned A1 by changing minimal number of bases to preserve its binding motifs. We removed the 2 over-hang strands and closed the loop near 5'- and 3'- end by modifying sequences for base-pairing (**Figure 5.5B**). The modified version of A1 was named tA1. tA1 was used in the binding studies and cell killing studies onwards.

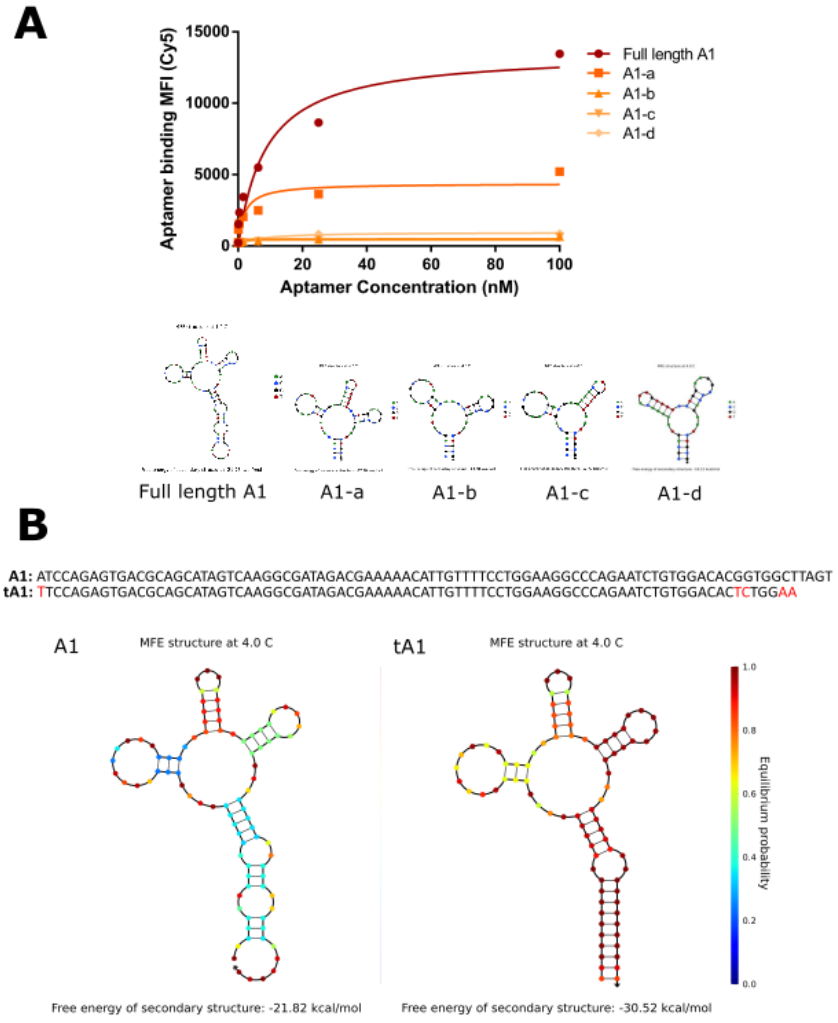

Figure 5.5. Modification of A1. (A) Upper: Binding curves of truncated A1 variants on IL-2 media incubated $CD4^+$ T cells. Lower: NUPACK simulated secondary structures of truncated A1 variants. (B) Sequence and secondary structure of A1 and tA1 predicted by NUPACK. MFI: median fluorescent intensity; Cy5: Cyanine 5. NUPACK settings: temperature = 4 °C; Na^+ = 137 mM; Mg^{2+} = 5.5mM.

5.3.5 Conjugating drug release linker and toxin to tA1

tA1 was conjugated with a Val-Cit dipeptide linker that links to a MMAE toxin. This construct was chosen because Val-Cit has shown successful cleavage and toxin release in Hodgkin's lymphoma[10,41], and several solid tumor cell lines.[26–28] The Val-Cit-cleaving protease, cathepsin B, has been reported to be overexpressed in cancer cell lines which could be one of the reasons the linker is suitable for cancer drug delivery.[16] The released MMAE has high potency to sufficiently inhibit cancer cell growth through blocking their tubulin polymerization during cell division.[42] tA1 and RAN aptamer were labeled with thiol group on their 5'-ends, while the Val-Cit-MMAE was modified to carry a maleimide group (MC-Val-Cit-PAB-MMAE, BOC sciences). Crosslinking of the thiol and maleimide groups yields a stable thioether bond that is not cleavable. After conjugation, we observed a delayed elution of conjugated DNA on HPLC due to their change of polarity. The conjugation efficiency was close to 100% for both aptamers (**Figure 5.6A**). The conjugated tA1-vc-MMAE showed similar degree of binding compared to its parent aptamer on both resting $CD4^+$ T cells and activated $CD4^+$ T cells (**Figure 5.6B**).

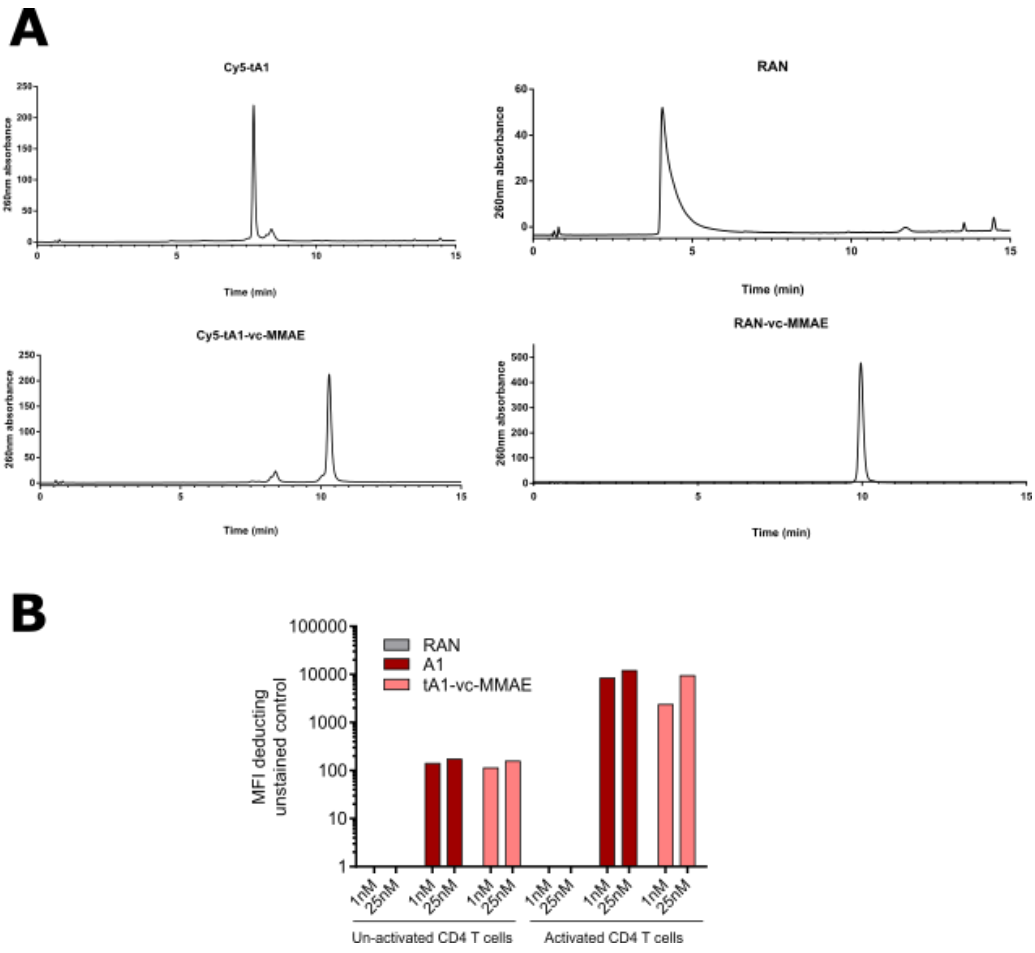

Figure 5.6. tA1 conjugation and binding of tA1 conjugate. (A) Time course of 260 nm absorbance on HPLC. (B) Flow cytometry binding study of tA1-vc-MMAE and A1 on resting, and cytokine and stimulation beads activated $CD4^+$ T cells. MFI: median fluorescent intensity.

5.3.6 Towards viability inhibition on targeted acute lymphoblast leukemia T cell line

MMAE has been tested on cancer cell lines with IC_{50} around 1 nM or less in its free-form without peptide linker.[43] After being conjugated with a linker, the cytotoxicity of the linker-MMAE constructs vary due to its change in membrane permeability. This was seen in the case of MC-Val-Cit-PAB-MMAE (vc-MMAE). We incubated vc-MMAE with J.RT3-T3.5 cells for 72 and 96 hours without washing the cells. Even with long incubations, the IC_{50} of vc-MMAE on J.RT3-T3.5 cells was around 220-250 nM (**Figure 5.7A**), of which the internalization was likely due to by-stander effect.

In a preliminary test, with ligand assisting internalization of the aptamer-drug conjugates, we saw inhibited viability on J.RT3-T3.5 cells pulsed for 1 hour with tA1-vc-MMAE. The cells pulsed with RAN-vc-MMAE were not inhibited unless using the maximum concentration. Unexpectedly, this targeted killing effect was not consistent in the next two biological repeats (**Figure 5.7B**). Since the free vc-MMAE incubated cells eventually show certain degree of cell killing (**Figure 5.7A**), we suspect the targeted labeling of tA1-vc-MMAE on J.RT3-T3.5 cells was not delivering enough MMAE into the cells. When we incubated tA1-vc-MMAE with activated T cells, no inhibition was observed either (**Figure 5.7C**).

We turned to a drug delivery system design that is easy to generate and carries multiple drug molecules on each aptamer sequence that is by intercalating doxorubicin (dox) into the double-stranded structure of DNA aptamers.[44] The intercalation can be achieved by simply mixing and incubating annealed aptamers with doxorubicin. After incubation, we used 10k molecular weight cut off spin column to replace dox solution with buffer. Both RAN- and A1-dox still show strong absorbance at 480 nm after washes, whereas the free dox without DNA control showed complete removal of the small molecule toxin (**Figure 5.8A**). After the RAN-dox and A1-dox complexes were formed, we applied the complexes to J.RT3-T3.5 cells for a short incubation, followed by repeated washing. However, even with 15 minutes of aptamer-dox incubation, both complexes showed high potency on J.RT3-T3.5 cells at a similar degree (**Figure 5.8B**). We will

need to further optimize the staining conditions such as incubation temperature and anionic blockers to reduce the background toxicity of RAN-dox.

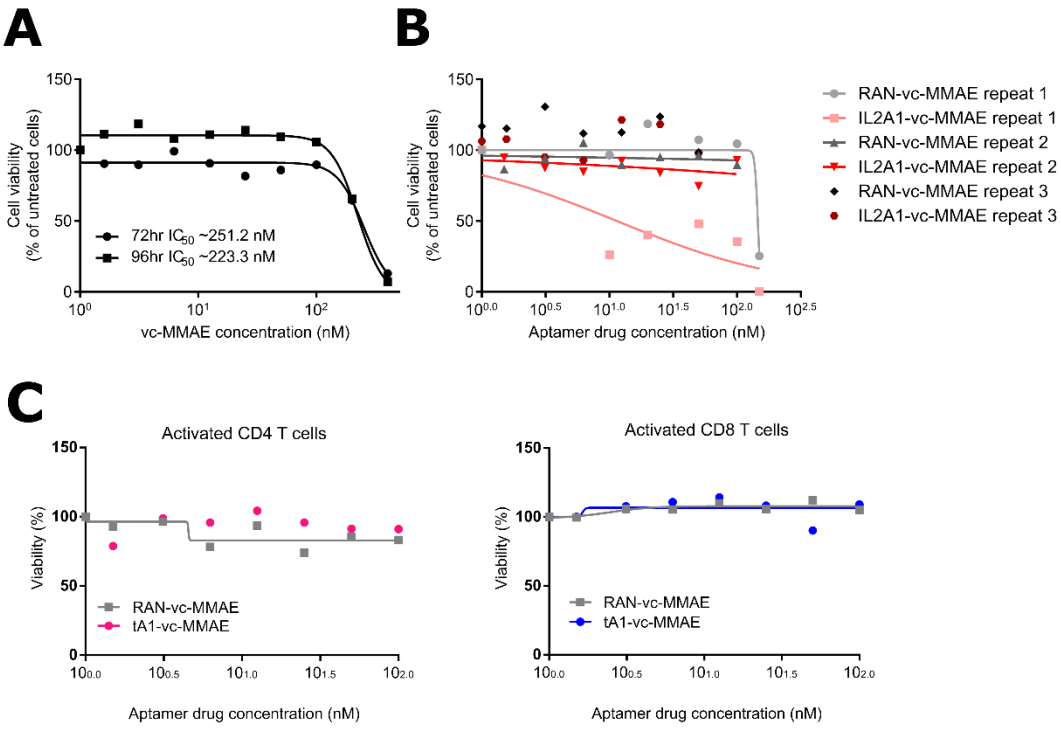

Figure 5.7. Killing curves of (A) unconjugated vc-MMAE treating J.RT3-T3.5 cells for 72 or 96 hours, (B) 96-hour post treatment with aptamer-drug conjugates tA1-vc-MMAE and RAN-vc-MMAE pulsing for 1 hour on J.RT3-T3.5 cells, and (C) 96-hour post-treatment using aptamer-drug conjugates tA1-vc-MMAE and RAN-vc-MMAE pulsing for 1 hour on activated $CD4^+$ and $CD8^+$ T cells. Viability was calculated by deducting the blank control without cells and normalize to the untreated cells as 100%.

A

	Total dox (uM)
800nM A1 dox after clearing	4.6
800nM RAN dox after clearing	3.9
Dox after clearing	0
NS only (no dox control)	0.3

B

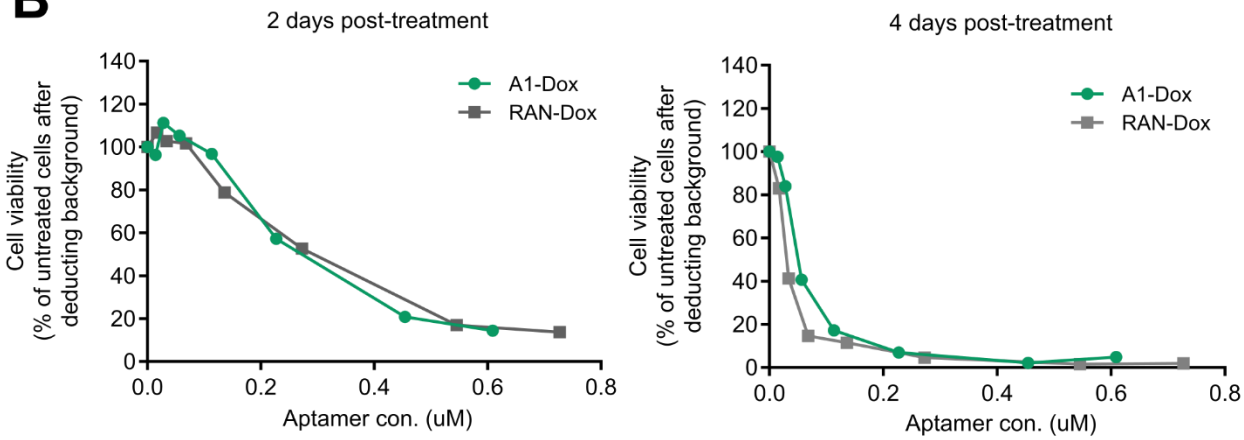

Figure 5.8. J.RT3-T3.5 cells cytotoxicity assay using A1- and RAN-dox. (A) Dox concentration after removing free dox from the aptamer-dox solutions. (B) Post-treatment killing curves of A1- and RAN-dox treating J.RT3-T3.5 cells and incubated for additional 48 or 96 hours.

5.4 Conclusion and future work

We identified a novel aptamer, A1, across two sets of combinational cell-SELEX designated for selecting $CD4^+$ T cell and general T cell binders. On $CD4^+$ T cells, A1 has shown incubation dependency as it binds to pre-incubated $CD4^+$ T cells with higher saturated binding. However, the enrichment of A1 in the cell-SELEX process was not dependent on the cell incubation step. In addition, A1 showed high affinity binding to CD4 T cells (sub-nanomolar K_D) regardless of the pre-incubation step. A1 also binds to $CD8^+$ T cells, NK cells, B cells, as well as J.RT3-T3.5 leukemic cells in varying degrees. We further explored the potential of using A1 for delivering toxic cargos into target cells after establishing that A1 can be internalized by target cells upon receptor binding. Therefore, we modified A1 to be used in an aptamer-drug conjugate delivery system targeting T-ALL tumor. The modified A1, named tA1, has a more stable structure and comparable target binding to its parent aptamer. We conjugated tA1 with Val-Cit linker and MMAE toxin for prolonged treatment (1 hour) on J.RT3-T3.5 cells. We also mixed A1 with dox to form aptamer-drug complex for shortened treatments (15 minutes) but with larger cargo capacity. The two methods have their own merits and drawbacks. The aptamer-drug conjugates are

theoretically more stable, without unintentional release of toxin outside of cells, with the covalent link and cleavable linker between the toxin and the ligand. However, this conjugate design only enables aptamers carrying one toxin per strand. The potency was inconsistent likely because of the limited toxin transport. The aptamer-drug complex, on the other hand, showed high potency due to the high intrinsic toxicity of the toxin and/or the increased drug load on the aptamers. However, the background toxicity is so high that the treatment effect is not only dependent on the ligand targeting and delivery.

The next steps of this study include further evaluation of potential A1 binding antigens by including more or different photoreactive analogues in the aptamer sequence for improved crosslinking in the pull-down assays, as well as optimizing the cytotoxicity assays of aptamer-dox complexes inhibiting J.RT3-T3.5 cells. We can potentially reduce the background interaction of aptamer-dox and the cells by reducing the incubation temperature or by including certain anionic blockers.

5.5 Acknowledgements

This research was supported by Juno Therapeutics (a Bristol Myers Squibb company). We thank Dr. Chris Ramsborg (Juno), Dr. Allison Bianchi (Juno), Dr. Julie Shi (Juno), and Dr. Michael C. Jensen (Seattle Children's Research Institute) for their valuable discussions and suggestions. We thank Dr. Julie Shi for coordinating and providing primary cells. We thank Dr. Stephan Salipante for collecting and processing the NGS data. We also thank Dr. Philip Gafken and Lisa Jones (Fred Hutchinson Cancer Research Center) for preparing and running the mass spectrometry samples.

5.6 References

1. Terwilliger, T. & Abdul-Hay, M. Acute lymphoblastic leukemia: a comprehensive review and 2017 update. *Blood Cancer J.* (2017) doi:10.1038/bcj.2017.53.

2. Fattizzo, B., Rosa, J., Giannotta, J. A., Baldini, L. & Fracchiolla, N. S. The Physiopathology of T- Cell Acute Lymphoblastic Leukemia: Focus on Molecular Aspects. *Frontiers in Oncology* (2020) doi:10.3389/fonc.2020.00273.

3. Raetz, E. A. & Teachey, D. T. T-cell acute lymphoblastic leukemia. *Hematology* (2016) doi:10.1182/asheducation-2016.1.580.

4. Roecker, A. M., Stockert, A. & Kisor, D. F. Nelarabine in the treatment of refractory T-Cell malignancies. *Clinical Medicine Insights: Oncology* (2010) doi:10.4137/CMO.S4364.

5. Luskin, M. R. & DeAngelo, D. J. T-cell acute lymphoblastic leukemia: Current approach and future directions. *Adv. CELL GENE Ther.* (2019) doi:10.1002/acg2.70.

6. Walter, R. B. Brief overview of antibody–drug conjugate therapy for acute leukemia. *Expert Opin. Biol. Ther.* 1–5 (2020) doi:10.1080/14712598.2020.1817373.

7. Jabbour, E., O'Brien, S., Ravandi, F. & Kantarjian, H. Monoclonal antibodies in acute lymphoblastic leukemia. *Blood* (2015) doi:10.1182/blood-2014-08-596403.

8. Cooper, M. L., Choi, J., Staser, K., Ritchey, J. K., Devenport, J. M., Eckardt, K., Rettig, M. P., Wang, B., Eissenberg, L. G., Ghobadi, A., Gehrs, L. N., Prior, J. L., Achilefu, S., Miller, C. A., Fronick, C. C., O'Neal, J., Gao, F., Weinstock, D. M., Gutierrez, A., Fulton, R. S. & DiPersio, J. F. An "off-the-shelf" fratricide-resistant CAR-T for the treatment of T cell hematologic malignancies. *Leukemia* (2018) doi:10.1038/s41375-018-0065-5.

9. Birrer, M. J., Moore, K. N., Betella, I. & Bates, R. C. Antibody-Drug Conjugate-Based Therapeutics: State of the Science. *J. Natl. Cancer Inst.* (2019) doi:10.1093/jnci/djz035.

10. Senter, P. D. & Sievers, E. L. The discovery and development of brentuximab vedotin for use in relapsed Hodgkin lymphoma and systemic anaplastic large cell lymphoma. *Nature Biotechnology* (2012) doi:10.1038/nbt.2289.

11. Salomon, P. L., Reid, E. E., Archer, K. E., Harris, L., Maloney, E. K., Wilhelm, A. J., Miller, M. L., Chari, R. V. J., Keating, T. A. & Singh, R. Optimizing Lysosomal Activation of Antibody-Drug Conjugates (ADCs) by Incorporation of Novel Cleavable Dipeptide Linkers. *Mol. Pharm.* (2019) doi:10.1021/acs.molpharmaceut.9b00696.

12. Buck, M. R., Karustis, D. G., Day, N. A., Honn, K. V. & Sloane, B. F. Degradation of extracellular-matrix proteins by human cathepsin B from normal and tumour tissues. *Biochem. J.* (1992) doi:10.1042/bj2820273.

13. Giusti, I., D'Ascenzo, S., Millimaggi, D., Taraboletti, G., Carta, G., Franceschini, N., Pavan, A. & Dolo, V. Cathepsin B mediates the pH-dependent proinvasive activity of tumor-shed microvesicles. *Neoplasia* (2008) doi:10.1593/neo.08178.

14. Chen, H., Lin, Z., Arnst, K. E., Miller, D. D. & Li, W. Tubulin inhibitor-based antibody-

drug conjugates for cancer therapy. *Molecules* (2017) doi:10.3390/molecules22081281.

15. Sedlik, C., Heitzmann, A., Viel, S., Ait Sarkouh, R., Batisse, C., Schmidt, F., De La Rochere, P., Amzallag, N., Osinaga, E., Oppezzo, P., Pritsch, O., Sastre-Garau, X., Hubert, P., Amigorena, S. & Piaggio, E. Effective antitumor therapy based on a novel antibody-drug conjugate targeting the Tn carbohydrate antigen. *Oncoimmunology* **5**, e1171434–e1171434 (2016).

16. Gondi, C. S. & Rao, J. S. Cathepsin B as a cancer target. *Expert Opin. Ther. Targets* **17**, 281–291 (2013).

17. Keefe, A. D., Pai, S. & Ellington, A. Aptamers as therapeutics. *Nature Reviews Drug Discovery* (2010) doi:10.1038/nrd3141.

18. Zhou, J. & Rossi, J. Aptamers as targeted therapeutics: Current potential and challenges. *Nature Reviews Drug Discovery* (2017) doi:10.1038/nrd.2016.199.

19. Xiang, D., Zheng, C., Zhou, S.-F., Qiao, S., Tran, P. H.-L., Pu, C., Li, Y., Kong, L., Kouzani, A. Z., Lin, J., Liu, K., Li, L., Shigdar, S. & Duan, W. Superior Performance of Aptamer in Tumor Penetration over Antibody: Implication of Aptamer-Based Theranostics in Solid Tumors. *Theranostics* **5**, 1083–1097 (2015).

20. Guyer, D. R., Fish, G., Haller, J. A., Ho, A. C., Klein, M., Loewenstein, J., Martin, D., Orth, D., Rosen, R. B., Sanislo, S., Schwartz, S. D., Singerman, L. J. & Williams, G. Anti-vascular endothelial growth factor therapy for subfoveal choroidal neovascularization secondary to age-related macular degeneration: Phase II study results. *Ophthalmology* (2003) doi:10.1016/S0161-6420(03)00085-X.

21. Taghdisi, S. M., Abnous, K., Mosaffa, F. & Behravan, J. Targeted delivery of daunorubicin to T-cell acute lymphoblastic leukemia by aptamer. *J. Drug Target.* (2010) doi:10.3109/10611860903434050.

22. Wen, J., Tao, W., Hao, S., Iyer, S. P. & Zu, Y. A unique aptamer-drug conjugate for targeted therapy of multiple myeloma. *Leukemia* (2016) doi:10.1038/leu.2015.216.

23. Zhao, N., Pei, S. N., Qi, J., Zeng, Z., Iyer, S. P., Lin, P., Tung, C. H. & Zu, Y. Oligonucleotide aptamer-drug conjugates for targeted therapy of acute myeloid leukemia. *Biomaterials* (2015) doi:10.1016/j.biomaterials.2015.07.025.

24. Yoon, S., Huang, K. W., Reebye, V., Spalding, D., Przytycka, T. M., Wang, Y., Swiderski, P., Li, L., Armstrong, B., Reccia, I., Zacharoulis, D., Dimas, K., Kusano, T., Shively, J., Habib, N. & Rossi, J. J. Aptamer-Drug Conjugates of Active Metabolites of Nucleoside Analogs and Cytotoxic Agents Inhibit Pancreatic Tumor Cell Growth. *Mol. Ther. - Nucleic Acids* (2017) doi:10.1016/j.omtn.2016.11.008.

25. Zhou, F., Wang, P., Peng, Y., Zhang, P., Huang, Q., Sun, W., He, N., Fu, T., Zhao, Z., Fang, X. & Tan, W. Molecular Engineering-Based Aptamer–Drug Conjugates with Accurate Tunability of Drug Ratios for Drug Combination Targeted Cancer Therapy. *Angew. Chemie - Int. Ed.* (2019) doi:10.1002/anie.201903807.

26. Powell Gray, B., Kelly, L., Ahrens, D. P., Barry, A. P., Kratschmer, C., Levy, M. & Sullenger, B. A. Tunable cytotoxic aptamer–drug conjugates for the treatment of prostate

cancer. *Proc. Natl. Acad. Sci.* **115**, 4761 LP – 4766 (2018).

27. Sun, Y., Gao, F., Yang, C., Li, Y., Jin, C., Xie, S., Lv, C., Ding, D., Han, D., Li, J., Wang, R., Wang, R., Tan, W., Tan, W. & Tan, W. Construction of Bispecific Aptamer-Drug Conjugate by a Hybrid Chemical and Biological Approach. *Bioconjug. Chem.* (2020) doi:10.1021/acs.bioconjchem.0c00071.

28. Kratschmer, C. & Levy, M. Targeted Delivery of Auristatin-Modified Toxins to Pancreatic Cancer Using Aptamers. *Mol. Ther. - Nucleic Acids* **10**, 227–236 (2018).

29. Sefah, K., Shangguan, D., Xiong, X., O'Donoghue, M. B. & Tan, W. Development of DNA aptamers using cell-selex. *Nat. Protoc.* (2010) doi:10.1038/nprot.2010.66.

30. Kacherovsky, N., Cardle, I. I., Cheng, E. L., Yu, J. L., Baldwin, M. L., Salipante, S. J., Jensen, M. C. & Pun, S. H. Traceless aptamer-mediated isolation of CD8+ T cells for chimeric antigen receptor T-cell therapy. *Nat. Biomed. Eng.* (2019) doi:10.1038/s41551-019-0411-6.

31. Alam, K. K., Chang, J. L. & Burke, D. H. FASTAptamer: A bioinformatic toolkit for high-throughput sequence analysis of combinatorial selections. *Mol. Ther. - Nucleic Acids* **4**, (2015).

32. Bailey, T. L., Boden, M., Buske, F. A., Frith, M., Grant, C. E., Clementi, L., Ren, J., Li, W. W. & Noble, W. S. MEME Suite: Tools for motif discovery and searching. *Nucleic Acids Res.* (2009) doi:10.1093/nar/gkp335.

33. McWilliam, H., Li, W., Uludag, M., Squizzato, S., Park, Y. M., Buso, N., Cowley, A. P. & Lopez, R. Analysis Tool Web Services from the EMBL-EBI. *Nucleic Acids Res.* (2013) doi:10.1093/nar/gkt376.

34. Zadeh, J. N., Steenberg, C. D., Bois, J. S., Wolfe, B. R., Pierce, M. B., Khan, A. R., Dirks, R. M. & Pierce, N. A. NUPACK: Analysis and design of nucleic acid systems. *J. Comput. Chem.* (2011) doi:10.1002/jcc.21596.

35. Shangguan, D., Cao, Z., Meng, L., Mallikaratchy, P., Sefah, K., Wang, H., Li, Y. & Tan, W. Cell-specific aptamer probes for membrane protein elucidation in cancer cells. *J. Proteome Res.* (2008) doi:10.1021/pr700894d.

36. Pacholarz, K. J. & Barran, P. E. Use of a charge reducing agent to enable intact mass analysis of cysteine-linked antibody-drug-conjugates by native mass spectrometry. *EuPA Open Proteomics* (2016) doi:10.1016/j.euprot.2016.02.004.

37. Caroli, J., Taccioli, C., De La Fuente, A., Serafini, P. & Bicciato, S. APTANI: A computational tool to select aptamers through sequence-structure motif analysis of HT-SELEX data. *Bioinformatics* (2016) doi:10.1093/bioinformatics/btv545.

38. Meisenheimer, K. M. & Koch, T. H. Photocross-linking of nucleic acids to associated proteins. *Critical Reviews in Biochemistry and Molecular Biology* (1997) doi:10.3109/10409239709108550.

39. Hafner, M., Landthaler, M., Burger, L., Khorshid, M., Hausser, J., Berninger, P., Rothballer, A., Ascano, M., Jungkamp, A. C., Munschauer, M., Ulrich, A., Wardle, G. S.,

Dewell, S., Zavolan, M. & Tuschl, T. Transcriptome-wide Identification of RNA-Binding Protein and MicroRNA Target Sites by PAR-CLIP. *Cell* (2010) doi:10.1016/j.cell.2010.03.009.

40. Tortorella, S. & Karagiannis, T. C. Transferrin receptor-mediated endocytosis: A useful target for cancer therapy. *Journal of Membrane Biology* (2014) doi:10.1007/s00232-014-9637-0.

41. Doronina, S. O., Toki, B. E., Torgov, M. Y., Mendelsohn, B. A., Cerveny, C. G., Chace, D. F., DeBlanc, R. L., Gearing, R. P., Bovee, T. D., Siegall, C. B., Francisco, J. A., Wahl, A. F., Meyer, D. L. & Senter, P. D. Development of potent monoclonal antibody auristatin conjugates for cancer therapy. *Nat. Biotechnol.* (2003) doi:10.1038/nbt832.

42. Waight, A. B., Bargsten, K., Doronina, S., Steinmetz, M. O., Sussman, D. & Prota, A. E. Structural basis of microtubule destabilization by potent auristatin anti-mitotics. *PLoS One* (2016) doi:10.1371/journal.pone.0160890.

43. Koga, Y., Manabe, S., Aihara, Y., Sato, R., Tsumura, R., Iwafuji, H., Furuya, F., Fuchigami, H., Fujiwara, Y., Hisada, Y., Yamamoto, Y., Yasunaga, M. & Matsumura, Y. Antitumor effect of antitissue factor antibody-MMAE conjugate in human pancreatic tumor xenografts. *Int. J. Cancer* (2015) doi:10.1002/ijc.29492.

44. Zhu, G., Zheng, J., Song, E., Donovan, M., Zhang, K., Liu, C. & Tan, W. Self-assembled, aptamer-tethered DNA nanotrains for targeted transport of molecular drugs in cancer theranostics. *Proc. Natl. Acad. Sci. U. S. A.* (2013) doi:10.1073/pnas.1220817110.

5.7 Supplementary information

Supplementary Table 1. Aptamer sequences used in this study.

Name	Sequence
RAN	5'-ATCCAGAGTGACGCAGCAAATTCCAAACTCGAGTAAGCGTAGAGCCTCTCATCGCCTCAATAATGGACACGGTGGCTTAGT -3'
A1	5'-ATCCAGAGTGACGCAGCATAGTCAAGGCGATAGACGAAAAACATTGTTTTCCTGGAAGGCCCAGAATCTGTGG ACACGGTGGCTTAGT -3'
tA1	5'-TTCCAGAGTGACGCAGCATAGTCAAGGCGATAGACGAAAAACATTGTTTTCCTGGAAGGCCCAGAATCTGTGGACACTCTGGAA -3'
BrdU-A1 (hairpin loop)	5'-ATCCAGAGTGACGCAGCA/i5BrdU/AGTCAAGGCGATAGACGAAAAACATTGTTTTCCTGGAAGGCCCAGAATCTGTGGACACGGTGGCTTAGT -3'
BrdU-A1 (3' overhang)	5'-ATCCAGAGTGACGCAGCATAGTCAAGGCGATAGACGAAAAACATTGTTTTCCTGGAAGGCCCAGAATCTGTGGACACGGTGGCTTAG/i5Br-dU/T -3'

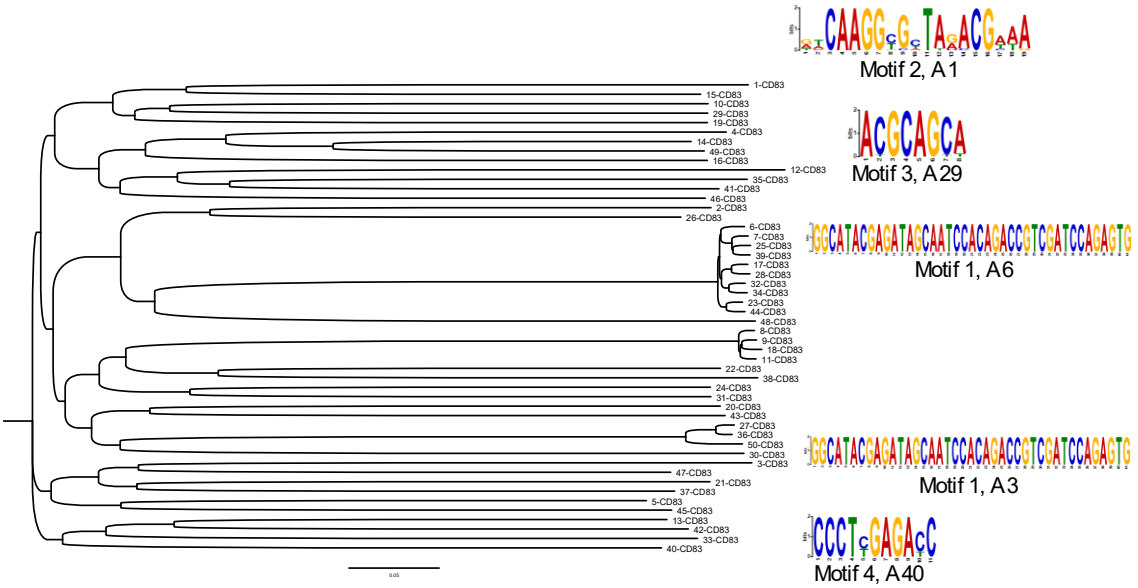

Supplementary Figure 5.1. Phylogenic tree with the selected aptamer candidates located on the branches and their predicted motifs.

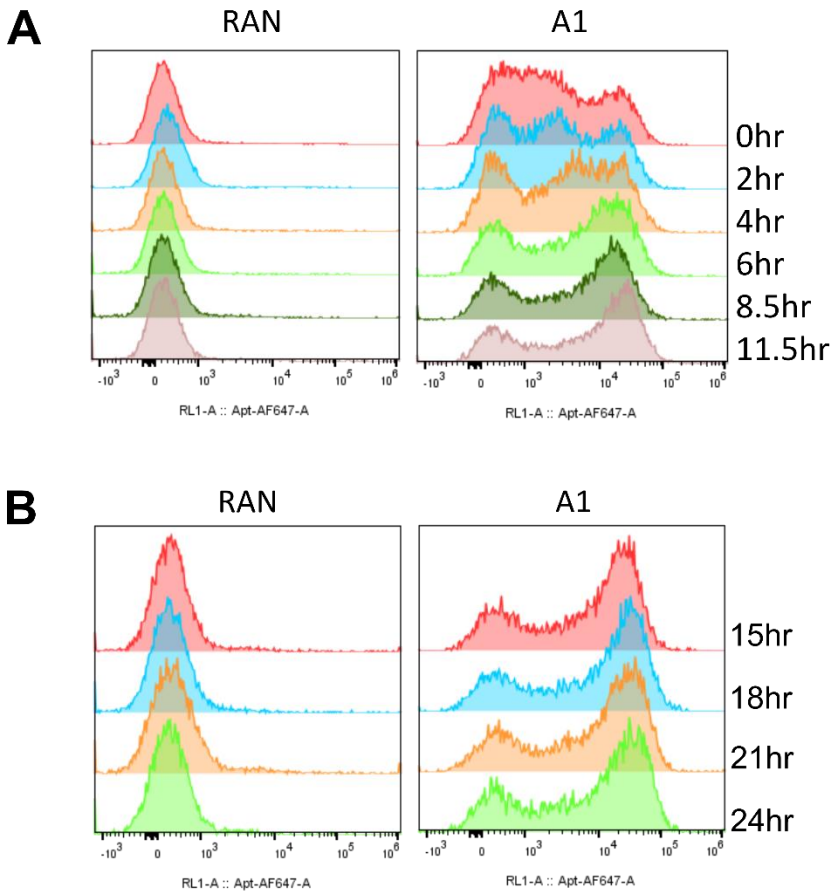

Supplementary Figure 5.2. Time course changes in 20 nM A1 binding to $CD4^+$ T cells incubated in RPMI with 10% FBS for (A) 0-11.5 hours, and (B) 15-24 hours.

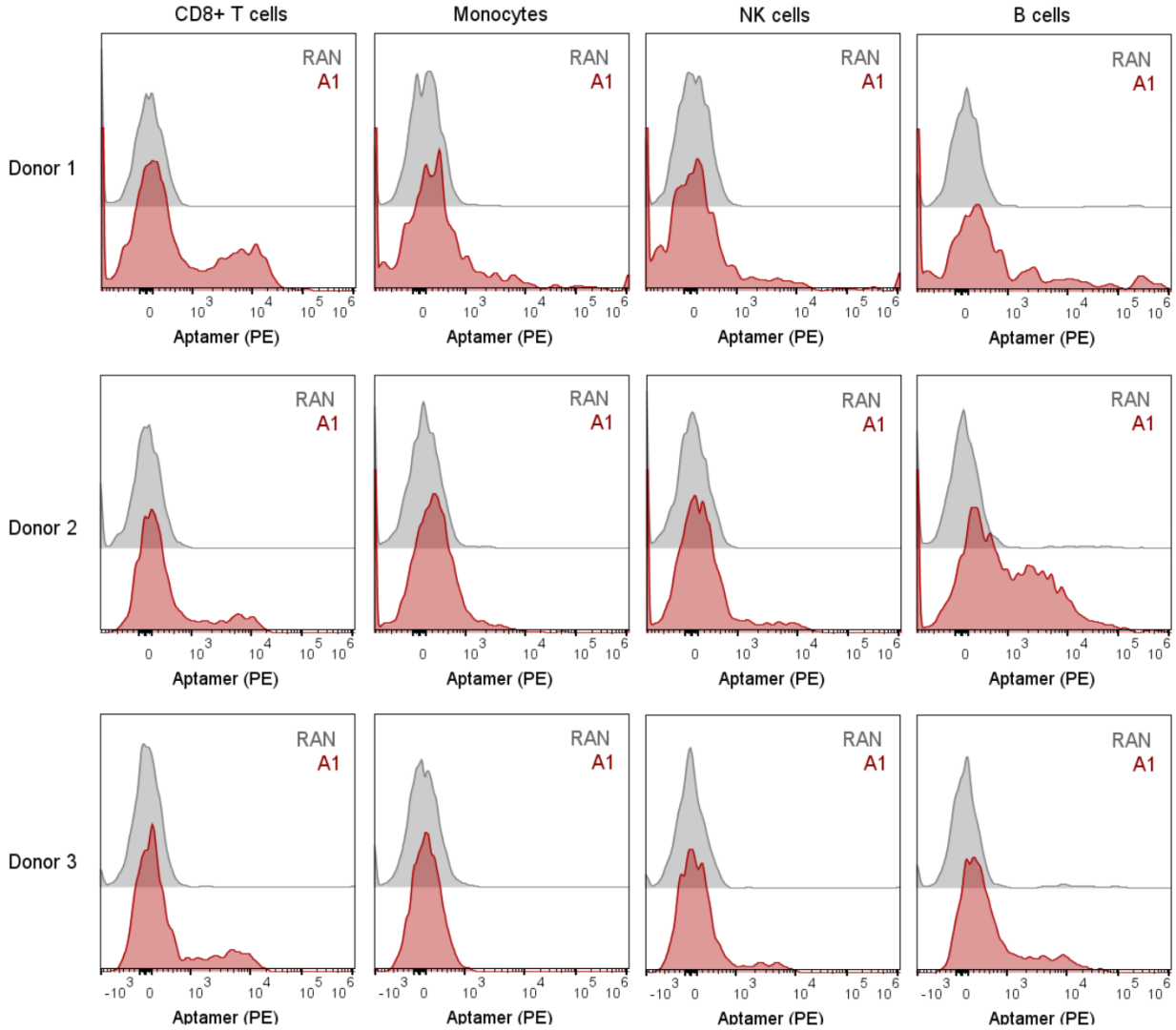

Supplementary Figure 5.3. 10 nM A1 binding to PBMCs. Aptamer binding was evaluated by gating on different cell types. $CD8^+$ T cells were gated on $CD8^{hi}$ cells. Monocytes were gated on $CD14^+$ cells. NK cells were gated on $CD56^+$ cells. B cells were gated on $CD19^+$ cells. PE: phycoerythrin.

A

		Positive selection			Negative selection			
Round	Library	Cell type and #	Time	Wash	Protein blocker	Cell type and #	Time	Protein blocker
1.	13.7uM	10 million CD4+ cells	1h	3x	0.1% BSA	None	1h	0.1% BSA
2.	500nM	5 million CD4+ cells	1h	4x	0.1% BSA	10 million CD8+ cells	1h	0.1% BSA
3.	250nM	5 million CD4+ cells	0.5h	4x	1% BSA	10 million CD8+ cells	0.5h	1% BSA
4.	250nM	5 million CD4+ cells	0.5h	4x	1% BSA	20 million CD8+ cells	0.5h	1% BSA
5.	250nM	5 million PBMCs with FACS isolating T cells	0.5h	4x	1% BSA	20 million CD8+ cells	0.5h	1% BSA

B

Ranking	Sequence	% total reads
1	TGTCTACGCAGTTGAACATCAAAACTACAACGAGTAACTCTCCAGTTCCTCC	20.9%
2	TAGTCAAGGCGATAGACGAAAAACATTGTTTTCCTGGAAGGCCCAGAATCTG	11%
3	CGCAGCACAGGGATTGAGCCGATTTGAGGCGTTGTTGTGGGCCCATGAGTGG	8.0%
4	AACCTGACTCAAAAGCTTAGGTCTACGCACGATCAGAGGAGTAACTCTAATT	2.3%
5	CGCAGCAGTGGGCCAAATGGATTGGATTAGGGTTGGGCCGCCCGGGAGGGGT	1.7%
6	CGCAGCAAATTCCAAACTCGAGTAAGCGTAGAGCCTCTCATCGCCTCAATAA	1.4%
7	GACCTCCACACGCGGAACGAGGGCGTGTTTCGACATACAATTCAACACACTA	1.3%
8	CGCAGCAGCTTGGGAAAGACCACCCTTGAATGTCTGTAAGTGGCAAGAACCC	0.9%
9	CGGAACCAACAACCTTCTGGAACGAGGTATTGTACCTCTCCACCAGGACGTA	0.9%
10	GACGAATGGCGTACTCCACTTTAGTACACAAGACAACAAGGCCGTAAGTTGA	0.8%

Supplementary Figure 5.4. Second combinational cell-SELEX. (A) Combinational cell-SELEX using $CD4^+$ T cells without cytokine treatment as target cells, and CD8 T cells without cytokine treatment as control cells. Round 5 (R5) was done with negative selection first, followed by positive selection on PBMCs combining FACS isolating T cells. (B) The top sequences identified in the R5 library enriched from the second SELEX with A1 aptamer shaded in orange.

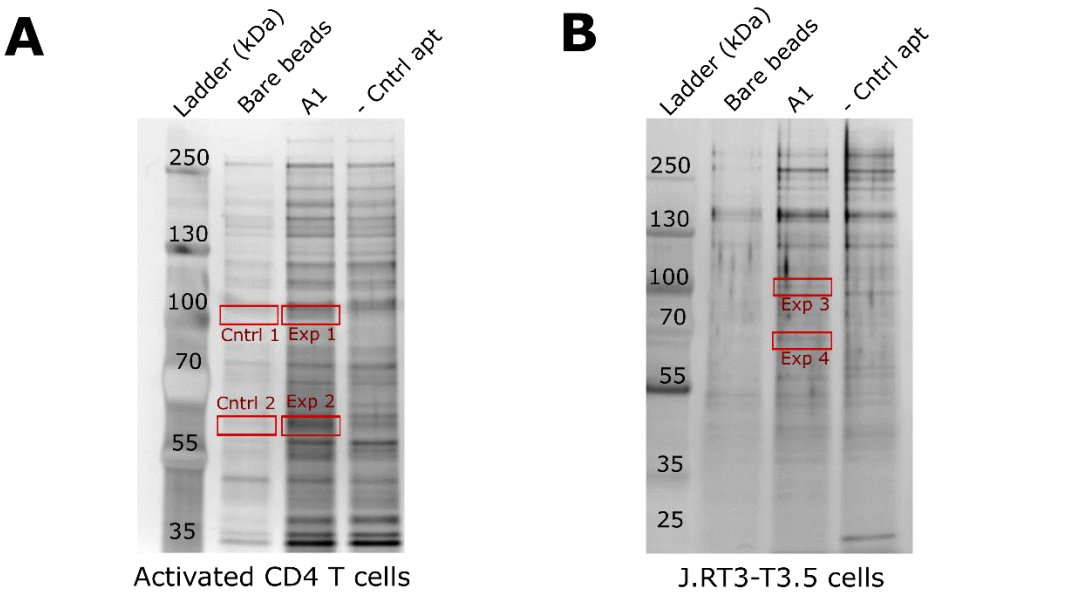

C

Protein identified	*Control 1 Peptide coverage %*	*Exp 1 Peptide coverage %*	*Control 1 Peptide #*	*Exp 1 Peptide #*	*Control 1 Score*	*Exp 1 Score*
Leukosialin	N/A	2	N/A	1	N/A	1.88

Protein identified	*Exp 3 Peptide coverage %*	*Exp 3 Peptide #*	*Exp 3 Score*
Sodium/potassium-transporting ATPase subunit alpha-1	25	24	69.36
Integrin beta-2	10	7	12.59
4F2 cell-surface antigen heavy chain	2	1	3.24
Leukosialin	2	1	2.08

Protein identified	*Exp 4 Peptide coverage %*	*Exp 4 Peptide #*	*Exp 4 Score*
T-cell surface glycoprotein CD5	10	4	11.4
Leukosialin	3	1	2.17

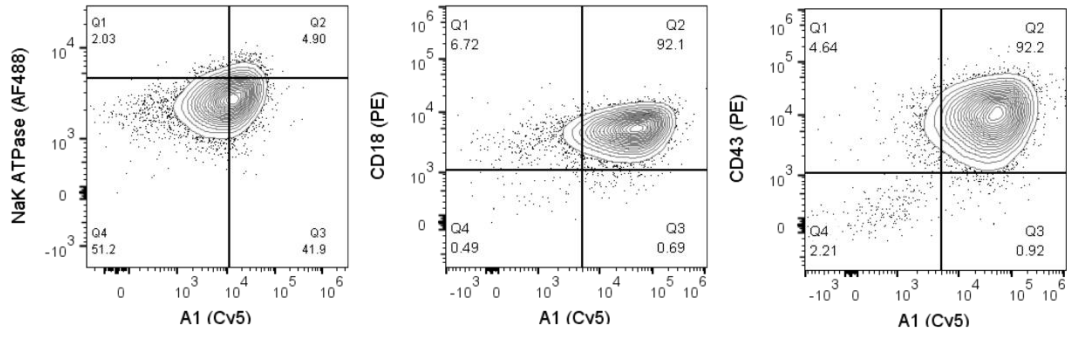

Supplementary Figure 5.5 A1 receptor identification with membrane protein extracted from activated $CD4^+$ T cells and J.RT3-T3.5 cells. (A) Activated $CD4^+$ T cell protein purified using streptavidin beads and biotinylated A1 or control aptamer. Purified targets were separated on 8% polyacrylamide gel. Excised bands of interest are indicated with red boxes. (B) J.RT3-T3.5 cell protein extract purified using streptavidin beads and biotinylated A1 or control aptamer. Purified

targets were separated on 4-20% gradient polyacrylamide gel. Excised target band of interest are indicated with red boxes. (C) Relevant proteins identified by mass spectrometry analysis on the excised target bands. No relevant protein candidates were identified in control 2 and experimental 2. (D) Binding correlation study with antibodies label potential targets and A1.

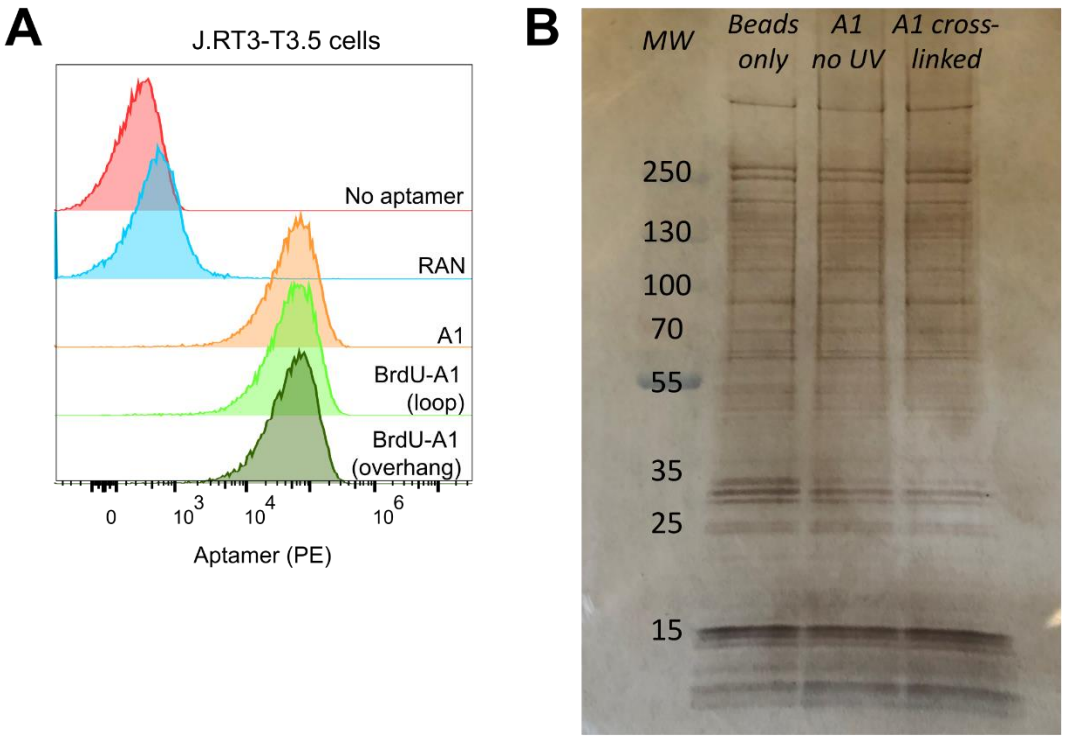

Supplementary Figure 5.6 BrdU-A1 receptor identification by staining J.RT3-T3.5 cells and followed by UV exposure. (A) Flow cytometry binding study using biotinylated-A1 variants followed by streptavidin-PE staining. (B) The membrane protein of treated J.RT3-T3.5 cells were extracted and enriched using streptavidin beads. Purified targets were separated on 4-20% polyacrylamide gel and stained with SilverQuest. PE: phycoerythrin.

Chapter 6. Summary of major findings and future work recommendations

6.1 Summary of major findings

6.1.1 Characterization and applications of a transferrin receptor 1-binding aptamer

A novel DNA ligand, JBA8.1 (Jurkat binding aptamer 8.1), was discovered in a cell-SELEX process using $CD3^+CD28^+$ Jurkat cells as selection target and $CD3^-CD28^-$ J.RT3-T3.5 cells as counter selection control. JBA8.1 was truncated to remove non-functional structures and to yield tJBA8.1 (truncated Jurkat binding aptamer 8.1) which has similar binding affinity (apparent K_D 10.9 nM) to the full-length version. We performed pull-down assay, as well as siRNA knockdown assay and identified one of the receptors of tJBA8.1 as transferrin receptor 1 (TfR1). This new TfR1 aptamer was compared with a previously identified sequence, XQ-2d. We found that tJBA8.1 shares overlapping binding sites with XQ-2d and holo-transferrin, but also has additional unknown binding sites on Jurkat cells. By incorporating tJBA8.1 into a magnetic cell isolation system, we depleted TfR^+ cancerous cell contamination from the healthy PBMCs. The resulting "cleared" PBMCs could be a better starting material for CAR T cell manufacturing.[1] Lastly, we identified another promising sequence, JBA8.26, from the sequencing result that has improved binding affinity compared to tJBA8.1. Both tJBA8.1 and JBA8.26 can both be used in the CAR T cell manufacturing process to capture cancerous cells with varying degree of TfR expressions.

6.1.2 Identify impactful modifications that improve efficacy of aptamer displacement with antidotes

Continuing from chapter 2, we modified the newly discovered TfR1 aptamer, JBA8.1, for traceless cell isolation in chapter 3. The mutations made on JBA8.1 for effective antidote annealing include switching out certain sequences to reduce overall stability of the aptamer and adding an 8 nt overhang toehold on the 3'-end. The overhang sequence was optimized in terms of G-C content, which led to little impact on the binding structure of the aptamer, but not significantly on strand displacement efficiency. Different antidote length was tested for aptamer displacement as well. Our result suggests that a sequence that is long enough to disrupt crucial binding structure on the

aptamer, but short enough to bypass the steric hindrance of aptamer-protein complex leads to optimal aptamer removal. Lastly, different magnetic isolation methods including using MACS columns set on a magnetic separator and Dynabeads resuspended in Eppendorf tubes, were also explored in this chapter. While the MACS system is more efficient in capturing the lower expressors, rotating Dynabeads in solutions is a better way to recover most of the target cells by antidote displacements. These optimizations are useful for modifying other novel aptamers discovered in the future.

6.1.3 Demonstration of a dual selection workflow

Continuing from section 6.1.2, If the modified JBA8.1, renamed as rvCD71apt, has enough sequence distinction from the A3t aptamer,[2] renamed as rvCD8apt, we can use two pairs of aptamers and antidotes together for a dual selection workflow consist of one step of ligand staining and two serial steps of antidote elution. This new cell isolation method reduces the operation time and the material needed, and yields target cells with less isolation material residual. In chapter 3, we demonstrated this workflow as a proof-of-concept by using activated $CD4^+CD71^+$ T cells mixed with PBMCs which contains $CD8^+CD71^-$ T cells as the starting cell population. By using dual selection, we isolated about 50% of the inputting activated $CD4^+CD71^+$ T cells with over 90% purity, and about 25% of inputting $CD8^+CD71^-$ T cells at around 85% purity. The impurity observed through flow cytometry suggests that we had some non-target cells associating with the isolation beads through non-specific interactions. Other solid support options with reduced non-specific interactions can be explored in the future to improve the target cell purity.

6.1.4 $CD4^+$ T cell-binding aptamer discovery

In chapter 4 and 5, we discovered a $CD4^+$ T cell-binding aptamer, A1, which shows high binding affinity to $CD4^+$ T cells, however, also shows targeted binding to several other PBMCs except for monocytes. Interestingly, the binding of A1 to $CD4^+$ T cells increased after the cells were incubated in culture media. This indicates the target receptor may have been upregulated by *ex vivo* incubation. We attempted to identify the target protein of A1 using pull-down assay.

However, the receptor might be expressed at low abundance or being bound with high off-rate. A new pull-down method that secures the association between A1 and its target is needed.

6.2 Future work recommendations

6.2.1 Optimizing UV crosslinking-assisted receptor identification of novel aptamers

6.2.1.1 Background and significance

Cell-SELEX is a commonly used panning method for developing novel ligands target certain cell types. By using cell-SELEX, the pre-acknowledgment of the target receptor is not required.[3] However, it is challenging to identify the protein target of the developed aptamers after selections. In this thesis, a pull-down assay was used in chapter 2 to identify the target protein of tJBA8.1 as transferrin receptor 1. However, when we applied the same method in chapter 5 to identify the target of A1, the enrichment of target proteins was not sufficient to yield reliable result. Since the pull-down assay is a lengthy process and depends on secure association of aptamer and its target proteins, crosslinking A1 and its target proteins could improve the probability of successful identification.

6.2.1.2 Aim 1: Use recombinant DNA-binding proteins to screen for effective UV crosslinking analogues

In **Supplementary Figure 5.6**, we showed incorporating one bromodeoxyuridine[4,5] on each aptamer strand was not sufficient to crosslink aptamer with its target protein. According to the literatures, there are different photoactive analogues can be used to crosslink RNA and protein for identifying cellular RNA-binding proteins[5,6], as well as applied to SELEX strategies[4] and aptamer receptor identifications[3]. Substituting 2-4% nucleotides with photoreactive analogues has been shown to increase immunoprecipitation of RNA-crosslinked proteins by hundreds folds compared to un-modified RNA.[7] Aside from bromodeoxyuridine, which can be purchased from IDT, thiouridine and iodouridine are other analogues that have been shown to have higher sensitivity to UV exposure, but are more expansive to purchase.[3,6,7] Increasing the amount of photosensitive analogues and/or choosing the modification sites closer to a crosslink-able amino

acids might improve the success rate of crosslinking. Therefore, screening through a panel of different types of photoreactive analogues, different number of analogues, and different modification sites on the aptamer will help identify the key parameters that lead to A1 crosslinking with proteins. Since the target of A1 is unknown, a DNA-binding protein such as single-stranded DNA binding protein (SSB) or DNA polymerase can be used as model proteins. The crosslinking effectiveness can be evaluated using SDS-PAGE to separate crosslinked proteins followed by silver staining.

6.2.1.3 Aim 2: Evaluate aptamer target binding affinity after including photosensitive analogues

As mentioned previously in section 6.2.1.2, a panel of A1 with different analogue insertions will be used in a design of experiments-style testing to identify the important parameters that promote crosslinking upon UV exposure. These changes, however, could also impact the binding of A1. As we demonstrated in **Figure 5.5**, A1 requires all of its secondary structure for maximum target binding. Therefore, testing the binding of each A1 variants in the screened panel is important before using the aptamer for receptor identification.

6.2.1.4 Aim 3: Receptor identification using photosensitive A1

Lastly, the A1 variants with optimal UV crosslinking efficiency and maintain their binding affinities will be used for receptor identification. We will first stain J.RT3-T3.5 cells with different A1 variants, followed by UV exposure. These crosslinked proteins will next be collected by cell membrane protein extraction, immunoprecipitation, separation with electrophoresis, and visualization with silver staining, as detailed in section 5.2.6. Once we observe indications of successful crosslinking, such as increased darkness of protein bands on SDS-PAGE gel, we will run the experiment by including RAN aptamer as a control group. The distinct bands enriched by A1 variants will be excised and submitted to the Proteomics Core at Fred Hutch Cancer Research Center to identify the enriched protein peptides. The verification of the identified proteins can be done with siRNA knockdown, bio-layer interferometry, colorimetric binding assays, and antibody/aptamer binding correlation with flow cytometry.

6.2.2 A1 targeted drug delivery with increased cargo

6.2.2.1 Background and significance

In chapter 5, we demonstrated the generation of two kinds of drug delivery systems with A1. Including A1 directly conjugated with MMAE and A1 complexed with dox using mostly its stem structure. The A1-vc-MMAE conjugate consists of one drug on each aptamer strand, bridged with a cleavable linker (**Scheme 5.1**). The A1-dox complex has about 4-5 drug molecules (**Figure 5.8**) on each aptamer. Along with the RAN aptamer control groups, we applied these two types of drug carriers to J.RT3-T3.5 cells. Surprisingly, we did not see significant differences between the A1 drug carriers and RAN drug carriers treated cells (**Figure 5.7 and 5.8**). A1-vc-MMAE could be carrying insufficient amount of toxin that targeted delivery was not enough to cause consistent killing. Whereas the A1-dox complex showed high background killing likely due to higher sensitivity of J.RT3-T3.5 cells to the toxin. A1 carrying more MMAE and dox might help increase the cytotoxicity differences between RAN- and A1-dox.

6.2.2.2 Aim 1: Design of A1 with longer double stranded region for carrying drug

A simple method to increase the double stranded region on an aptamer is to extend the stem region with hybridization of complementary strands. It has been demonstrated that the extended region of aptamer can be used to intercalate dox molecules for increased drug load on aptamers.[8,9] By using NUPACK structure simulating software, we designed elongated stem for A1 through hybridization of two short single strands with the original A1 sequence (**Table 6.1** and **Figure 6.1**). This new structure will be conjugated with vc-MMAE peptide by incorporating internal dithiol side chains (IDT code “iDTPA”) and use the method described in section 5.2.9 for conjugation. A1 with longer stem but without dithiol side chains will be used to intercalate dox using the method described in section 5.2.11.

Table 6.1. Sequences for A1 and strands for hybridization

Name	Sequence
A1	5'- ATCCAGAGTGACGCAGCATAGTCAAGGCGATAGACGAAAAACATTGTTTTCCTGGAAGGCCCAGAA TCTGTGG ACACGGTGGCTTAGT -3'
Strand 1	5'- CAATACCTACTAA -3'
Strand 2	5'- GGTATTGTTTAGT -3'

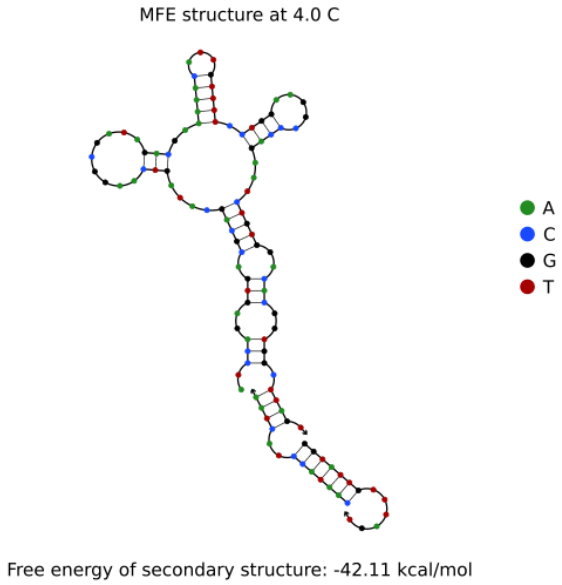

Figure 6.1. A1 with hybridized stem using sequences in **Table 6.1**.

6.2.2.3 Aim 2: Evaluation of drug delivery to target cells using A1-drug conjugate and complex

The A1-drug conjugate and complex generated in section 6.2.2.2, will be applied to J.RT3-T3.5 cells for various treatment time. 0.5, 1, 2 hours for aptamer-MMAE conjugates and 5, 10, 15 minutes for aptamer-dox complexes due to their differences in background killing. Various incubation temperatures and anionic blocker compositions will be optimized to minimize background killing as well. The optimal condition and different drug carrier concentrations will be applied to the cells to generate IC_{50} curves. After incubation, the cells will be washed to remove drug conjugates and complexes. MTS assay will be used to assess cell viability.

6.3 References

1. Ruella, M., Xu, J., Barrett, D. M., Fraietta, J. A., Reich, T. J., Ambrose, D. E., Klichinsky, M., Shestova, O., Patel, P. R., Kulikovskaya, I., Nazimuddin, F., Bhoj, V. G., Orlando, E. J., Fry, T. J., Bitter, H., Maude, S. L., Levine, B. L., Nobles, C. L., Bushman, F. D., Young, R. M., Scholler, J., Gill, S. I., June, C. H., Grupp, S. A., Lacey, S. F. & Melenhorst, J. J. Induction of resistance to chimeric antigen receptor T cell therapy by transduction of a single leukemic B cell. *Nat. Med.* (2018) doi:10.1038/s41591-018-0201-9.

2. Kacherovsky, N., Cardle, I. I., Cheng, E. L., Yu, J. L., Baldwin, M. L., Salipante, S. J., Jensen, M. C. & Pun, S. H. Traceless aptamer-mediated isolation of CD8+ T cells for chimeric antigen receptor T-cell therapy. *Nat. Biomed. Eng.* (2019) doi:10.1038/s41551-019-0411-6.

3. Mallikaratchy, P., Tang, Z., Kwame, S., Meng, L., Shangguan, D. & Tan, W. Aptamer directly evolved from live cells recognizes membrane bound immunoglobin heavy mu chain in Burkitt's lymphoma cells. *Mol. Cell. Proteomics* (2007) doi:10.1074/mcp.M700026-MCP200.

4. Golden, M. C., Collins, B. D., Willis, M. C. & Koch, T. H. Diagnostic potential of PhotoSELEX-evolved ssDNA aptamers. *J. Biotechnol.* (2000) doi:10.1016/S0168-1656(00)00290-X.

5. Meisenheimer, K. M. & Koch, T. H. Photocross-linking of nucleic acids to associated proteins. *Critical Reviews in Biochemistry and Molecular Biology* (1997) doi:10.3109/10409239709108550.

6. Hafner, M., Landthaler, M., Burger, L., Khorshid, M., Hausser, J., Berninger, P., Rothballer, A., Ascano, M., Jungkamp, A. C., Munschauer, M., Ulrich, A., Wardle, G. S., Dewell, S., Zavolan, M. & Tuschl, T. Transcriptome-wide Identification of RNA-Binding Protein and MicroRNA Target Sites by PAR-CLIP. *Cell* (2010) doi:10.1016/j.cell.2010.03.009.

7. Ascano, M., Hafner, M., Cekan, P., Gerstberger, S. & Tuschl, T. Identification of RNA-

protein interaction networks using PAR-CLIP. *Wiley Interdisciplinary Reviews: RNA* (2012) doi:10.1002/wrna.1103.

8. Zhu, G., Zheng, J., Song, E., Donovan, M., Zhang, K., Liu, C. & Tan, W. Self-assembled, aptamer-tethered DNA nanotrains for targeted transport of molecular drugs in cancer theranostics. *Proc. Natl. Acad. Sci. U. S. A.* (2013) doi:10.1073/pnas.1220817110.

9. Zhang, L., Wang, S., Yang, Z., Hoshika, S., Xie, S., Li, J., Chen, X., Wan, S., Li, L., Benner, S. A. & Tan, W. An Aptamer-Nanotrain Assembled from Six-Letter DNA Delivers Doxorubicin Selectively to Liver Cancer Cells. *Angew. Chemie* (2020) doi:10.1002/ange.201909691.